INFORMATION TO USERS

This manuscript has been reproduced from the microfilm master. UMI films the text directly from the original or copy submitted. Thus, some thesis and dissertation copies are in typewriter face, while others may be from any type of computer printer.

The quality of this reproduction is dependent upon the quality of the copy submitted. Broken or indistinct print, colored or poor quality illustrations and photographs, print bleedthrough, substandard margins, and improper alignment can adversely affect reproduction.

In the unlikely event that the author did not send UMI a complete manuscript and there are missing pages, these will be noted. Also, if unauthorized copyright material had to be removed, a note will indicate the deletion.

Oversize materials (e.g., maps, drawings, charts) are reproduced by sectioning the original, beginning at the upper left-hand corner and continuing from left to right in equal sections with small overlaps.

Photographs included in the original manuscript have been reproduced xerographically in this copy. Higher quality 6" x 9" black and white photographic prints are available for any photographs or illustrations appearing in this copy for an additional charge. Contact UMI directly to order.

ProQuest Information and Learning
300 North Zeeb Road, Ann Arbor, MI 48106-1346 USA
800-521-0600

DISSERTATION

POLYFLUOROALKOXYALUMINATES AND BORATES AS NEW WEAKLY COORDINATING ANIONS AND AS COMPONENTS OF BATTERY ELECTROLYTES.

Submitted by

Benjamin G. Nolan

Department of Chemistry

In partial fulfillment of the requirements

for the Degree of Doctor of Philosophy

Colorado State University

Fort Collins, Colorado

Spring 2001

Bell & Howell Information and Learning Company
300 North Zeeb Road
P.O. Box 1346
Ann Arbor, MI 48106-1346

COLORADO STATE UNIVERSITY

December 13, 2000

WE HEREBY RECOMMEND THAT THE DISSERTATION PREPARED UNDER OUR SUPERVISION BY BENJAMIN G. NOLAN ENTITLED POLYFLUOROALKOXYALUMINATES AND BORATES AS NEW WEAKLY COORDINATING ANIONS AND AS COMPONENTS OF BATTERY ELECTROLYTES. BE ACCEPTED AS FULFILLING IN PART THE REQUIREMENTS FOR THE DEGREE OF DOCTOR OF PHILOSOPHY.

Committee on Graduate Work

Advisor

Department Head

Abstract of Dissertation

POLYFLUOROALKOXYALUMINATES AND BORATES AS NEW WEAKLY COORDINATING ANIONS AND AS COMPONENTS OF BATTERY ELECTROLYTES

The synthesis and characterization of salts of new weakly coordinating anions based on the general formulas $B(O_2L_f)_2^-$ and $Al(OR_f)_4^-$ are reported. New $B(O_2L_f)_2^-$ anions are $B(OC(2\text{-}C_6H_4O)(CF_3)_2)_2^-$, $B(OC(2\text{-}(O)\text{-}3\text{-}C_6H_3F)(CF_3)_2)_2^-$, $B(OC(2\text{-}(O)\text{-}4\text{-}C_6H_3F)(CF_3)_2)_2^-$, $B(OC(2\text{-}(O)\text{-}5\text{-}C_6H_3F)(CF_3)_2)_2^-$, $B(OC(2\text{-}(O)\text{-}3,5\text{-}C_6H_2F_2)(CF_3)_2)_2^-$, $B(OC(2\text{-}(O)\text{-}4,5\text{-}C_6H_2F_2)(CF_3)_2)_2^-$, $B(OC(2\text{-}(O)\text{-}4,6\text{-}C_6H_2F_2)(CF_3)_2)_2^-$, $B(OC(2\text{-}(O)\text{-}3,4,5\text{-}C_6HF_3)(CF_3)_2)_2^-$, $B(OC(2\text{-}(O)\text{-}4,5,6\text{-}C_6HF_3)(CF_3)_2)_2^-$, $B(OC(2\text{-}(O)\text{-}3\text{-}t\text{-}Bu\text{-}5\text{-}Me\text{-}C_6H_2)(CF_3)_2)_2^-$, $B(OC(2\text{-}(O)\text{-}3,5\text{-}C_6H_2(t\text{-}Bu)_2)(CF_3)_2)_2^-$, $B(OC(2\text{-}(O)\text{-}3\text{-}C_6H_3I)(CF_3)_2)_2^-$. Except for $HOC(2\text{-}C_6H_4(OH))(CF_3)_2$, $HOC(2\text{-}(OH)\text{-}4\text{-}C_6H_3F)(CF_3)_2$, and $HOC(2\text{-}(OH)\text{-}3,5\text{-}C_6H_2(t\text{-}Bu)_2)(CF_3)_2$, all of the diols used as ligand precursors in the new borate anions are new compounds. The new $LiAl(OR_f)_4$ salts prepared are $LiAl(OCH(CF_3)_2)_4$, $LiAl(OC(cyclo\text{-}C_6H_{11})(CF_3)_2)_4$, and $LiAl(OC(C_6H_5)(CF_3)_2)_4$. Four Li^+ salts of the new borates and aluminates were structurally characterized by X-ray crystallography: $Li(OC(CH_3)_2)(B(OC(2\text{-}(O)\text{-}3,4,5\text{-}C_6HF_3)(CF_3)_2)_2$, $Li_2(CH_3O(CH_2)_2OCH_3)(B(OC(2\text{-}C_6H_4O)(CF_3)_2)_2)$, $LiAl(OCH(CF_3)_2)_4$, and $LiAl(OC(cyclo\text{-}C_6H_{11})(CF_3)_2)_4$.

Conductivities of solutions of many of the new salts were determined for the solvents 1,2-dimethoxyethane, tetrahydrofuran, propylene carbonate, acetonitrile, and various mixtures of ethylene carbonate and dimethyl carbonate. Conductivities were also measured for the first time for the known salts $LiAl(OC(CH_3)(CF_3)_2)_4$, $LiAl(OCH(C_6H_5)(CF_3)_2)_4$, $LiAl(OC(4\text{-}C_6H_4(CH_3)(CF_3)_2)_4$, $LiAl(OC(4\text{-}C_6H_4(t\text{-}Bu))(CF_3)_2)_4$, $LiAl(OC(C_6H_5)(CF_3)_2)_4$, and $LiAl(OC(CF_3)_3)_4$. Based on these measurements, it was determined that all of the anions are more weakly coordinating and more weakly ion-pairing than the commonly-used weakly coordinating anion $CF_3SO_3^-$. For the $B(O_2L_f)_2^-$ anions, it was found that the ion-pairing strength depends not only on the number of fluorine atoms incorporated into the phenyl groups in the anions but also on their relative positions. Maximum conductivities in 1,2-dimethoxyethane (DME) solution were also determined for several lithium salts, and these exceed the minimum value for practical use in lithium batteries. The maximum value for any $LiB(O_2L_f)_2$ salt studied was observed for a 0.5 M DME solution of $LiB(OC(2\text{-}(O)\text{-}4,5,6\text{-}C_6HF_3)(CF_3)_2)_2$ (8.39 mS cm^{-1}). The maximum value for the $LiAl(OR_f)_4$ salts studied was observed in a 0.5 M solution of $LiAl(OCH(CF_3)_2)_4$ (11.2 mS cm^{-1}). Electrochemical stabilities (oxidative, reductive, aluminum corrosion) of the new lithium salts were also examined, and it was found that in almost every case all requirements for practical use were satisfied.

The solubility in hexane of $LiAl(OR_f)_4$ salts was determined for $LiAl(OCH(CF_3)_2)_4$, $LiAl(OC(C_6H_5)(CF_3)_4$, $LiAl(OC(C_6H_5)_2(CF_3))_4$, $LiAl(OC(cyclo\text{-}C_6H_{11})(CF_3)_2$, $LiAl(OC(CH_3)(CF_3)_2)_4$, $LiAl(OC(4\text{-}C_6H_4(CH_3))(CF_3)_2)_4$, and

$LiAl(OC(4\text{-}C_6H_4(t\text{-}Bu))(CF_3)_2)_4$. Some trends according to ligand type and coordination environment were suggested.

Three other classes of weakly coordinating anions were studied in terms of the conductivities of their lithium salts in 1,2-dimethoxyethane, tetrahydrofuran, and propylene carbonate: $B(C_6F_5)_3(OR_f)^-$ ($OR_f = OCH(CF_3)_2$, $OC(C_6H_5)_2(CF_3)$, $OC(CF_3)_3$); carborane anions ($CB_{11}H_{12}^-$, 7,8,9,10,11,12-$CB_{11}H_6Br_6^-$, 1-CH_3-$CB_{11}F_{11}^-$); and the anion based on the hydrogen-bonded complex of $CF_3CO_2^-$ and CF_3COOH, $H(CF_3CO_2)_2^-$.

Benjamin G. Nolan
Department of Chemistry
Colorado State University
Fort Collins, CO 80523
Spring 2001

ACKNOWLEDGEMENTS

I have been told that choosing an advisor is the single most important decision one will make in graduate school. I must say that I made a fantastic choice – Steve Strauss has been everything I could ask for in an advisor, and I owe him a large debt of gratitude for this. I would also like to thank all of my co-workers that have helped me to get to this point for their advice, consultation, and support. Also, special thanks go to Tony Rappé, who was extremely helpful and a valuable resource during the preparation of this dissertation. Finally, I would like express deep appreciation to my family and friends; the last four and a half years have been a wild ride, and they have always been there for me.

To

My parents, Richard and Pamela Nolan,

without whom this would never have been possible

Table of Contents

List of Figures

List of Tables

CHAPTER 1

Introduction

Weakly Coordinating Anions

Research in the field of weakly coordinating anions (*WCA*s) has received considerable attention in recent years, due to the important role these species can play in a variety of applications.[1] Such applications center around the use of a *WCA* to generate a "free" cation, and include the following: isolation and study of reactive cations (e.g. Xe_2^+,[2] $H(C_6(CH_3)_6)^+$,[3] $Cu(CO)_4^+$ [4]); polymerization catalysis;[5] organic transformation catalysis (e.g. 1,4 conjugate addition reactions, Diels-Alder reactions);[6] and lithium batteries (i.e. as components of solution or solid-polymer electrolytes).[7]

Due to the wide range of conditions used in the applications listed above and others where a *WCA* is necessary, the notion of a "universal" anion, one that would be well suited for every possible use, is unrealistic. Many anions are needed, each with different properties to meet the specific requirements of a variety of applications. However, there is one characteristic that is necessary for all *WCA*s: low Lewis basicity. For ion pairs, this means a weak interaction between a *WCA* and its countercation. To minimize this interaction, there are several *WCA* design criteria that are important to consider. First, the overall charge should be low (ideally –1). Size is another issue. As a first approximation, the effect of size on the strength of a cation-anion electrostatic interaction is described by Coulomb's Law (eq. 1).

$$force = \frac{Z^- Z^- e^2}{r^2} \qquad \text{(eq. 1)}$$

This expresses the force of attraction or repulsion between two point charges, and decreases as $1/r^2$, where r is the distance between the two charges. Although cations and anions cannot be accurately portrayed as point charges, the same principle applies: as anion size increases, the distance between the centers of charge for the ions increases, thereby decreasing the attractive force between the ion pair.

While Coulomb's Law is a useful starting point for understanding the basis of coordinating ability, it does not address some important other issues. One of these is the nature of the charge distribution. Large size is beneficial in this regard as well, as the negative charge has many atoms over which it can be distributed. In principle, as the number of atoms increases, the fraction of charge at each site on the anion decreases. Since a cation can only coordinate to a limited number of sites, the negative charge that it experiences, or the *effective charge*, also decreases. To illustrate the meaning of this term, consider the comparison of LiF and $LiPF_6$. In the simple case of LiF, the fluoride anion coordinates to the lithium cation, and the two are close enough to each other that the cation experiences most, if not all, of the F^- negative charge. Thus, the effective charge of F^- is approximately negative one. For $LiPF_6$, the larger size of the anion prevents Li^+ from coordinating to every site. For the sake of this discussion, assume that the cation coordinates to one face composed of three fluorine atoms, as shown below.

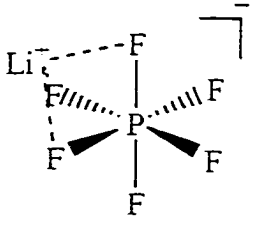

Hypothetical coordination of Li^+ to PF_6^-.

There may be weak interactions with the remaining fluorine atoms, but it is assumed that these lie beyond a certain distance of separation (arbitrarily defined for this example) where the strength of these is negligible. If the charge on PF_6^- can be thought of as shared equally among the six fluorine atoms, the effective charge experienced by Li^+ is therefore only approximately –0.5. Although *WCA*s possess a full negative charge, a high degree of charge dispersal thus acts to decrease its *effective* charge, making it a weaker Lewis base.

A third important characteristic of a *WCA* is the nature of the atoms on the periphery. Usually, a cation is coordinated primarily by sites on the outer portion of an anion. To minimize Lewis basicity, the periphery is ideally composed of weak donor atoms that do not release a significant amount of charge density in coordinating to a cation. As donor strength decreases, the effective charge experienced by the cation becomes less. The best-suited atoms in this respect are hydrogen and fluorine. Hydrogen atoms have no lone pairs to coordinate to a cation, and although fluorine atoms do, these atoms usually form strong bonds with only one atom at a time. Other halogens (Cl, Br, I) are also good candidates for peripheral atoms, but they are more strongly donating than both hydrogen and fluorine atoms.

Another requirement for *WCA*s, one that is not related to coordinating ability, is stability. To be useful, an anion must exhibit thermal, chemical, and electrochemical stability, as well as stability with respect to fragmentation in the presence of highly electrophilic cations. Toxicity is another consideration, and ideally the *WCA* would be inexpensive to manufacture.

The development of *WCA*s began with relatively simple species such as ClO_4^-, BF_4^-, $AlCl_4^-$, PF_6^-, AsF_6^-, SbF_6^-, $B(C_6H_5)_4^-$, and $CF_3SO_3^-$. These were suitable for

many applications, and many are still used today. However, the desire to pursue and study increasingly reactive cationic species has rendered these anions obsolete. Aside from the fact that none are weakly coordinating enough to yield the desired cationic reactivity in many cases, there are stability issues as well. Certain salts of these anions are unstable towards water, undergoing hydrolysis. Also, many are not oxidatively stable, or will decompose in the presence of a highly electrophilic cation. The need for more weakly coordinating and more robust anions has resulted in the development of several new classes of *WCA*s, which are listed with selected examples in Table 1.

Table 1. Examples of the new classes of weakly coordinating anions.

class	examples
1. Nitrogen and carbon perfluoroalkylsulfonyl derivatives	$N(SO_2CF_3)_2^-$, $C(SO_2CF_3)_3^-$
2. Central anion surrounded by two or more Lewis acids	$Sb_nF_{5n+1}^-$ (n = 2, 3, 4), *cyclo*-$(Hg(1,2\text{-}C_2B_{10}H_8R_2))_4Cl^-$ (R = H, 4-C_6H_4F)
3. Central cation surrounded by two or more anions	$B(C_6F_5)_4^-$, $B(3,5\text{-}C_6H_3(CF_3)_2)_4^-$, $Al(OC(C_6H_5)(CF_3)_2)_4^-$, $Nb(OCH(CF_3)_2)_6^-$, $B(OCH(CF_3)_2)_4^-$, $Al(OC_6F_5)_4^-$, $B(OTeF_5)_4^-$, $Nb(OTeF_5)_6^-$, $Co(C_2B_9H_{11})_2^-$
4. Cluster anions containing d- and/or p-block atoms	$CB_{11}H_6X_6^-$ (X = F, Cl, Br, I), 1-R-$CB_{11}X_{11}$ (R = H, F, alkyl, X = F, Cl, Br, I) $CB_{11}(CH_3)_{12}^-$, $CB_{11}(CF_3)_{12}^-$, $PW_{12}O_{40}^{3-}$

The class of nitrogen and carbon perfluoroalkylsulfonyl derivatives was developed at 3M (imide)[8] and Covalent Associates (methide).[9] Due in part to their molecular structure, these anions exhibit high degrees of thermal and chemical stability. This, combined with their weak coordinating ability, has made these species useful for a variety of applications including lithium batteries, organic transformation catalysis, and the isolation of reactive cations. However, they are not viable as counterions in systems

where the presence of oxygen atoms is undesirable. For example, some cationic transition metal catalysts have been found to be inactive in the presence of $N(SO_2CF_3)_2^-$, due to relatively strong coordination of the sulfonyl oxygen atoms to the metal center.[10]

The series of anions based on the formula $Sb_nF_{5n+1}^-$ ($n = 2, 3, 4$) are generated in the superacid mixture of 1:1 HF:SbF_5.[11] The different values of n correspond to higher-order oligomers composed of SbF_5–SbF_6^- Lewis acid–conjugate base complex units. They have been used to isolate highly reactive cations such as Xe_2^+,[2] *cyclo*-$Cl_2O_2^+$,[12] and a variety of homoleptic carbonyl cations such as $[Hg(CO)_2]^{2+}$,[13] high-spin $[Fe(CO)_6]^{2+}$,[14] HCO^+,[15] and $N(CO)_2^+$.[16] However, the success of these anions is tempered by their instability with respect to water, fragmentation, and/or reduction. Furthermore, the superacid system in which the anions are generated is toxic and corrosive.

The third class contains the well-known aryl borates, which have been used extensively in polymerization catalysis.[5] These are based on the parent $B(C_6H_5)_4^-$ anion, which suffers from a variety of problems: oxidative instability, coordination of the phenyl rings to metal centers via π–phenyl interactions, metalation, and phenyl group abstraction. Fluorination of the phenyl rings, either by substitution of hydrogen atoms with fluorine atoms or with trifluoromethyl groups, has resulted in borates with improved properties.[17] They are more stable towards oxidation, and no coordination to metal centers through π–phenyl interactions has been observed. Coordination does occur through C–F bonds, but it is a much weaker interaction. Stability is still an issue in terms of aryl abstraction: one report described the reaction of $B(C_6F_5)_4^-$ with a zirconium complex to form a Zr–C_6F_5 species;[18] in another, the reaction of $AlMe_3$ with $[CPh_3][B(C_6F_5)_4]$ to produce $AlMe_{3-x}(C_6F_5)_x$ was observed.[18] There has also been a

report of aryl transfer to Pt in the complex [*trans*-$PtMe(OEt_2)(PPh_3)_2$][$B(3,5\text{-}C_6H_3(CF_3)_2)_4$] to produce [*trans*-$Pt(3,5\text{-}C_6H_3(CF_3)_2)_2(PPh_3)_2$] and other unidentified products.[19] The other major family of anions in this class consists of fluoroalkoxy- and fluorophenoxyaluminates, –niobates, and –borates. These will be discussed in detail in a later section.

Another subset of the third class of *WCA*s is based on pentafluorooxotellurate (teflate, $-OTeF_5$) ligands.[20] Although an oxygen atom is present, it is made weakly basic by virtue of the highly electron-withdrawing $-TeF_5$ group. Furthermore, in metal complexes with these ligands, the oxygen atoms reside in the core of the anion, and the periphery is composed exclusively of fluorine atoms. New *WCA*s based on this theme include $B(OTeF_5)_4^-$,[21] $Nb(OTeF_5)_6^-$,[22] and $Sb(OTeF_5)_6^-$.[22,23] Their weakly coordinating ability is evidenced by the synthesis and isolation of unusual cationic silver complexes of carbon monoxide,[21d] dichloromethane,[22a] and dichloroethane.[24]

The last class is composed of the cluster anions, and is dominated by monocarborane anions based on $CB_{11}H_{12}^-$.[25] This anion has been shown to be weakly coordinating in its own right,[1b,26] and exhibits good thermal stability. However, one important problem is the apparent lack of stability of its trityl salt, presumably due to hydride abstraction from the cluster.[27] It is likely that salts composed of other strong electrophiles would behave in a similar manner. This limits the number of metathesis salts that can be made with this anion, and thus its usefulness. Efforts to improve $CB_{11}H_{12}^-$ have consisted of substituting the hydrogen atoms with a variety of substituents: halogens (F,[28] Cl,[29] Br,[30] I[31]), methyl groups,[32] and trifluoromethyl groups.[33] It was found that that the polyhalogenated anions are stable in the presence of strong electrophiles such as $Si(i\text{-}Pr)_3^+$ [28,34] and $H(C_6H_6)^+$.[35] Stability studies were

performed on 1-H-$CB_{11}F_{11}^-$, where it was found that the cesium salt of this anion is stable in the presence of F_2/HF, 98% H_2SO_4, 1 M aqueous HNO_3, and excess $AlEt_3$, although it did react slowly with Ce^{4+}, as well as with metallic sodium to yield 1,12-$CB_{11}H_2F_{10}^-$.[28] The lithium salt of 1-H-$CB_{11}F_{11}^-$ was found to be stable to at least 230 °C under vacuum. These anions have very few limitations, but one is their high cost.

The various anions listed above possess many favorable properties, and have proven to be very useful. However, each has its limitations, and as described earlier, there is a need for many different *WCA*s with a range of properties. For these reasons, the development of new *WCA*s continues to be an active and necessary endeavor.

Fluorinated Alkoxides as Ligands for New WCA*s*

Highly fluorinated alcohols and the metal alkoxides that can be derived from them are of interest for a number of reasons.[36,37] In general, they are chemically stable and resistant to oxidation, enabling them to be used as ligands to stabilize metal atoms in high oxidation states. In addition, the high electronegativity of the fluorinated substituents reduces the basicity of the oxygen atom, disfavoring the formation of extended alkoxy-bridged species. Furthermore, the steric and electronic properties can be readily modified, allowing for a wide variety of possible ligands. One area where they are important is in the design of metathesis catalysts, where they are used as components of complexes based on tungsten and molybdenum.[38] As part of this research, it was found that varying the character of the fluoroalkoxide ligand had a significant effect on catalyst activity. Metal fluoroalkoxides have also found use as precursors for chemical vapor deposition of metal fluorides[39] and fluorine-doped metal oxides.[40]

The idea of using fluoroalkoxides as ligands to synthesize new *WCA*s follows from work done by Strauss with metal teflates.[20] While $M(OTeF_5)_n^-$ anions are very weakly coordinating, both the anions and $OTeF_5$ groups are extremely sensitive to traces of water and produce highly toxic decomposition products (including HF). Using tellurium also introduces significant cost. Fluoroalkoxides are less expensive and are more stable than the teflate anion. The oxygen atom is more basic than that in $-OTeF_5$, but is still a weak donor. For comparison, $HOTeF_5$ has an acidity similar to HCl (pK_a = –7.0), while the fluoroalcohols $HOCH(CF_3)_2$ and $HOC(CF_3)_3$ have pK_a values of 9.3 and 5.4, respectively.[36] However, due to the larger size of the fluoroalkoxides, a greater degree of charge dispersal can be achieved in the anion as a whole. The size of the

fluoroalkoxide may also introduce kinetic barriers to cation coordination by the oxygen atoms, in the form of steric hindrance. Also, the ease of structural variation of these ligands facilitates tuning of steric and electronic properties, allowing a wide variety of anions to be created.

Prior to the work done by Strauss, there were only a few published examples of homoleptic anions containing fluoroalkoxide ligands. These are $Y(OC(CH_3)(CF_3)_2)_5^{2-}$,[41] $YOCH(CF_3)_2)_5^{2-}$,[42] $Zr(OCH(CF_3)_2)_6^{2-}$,[43] and $Cu(OCH(CF_3)_2)_4^{2-}$.[44] Note that all of these are dianionic. The first salt of a 1– anion of this type, $LiAl(OC(C_6H_5)(CF_3)_2)_4$, was reported by Barbarich *et al.* in 1996.[6f] In 1997, the first salt of anion of this type based on niobium, $LiNb(OCH(CF_3)_2)_6$, was reported by Rockwell *et al.*[45] Work has continued since that time on the development of new anions based on these prototypes, with the goal of improving them in terms of weak coordinating ability, solubility, and stability. A closely related series of anions incorporating fluorinated *phenoxide* ligands, including $Al(OC_6F_5)_4^-$, $Nb(OC_6F_5)_4^-$, and $Ta(OC_6F_5)_4^-$, has been developed by Marks and co-workers.[46]

One interesting aspect of the lithium fluoroalkoxyaluminates developed thus far is the nature of the bonding between Li^+ and the anion. For example, in the solid state structure of $LiAl(OC(C_6H_5)(CF_3)_2)_4$, there are four Li–F(C) bonds that, albeit weak, are significant to the overall coordination of Li^+. There are other examples of very weak metal-ligand (or metal-solvent) bonding, incldiuing $Ag(CH_2Cl_2)^+$,[22a] $Ag(CO)^+$,[21d] $Na(\eta^6\text{-}C_6H_6)^+$,[43] (porphyrin)$Fe(\eta^2\text{-}C_6H_4R_2)^+$,[47] and $Tl(\eta^6\text{-}C_6H_3R_3)^+$ [21a,48] Understanding the nature of these types of bonds is critical to understanding how they affect the structure and reactivity of a metal complex, and the growing number of these complexes that have been structurally characterized has allowed the development of

various approaches to do this. One qualitative method that has been used with some success is based on the concept of secondary bonding.[49] In this approach, atoms separated by a distance that falls within the sum of the two van der Waals radii but is longer than the sum of the two covalent radii are said to be joined by a secondary bond, which may affect the structure and reactivity of the complex. This works well for nonmetallic elements,[49] but is not well suited for metallic elements. This is because the concept of a van der Waals radius is more meaningful for nonmetallic elements than for metallic elements, since metal atoms or ions are usually shielded by their ligands from nonbonded contacts.[50]

A more quantitative method is through bond valence analysis.[51] In this approach, the valence of an atom is assumed to be distributed among the bonds it forms. Thus, the sum of the individual bond valences, s, should be equal to the valence of an atom or ion, which for a singly charged cation is one. Equation 2 gives a two parameter empirical relationship that has been developed by Brown and Shannon after examining thousands of crystal structures, and with which an individual bond's contribution to the valence of the atom or ion can be determined:[51a]

$$s = (r/r_0)^{-N} \qquad \text{(eq. 2)}$$

The sum of the individual bond valences should be within 0.05 valence units of the valence of the atom. The variable r is the experimentally determined interatomic distance for a particular bond. The parameters r_0 and N were empirically derived for a given bond type. The parameter r_0 can be thought of as the length of a bond with a unit bond valence, although the relationship $s = (r/r_0)^{-N}$ may only be valid over the central part of

the range of r values for a given bond type.[51c] Self-consistent sets of parameters r_0 and N for many types of bonds have been determined.[51a] For the two types of bonds to be discussed below, the parameters are: Li–O, $r_0 = 1.378$, $N = 4.065$; and Li–F, $r_0 = 1.288$, $N = 3.9$.

The bond valence method possesses the key benefit of being able to assess the relative strengths of bonds: a higher s value indicates a stronger bond. However, at what point does an interaction become weak enough that it is no longer considered to be a bond? It is proposed here that the limit be taken as an s value of 0.03, or when a bond contributes only 3% to the total valence, leading to a maximum bonding distance of 3.165 Å for Li–F bonds. Since the van der Waals radius of fluorine is 1.47 Å,[50] the lithium cation portion of the $s = 0.03$ distance is 1.70 Å, which is remarkably close to the published van der Waals radius of 1.82 Å for this atom.[50] For Li–O bonds, the lithium cation portion of the $s = 0.03$ distance is 1.75 Å. It will be interesting to see if the $s = 0.03$ limit correlates with van der Waals radii for other metal ions because, if it does, the bond valence method could be used to determine unknown metal-ion van der Waals radii.

Salts of WCA*s as Components of Solution Electrolytes*

The success of primary and secondary lithium batteries depends upon many factors, one important one being the availability of electrolyte salts that satisfy an array of requirements. The salt must be highly conducting in solution (at least 5 mS cm^{-1}) over a wide temperature range. It must be thermally stable, chemically stable (e.g. in contact with anode and cathode materials and with solvent), electrochemically stable, of low toxicity, and inexpensive. The requirement of electrochemical stability includes several

conditions: oxidation (>4.2 V $Li^{0/+}$); reduction (<–0.5 V vs. $Li^{0/+}$); in contact with anode (reducing conditions, e.g. 0 – 2.0 V vs. $Li^{0/+}$) and cathode (oxidizing conditions, e.g. 2 – 4.2 V vs. $Li^{0/+}$) materials; and in contact with aluminum over the entire working potential range of the battery. Aluminum is used as the current collector in lithium batteries, and some lithium salts have been shown to promote its corrosion.

The earliest electrolytes consisted of lithium salts of relatively simple anions, and included the following: $LiClO_4$; $LiPF_6$; $LiAsF_6$; $LiBF_4$; and $LiCF_3SO_3$. These satisfy many of the requirements listed above, and found practical use in primary lithium cells. However, each has certain problems that warrant the search for new and better electrolytes. For example, perchlorate is a strong oxidizing agent, and poses explosion risks in ether solutions. The compound $LiPF_6$ is thermally unstable, decomposing at 40 °C in the solid state and 70 °C in solution (EC/DMC 50:50 mol%) to form LiF and PF_5.[52] The compound LiF is a poor electrolyte, and PF_5 is a Lewis acid that can initiate the polymerization of cyclic ethers, common solvents used in batteries.[53] The salt $LiAsF_6$ is more thermally stable, but the same degradation pathway is possible to form LiF and AsF_5. The latter compound is highly toxic and additional decomposition pathways exist for $LiAsF_6$ that can result in the formation of other toxic substances. The salt $LiBF_4$ is somewhat more stable with respect to decomposition to LiF and BF_3, but this reaction still does occur. In any event, this salt also does not form highly-conducting solutions with any suitable solvent. The compound $LiCF_3SO_3$ has several favorable properties, but promotes the corrosion of aluminum at 3.0 V vs. $Li^{0/+}$.

Despite its drawbacks, $LiPF_6$ is currently the salt most commonly found in lithium batteries. It is highly conducting (11.5 mS cm^{-1} in ethylene carbonate/dimethyl carbonate (EC/DMC), 50:50 mol%), electrochemically stable in all respects, and

relatively inexpensive. Nevertheless, there is still much room for improvement, and research in recent years has been directed towards synthesizing new and better salts. Notable examples include the series of lithium fluoroalkylsulfonyl imides and methides including $LiN(SO_2CF_3)_2$ [8] and $LiC(SO_2CF_3)_3$,[9] respectively, and the family of lithium chelatoborates based on the general formula $LiB(O_2L)_2$.

The class of lithium salts based on $LiB(O_2L)_2$ deserves additional discussion, as the compounds described in the current work are of a similar variety. These were developed by Barthel and Gores, and the ligands they have used thus far are shown in Figure 1. The first lithium chelatoborates incorporated catechol and fluorinated analogs as ligands.[54] The resulting salts exhibited many favorable properties: high conductivity, high thermal stability, hydrolytic stability, and reductive stability. One problem was the oxidative stability – even the perfluorinated anion was oxidized at 4.1 V vs. $Li^{0/+}$, below the 4.2 V practical minimum. Other chelating ligands containing two oxygen donors were explored in an effort to improve the oxidative stability, including 2,2'-biphenyldiolate,[55] 2,3-naphthalenediolate,[54c] salicylate,[55] 4-(trifluoromethyl)-salicylate,[56] 2-olate-1-benzenesulfonate,[56] 5-fluoro-2-olate-1-benzenesulfonate,[57] and 2,3-pyridinediolate.[58] The lithium salt derived from salicylate showed an oxidative limit of 4.5 V vs. $Li^{0/+}$, but is reduced at 0.7 V. However, the lithium borate derived from 5-fluoro-2-olate-1-benzenesulfonate exhibited an oxidative stability of 4.6 V vs. $Li^{0/+}$, as well as the required reductive stability. Although the conductivity data have not yet been reported, from the available information this compound appears to be a promising candidate for practical use.

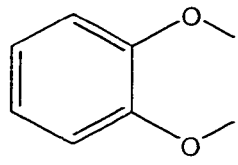

1,2-Benzenediolate

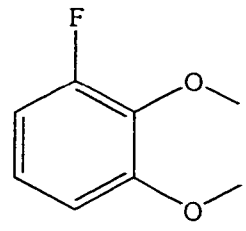

3-Fluoro-1,2-benzenediolate

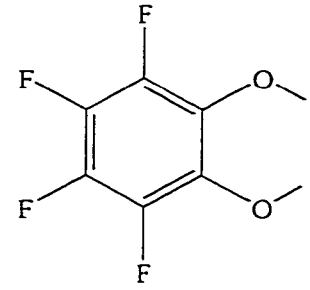

Tetrafluoro-1,2-benzenediolate

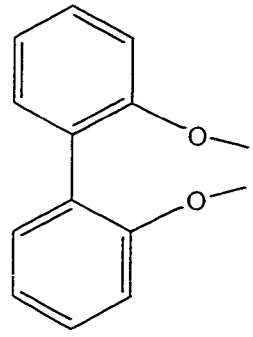

2,2'-Biphenyldiolate

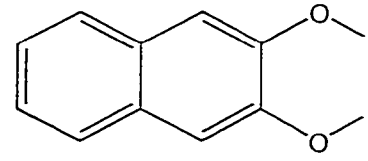

2,3-Napthalenediolate

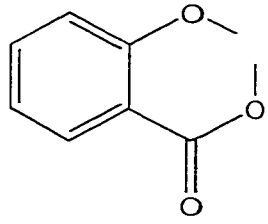

Salicylate

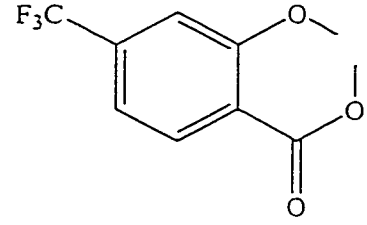

4-(trifluoromethyl)-salicylate

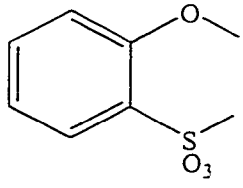

2-Olate-1-benzenesulfonate

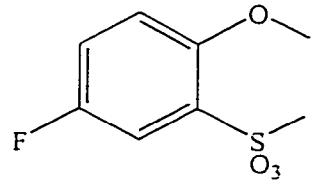

5-Fluoro2-olate-1-benzenesulfonate

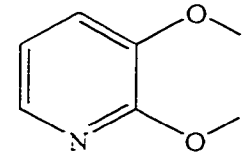

2,3-Pyridinediolate

Figure 1. Ligands used by Barthel and Gores to make lithium borate electrolytes

References

1. (a) Lupinetti, A.J.; Strauss, S.H. *Chemtracts–Inorganic Chemistry* **1998**, *11*, 565. (b) Strauss, S.H. *Chem. Rev.* **1993**, *93*, 927.
2. Drews, T.; Seppelt, K. *Angw. Chem. Int. Ed. Engl.* **1997**, *36*, 273.
3. Reed, C.A.; Fackler, N.L.P.; Kim, K.-C.; Stasko, D.; Evans, D. *J. Am. Chem. Soc.* **1999**, *121*, 6314.
4. Ivanova, S.M.; Ivanov, S.V.; Miller, S.M.; Anderson, O.P.; Solntsev, K.A.; Strauss, S.H. *Inorg. Chem.* **1999**, *38*, 3756.
5. Chen, E.Y.-X.; Marks, T.J.*Chem. Rev.* **2000**, *100*, 1391.
6. (a) DuBay, W.J.; Grieco, P.A.; Todd, L.J. *J. Org. Chem.* **1994**, *59*, 6898. (b) Saidi, M.R.; Heydari, A.; Ipaktschi, J. *Chem. Ber.* **1994**, *127*, 1761. (c) Kobayashi, H.; Nie, J.; Sonoda, T. *Chem. Lett.* **1995**, 307. (d) Arai, T.; Sasai, H.; Aoe, K.; Okamura, K.; Date, T.; Shibasaki, M. *Angew. Chem. Int. Ed. Engl.* **1996**, *35*, 104. (e) Handy, S.T.; Grieco, P.A.; Mineur, C.; Ghosez, L. *Syn. Lett.* **1995**, 565. (f) Barbarich, T.J.; Handy, S.T.; Miller S.M.; Anderson, O.P.; Grieco, P.A.; Strauss, S.H. *Organometallics* **1996**, *15*, 3776.
7. Barthel, J.; Gores, H.J.; In *Handbook of Battery Materials*; Besenhard, J.O., Ed.; VCH Publishers: New York, 1999; Ch. 7.
8. (a) Armand, M.; Mourslı, F. Fr. Patent FR 2527602, 1985; *Chem. Abstr.* **1985**, *100*, 195112. (b) Armand, M.; Gauthier, M.; Muller, D. Fr. Patent FR 2606217, 1989; *Chem. Abstr.* **1989**, *110*, 98805. (c) Dominey, L.A.; Goldman, J.L.; Koch, V.R.; Nanjundiah, C. In *Rechargeable Lithium Batteries*; Subbarao, S., Koch, V.R., Owens, B.B., Smyrl, W.H., Eds.; The Electrochemical Society Proceeding Series PV 90-5;

The Electrochemical Society: Pennington, NJ, 1990; 56. (d) Turowsky, L.; Seppelt, K. *Inorg. Chem.* **1988**, *27*, 2135. (e) Foropolous Jr., J.; DesMarteau, D.D. *Inorg. Chem.* **1984**, *23*, 3720. (f) Armand, M.B.; Gorecki, W.; Adréani, R. In *Second International Symposium on Polymer Electrolytes*; Scrosati, B., Ed.; Elsevier: London, 1990; 91. (g) Webber, A. *J. Electrochem. Soc.* **1991**, *138*, 2586.

9. (a) Dominey, L.A.; Koch, V.R.; Blakeley, T.J. *Electrochim. Acta* **1992**, *37*, 1551. (b) Croce, F.; D'Aprano, A.; Nanjundiah, C.; Koch, V.R.; Walker Jr., C.W.; Salomon, M. *J. Electrochem. Soc.* **1996**, *143*, L80. (c) Walker Jr., C.W.; Cox, J.D.; Salomon, M. *J. Electrochem. Soc.* **1996**, *143*, 154. (d) Dominey, L.A. *Chem. Abstr.* **1992**, *143*, 93735.
10. Siedle, A.R.; Newmark, R.A.; Gleason, W.B.; Lammana, W.M. *Organometallics* **1990**, *9*, 1990.
11. (a) Olah, G.A.; Prakash, G.K.S.; Sommer, J. *Superacids*; J. Wiley: New York, 1985. (b) O'Donnell, T.A. *Superacids and Acidic Melts as Inorganic Chemical Reaction Media*; VCH Publishers: Weinheim, Germany, 1993 and references therein.
12. Drews, T.; Koch, W.; Seppelt, K. *J. Am. Chem. Soc.* **1999**, *121*, 4379.
13. Bodenbinder, M.; Balzer-Jöllenbeck, G.; Willner, H.; Batchelor, R.J.; Einstein, F.W.B.; Wang, C.; Aubke, F. *Inorg. Chem.* **1996**, *35*, 82.
14. Willner, H.; Aubke, F. *Angew. Chem., Int. Ed. Engl.* **1997**, *36*, 2402.
15. de Rege, P.J.F.; Gladysz, J.A.; Horváth, I.T. *Science* **1997**, *276*, 776.
16. Bernhardi, E.; Drews, T.; Seppelt, K. *Angew. Chem.* **1999**, *38*, 2232.
17. (a) Nishida, H.; Takura, N.; Yoshimura, M.; Sonoda, T.; Kobayashi, H. *Bull Chem. Soc. Jpn.* **1984**, *1957*, 2600. (b) Massey, A.G.; Park, A.J. *J. Organomet. Chem.* **1964**,

2, 245. (c) Jia, L.; Yang, X.; Ishihara, A.; Marks, T.J. *Organometallics* **1995**, *14*, 3135.

18. Bochmann, M. Noncoordinating anions as ligands and synthetic reagents, 215th ACS National Meeting, Dallas, TX, March/April 1998, abstract INOR 264.
19. Konze, W.V.; Scott, B.L.; Kubas, G.J. *Chem. Commun.* **1999**, *18*, 1807.
20. Miller, P.K.; Abney, K.D.; Rappé, A.K.; Anderson, O.P.; Strauss, S.H. *Inorg. Chem.* **1988**, *28*, 2255.
21. (a) Noirot, M.D.; Anderson, O.P.; Strauss, S.H. *Inorg. Chem.* **1987**, *26*, 2216. (b) Strauss, S.H.; Noirot, M.D.; Anderson, O.P. *Inorg. Chem.* **1986**, *25*, 3850. (c) Van Seggen, D.M.; Hurlburt, P.K.; Noirot, M.D.; Anderson, O.P.; Strauss, S.H. *Inorg. Chem.* **1992**, *31*, 1423. (d) Hurlburt, P.K.; Anderson, O.P.; Strauss, S.H. *J. Am. Chem. Soc.* **1991**, *113*, 6277.
22. (a) Van Seggen, D.M.; Hurlburt, P.K.; Anderson, O.P.; Strauss, S.H. *Inorg. Chem.* **1995**, *34*, 3453. (b) Moock, K.; Seppelt, K. *Z. anorg. allg. Chemie* **1988**, *561*, 132.
23. Mercier, H.P.A.; Sanders, J.C.P.; Schrobilgen, G.J. *J. Am. Chem. Soc.* **1994**, *116*, 2921.
24. (a) Hurlburt, P.K.; Rack, J.J.; Luck, J.S.; Dec, S.F.; Webb, J.D.; Anderson, O.P.; Strauss, S.H. *J. Am. Chem. Soc.* **1994**, *116*, 10003. (b) Rack, J.J.; Moasser, B.; Gargulak, J.D.; Gladfelter, W.L.; Hochheimer, H.D.; Strauss, S.H. *J. Am. Chem. Soc., Chem. Commun.* **1994**, 685. (c) Hurlburt, P.K.; Rack, J.J.; Dec, S.F.; Anderson, O.P.; Strauss, S.H. *Inorg. Chem* **1993**, *32*, 373.
25. (a) Knoth, W.H. *J. Am. Chem. Soc.* **1967**, *89*, 1274. (b) Knoth, W.H. *Inorg. Chem.* **1971**, *10*, 598.

26. (a) Shelly, K.; Finster, D.C.; Lee, Y.J.; Scheidt, W.R.; Reed, C.A. *J. Am. Chem. Soc.* **1985**, *107*, 5955. (b) Shelly, K.; Reed, C.A.; Lee, Y.J.; Scheidt, W.R. *J. Am. Chem. Soc.* **1986**, *108*, 3117. (c) Liston, D.J.; Reed, C.A.; Eigenbrot, C.W.; Scheidt, W.R. *Inorg. Chem.* **1987**, *26*, 2739. (d) Liston, D.J.; Lee, Y.J.; Scheidt, W.R.; Reed, C.A. *J. Am Chem. Soc.* **1989**, *111*, 6643.

27. Jelínek, T.; Baldwin, P.; Scheidt, W.R.; Reed, C.A. *Inorg. Chem.* **1993**, *32*, 1982.

28. Ivanov, S.V.; Rockwell, J.R.; Polyakov, O.G.; Gaudinski, C.M.; Anderson, O.P.; Solntsev, K.A.; Strauss, S.H. *J. Am. Chem. Soc.* **1998**, *120*, 4224.

29. Xie, Z.; Tsang, C.-W.; Xue, F.; Mak, T.C.W. *Inorg. Chem.* **1997**, *36*, 2246.

30. Xie, Z.; Tsang, C.-W.; Sze, E.T.-P.; Yang, Q.; Chan, D.T.W.; Mak, T.C.W. *Inorg. Chem.* **1998**, *37*, 6444.

31. Srivastava, R.R.; Hamlin, D.K.; Wilbur, D.S. *J. Org. Chem.* **1996**, *61*, 9041.

32. King, B.T.; Janousek, Z.; Gruener, B.; Trammell, M.; Noll, B.C.; Michl, J. *J. Am. Chem. Soc.* **1996**, *118*, 3313.

33. King, B.T., Michl, J. *J. Am. Chem. Soc.* **2000**, *122*, 10253.

34. (a) Reed, C.A.; Xie, Z.A.; Bau, R.; Benesi, A. *Science* **1993**, *262*, 402. (b) Xie, Z.; Manning, J.; Reed, R.W.; Mathur, R.; Boyd, P.D.W.; Benesi, A.; Reed, C.A. *J. Am. Chem. Soc.* **1996**, *118*, 2922.

35. Dagani, R. *Chem. Eng. News* **1998**; May 4: 49.

36. Willis, C.J. *Coord. Chem. Rev.* **1988**, *88*, 133.

37. Purdy, A.P.; George, C.F. in: J.S. Thrasher, S.H. Strauss (Eds.), Inorganic Fluorine Towards the 21st Century, A.C.S. Symposium Series, 555, American Chemical Society; Washington DC, 1994, p. 405.

38. (a) Freudenberger, J.H.; Schrock, R.R.; Churchill, M.R.; Rheingold, A.L.; Ziller, J.W. *Organometallics* **1984**, *3*, 1563. (b) Schrock, R.R.; DePue, R.T.; Feldman, J.; Schaverien, C.J.; Dewan, J.C.; Liu, A.H. *J. Am. Chem. Soc.* **1988**, *110*, 1423. (c) Schrock, R.R.; Murdzek, J.S.; Bazan, G.C.; Robbins, J.; DiMare, M.; O'Regan, M.; *J. Am. Chem. Soc.* **1990**, *112*, 3875. (d) Johnson, L.K.; Virgil, S.C.; Grubbs, R.H. *J. Am. Chem. Soc.* **1990**, *112*, 5384.

39. (a) Lingg, L.J.; Berry, A.D.; Purdy, A.P.; Ewing, K.J. *Thin Solid Films* **1992**, *209*, 9. (b) Samuels, J.A.; Chiang, W.-C.; Yu, C.-P.; Apen, E.; Smith, D.C.; Baxter, D.V.; Caulton, K.G. *Chem. Mater.* **1994**, *6*, 1684.

40. (a) Suh, S.; Hoffman, D.M. *Inorg. Chem.* **1996**, *35*, 6164. (b) Mîinea, L.; Suh, S.; Bott, S.G.; Liu, J.-R.; Chu, W.-K.; Hoffman, D.M. *J. Mater. Chem.* **1999**, *9*, 929.

41. Laurent, F.; Huffman, J.C.; Folting, K.; Caulton, K.G. *Inorg. Chem.* **1995**, *34*, 3980.

42. Labrize, F.; Hubert-Pfalzgraf, L.G. *Polyhedron* **1994**, *34*, 881.

43. Samuels, J.A.; Lobkovsky, E.B.; Strieb, W.E.; Folting, K.; Huffman, J.C.; Zwanziger, J.W.; Caulton, K.G. *J. Am. Chem. Soc.* **1993**, *115*, 5093.

44. Purdy, A.P.; George, C.F.; Callahan, J.H. *Inorg. Chem.* **1991**, *30*, 2812.

45. Rockwell, J.J.; Kloster, G.M.; Dubay, W.J.; Grieco, P.A.; Shriver, D.F.; Strauss, S.H. *Inorg. Chim. Acta* **1997**, *263*, 195.

46. Sun, Y.; Metz, M.V.; Stern, C.L.; Marks, T.J. *Organometallics* **2000**, *19*, 1625.

47. Xie, Z.; Bau, R.; Reed, C.A. *Angew. Chem., Int. Ed. Engl.* **1994**, *33*, 2433.

48. Schmidbaur, H.; Bublak, W.; Reide, J.; Müller, G. *Angew. Chem., Int. Ed. Engl.* **1985**, *24*, 414.

49. Alcock, N.W. *Adv. Inorg. Chem. Radiochem.* **1972**, *15*, 1.

50. Bondi, A. *J. Phys. Chem.* **1964**, *68*, 441.

51. (a) Brown, I.D.; In *Structure and Bonding in Crystals*; O'Keefe, M., Navrotsky, A., Eds.; Academic Press: New York, 1981; vol. II, ch. 14, p. 1. (b) Brown, I.D.; Altermatt, D. *Acta Cryst. B* **1985**, *41*, 244. (c) O'Keefe, M. *Structure and Bonding*; Springer-Verlag: Berlin, 1989; vol. 71, p. 161.

52. Ehlert, T.C.; Hsia, M.M. *J. Chem. Eng. Data* **1972**, *17*, 18.

53. Gorin, S.; Monniere, L.; Laforest, J. *Bull. Soc. Chim. France* **1967**, *4*, 1265.

54. (a) Barthel, J.; Wühr, Buestrich, R.; Gores, H.J. *J. Electrochem. Soc.* **1995**, *142*, 2527. (b) Barthel, J.; Buestrich, R.; Carl, E.; Gores, H.J. *J. Electrochem. Soc.* **1996**, *143*, 3565. (c) Barthel, J.; Buestrich, R.; Carl, E.; Gores, H.J. *J. Electrochem. Soc.* **1996**, *143*, 3572.

55. Barthel, J.; Buestrich, R., Gores, H.J., Schmidt, M.; Wühr, M. *J. Electrochem. Soc.* **1997**, *144*, 3866.

56. Barthel, J.; Gores, H.J.; Neueder, R.; Schmid, A. *Pure Appl. Chem.* **1999**, *71*, 1705.

57. Barthel, J.; Schmidt, M.; Gores, H.J. *J. Electrochem. Soc.* **1998**, *145*, L17.

58. Schmid, A.; Gores, H.J. *J. Electrochem. Soc.* **2000**, *147*, 21.

CHAPTER 2

A New Class of Weakly Coordinating Anions Based on Polyfluorodiolato Borates

Three of the anions discussed in the introduction, $Al(OC(C_6H_5)(CF_3)_2)_4^-$, $Nb(OCH(CF_3)_2)_6^-$, and $B(OCH(CF_3)_2)_4^-$, are examples of a new class of *WCA*s based on polyfluoroalkoxide ligands. There are many advantages to this design: a high degree of charge dispersal; a weakly basic periphery composed of mostly fluorine atoms; and a high degree of compositional flexibility due the wide array of available fluoroalcohols. Their use in applications such as Lewis-acid catalysis, late-transition-metal catalysis, and lithium batteries have been investigated, and in each case the results have been very encouraging. Analogous anions incorporating fluorinated phenoxide ligands, $Al(OC_6F_5)_4^-$, $Nb(OC_6F_5)_6^-$, and $Ta(OC_6F_5)_6^-$, were also mentioned above. This chapter describes the development of a new class of anions that *combines* aspects of each of these varieties of anion, a class based on new bifunctional ligands that have one alkoxide and one phenoxide oxygen atom. Many compounds are discussed, and each has an abbreviation; see Table 2 for definitions of these abbreviations and structures.

Experimental

Materials

Schlenk, glovebox, and high vacuum techniques were employed, with purified argon used when an inert atmosphere was required. All reagents and solvents were reagent grade or better. The compounds $AlCl_3$ (Aldrich, 99%), hexafluoroacetone

Table 2. Abbreviations, formulas, names, and structures.

abbreviation	formula/name	structure
HFIP	$-OCH(CF_3)_2$	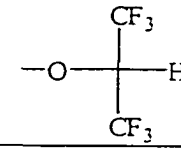
HFTB	$-OC(CH_3)(CF_3)_2$	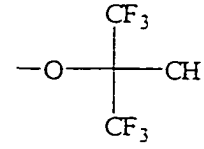
HFPP	$-OC(C_6H_5)(CF_3)_2$	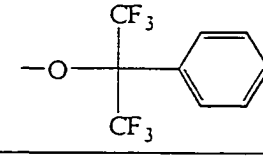
HFTP	$-OC(4\text{-}C_6H_4(CH_3))(CF_3)_2$	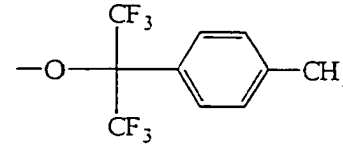
HFBuPP	$-OC(4\text{-}C_6H_4(t\text{-}Bu))(CF_3)_2$	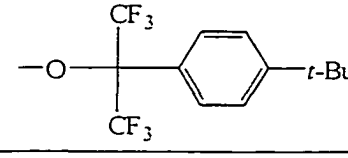
HFCP	$-OC(cyclo\text{-}C_6H_{11})(CF_3)_2$	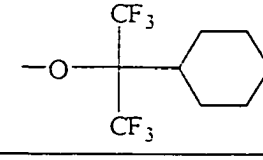
PFTB	$-OC(CF_3)_3$	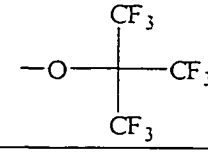
DPTE	$-OC(C_6H_5)_2(CF_3)$	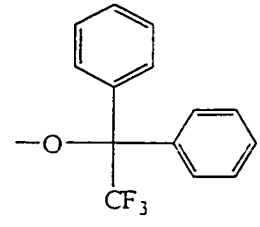

Table 2 (continued).

DCTE	$-OC(cyclo\text{-}C_6H_{11})_2(CF_3)$	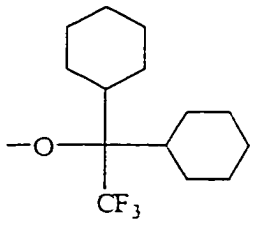
TFPE	$-OCH(C_6H_5)(CF_3)$	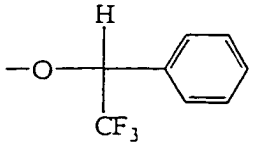
1,2-HFAB	$-OC(2\text{-}C_6H_4(OC(CF_3)_2)(CF_3)_2$	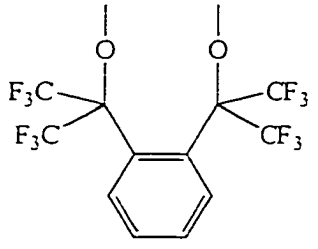
HFPOP	$-OC(2\text{-}C_6H_4O)(CF_3)_2$	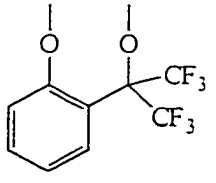
HFFPOP-2	$-OC(2\text{-}(O)\text{-}3\text{-}C_6H_3F)(CF_3)_2$	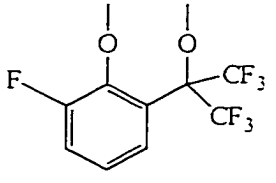

Table 2 (continued).

HFFPOP-3	–OC(2-(O)-4-C_6H_3F)$(CF_3)_2$	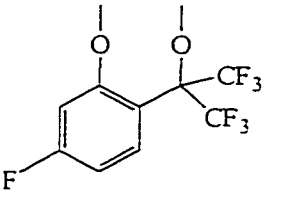
HFFPOP-4	–OC(2-(O)-5-C_6H_3F)$(CF_3)_2$	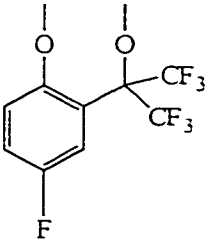
HFDPOP-2,4	–OC(2-(O)-3,5-$C_6H_2F_2$)$(CF_3)_2$	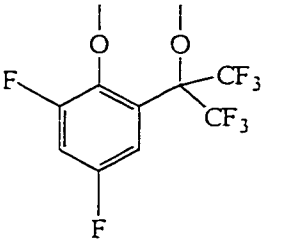
HFDPOP-3,4	–OC(2-(O)-4,5-$C_6H_2F_2$)$(CF_3)_2$	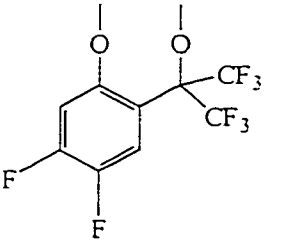
HFDPOP-3,5	–OC(2-(O)-4,6-$C_6H_2F_2$)$(CF_3)_2$	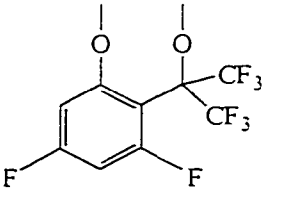

Table 2 (continued).

HFTPOP-2,3,4	–OC(2-(O)-3,4,5-C_6HF_3)$(CF_3)_2$	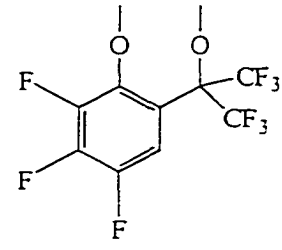
HFTPOP-3,4,5	–OC(2-(O)-4,5,6-C_6HF_3)$(CF_3)_2$	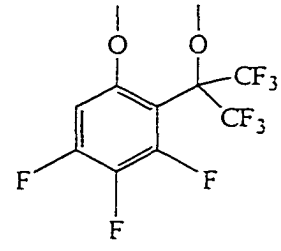
HFAPOP	–OC(2-(O)-3-*t*-Bu-5-Me-C_6H_2)$(CF_3)_2$	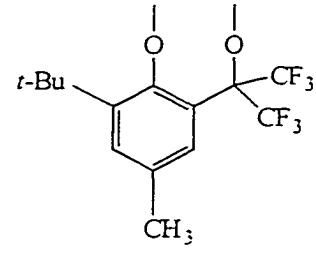
HFBPOP	–OC(2-(O)-3,5-C_6H_2(*t*-Bu)$_2$)$(CF_3)_2$	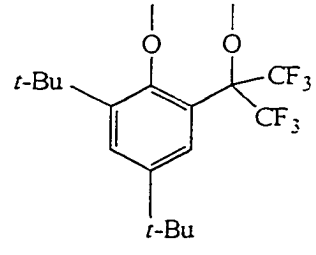
HFIPOP	–OC(2-(O)-3-C_6H_3I)$(CF_3)_2$	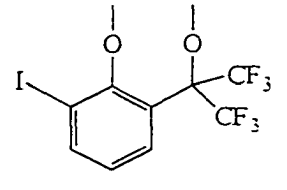

(Aldrich, 97%), 2-iodophenol (Fluorochem, 98%), phenol (Aldrich, 99+%), 2-*t*-butyl-4-methylphenol (Aldrich, 99%), 2,4-di-*t*-butylphenol (Aldrich, 99%), 2-fluorophenol (Fluorochem, 98%), 3-fluorophenol (Fluorochem, 98%), 4-fluorophenol (Fluorochem, 99%), 2,4-difluorophenol (Alfa Aesar, 98+%), 3,4-difluorophenol (Fluorochem, 99%), 3,5-difluorophenol (Fluorochem, 99%), 2,3,4-trifluorophenol (Fluorochem, 97%), 3,4,5-trifluorophenol (Fluorochem, 97%), $LiOH{\cdot}H_2O$ (Aldrich, 98%), $B(OH_3)$ (Fisher, 99%), and $MgSO_4$ (Fisher, anhydrous) were used as received. The compound 12-crown-4 (Aldrich, 98%) was dried over Na and vacuum distilled. The following solvents were purified by distillation under nitrogen or under vacuum from the indicated drying agent: 1,2-dichloroethane (Fisher, P_2O_5); 1,2-dimethoxyethane (DME, Acros, Na); acetonitrile-d_3 (Cambridge, CaH_2); benzene-d_6 (Cambridge, Na); hexafluorobenzene (Fluorochem, P_2O_5). Ethylene carbonate (EC, Mitsubishi Chem.) and dimethyl carbonate (DMC, Mitsubishi Chem.) were battery grade and used as received.

$HOC(2\text{-}C_6H_4OH)(CF_3)_2$ (H_2(HFPOP)). This synthesis is a modified version of that reported by Gilbert *et al.*[1] Phenol (6.50 g, 69.2 mmol) and $AlCl_3$ (0.0947 g, 0.692 mmol) were dissolved in 120 mL of dry 1,2-dichloroethane. After degassing this solution, hexafluoroacetone (5.74 g, 34.6 mmol), which had been measured out in a calibrated bulb using a high-vacuum (10^{-5} torr) line, was then added to the partially frozen mixture. The mixture was stirred at room temperature for 16 h, after which time the pressure had decreased by a factor of 2.3. The system volume was reduced, and the mixture stirred for an additional 14 h. The pressure continued to decrease, and the value after this time indicated that most of the hexafluoroacetone had dissolved in solution. The flask was closed, and the mixture stirred for an additional 18 h. The flask was then opened to air and 50 mL of distilled water added, resulting in the formation of a white

precipitate. After 6 h of stirring, the organic layer was isolated, and the aqueous layer washed twice with 20 mL portions of fresh 1,2-dichloroethane. The organic fractions were combined and dried over $MgSO_4$ for 4 h. Following filtration, solvent was removed using a rotary evaporator to leave a cloudy oil. This solidified upon standing, and was sublimed at 60 °C under vacuum to yield H_2(HFPOP) as a white crystalline solid (6.01 g, 67%). ^{1}H NMR (C_6D_6/C_6F_6, δ): 7.43 (s, 1 H), 7.20 (d, 1H, $J_{H\text{-}H}$ = 8.1 Hz), 6.80 (t, 1 H, $J_{H\text{-}H}$ = 7.8 Hz), 6.55 (t, 1 H, $J_{H\text{-}H}$ = 7.8 Hz), 6.13 (d, 1 H, $J_{H\text{-}H}$ = 8.1 Hz), 5.66 (s, 1 H), 5.39 (s, 1 H). ^{19}F NMR (C_6D_6/C_6F_6, δ): –75.98 (s).

HOC(2-(OH)-3-C_6H_3F)(CF_3)$_2$ (H_2(HFFPOP-2)). The compounds $AlCl_3$ (0.616 g, 4.62 mmol) and 2-fluorophenol (10.3 g, 92.3 mmol) were first dissolved in 135 mL 1,2-dichloroethane. After degassing this solution, hexafluoroacetone (15.3 g, 92.3 mmol), which had been measured out in a calibrated bulb using a high-vacuum (10^{-5} torr) line, was then added to the partially frozen mixture. The pressure decreased very slowly, and the mixture was stirred at room temperature for three weeks. Not all of the hexafluoroacetone had dissolved and/or reacted, but there was no further change in pressure after this point. Vapors from the flask were bubbled through water, and 60 mL of distilled water were added and the mixture stirred for 1 h. The organic layer was isolated, and the aqueous layer washed twice with 30 mL portions of fresh 1,2-dichloroethane. The organic fractions were combined and dried over $MgSO_4$ for 4 h. Filtering left a clear yellow solution. Solvent was removed using a rotary evaporator to leave an off-white solid. Sublimation at 60 °C under vacuum and subsequent recrystallization from hexane/$CHCl_3$ (4:1 v:v) yielded H_2(HFFPOP-2) as a white crystalline solid (9.15 g, 36%). ^{1}H NMR (C_6D_6/C_6F_6, δ): 7.12 (m, 1 H), 6.48 (m, 1 H),

6.23 (m, 1 H), 6.16 (s, 1 H), 5.53 (s, 1 H). ^{19}F NMR (C_6D_6/C_6F_6, δ): –75.35 (s, 6 F), –137.53 (m, 1 F).

HOC(2-(OH)-4-C_6H_3F)(CF_3)$_2$ (H_2(HFFPOP-3)). The compounds $AlCl_3$ (0.494 g, 3.71 mmol) and 3-fluorophenol (4.49 g, 40 mmol) were dissolved in 25 mL of 1,2-dichloroethane to make a clear, red solution. After degassing this solution, hexafluoroacetone (6.64 g, 40 mmol), which had been measured out in a calibrated bulb using a high-vacuum (10^{-5} torr) line, was then added to the partially frozen mixture. The pressure decreased rapidly, and the mixture was stirred at room temperature for 18 h. The system volume was reduced, and the mixture was stirred for an additional 18 h. The flask was then opened to air, and 20 mL of distilled water was added and stirred for 1 h. The organic layer was isolated, and the aqueous layer washed twice with 20 mL portions of fresh 1,2-dichloroethane. The organic fractions were combined and dried over $MgSO_4$ for 18 h. Filtering left a clear red solution. Solvent was removed using a rotary evaporator to leave a red solid. This was recrystallized from hexane/$CHCl_3$ (10:1 v:v) to yield red crystals. These were sublimed twice at 65 °C under vacuum to yield H_2(HFFPOP-3) as a white solid (6.95 g, 63%). ^1H NMR (C_6D_6/C_6F_6, δ): 7.15 (m, 1 H), 6.19 (m, 1 H), 6.03 (s, 1 H), 5.97 (m, 1H), 4.74 (s, 1H); ^{19}F NMR (C_6D_6/C_6F_6, δ): –75.65 (s, 6 F), –108.65 (m, 1 F).

HOC(2-(OH)-5-C_6H_3F)(CF_3)$_2$ (H_2(HFFPOP-4)). The compounds $AlCl_3$ (0.616 g, 4.62 mmol) and 4-fluorophenol (4.43 g, 39.6 mmol) were dissolved in 100 mL of dry 1,2-dichloroethane to make a clear, orange solution. After degassing this solution, hexafluoroacetone (15.3 g, 92.3 mmol), which had been measured out in a calibrated bulb using a high-vacuum (10^{-5} torr) line, was then added to the partially frozen mixture. The pressure decreased slowly, and the mixture was stirred at room temperature for two days.

The system volume was reduced, and the mixture was stirred for an additional 18 h. The flask was then closed, and the mixture stirred for 18 h. The flask was then opened to air, and 50 mL of distilled water was added and stirred for 1 h. The organic layer was isolated, and the aqueous layer washed twice with 30 mL portions of fresh 1,2-dichloroethane. The organic fractions were combined and dried over $MgSO_4$ for 4 h. Filtering left a clear yellow solution. Solvent was removed using a rotary evaporator to leave a yellow solid. Sublimation at 55 °C under vacuum and subsequent recrystallization from hexane/$CHCl_3$ (5:1 v:v) yielded H_2(HFFPOP-4) as a white cotton-like solid (6.00 g, 54%). ^{1}H NMR (C_6D_6/C_6F_6, δ): 7.31 (m, 1 H), 6.46 (m, 1 H), 5.93 (m, 1 H), 5.57 (s, 1 H), 5.48 (s, 1 H). ^{19}F NMR (C_6D_6/C_6F_6, δ): –75.51 (s, 6 F), –120.74 (m, 1 F).

HOC(2-(OH)-3,5-$C_6H_2F_2$)(CF_3)$_2$ (H_2(HFDPOP-2,4)). The compounds $AlCl_3$ (0.383 g, 2.87 mmol) and 2,4-difluorophenol (7.47 g, 57.5 mmol) were dissolved in 125 of mL 1,2-dichloroethane to make a clear, deep amber solution. After degassing this solution, hexafluoroacetone (6.39 g, 38.5 mmol), which had been measured out in a calibrated bulb using a high-vacuum (10^{-5} torr) line, was then added to the partially frozen mixture. The pressure decreased rapidly, and the mixture was stirred at room temperature for 18 h, after which time the system volume was reduced and the mixture stirred for an additional 18 h. The flask was then closed, and the mixture stirred for 18 h. After this time, the flask was opened to air and 50 mL of distilled water was added and stirred for 2 h. The organic layer was isolated, and the aqueous layer washed twice with 30 mL portions of fresh 1,2-dichloroethane. The organic fractions were combined and dried over $MgSO_4$ for 4 h. After filtering, solvent was removed using a rotary evaporator to leave a yellow solid. Sublimation at 70 °C under vacuum yielded H_2(HFDPOP-2,4) as

a white crystalline solid (8.04 g, 47%). ^{1}H NMR (C_6D_6/C_6F_6, δ): 7.04 (m, 1 H), 6.18 (m, 1 H), 5.75 (s, 1 H), 5.03 (s, 1H). ^{19}F NMR (C_6D_6/C_6F_6, δ): –75.43 (s, 6 F), –117.39 (m, 1 F), –132.22 (m, 1 F).

HOC(2-(OH)-4,5-$C_6H_2F_2$)(CF_3)$_2$ (H_2(HFDPOP-3,4)). The compounds 3,4-difluorophenol (5.00 g, 38.5 mmol) and $AlCl_3$ (0.341 g, 2.60 mmol) were dissolved in 40 mL of 1,2-dichloroethane to make a clear, pink solution. After degassing this solution, hexafluoroacetone (6.39 g, 38.5 mmol), which had been measured out in a calibrated bulb using a high-vacuum (10^{-5} torr) line, was then added to the partially frozen mixture. The pressure decreased slowly, and the mixture was stirred at room temperature for two days, after which time the system volume was reduced and the mixture stirred for an additional 18 h. The flask was then closed, and the mixture stirred for 18 h. After this time, the flask was opened to air and 30 mL of distilled water was added and stirred for 2 h. The organic layer was isolated, and the aqueous layer washed twice with 30 mL portions of fresh 1,2-dichloroethane. The organic fractions were combined and dried over $MgSO_4$ for 4 h. After filtering, solvent was removed using a rotary evaporator to leave a pink solid. Recrystallization from hexane/$CHCl_3$ (5:1 v:v) yielded H_2(HFDPOP-3,4) as a slightly pink crystalline solid (7.07 g, 62%). ^{1}H NMR (C_6D_6/C_6F_6, δ): 7.16 (m, 1 H), 5.90 (s, 1 H), 5.85 (m, 1 H), 4.82 (s, 1 H). ^{19}F NMR (C_6D_6/C_6F_6, δ): –75.76 (s, 6 F), –131.33 (m, 1 F), –145.05 (m, 1 F).

HOC(2-(OH)-4,6-$C_6H_2F_2$)(CF_3)$_2$ (H_2(HFDPOP-3,5)). The compounds 3,5-difluorophenol (5.05 g, 38.9 mmol) and $AlCl_3$ (0.260 g, 1.94 mmol) were dissolved in 40 mL 1,2-dichloroethane to make a clear, tan suspension. After degassing this solution, hexafluoroacetone (6.45 g, 38.9 mmol), which had been measured out in a calibrated bulb using a high-vacuum (10^{-5} torr) line, was then added to the partially frozen mixture. The

pressure decreased rapidly, and the mixture was stirred at room temperature for 18 h. The flask was then closed, and the mixture stirred for an additional 18 h. After this time, the flask was opened to air and 30 mL of distilled water was added and stirred for 1 h. The organic layer was isolated, and the aqueous layer washed twice with 30 mL portions of fresh 1,2-dichloroethane. The organic fractions were combined and dried over $MgSO_4$ for 4 h. After filtering, solvent was removed using a rotary evaporator to leave an off-white solid. Recrystallization from hexane/$CHCl_3$ (4:1 v:v) yielded H_2(HFDPOP-3,5) as a white crystalline solid (7.68 g, 67%). ^1H NMR (C_6D_6/C_6F_6, δ): 7.71 (s, 1H), 6.09 (m, 1 H), 5.92 (m, 1 H), 3.87 (s, 1H). ^{19}F NMR (C_6D_6/C_6F_6, δ): –75.76 (m, 6 F), –102.81 (m, 1 F), –105.60 (m, 1 F).

HOC(2-(OH)-3,4,5-C_6HF_3)(CF_3)$_2$ (H_2(HFTPOP-2,3,4)). The compounds 2,3,4-trifluorophenol (4.81 g, 32.5 mmol) and $AlCl_3$ (0.217 g, 1.63 mmol) were dissolved in 100 mL dry 1,2-dichloroethane to make a clear, yellow solution. After degassing this solution, hexafluoroacetone (5.40 g, 32.5 mmol), which had been measured out in a calibrated bulb using a high-vacuum (10^{-5} torr) line, was then added to the partially frozen mixture. The mixture was stirred for 11 h at room temperature, after which time the pressure had decreased by a factor of 0.4. At this point the system volume was reduced, and the mixture stirred for an additional 24 h. The pressure continued to decrease, and after this time the flask was closed, and the mixture stirred for an additional 18 h. The flask was then opened to air, and 100 mL of distilled water added and stirred for 1 h. The organic layer was isolated, and the aqueous layer washed twice with 30 mL portions of fresh 1,2-dichloroethane. The organic fractions were combined and dried over $MgSO_4$ for 4 h. After filtering, solvent was removed using a rotary evaporator to leave an off-white solid. Sublimation at 65 °C under vacuum yielded H_2(HFTPOP-2,3,4)

as a white crystalline solid (7.01 g, 69%). ^{1}H NMR (C_6D_6/C_6F_6, δ): 6.94 (t, 1 H, J_{H-F} = 9.52 Hz), 5.46 (s, 1 H), 4.85 (s, 1 H). ^{19}F NMR (C_6D_6/C_6F_6, δ): –75.75 (m, 6 F), –142.40 (m, 1 F), –153.50 (m, 1 H), –154.30 (m, 1 F).

HOC(2-(OH)-4,5,6-C_6HF_3)(CF_3)$_2$ (H_2(HFTPOP-3,4,5)). The compounds 3,4,5-trifluorophenol (3.25 g, 21.9 mmol) and $AlCl_3$ (0.211 g, 1.60 mmol) were dissolved in 40 mL of 1,2-dichloroethane to make a clear, yellow solution. After degassing this solution, hexafluoroacetone (6.45 g, 38.9 mmol), which had been measured out in a calibrated bulb using a high-vacuum (10^{-5} torr) line, was then added to the partially frozen mixture. The pressure decreased rapidly, and the mixture was stirred for 18 h at room temperature. The system volume was then reduced, and the mixture stirred for an additional 18 h. After this time, the flask was closed and the mixture stirred for two days. The flask was then opened to air, and 30 mL of distilled water was added stirred for 2 h. The organic layer was isolated, and the aqueous layer washed twice with 30 mL portions of fresh 1,2-dichloroethane. The organic fractions were combined and dried over $MgSO_4$ for 4 h. After filtering, solvent was removed from the filtrate using a rotary evaporator to leave an off-white solid. Recrystallization from hexane/$CHCl_3$ (5:1 v:v) yielded H_2(HFTPOP-3,4,5) as a white crystalline solid (4.02 g, 59%). ^{1}H NMR (C_6D_6/C_6F_6, δ): 7.36 (s, 1 H), 5.88 (m, 1 H), 4.00 (s, 1 H). ^{19}F NMR (C_6D_6/C_6F_6, δ): –75.71 (m, 6 F), –128.64 (m, 1 F), –129.07 (m, 1 H), –169.09 (m, 1 F).

HOC(2-(OH)-3-*t*-Bu-5-Me-C_6H_2)(CF_3)$_2$ (H_2(HFAPOP)). The compounds 2-*t*-butyl-4-methylphenol (4.63 g, 28.3 mmol) and $AlCl_3$ (0.152 g, 1.14 mmol) were dissolved in 120 mL of dry 1,2-dichloroethane to make clear red solution. After degassing this solution, hexafluoroacetone (5.74 g, 34.6 mmol), which had been measured in a calibrated bulb using a high-vacuum (10^{-5} torr) line, was then added to the

partially frozen mixture. The mixture was stirred for 11 h at room temperature, after which time the pressure had decreased by a factor of 0.4. After stirring at room temperature for 12 h, the system volume was reduced, and after an additional 9 h was reduced again to just the flask. The mixture was stirred for 18 h, and then the flask was opened to air and 50 mL of distilled H_2O added, resulting in the formation of a white precipitate. After 2 h of stirring, the organic layer was isolated, and the aqueous layer washed twice with 20 mL portions of fresh 1,2-dichlorethane. Solvent was removed using a rotary evaporator to leave a cloudy oil, which solidified upon standing. This was sublimed at 60 °C under vacuum to yield H_2(HFAPOP) as a white crystalline solid (5.94 g, 64%). ^{1}H NMR (C_6D_6/C_6F_6, δ): 8.07 (s, 1 H), 7.20 (s, 1H), 7.12 (m, 1 H), 3.84 (s, 1 H), 2.00 (s, 3 H), 1.42 (s, 9 H). ^{19}F NMR (C_6D_6/C_6F_6, δ): –75.60 (s).

HOC(2-(OH)-3,5-C_6H_2(*t*-Bu)$_2$)(CF_3)$_2$ (H_2(HFBPOP)). The compounds 2,4-di-*t*-butylphenol (6.45 g, 31.3 mmol) and $AlCl_3$ (0.325 g, 2.4 mmol) were dissolved in 100 mL of 1,2-dichloroethane. After degassing this solution, hexafluoroacetone (5.20 g, 31.3 mmol), which had been measured out in a calibrated bulb using a high-vacuum (10^{-5} torr) line, was added to the partially frozen mixture. The pressure decreased at a moderate rate, and the mixture was stirred at room temperature for 18 h. After this time, the system volume was reduced, and stirring continued for an additional 18 h. The volume was then reduced to just the flask, and the mixture stirred for 18 h. After this time, 50 mL of distilled water was added. The organic layer was isolated, and the aqueous layer washed twice with 20 mL portions of fresh 1,2-dichloroethane. Volatiles were removed from the combined fractions to yield an off-white solid. This was recrystallized from hexane, and then sublimed under vacuum at 60 °C to yield H_2(HFBPOP) as a white solid (2.50 g, 21%), with a small amount (~3% based on ^{19}F

NMR signal intensity) of an unknown impurity. ^{1}H NMR (C_6D_6, δ): 8.07 (s, 1 H), 7.52 (s, 1 H), 7.49 (s, 1 H), 3.77 (s, 1 H), 1.45 (s, 9 H), 1.19 (s, 9 H). ^{19}F NMR (C_6D_6, δ): –78.19 (s).

HOC(2-(OH)-3-C_6H_3I)(CF_3)$_2$ (H_2(HFIPOP)). The compounds 2-iodophenol (3.11 g, 14.2 mmol) and $AlCl_3$ (0.095 g, 0.71 mmol) were dissolved in 45 mL 1,2-dichloroethane. After degassing this solution, hexafluoroacetone (2.35 g, 14.2 mmol), which had been measured out in a calibrated bulb using a high-vacuum (10^{-5} torr) line, was added to the partially frozen mixture. The mixture was stirred for 15 h at room temperature, after which time the pressure had decreased by a factor of 0.2. The system volume was reduced, and stirring continued for 12 h. The volume was then reduced to just the flask, and mixture was stirred for 18 h. The flask was then opened to air, and 50 mL of distilled water was added. The organic layer was isolated, and the aqueous layer washed twice with 20 mL portions of fresh 1,2-dichloroethane. This was distilled at 100 °C under vacuum to yield a clear colorless oil. Residual impurities were distilled away from the desired product at 80 °C under vacuum to yield H_2(HFIPOP) as a clear colorless oil (2.71 g, 50%). ^{1}H NMR (C_6D_6/C_6F_6, δ): 7.31 (d, J_{H-H} = 9 Hz, 1 H), 7.18 (d, J_{H-H} = 9 Hz, 1 H), 6.05 (t, J_{H-H} = 9 Hz, 1 H). ^{19}F NMR (C_6D_6/C_6F_6, δ): –75.56 (s).

LiB(HFPOP)$_2$. The compounds $LiOH·H_2O$ (0.813 g, 19.4 mmol) and $B(OH)_3$ (1.20 g, 19.4 mmol) were dissolved in 200 mL of distilled water and stirred at reflux for 2 h. H_2(HFPOP) (10.1 g, 38.7 mmol) was then added as a solution in acetonitrile (20 mL). This mixture was stirred at reflux for 20 h, after which time it was clear and colorless. Water and acetonitrile were removed using a rotary evaporator to leave a white solid. This was heated under high-vacuum conditions (10^{-5} torr) in two stages: 100 °C for 18 h, and 130 °C for 18 h. LiB(HFPOP)$_2$ was isolated as a white powder (9.83 g, 95%). ^{1}H

NMR (CD_3CN, δ): 7.38 (m, 2 H), 7.25 (t, 1 H, J_{H-H} = 7.8 Hz), 6.80 (t, 1 H, J_{H-H} = 7.8 Hz), 6.70 (d, 1 H, J_{H-H} = 8.4 Hz); ^{19}F NMR (CD_3CN, δ): –75.26 (s). Low-resolution mass spectrum ((–)ES-MS, CH_3CN solution) *m/z* 527.1 [$(M - Li)^-$; calcd for $C_{18}H_8BF_{12}O_4$ 527.0].

LiB(HFFPOP-2)$_2$. The compounds $LiOH·H_2O$ (0.220 g, 5.25 mmol) and $B(OH)_3$ (0.324 g, 5.25 mmol) were dissolved in 110 mL of distilled water and stirred at reflux for 6 h. H_2(HFFPOP-2) (2.92 g, 10.5 mmol) was then added as a solution in acetonitrile (20 mL). This mixture was stirred at reflux for 20 h, after which time it was clear and colorless. Water and acetonitrile were removed using a rotary evaporator to leave a white solid. This was heated under high-vacuum conditions (10^{-5} torr) in three stages: 100 °C for 18 h, 120 °C for 18 h, and 140 °C for 18 h. LiB(HFFPOP-2)$_2$ was isolated as a white powder (2.75 g, 92%). ^1H NMR (CD_3CN, δ): 7.26 (m, 2 H), 7.18 (m, 2 H), 6.83 (m, 2 H). ^{19}F NMR (CD_3CN, δ): –75.42 (s, 12 F), –136.94 (m, 2 F). Low-resolution mass spectrum ((-)ES-MS, CH_3CN solution) *m/z* 563.1 [$(M - Li)^-$; calcd for $C_{18}H_6BF_{14}O_4$ 563.0].

LiB(HFFPOP-3)$_2$. The compounds $LiOH·H_2O$ (0.282 g, 6.71 mmol) and $B(OH)_3$ (0.415 g, 6.71 mmol) were dissolved in 110 mL of distilled water and stirred at reflux for 6 h. H_2(HFFPOP-3) (3.73 g, 13.4 mmol) was then added as a solution in acetonitrile (25 mL). This mixture was stirred at reflux for 20 h, after which time it was clear and colorless. Water and acetonitrile were removed using a rotary evaporator to leave a clear colorless oil. This was placed under vacuum overnight, and then heated under high-vacuum conditions (10^{-5} torr) in three stages: 100 °C for 18 h, and 130 °C for 48 h. LiB(HFFPOP-3)$_2$ was isolated as a white powder (3.62 g, 95%). ^1H NMR (CD_3CN, δ): 7.43 (t, 2 H), 6.63 (t, 2 H), 6.51 (t, 2 H). ^{19}F NMR (CD_3CN, δ): –75.60 (s,

12 F), –111.61 (m, 2 F). Low-resolution mass spectrum ((-)ES-MS, CH_3CN solution) *m/z* 563.1 [$(M - Li)^-$; calcd for $C_{18}H_6BF_{14}O_4$ 563.0].

LiB(HFFPOP-4)$_2$. The compounds $LiOH{\cdot}H_2O$ (0.206 g, 4.9 mmol) and $B(OH)_3$ (0.303 g, 4.9 mmol) were dissolved in 100 mL of distilled water and stirred at reflux for 6 h. H_2(HFFPOP-4) (2.73 g, 9.8 mmol) was then added as a solution in acetonitrile (20 mL). This mixture was stirred at reflux for 18 h, after which time it was clear and colorless. Water and acetonitrile were removed using a rotary evaporator to leave a clear colorless oil. Initial drying was accomplished by azeotropic distillation with toluene, followed by heating under high-vacuum conditions (10^{-5} torr) in two stages: at 100 °C for 18 h, then at 138 °C for four days. LiB(HFFPOP-4)$_2$ was isolated as a white powder (2.56 g, 92%). ^1H NMR (CD_3CN, δ): 7.18 (m, 2 H), 7.09 (m, 2 H), 6.75 (m, 2 H). ^{19}F NMR (CD_3CN, δ): –75.46 (s, 12 F), –126.38 (m, 2 F). Low-resolution mass spectrum ((-)ES-MS, CH_3CN solution) *m/z* 563.1 [$(M - Li)^-$; calcd for $C_{18}H_6BF_{14}O_4$ 563.0].

LiB(HFDPOP-2,4)$_2$. The compounds $LiOH{\cdot}H_2O$ (0.156 g, 3.72 mmol) and $B(OH)_3$ (0.230 g, 3.72 mmol) were dissolved in 110 mL of distilled water and stirred at reflux for 6 h. H_2(HFDPOP-2,4) (2.20 g, 7.43 mmol) was then added as a solution in acetonitrile (15 mL). This mixture was stirred at reflux for 36 h, after which time it was clear and colorless. Water and acetonitrile were removed using a rotary evaporator to leave a clear colorless oil. Initial drying was accomplished by azeotropic distillation with toluene. The resulting white solid was then heated under high-vacuum conditions (10^{-5} torr) in three stages: 90 °C for 18 h, 132 °C for 18 h, and 152 °C for 18 h. LiB(HFDPOP-2,4)$_2$ was isolated as a white powder (1.96 g, 87%). ^1H NMR (CD_3CN, δ): 7.07 (m, 4 H). ^{19}F NMR (CD_3CN, δ): –75.52 (s, 12 F), –124.04 (m, 2 F), –132.50 (m, 2F). Low-

resolution mass spectrum ((-)ES-MS, CH_3CN solution) *m/z* 599.0 [$(M - Li)^-$; calcd for $C_{18}H_4BF_{16}O_4$ 599.0].

LiB(HFDPOP-3,4)$_2$. The compounds $LiOH \cdot H_2O$ (0.356 g, 8.48 mmol) and $B(OH)_3$ (0.524 g, 8.48 mmol) were dissolved in 110 mL of distilled water and stirred at reflux for 6 h. H_2(HFDPOP-3,4) (5.02 g, 17.0 mmol) was then added as a solution in acetonitrile (25 mL). This mixture was stirred at reflux for 20 h, after which time it was clear and colorless. Water and acetonitrile were removed using a rotary evaporator to leave a clear colorless oil. Initial drying was accomplished by azeotropic distillation with toluene. The resulting white solid was then heated under high-vacuum conditions (10^{-5} torr) in two stages: 90 °C for 18 h, and 145 °C for 48 h. LiB(HFDPOP-3,4)$_2$ was isolated as an off-white powder (4.40 g, 86%). ^1H NMR (CD_3CN, δ): 7.33 (m, 2 H), 6.68 (m, 2 H). ^{19}F NMR (CD_3CN, δ): –75.72 (s, 12 F), –135.39 (m, 2 F), –151.07 (m, 2 F). Low-resolution mass spectrum ((-)ES-MS, CH_3CN solution) *m/z* 599.0 [$(M - Li)^-$; calcd for $C_{18}H_4BF_{16}O_4$ 599.0].

LiB(HFDPOP-3,5)$_2$. The compounds $LiOH \cdot H_2O$ (0.287 g, 6.82 mmol) and $B(OH)_3$ (0.422 g, 6.82 mmol) were dissolved in 110 mL of distilled water and stirred at reflux for 6 h. H_2(HFDPOP-3,5) (4.04 g, 13.6 mmol) was then added as a solution in acetonitrile (20 mL). This mixture was stirred at reflux for 20 h, after which time it was clear and colorless. Water and acetonitrile were removed using a rotary evaporator to leave a clear colorless oil. Initial drying was accomplished by azeotropic distillation with toluene. The resulting white solid was then heated under high-vacuum conditions (10^{-5} torr) in two stages: 90 °C for 18 h, and at 135 °C for 48 h. LiB(HFDPOP-3,5)$_2$ was isolated as a white powder (3.67 g, 89%). ^1H NMR (CD_3CN, δ): 6.48 (m, 2 H), 6.40 (m, 2 H). ^{19}F NMR (CD_3CN, δ): –75.18 (m, 12 F), –105.27 (m, 2 F), –109.31 (m, 2 F).

Low-resolution mass spectrum ((-)ES-MS, CH_3CN solution) *m/z* 599.1 [$(M - Li)^-$; calcd for $C_{18}H_4BF_{16}O_4$ 599.0].

LiB(HFTPOP-2,3,4)$_2$. The compounds $LiOH{\cdot}H_2O$ (0.156 g, 3.72 mmol) and $B(OH)_3$ (0.230 g, 3.72 mmol) were dissolved in 110 mL of distilled water and stirred at reflux for 5 h. H_2(HFTPOP-2,3,4) (2.45 g, 7.43 mmol) was then added as a solid, as well 15 mL diethyl ether. This mixture was stirred at reflux for 20 h, after which time it was clear and colorless. Water and ether were removed using a rotary evaporator to leave a clear colorless oil. Initial drying was accomplished using azeotropic distillation with toluene. The resulting oil was then heated under high-vacuum conditions (10^{-5} torr) in two stages: first at 100 °C for 18 h; then at 150 °C for an additional 48 h. LiB(HFTPOP-2,3,4)$_2$ was isolated as a white powder (2.07 g, 87%). ^1H NMR (CD_3CN, δ): 7.16 (m, 2 H). ^{19}F NMR (CD_3CN, δ): –75.69 (s, 12 F), –149.11 (m, 2 F), –157.77 (m, 4 F), –173.02. Low-resolution mass spectrum ((-)ES-MS, CH_3CN solution) *m/z* 634.8 [$(M - Li)^-$; calcd for $C_{18}H_2BF_{18}O_4$ 635.0].

LiB(HFTPOP-3,4,5)$_2$. The compounds $LiOH{\cdot}H_2O$ (0.267 g, 6.36 mmol) and $B(OH)_3$ (0.393 g, 6.36 mmol) were dissolved in 110 mL of distilled water and stirred at reflux for 6 h. H_2(HFTPOP-3,4,5) (4.00 g, 12.7 mmol) was then added as a solution in acetonitrile (20 mL). This mixture was stirred at reflux for 20 h, after which time it was clear and colorless. Water and acetonitrile were removed using a rotary evaporator to leave a clear colorless oil. Initial drying was accomplished by azeotropic distillation with toluene. The resulting oil was then heated under high-vacuum conditions (10^{-5} torr) in two stages: 100 °C for 48 h, and 143 °C for 96 h. LiB(HFTPOP-3,4,5)$_2$ was isolated as a white powder (3.63 g, 89%). ^1H NMR (CD_3CN, δ): 6.64 (m). ^{19}F NMR (CD_3CN, δ): –75.30 (m, 12 F), –131.35 (m, 2 F), –133.72 (m, 2 F), –174.13 (m, 2 F). Low-resolution

mass spectrum ((-)ES-MS, CH_3CN solution) *m/z* 634.9 [(M – Li)$^-$; calcd for $C_{18}H_2BF_{18}O_4$ 635.0].

LiB(HFAPOP)$_2$. The compounds $LiOH{\cdot}H_2O$ (0.152 g, 3.62 mmol) and $B(OH)_3$ (0.224 g, 3.62 mmol) were dissolved in 115 mL of distilled water and stirred at reflux for 18 h. H_2(HFAPOP) (2.51 g, 7.61 mmol) was then added as a solution in diethyl ether (15 mL). This mixture was stirred at reflux for 18 h, after which time it was clear and colorless. Water and ether were removed using a rotary evaporator to leave a clear colorless oil. This was heated under high-vacuum conditions (10^{-5} torr) at 105 °C for six days. LiB(HFAPOP)$_2$ was isolated as a white powder (1.97 g, 82%). ^{1}H NMR (C_6D_6/C_6F_6, δ): 7.37 (s, 2 H), 7.13 (m, 2 H), 2.07 (s, 6 H), 1.27 (s, 18 H). ^{19}F NMR (C_6D_6/C_6F_6, δ): –72.80 (m, 6 F), –76.44 (m, 6 F). Low-resolution mass spectrum ((-)ES-MS, CH_3CN solution) *m/z* 667.0 [(M – Li)$^-$; calcd for $C_{28}H_{28}BF_{12}O_4$ 667.0].

LiB(HFBPOP)$_2$. Them compounds $LiOH{\cdot}H_2O$ (0.141 g, 3.35 mmol) and $B(OH)_3$ (0.207 g, 3.35 mmol) were dissolved in 110 mL of distilled water and stirred at reflux for 6 h. H_2(HFBPOP) (2.49 g, 6.7 mmol) was then added as a solution in acetonitrile (35 mL), and the mixture stirred at reflux for 22 h. After this time, volatiles were removed by heating the solution in air (use of a rotary evaporator led to excessive foaming), and placing the resulting oil under vacuum for 18 h. The white solid was recrystallized from dichloromethane at –22 °C, and dried under high-vacuum conditions (10^{-5} torr) at 100 °C for two days to yield LiB(HFBPOP)$_2$ as a yellow solid (0.432 g, 17%). ^{1}H NMR (CD_3CN, δ): 7.35 (s, 2 H), 7.30 (s, 2 H), 1.324 (s, 18 H), 1.320 (s, 18 H). ^{19}F NMR (CD_3CN, δ): –74.56 (m, 6 F), –75.44 (m, 6 F). Low-resolution mass spectrum ((-)ES-MS, CH_3CN solution) *m/z* 751.4 [(M – Li)$^-$; calcd for $C_{34}H_{40}BF_{12}O_4$ 751.0].

$LiB(HFIPOP)_2$. The compounds $LiOH{\cdot}H_2O$ (0.100 g, 2.39 mmol) and $B(OH)_3$ (0.148 g, 2.39 mmol) were dissolved in 115 mL of distilled water and stirred at reflux for 2 h. H_2(HFIPOP) (1.99 g, 5.15 mmol) was then added as a solution in diethyl ether (20 mL). This mixture was stirred at reflux for 18 h, after which time it was clear and colorless. Water and acetonitrile were removed using a rotary evaporator to leave a clear colorless oil. Initial drying was accomplished by azeotropic distillation with toluene. The resulting white solid was then heated under high-vacuum conditions (10^{-5} torr) in three stages: 143 °C for 48 h, 150 °C for 48 h, and 170 °C for 18 h. During this time the solid turned purple. $LiB(HFIPOP)_2$ was isolated as a purple powder (1.20 g, 64%). ^1H NMR (CD_3CN, δ): 7.16 (m, 2 H), 7.08 (m, 2 H), 6.75 (m, 1 H). ^{19}F NMR (CD_3CN, δ): –74.56 (m, 6 F), –75.44 (m, 6 F). Low-resolution mass spectrum ((-)ES-MS, CH_3CN solution) *m/z* 778.0 [$(M - Li)^-$; calcd for $C_{18}H_6BF_{12}I_2O_4$ 779.0].

Physical Measurements

Samples for NMR spectroscopy were solutions in 5-mm glass tubes, equipped with a teflon seal when protection from air was necessary. NMR spectra were recorded on a Varian 300 spectrometer operating at the indicated frequencies: ^1H, 300.1 MHz; ^{19}F, 282.4 MHz. Chemical shifts (δ scale) are relative to $SiMe_4$ (δ = 0 for ^1H NMR) and $CFCl_3$ (δ = 0 for ^{19}F NMR). Negative-ion electrospray mass spectra ((-)ES-MS) were recorded on a Fisons VG Quattro-SQ mass spectrometer. Solution conductances were measured at 24±1 °C using a YSI Model 3403 conductivity cell calibrated for inverted use (k = 0.9988 cm^{-1}) and a YSI Model 32 conductivity bridge. The bridge was operated

at 1 KHz (conductances > 100 μS) or at line frequency (50–60 Hz, conductances <100 μS). Measurements made using both modes were the same, but a sharper null point is observed at 1 KHz for higher conductances, and at line frequency for lower conductances. All samples were anhydrous as determined by ^{1}H NMR spectroscopy, and solutions of these were prepared in volumetric flasks in the glovebox. The error in measurement was determined to be < 1% using the same batch of material. Variation from one batch to another was found to be 2% or less. Cyclic voltammetry and chronoamperometry were performed using an EG&G Model 263 potentiostat. Experiments were performed in a glass cell in a Helium-filled glovebox at 24±1 °C. Platinum (0.02 cm^2) and stainless steel (0.48 cm^2) electrodes were polished with alumina, rinsed and sonicated with water, and dried before each use. Counter electrodes were platinum mesh and lithium foil. Reference electrodes were lithium foil (Aldrich, 99.9%). Aluminum electrodes (Strem, 99.997%, 2 cm^2) were cleaned and dried before use. All cyclic voltammetry experiments were performed at a scan rate of 10 mV s^{-1}.

Crystals of $LiB(HFTPOP\text{-}2,3,4)_2$ were grown by sublimation at 180 °C under vacuum. Crystals of $Li_2(DME)(B(HFPOP)_2)_2$ were grown at room temperature from a solution of $LiB(HFPOP)_2$ in CH_2Cl_2/DME (20:1 v:v). In each case, a suitable crystal was examined under an argon atmosphere and placed in the cold nitrogen stream of the low-temperature LT-2 unit of a Siemens SMART CCD diffractometer system. The diffraction data collection and subsequent structural computations were performed using the crystallographic software supplied by Siemens[2] or by Professor G.M. Sheldrick.[3] Lorentz and polarization corrections were applied to the data. Details of the crystallographic experiment and subsequent computations are summarized in Tables A.1 ($Li_2(DME)(B(HFPOP)_2)_2$) and A.2 ($Li(OC(CH_3)B(HFTPOP\text{-}2,3,4)_2$), and can be found

in the appendix.[4,5] The structures were solved by direct methods and were refined using full-matrix least-squares procedures on F^2 for all data. Non-hydrogen atoms were refined anisotropically. Hydrogen atoms were placed in calculated positions.

Results and Discussion

Synthesis of $HOC(ROH)(CF_3)_2$ and $LiB(O_2L_f)_2$ Compounds

The compound H_2(HFPOP) and its derivatives were chosen for study as an extension of previous work with fluoroalkoxyaluminates and -borates.[6,7] As mentioned above, these anions were found to be excellent *WCA*s, and most were comprised of fluoroalkoxide ligands with the general formula $-OCR(CF_3)_2$. However, one problem was a lack of hydrolytic stability; the E–O (E = B, Al) bonds in $ME(OR_f)_4$ ($M = Tl^+, Li^+$) are readily hydrolyzed in the presence of water. H_2(HFPOP) is derived from the same $-OCR(CF_3)_2$ formula, but with R being a phenoxy moiety; it was hoped that the combination of this strong donor and the chelate effect would result in hydrolytically-stable complexes. In related work, Barthel and Gores reported that lithium borates containing two catecholate or substituted catecholate ligands possessed this property.[8] They also explored the use of other diolate donor ligands listed in the introduction, and in each case, the lithium borate derived from these ligands exhibited hydrolytic stability. This turned out to be true when HFPOP and its derivatives were used as well, but only when boron was used as the central atom. Complexes formed with aluminum were *not* stable in water.[9] This may be due to the weaker Al–O (122(2) kcal/mol) bond strength compared to that of an average B–O bond (193(5) kcal/mol).[10]

With the exception of H_2(HFPOP), H_2(HFBPOP),[11] and H_2(HFFPOP-3),[12] all of the diols described in the experimental section are new, and are listed in Table 2 along with their abbreviations. The synthetic method is very similar to that developed by

Gilbert *et al.*,[1] which consists of mixing a phenol with hexafluoroacetone in the presence of a catalyst (5 mol% based on phenol), using xylene as the solvent. In his work, three catalysts were studied: $AlCl_3$, BF_3, and *p*-toluenesulfonic acid. It was found that the regiochemistry of the reaction depended on the nature of the catalyst: using BF_3 yielded primarily *para*-substituted phenols, while $AlCl_3$ and *p*-toluenesulfonic acid generally produced *ortho*-substituted products. The desired ligands for this work are the *ortho* isomers, as they form a stable six-membered chelate ring with a central atom such as boron. Of the two catalysts that give rise to these forms, it was found that $AlCl_3$ catalysis resulted in a higher yield of substituted phenol, and required less time to do so. As such, this catalyst was chosen to synthesize the new diols. The amount used was generally the same (5% based on phenol) as that used by Gilbert, but in some cases a slightly higher percentage was added to decrease the required reaction time. The only other modification on the original procedure was the solvent: 1,2-dichloroethane was used instead of xylene. Xylene has been shown to react with hexafluoroacetone in the presence of $AlCl_3$,[13] creating the possibility for an undesired side reaction to occur when this is used as the solvent.

The synthesis of the new lithium borates was based on the procedure developed by Barthel *et al.* used to synthesize other lithium borates with chelating diolate ligands.[8] One change was the addition of a small amount of acetonitrile to the reaction mixture. The diols are somewhat volatile and not highly soluble in water. It was observed that in the early stages of the reaction, the diol would sublime and collect in the condenser. Acetonitrile was added to continually wash the condenser over the course of the reaction; the diols are highly soluble in this solvent, even at low temperature, and thus did not become sequestered on the condenser walls. Another modification was the order of

addition of the reactants. For $LiB(HFPOP)_2$ and $LiB(HFAPOP)_2$, all reagents can be added simultaneously and the reaction proceeds smoothly. However, when fluorine atoms are added to the ring, using the same procedure yielded a product mixture that contains primarily $LiH(O_2L_f)$, with only a small amount of $LiB(O_2L_f)_2$. This most likely stems from the increased acidity of the fluorinated diols vs. the non-fluorinated varieties. A possible explanation is that the diol reacts with LiOH before the presumed $LiB(OH)_4$ can be formed, and the resulting $LiH(O_2L_f)$ is unreactive towards $B(OH)_3$. By refluxing LiOH and $B(OH)_3$ *before* adding the diol, only $LiB(O_2L_f)_2$ was observed in the product mixture. This result lends support to the proposed explanation, as the formation of $LiH(O_2L_f)$ is presumably avoided by allowing $LiB(OH)_4$ to form in the absence of diol. One major advantage of these salts over those made by Barthel *et al.* is that in most cases no purification was necessary other than the removal of water. The high thermal stability of the lithium borates allows facile drying, although it must be done in stages. The bulk of the water must be removed at a relatively low temperature (100 – 110 °C) or some decomposition occurs. However, after this has been done the salts can be heated to at least 180 °C to remove the last traces of water with no ill effects.

Solution Conductivity

The compound $LiB(HFPOP)_2$ was first evaluated as a possible battery electrolyte by measuring its conductivity at various concentrations, c, in DME in order to gain a better understanding of the nature of solution ion pairing. Equivalent conductivities, Λ, were determined from these values and plotted vs. $c^{1/2}$ as shown in Figure 2. The shape of the curve is characteristic of a low-dielectric electrolyte solution in which dissociation of the salt is concentration-dependent (a similar curve has been observed for $LiBF_4$ solutions in DME[14]). Starting at infinite dilution, where the ionic species have no interaction with each other, the equivalent conductivity decreases as square root of concentration increases. This reflects the formation of neutral, nonconducting ion pairs as a result of increasing ionic interactions. As the concentration approaches 0.1 $M^{1/2}$ (0.01 M), the rate of decrease slows, and eventually a local minimum is reached. This is the result of charge carrier formation, which Fuoss and Kraus attributed to the effects of the equilibria shown below.[15]

$$2\,[CA]_s \overset{K_T}{\rightleftharpoons} [C^+A^-C^+]_s{}^+A_s^-$$

$$2\,[CA]_s \overset{K_T}{\rightleftharpoons} C_s^+[A^-C^+A^-]_s$$

These equilibria describe the formation of triple ions, which can exist in two forms: bilateral simultaneous, where both $[C^+A^-C^+]_s^+$ and $[A^-C^+A^-]_s^-$ are present in equal concentrations; or unilateral, where only one or the other is formed. For cations and anions of approximately equal size, Fuoss and Kraus assumed bilateral triple-ion formation, with equal formation constants (K_T).[15] This assumption was verified in part

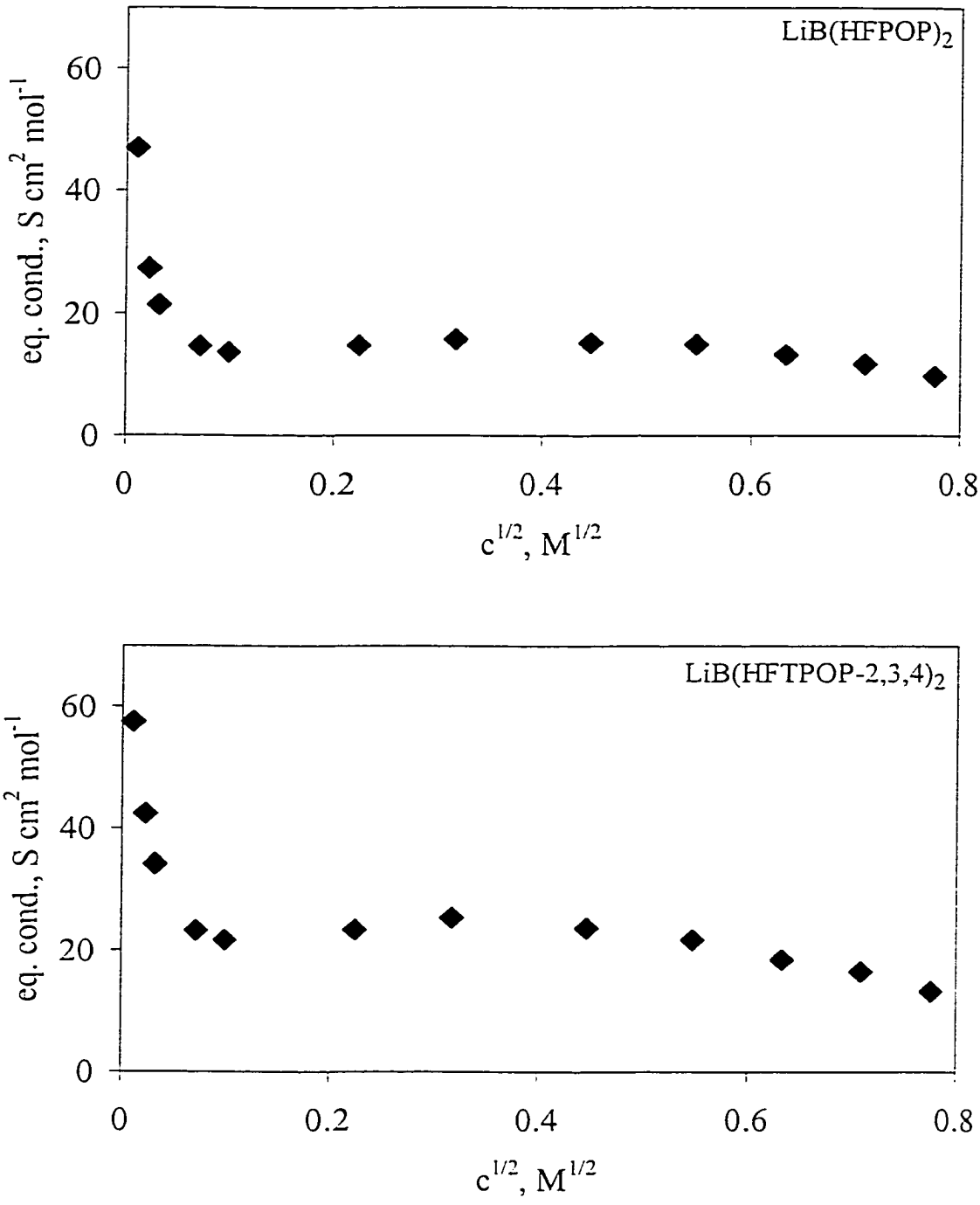

Figure 2. Plots of equivalent conductivity vs. square root of concentration for $LiB(HFPOP)_2$ and $LiB(HFTPOP\text{-}2,3,4)_2$ in DME. See Table 2 for definitions of abbreviations.

by the work of Hojo *et al.* in a study of the formation of triple ions composed of Li^+ and Cl^- in acetonitrile.[16]

$$2\,[LiCl]_s \overset{K_T}{\rightleftharpoons} [Li^+Cl^-Li^+]_s{}^+Cl_s^- \quad K_T = 10^{5.5}\,(dm^3\,mol^{-1})^{-2}$$

$$2\,[LiCl]_s \overset{K_T}{\rightleftharpoons} Li_s^+[Cl^-Li^+Cl^-]_s^- \quad K_T = 10^{4.7}\,(dm^3\,mol^{-1})^{-2}$$

Unilateral triple-ions are usually anionic, although some cationic complexes have been identified.[17] Anionic triple ions are generally composed of large anions and small cations.

As the concentration increases after the local minimum in Figure 2, the equivalent conductivity begins to steadily increase. According to the Fuoss-Kraus model,[15] this is due to the progressive formation of triple ions, which increases the relative amount of charge carriers in solution. Another possibility is that the increasing concentration of ionic species raises the dielectric constant of the solution, shifting dissociation equilibria towards the formation of free ions.[18] Thus, the relative number of charge carriers increases as the concentration is increased, thereby increasing the equivalent conductivity. For example, it was found that the permittivity of a dioxane solution of $LiClO_4$ increases from 6.95 at 0.19 mM to 8.61 and 0.12 M.[18b]

The equivalent conductivity increases in Figure 2 until a local maximum is reached at a concentration of approximately 0.32 $M^{1/2}$ (0.1 M). This occurs when a limit has been reached as to the number of available charge carriers. By increasing the electrolyte concentration, the average distance between ions decreases, and therefore the average electrostatic interactions among ions increase. This acts to increase the extent of ion association, effectively reducing the number of charge carriers. The extensive

interionic interactions at high concentrations also decrease ion mobilities, which leads to a lower equivalent conductivity. This effect can also be thought of in terms of an increased solution viscosity.[19]

The case for triple-ion formation in $LiB(HFPOP)_2$ solutions is substantiated by the existence of a triple-ion-like species in the structure of $Li_2(DME)(B(HFPOP)_2)_2$, shown in Figure 3. Crystals were grown from a solution of $LiB(HFPOP)_2$ in CH_2Cl_2/DME (20:1 v:v). Selected bond distances and angles are listed in Table 3. The structure consists of two $B(HFPOP)_2^-$ anions, one molecule of DME, and two lithium cations. Each boron atom is tetrahedrally coordinated by two 2-(hexafluoroisopropoxy)phenoxide (HFPOP) ligands. The four ligand chelate rings form very similar O–B–O angles ranging from 111.2(2) to 112.7(2)°, close to the ideal tetrahedral angle of 109.5°. The O–B–O angles including oxygen atoms bonded to Li^+ are smaller, ranging from 100.6(2) to 102.8(2)°. The oxygen atoms from the anion that bridge the boron and lithium atoms form B–O bonds ranging from 1.451(3) – 1.482(3) Å. Surprisingly, these are not considerably different from the other two B–O distances of 1.450(3) and 1.459(2) Å, which involve oxygen atoms *not* bonded to Li^+. Usually, coordination of a bond to a metal cation significantly ($\pm 3\sigma$) lengthens it relative to non-coordinated bonds.

There are two Li^+ coordination spheres in this structure. The first contains Li1, and consists of four Li–O and three Li–F contacts. The O3–B1–O4 unit forms a four-membered chelate ring with Li1, with Li–O bond distances of 1.962(4) and 2.060(4) Å, and an O3–Li1–O4 bond angle of 68.6(1)°. A five-membered O1–Li1–O2–C3–C2 chelate ring is also formed by coordination of DME to Li^+, with Li–O bond distances of 1.907(4) and 1.937(4) Å, and an O1–Li1–O2 bond angle of 85.1(2)°. The Li–F distances

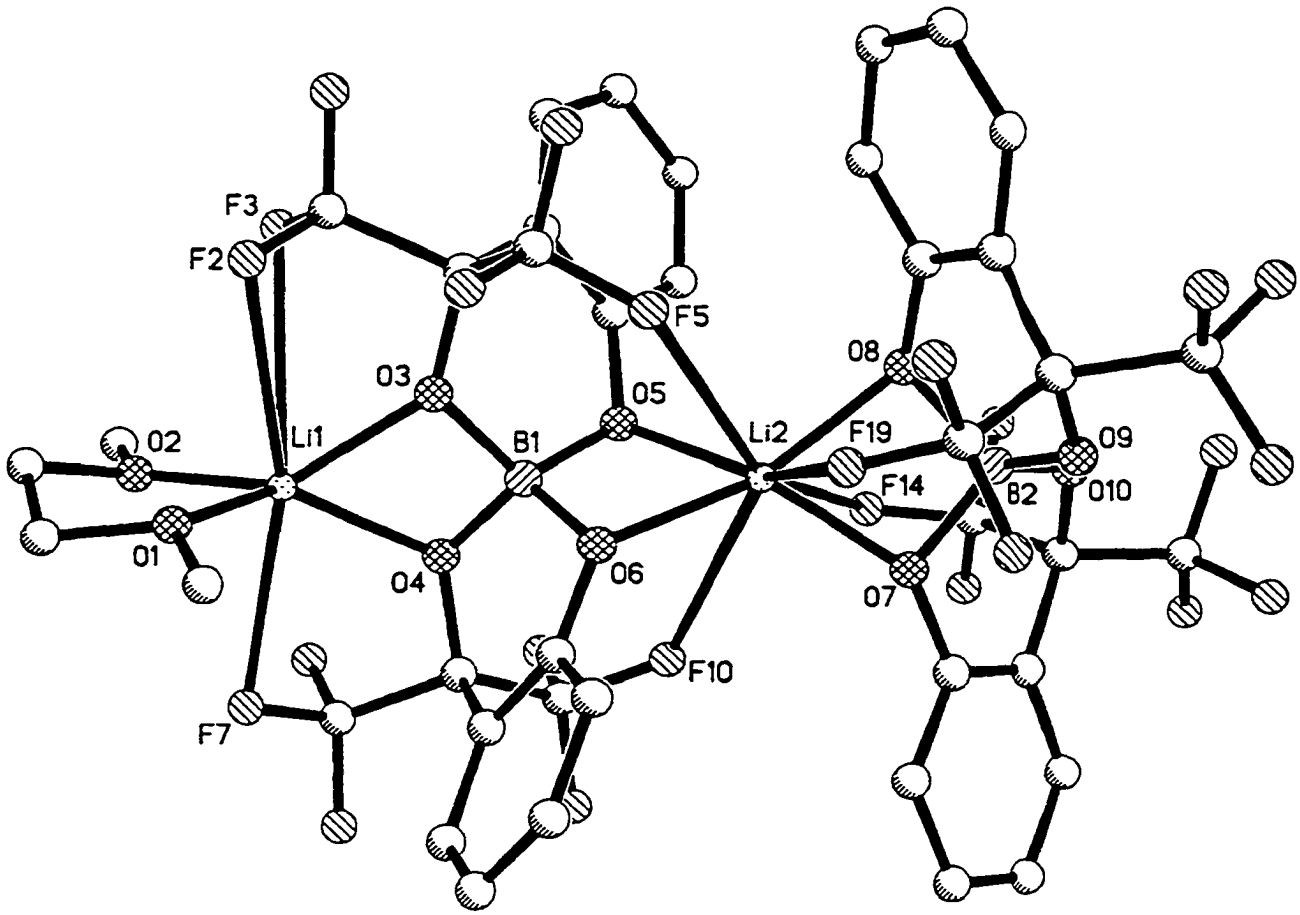

Figure 3. Drawing of the structure of $Li_2(DME)(B(HFPOP)_2)_2$ (hydrogen atoms omitted for clarity). The unlabeled partially shaded circles are carbon atoms, and the unlabeled circles fully shaded left to right are fluorine atoms. Selected interatomic distances (Å) and angles (deg): Li1–O1, 1.937(4); Li1–O2, 1.907(4); Li1–O3, 1.962(4); Li1–O4, 2.060(4); Li1–F2, 2.920(4); Li1–F3, 3.027(4); Li1–F7, 2.650(4); Li2–O5, 2.034(4); Li2–O6, 1.972(4); Li2–O7, 1.929(4); Li2–O8, 1.993(4); Li2–F5, 2.703(4); Li2–F10, 2.963(4); Li2–F14, 2.761(4); Li2–F19, 2.997(4); O5–Li–O6, 69.3(2); O7–Li–O8, 71.3(2). See Table 2 for definitions of abbreviations.

Table 3. Selected interatomic distances (Å) and angles (deg) for $Li_2(DME)(HFPOP)_2$.

Li1–O1	1.937(4)	Li1–O2	1.907(4)
Li1–O3	1.962(4)	Li1–O4	2.060(4)
Li1–F2	2.920(4)	Li1–F3	3.027(4)
Li1–F7	2.650(4)	Li2–O5	2.034(4)
Li2–O6	1.972(4)	Li2–O7	1.929(4)
Li2–O8	1.993(4)	Li2–F5	2.703(4)
Li2–F10	2.963(4)	Li2–F14	2.761(4)
Li2–F19	2.997(4)	B1–O3	1.470(3)
B1–O4	1.481(3)	B1–O5	1.451(3)
B1–O6	1.462(3)	B2–O7	1.477(3)
B2–O8	1.482(3)	B2–O9	1.450(3)
B2–O10	1.459(2)		
O5–B1–O6	102.8(2)	O5–B1–O3	112.5(2)
O6–B1–O3	114.7(2)	O5–B1–O4	115.7(2)
O6–B1–O4	111.2(2)	O3–B1–O4	100.6(2)
O9–B2–O10	106.6(2)	O9–B2–O7	113.5(2)
O10–B2–O7	111.7(2)	O9–B2–O8	112.7(2)
O10–B2–O8	111.3(2)	O7–B2–O8	101.2(2)
O2–Li–O1	85.1(2)	O2–Li–O3	141.8(2)
O1–Li–O3	112.2(2)	O2–Li–O4	123.7(2)

Table 2. (continued)

O1–Li–O4	134.3(2)	O3–Li–O4	68.7(2)
F2–Li–F3	42.0(3)	F2–Li–F7	154.9(3)
F3–Li–F7	155.9(3)	O7–Li2–O6	117.4(2)
O7–Li2–O8	71.3(2)	O6–Li2–O8	150.6(2)
O7–Li2–O5	153.5(2)	O6–Li2–O5	69.3(2)
O8–Li2–O5	116.5(2)	F5–Li2–F10	134.3(3)
F5–Li2–F14	144.7(3)	F5–Li2–F19	60.8(3)
F10–Li2–F14	62.8(3)	F10–Li2–F19	133.1(3)
F14–Li2–F19	136.9(3)		

See Table 2 for definition of abbreviation.

are 2.650(4), 2.920(4), and 3.027(4) Å. The next closest Li–F contact is at 3.324(4) Å. The geometry of the LiO_4F_3 coordination sphere, shown in Figure 4, is irregular. The second Li^+ coordination sphere contains Li2, and consists of four Li–O and four Li–F contacts. Two four-membered chelate rings are formed, one from each $B(HFPOP)_2^-$ anion. The Li–O bond distances range from 1.929(4) to 2.034(4) Å, and the two O–Li–O bond angles are 69.28(13)° (O5–Li2–O6) and 71.28(13)° (O7–Li2–O8). The Li–F distances are 2.703(4), 2.761(4), 2.963(4), and 2.997(4) Å. The next closest Li–F contact is at 4.493(4) Å. The geometry of the LiO_4F_4 coordination sphere is a distorted square antiprism, and is shown in Figure 5. The O5–F14–O8–F5 and O6–F10–O7–F19 least-squares planes are coplanar to within 0.11 Å. The dihedral angle between these two planes is only 0.5°. The Li2 atom is 0.944 Å from the centroid of the former plane and 1.099 Å from the centroid of the latter plane. The centroid···Li2···centroid angle is 177°.

This structure provides further evidence for the existence of $[Li(B(HFPOP)_2)_2]^-$ triple ions in solution, and illustrates one possible form for this species. However, it is not assumed that this is the *only* variety of triple ion found in DME solutions; at least three forms can be envisioned, as shown below. The lithium countercation for the triple ion is assumed to be completely solvated in all cases.

$[Li(DME)_2]^+[A^-Li^+A^-]^-$ **A**

$[Li(DME)_2]^+[A^-Li(DME)^+A^-]^-$ **B**

$[Li(DME)_2]^+[A^-Li(DME)_2^+A^-]^-$ **C**

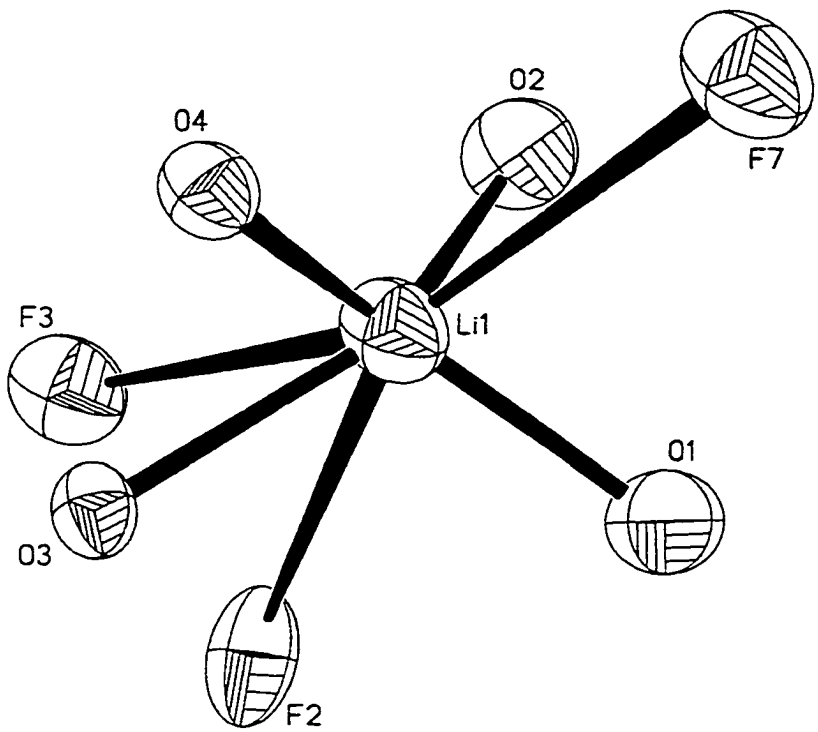

Figure 4. Drawing of the LiO_4F_3 coordination sphere for Li1 of $Li_2(DME)(B(HFPOP)_2)_2$ with 50% probability ellipsoids. See Table 2 for definitions of abbreviations.

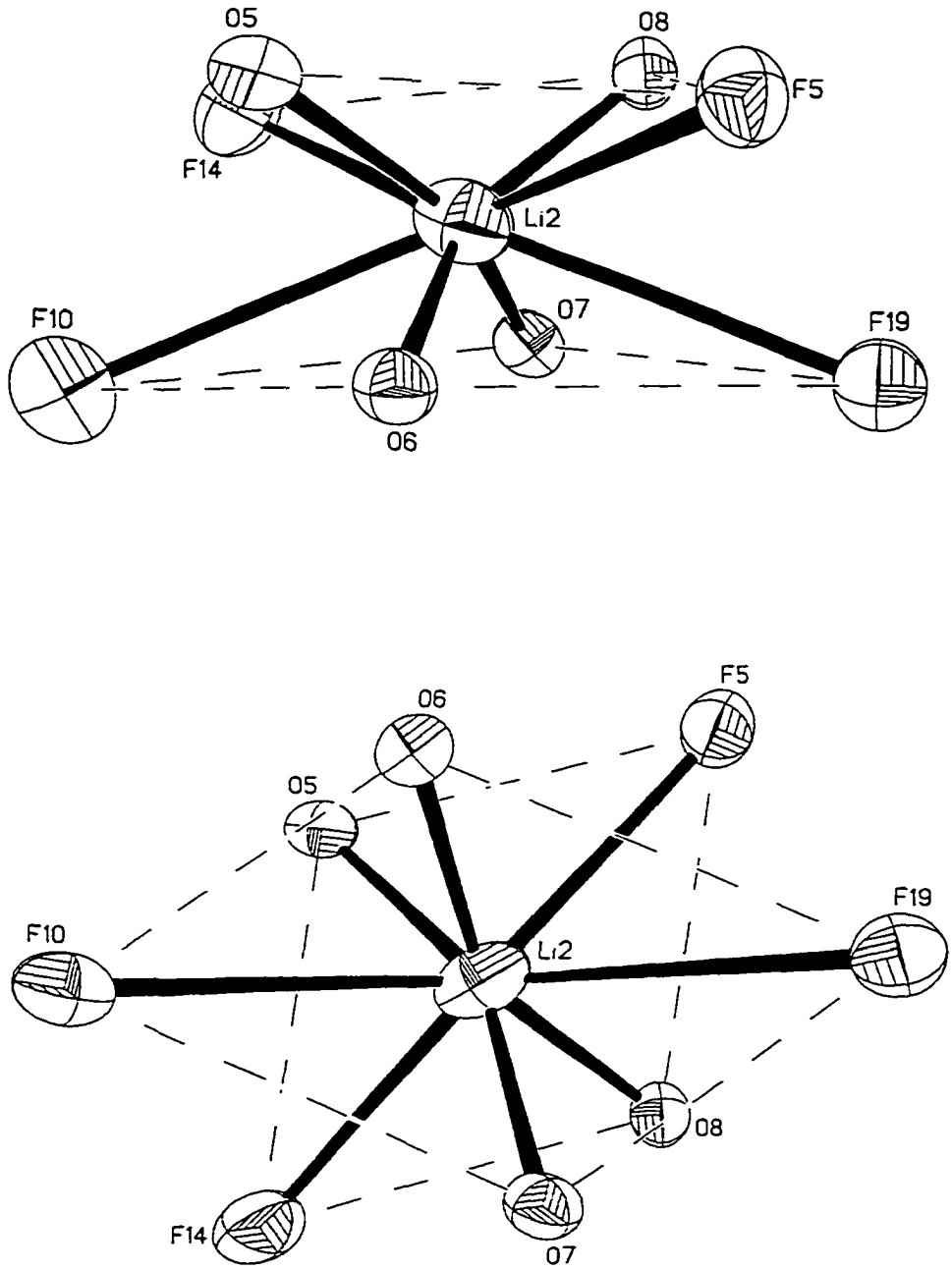

Figure 5. Drawings of LiO_4F_4 coordination sphere for Li2 of $Li_2(DME)(B(HFPOP)_2)_2$ with 50% ellipsoids, showing the square antiprismatic geometry. See Table 2 for definitions of abbreviations.

Structure **A** is similar to the structure discussed above, in that the lithium cation in the triple ion is coordinated only by the two anions. In case **B**, one molecule of DME is added to the coordination sphere of Li^+. In this form, Li^+ has contacts to DME and to the anions, but the contribution of the anions is less than in case **A**. The lithium cation in structure **C** is complexed by two DME molecules, and most likely has only weak direct contacts with each anion. The relative concentrations of each species will depend on anion basicity and steric considerations.

Considering only the $Li(B(HFPOP)_2)_2$ fragment of the $Li_2(DME)(B(HFPOP)_2)_2$ structure, it can be seen that each anion coordinates the lithium cation through its phenoxy oxygen atoms, presumably the strongest donor atoms in the anion. On the outside of the triple ion the second lithium cation is still coordinated by the complex anion, but this occurs through the two alkoxy oxygen atoms. A molecule of DME and several Li···F contacts complete its coordination sphere. The question may be raised as to why the lithium cations are coordinated in this manner, which can be answered in part using bond valence analysis as shown in Table 4. The contribution by Li–O bonds is nearly the same for Li1 (86%) and Li2 (82%). This indicates that the amount of stabilization of Li^+ by Li–O bonds is similar in both cases; that is, the stabilization afforded Li^+ by four phenoxy oxygen atoms is similar to that afforded by two DME oxygen atoms and two alkoxy oxygen atoms. There may also be steric factors contributing to structural arrangement of this compound, but in terms of thermodynamic stabilization of Li^+, it appears to be in the most stable arrangement.

To further understand the nature of ion pairing of $LiB(HFPOP)_2$ in DME, conductivity measurements of 0.01 M solutions of this salt were made with and without added 12-crown-4, a Li^+ complexing agent. Values are listed in Table 5. The effect of

Table 4. Bond valence values for $Li_2(DME)(B(HFPOP)_2)_2$.

Li1			Li2		
bond	distance, Å	bond valence (s)	bond	distance, Å	bond valence (s)
Li1–O1	1.937(4)	0.250	Li2–O1	2.034(4)	0.205
Li1–O2	1.907(4)	0.267	Li2–O2	1.972(4)	0.233
Li1–O3	1.962(4)	0.238	Li2–O7	1.929(4)	0.255
Li1–O4	2.060(4)	0.195	Li2–O8	1.993(4)	0.223
Li1–F2	2.920(4)	0.041	Li2–F5	2.703(4)	0.056
Li1–F3	3.027(4)	0.036	Li2–F10	2.963(4)	0.039
Li1–F7	2.650(4)	0.060	Li2–F14	2.761(4)	0.051
			Li2–F19	2.997(4)	0.037
total bond valence =		**1.087**	total bond valence =		**1.030**

The bond valence, s, is given by $s = (r/r_0)^{-N}$, where r_0(Li–O) = 1.378, N(Li–O) = 4.065, r_0(Li–F) = 1.288, and N(Li–F) = 3.9. See Table 2 for definition of abbreviation.

Table 5. 0.01 M Conductivities of $LiCF_3SO_3$ and $LiB(O_2L_f)_2$ salts in DME.

compound	conductivity, mS cm^{-1}
$LiB(HFPOP)_2$	0.136
$LiB(HFFPOP\text{-}2)_2$	0.123
$LiB(HFFPOP\text{-}3)_2$	0.177
$LiB(HFFPOP\text{-}4)_2$	0.190
$LiB(HFDPOP\text{-}2,4)_2$	0.179
$LiB(HFDPOP\text{-}3,4)_2$	0.231
$LiB(HFDPOP\text{-}3,5)_2$	0.212
$LiB(HFTPOP\text{-}2,3,4)_2$	0.218
$LiB(HFTPOP\text{-}3,4,5)_2$	0.260
$LiB(HFAPOP)_2$	0.160
$LiB(HFBPOP)_2$	0.160
$LiB(HFIPOP)_2$	0.157
$LiB(HFPOP)_2$ + 2 eq. 12-c-4	0.133
$LiCF_3SO_3$	0.004
$LiCF_3SO_3$ + 2 eq. 12-c-4	0.010

See Table 2 for definitions of abbreviations. 12-c-4 = 12-crown 4.

the crown ether on conductivity can be understood in the context of the equilibria shown below (all species are solvated by DME).

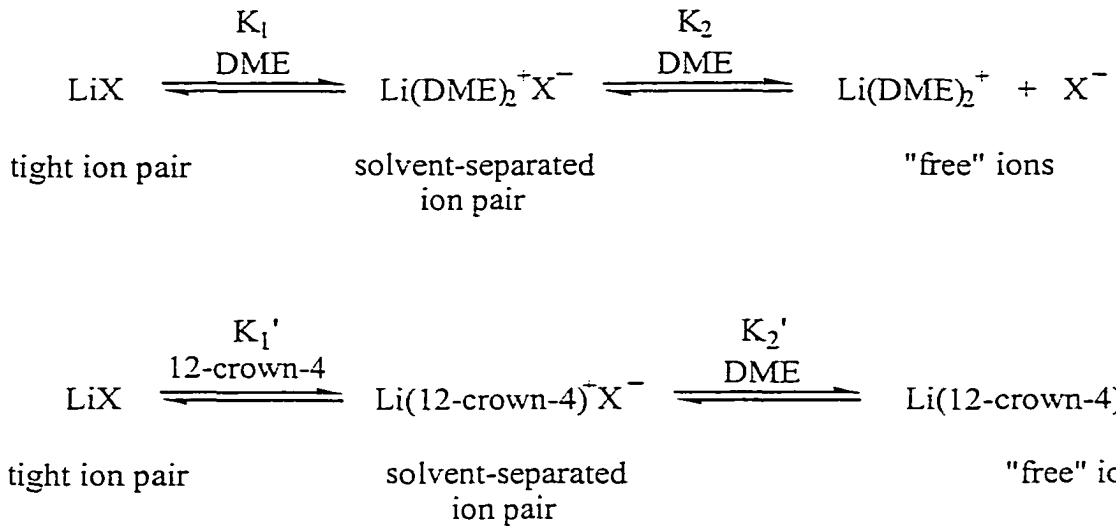

First consider the upper set of equilibria, without added 12-crown-4. The first equilibrium describes the relative concentrations of tight ion pairs and solvent-separated ion pairs, and is determined by the basicity, or coordinating strength, of the anion. These terms describe the strength of the direct interaction between the anion and cation. The more strongly coordinating the anion, the smaller K_1 will be. The second equilibrium describes the relative concentrations of solvent-separated ion pairs and free ions, and is determined not by the coordinating strength, but by the ion-pairing strength of the anion. Conductivity is determined by the number of free ions available to carry a charge in solution, and thus the position of the second equilibrium is more important than the first equilibrium in this respect.

The lower set of equilibria describes the effect of adding 12-crown-4 to a DME electrolyte solution. This compound forms a strong tetradentate chelate complex with

Li^+, and the position of the first equilibrium (defined by K_1') lies farther to the right than the equilibrium defined by K_1. This increases the concentration of solvent-separated ion pairs relative to the solution without added 12-crown-4. The magnitudes of K_2 and K_2' should not be very different, considering that $Li(DME)_2^+$ and $Li(12\text{-crown-4})^+$ are similar species. Thus, according to Le Châtelier's principle more free ions will be generated, thereby increasing conductivity. The more strongly coordinating the anion (i.e the greater the difference between K_1 and K_1'), the more pronounced the effect of adding 12-crown-4 on conductivity becomes.

When two equivalents of 12-crown-4 were added to a 0.01 M solution of $LiB(HFPOP)_2$ in DME, no change in conductivity was observed (Table 5). The number of charge carriers was not significantly increased, which indicates that the value of K_1' is not very different from K_1. The first equilibrium lies far to the right in both cases, providing evidence that in DME the lithium cation is predominantly in the *fully solvated* form. The presumably high K_1 indicates that the anion is only weakly associated, if at all, with the lithium cation. In this way, the $B(HFPOP)_2^-$ anion has been shown to be weakly coordinating. For comparison, the addition of two equivalents of 12-crown-4 to a 0.01 M solution of $LiCF_3SO_3$ increased the conductivity by 150% relative to a solution of this salt without added 12-crown-4 (Table 5). Although the triflate anion is often described as weakly coordinating, the results just described indicate that it is far more coordinating than the $B(HFPOP)_2^-$ anion.

In addition to showing that the $B(HFPOP)_2^-$ anion was weakly coordinating, the conductivitites for $LiCF_3SO_3$ and $LiB(HFPOP)_2$ in the presence of 12-crown-4 also provide information regarding the relative ion-pairing strengths of each anion. In both cases, the addition of 12-crown-4 drove the first equilibrium towards the formation of

solvent-separated ion pairs, and it is assumed that the concentration of tight ion pairs is negligible under these conditions. Thus, the effect of different coordinating abilities is not an issue, and the conductivities can be interpreted in terms of ion-pairing strength. The higher value for $LiB(HFPOP)_2$ (0.137 mS cm^{-1}) vs. $LiCF_3SO_3$ (0.010 mS cm^{-1}) indicates that the $B(HFPOP)_2^-$ anion is much more weakly ion-pairing than the $CF_3SO_3^-$ anion.

Although the conductivity results show that $B(HFPOP)_2^-$ is weakly ion-pairing, results from work with lithium fluoroalkoxyaluminates[20] demonstrate that there is still room for improvement in this respect. The conductivities of $LiAl(OR_f)_4$ salts are significantly higher (as much as 2.5 times higher than $LiB(HFPOP)_2$ in DME at 0.01 M), indicating that the borate ion-pairing strength is greater than for $Al(OR_f)_4^-$ anions. Thus, efforts were made to reduce this by modifying the diolate ligands. To intelligently design these new ligands, it was important to understand the nature of ion pairing between the anion and cation in DME solution. The experiment with 12-crown-4 provided a key insight in this respect, showing that the anion is not coordinated to the cation, and that the latter predominantly exists in the fully solvated form of $Li(DME)_2^+$. This cationic complex forms an ion pair with the anion, and presumably interacts most strongly with it at the point of highest negative charge density. Considering the structure of the anion, this is located in the area containing the boron and oxygen atoms (BO_4 core). With these points in mind, the $Li(DME)_2^+B(HFPOP)_2^-$ ion pair can be thought of in terms of the picture shown below.

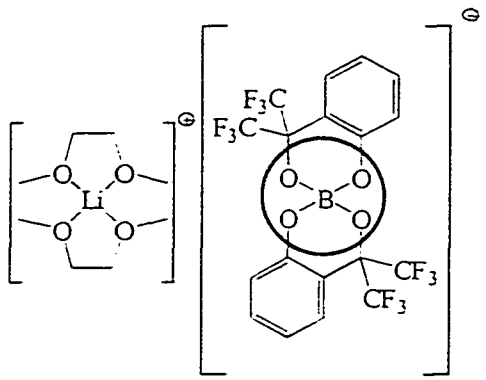

The circled area highlights the BO_4 core. A high amount of charge density in this region results in a strong cation-anion interaction; that is, the anion has a strong ion-pairing strength. A low amount of charge density in the BO_4 core leads to a weak cation-anion interaction, and a weak ion-pairing strength for the anion. The relative concentration of "free" ions in solution will be greater in the second case, and thus a higher conductivity should be observed. Thus, while the magnitude of the negative charge is the same for each hypothetical anion (–1), their ion-pairing strengths (and thus the conductivities of their lithium salts) vary depending on how this charge is distributed to affect the relative amount localized in the BO_4 core.

New ligand precursors were designed and synthesized with the goal of manipulating charge distribution in the corresponding borate anions to decrease charge density in the BO_4 core. Fluorine atoms were incorporated into the H_2(HFPOP) diol, which enhance the degree of charge dispersal as described in the Introduction. Several varieties were made, and the 0.01 M conductivities of their lithium salts measured in DME. Values are listed in Table 5, and illustrated graphically in Figure 6. It was initially believed that a higher degree of fluorination would lead to a higher conductivity, and it can be seen in Figure 6 that this hypothesis was, in general, correct. It is important

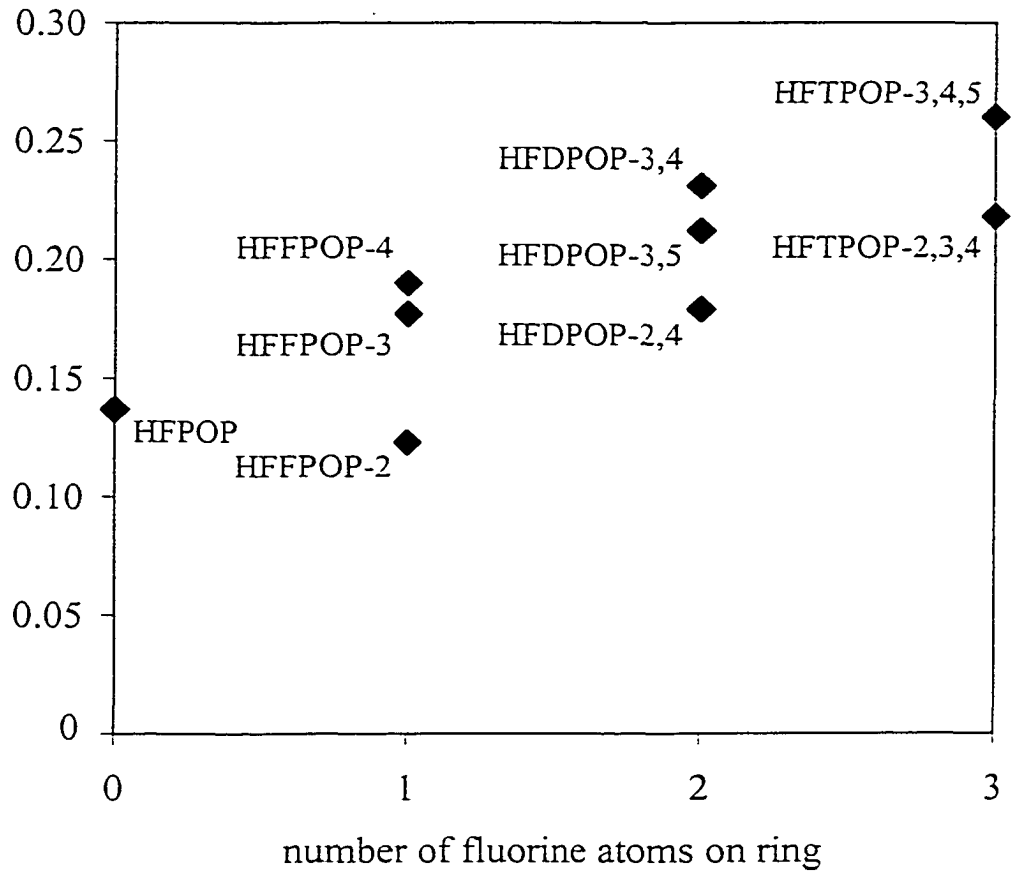

Figure 6. Plot of conductivity of $LiB(O_2L_f)_2$ salts (0.01 M, DME) vs. number of fluorine atoms on the phenyl ring of each diolate ligand. See Table 2 for definitions of abbreviations.

to note that conductivity reflects both ion-pairing strength and ion mobility. It might be suggested that substituting fluorine atoms for hydrogen atoms changes anion size, thereby affecting ion mobility and thus conductivity. However, given the similar sizes of hydrogen and fluorine atoms (van der Waals radii of 1.20 and 1.35 Å, respectively[10]), it can be assumed that all of the fluorinated $B(HFPOP)_2^-$ derivatives are essentially the same size, and differences in conductivity can be attributed to differences in ion-pairing strength, not ion mobility. The higher conductivities for lithium salts of the fluorinated anions reflect decreases in ion-pairing strength. The incorporation of fluorine atoms in the ligands enhances the degree of charge dispersal in the corresponding anions, and therefore most likely decreases the amount of charge density in the BO_4 core relative to $B(HFPOP)_2^-$. However, can a decrease in charge density in the BO_4 core be directly correlated with a decrease in ion-pairing strength (as measured by conductivity)? To help answer this question, the nature of charge distribution in each anion was examined in greater detail.

To gain an insight into the differences in charge distribution among the borate anions, the quadrupole moment for each was examined. This is illustrated in a general manner by the picture below.

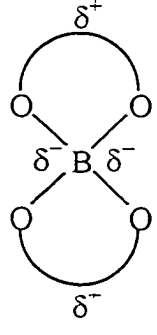

Quadrupole Moment of $B(O_2L_f)_2^-$

This property not only describes charge distribution, but also provides a measure of how much charge density resides in the center of the anion (i.e. the BO_4 region) by the value of δ^-. To calculate the quadrupole moment, each anion was modeled as its neutral analog, substituting carbon for boron. The geometry of the structure was optimized using the AM1 semi-empirical method, and a single point energy calculation was then performed using the *ab initio* Hartree-Fock (3-21G) method. The tensor elements for the quadrupole moment were obtained from the results of the second calculation. To calculate the magnitude of the overall quadrupole moment, the assumption was made that each compound was spherically symmetric. This allowed the XX, YY, and ZZ tensor elements to be averaged to obtain an overall R^2 "quadrupole moment." In reality, a molecule with spherical symmetry does not have a quadrupole moment, but the radial anisotropy of the charge distribution in the anion can be approximated using this model. Values for each anion analog are listed in Table 6, and illustrated graphically in a plot of conductivity vs. quadrupole moment magnitude in Figure 7. The plot shows that there is a strong linear correlation ($R^2 = 0.86$) between these two variables. With the assumption that a more negative quadrupole moment corresponds to less charge density in the center of the molecule (i.e. the BO_4 region), this plot provides support for the explanation proposed above.

Another way to consider the quadrupole moment is as a combination of two opposing dipole moments. For the borate anions, these correspond to the dipole moments of each ligand. To examine the anion system in this manner, each ligand was modeled, using Mg^{2+} as a substitute for the boron atom to yield a neutral species as illustrated below. The geometry of each structure was optimized using the AM1 semi-empirical method, and the dipole direction and magnitude were obtained from these calculations.

Table 6. Quadrupole moment tensor elements and averages for $C(O_2L_f)_2$ compounds.

model	XX tensor element	YY tensor element	ZZ tensor element	average, D Å
$C(HFPOP)_2$	–183.7	–194.5	–196.9	–191.7
$C(HFFPOP\text{-}2)_2$	–181.7	–205.1	–214.0	–200.3
$C(HFFPOP\text{-}3)_2$	–188.9	–219.4	–219.0	–209.1
$C(HFFPOP\text{-}4)_2$	–221.0	–206.6	–206.1	–211.2
$C(HFDPOP\text{-}2,4)_2$	–225.8	–215.9	–220.1	–220.6
$C(HFDPOP\text{-}3,4)_2$	–224.6	–229.5	–233.3	–229.1
$C(HFDPOP\text{-}3,5)_2$	–228.2	–214.6	–223.3	–222.0
$C(HFTPOP\text{-}2,3,4)_2$	–226.7	–246.4	–240.9	–238.0
$C(HFTPOP\text{-}3,4,5)_2$	–231.8	–256.2	–238.2	–242.1

See Table 2 for definitions of abbreviations.

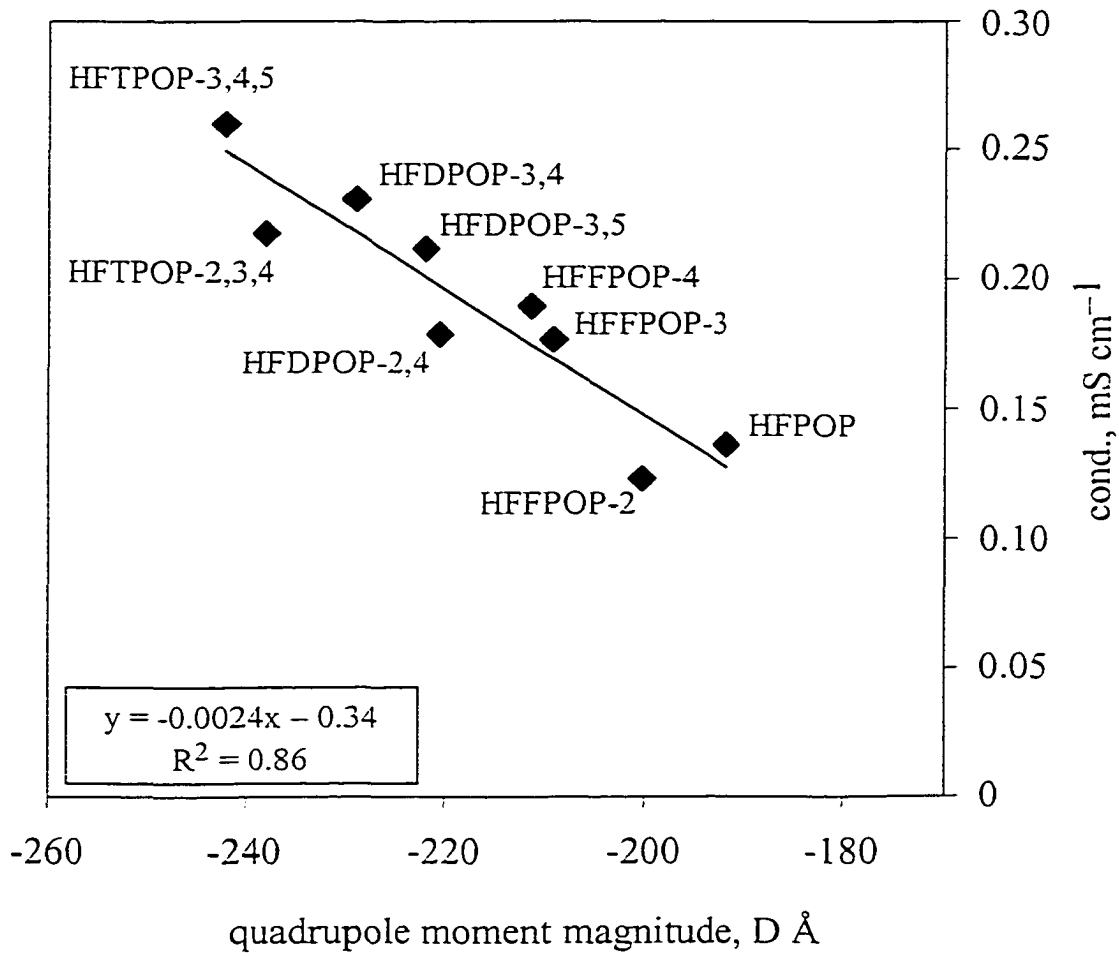

Figure 7. Conductivity of $LiB(O_2L_f)_2$ (0.01 M in DME) vs. calculated quadrupole moment magnitude. See Table 2 for definitions of abbreviations.

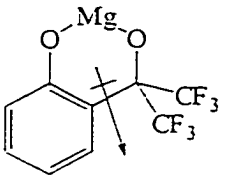

$Mg(O_2L_f)$ Model

For each structure, the dipole moment is oriented in the same direction (see above), but the magnitude varies. These values are listed in Table 7, and are displayed graphically in Figure 8 in a plot of conductivity vs. dipole moment magnitude. It can be seen that a strong linear correlation ($R^2 = 0.85$) between these two properties also exists. As the magnitude increases, the charge density in the BO_4 region decreases, thereby reducing the ion-pairing strength of the anion and increasing the conductivity of its lithium salt.

The discussion above provides evidence to support the conclusion that the amount of charge density in the BO_4 core determines ion-pairing strength, and thus conductivity. The next issue to address is the origin of differences among the borate anions in this respect. It was initially thought that the amount of charge density in the center of each anion might correlate directly with acidity trends of fluorophenols, which are fragments of the overall anion. The fluorophenoxy moiety contains the phenoxy oxygen atom, one of the two types of oxygen atoms that make up the BO_4 core. Consider the three anions with monofluorinated ligands. The trend in terms of increasing gas-phase acidity for the three analogous monofluorophenols is 4-fluorophenol < 3-fluorophenol < 2-fluorophenol.[21] The compound 2-fluorophenol is the strongest acid, so its conjugate base (2-fluorophenoxide) is the weakest of the three, and therefore has the least amount of charge density localized on the phenoxy oxygen atom. As such, the $B(HFFPOP\text{-}2)_2^-$

Table 7. Calculated dipole moment magnitudes for HFPOP ligands using the $Mg(O_2L_f)$ model.

ligand	dipole moment, D
HFPOP	6.289
HFFPOP-2	4.965
HFFPOP-3	6.311
HFFPOP-4	7.641
HFDPOP-2,4	6.494
HFDPOP-3.4	7.871
HFDPOP-3,5	7.621
HFTPOP-2,3,4	7.046
HFTPOP-3,4,5	9.103

See Table 2 for definitions of abbreviations.

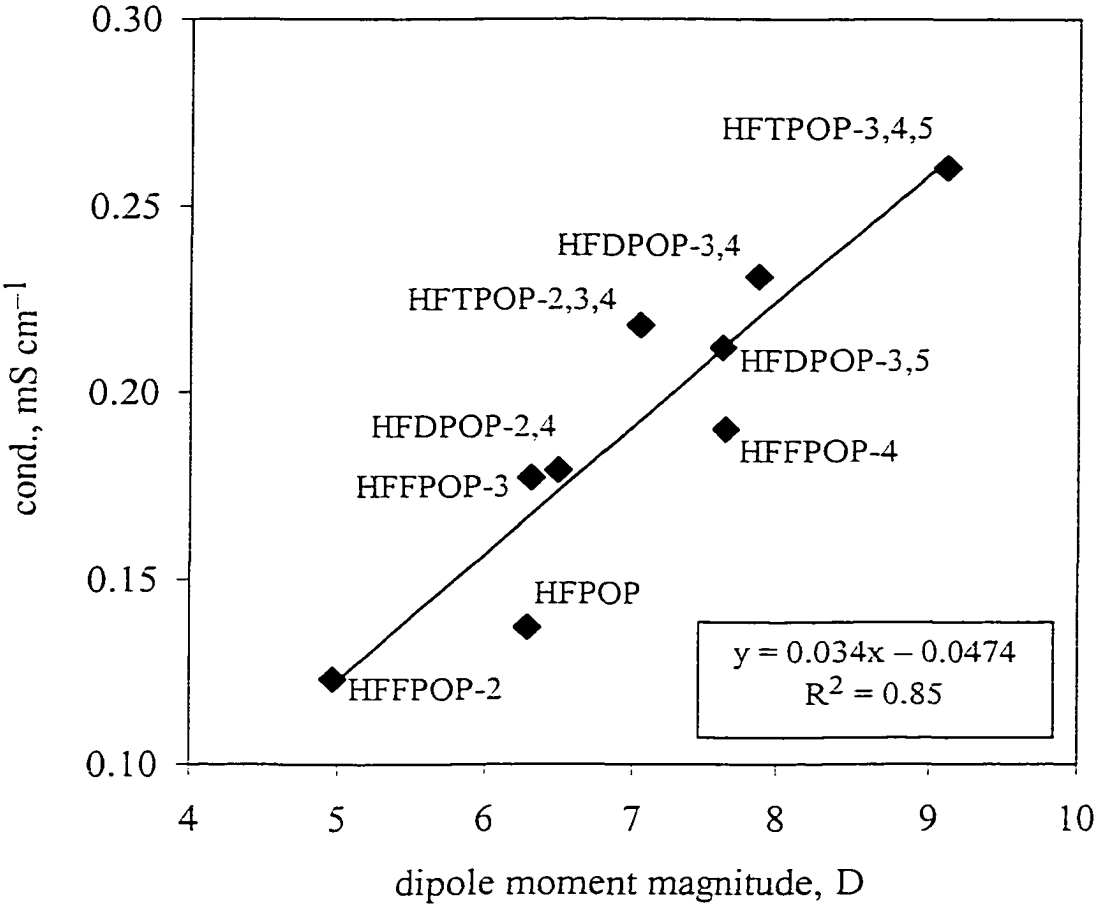

Figure 8. Plot of conductivity of $LiB(O_2L_f)_2$ salts (0.01 M, DME) vs. calculated dipole moment magnitude using the $Mg(O_2L_f)$ model. See Table 2 for definitions of abbreviations.

anion should be expected to have the least amount of charge density in the BO_4 region and thus the weakest ion-pairing strength, followed by $B(HFFPOP\text{-}3)_2^-$ and then $B(HFFPOP\text{-}4)_2^-$, with the conductivities of their lithium salts reflecting this progression. However, this was not observed. In fact, the exact *opposite* order was seen: $LiB(HFFPOP\text{-}4)_2$ had the highest conductivity (0.190 mS cm^{-1}), followed by $LiB(HFFPOP\text{-}3)_2$ (0.177 mS cm^{-1}), and $LiB(HFFPOP\text{-}2)_2$ had the lowest value (0.123 mS cm^{-1}). It is remarkable that the value for $LiB(HFFPOP\text{-}2)_2$ was lower than even the parent compound $LiB(HFPOP)_2$, which has no fluorine atoms on its two phenyl rings. The fluorophenoxide basicity trend is determined by the relative electron-withdrawing power of a fluorine atom in the *ortho*, *meta*, or *para* position on the phenoxide phenyl ring. Apparently, this effect is not the determining factor for the amount of charge density in the BO_4 core, and thus ion-pairing strength, in each analogous borate anion.

While the differences in ion-pairing strengths (i.e. conductivities) cannot be explained according to the reasoning used for the trend in fluorophenoxide basicity, it is still the placement of the fluorine atoms that is the determining factor. Local C–F dipoles are created, and these affect charge distribution and the amount of charge density in the BO_4 core, which can again be described by the quadrupole moment of the anion (see above). Depending on the orientation of the C–F dipoles, the magnitudes of the δ^- and δ^+ partial charges can increase or decrease relative to their values in $B(HFPOP)_2^-$. Once again consider the three anions $B(HFFPOP\text{-}2)_2^-$, $B(HFFPOP\text{-}3)_2^-$, and $B(HFFPOP\text{-}4)_2^-$. The local C–F dipole for each compound is shown below to isolate its effect on the overall anion quadrupole (only one of the two chelating diolate ligands is shown for each anion).

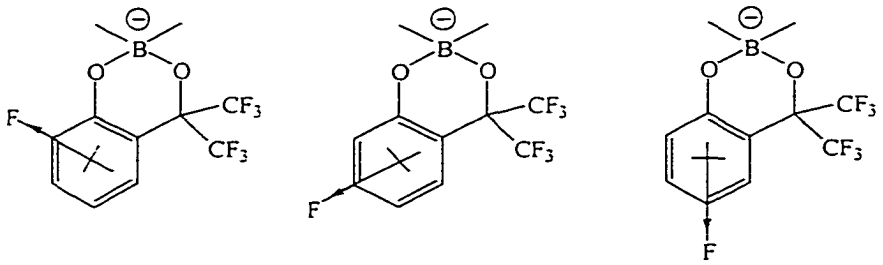

$B(HFFPOP\text{-}2)_2^-$ $B(HFFPOP\text{-}3)_2^-$ $B(HFFPOP\text{-}4)_2^-$

Progressing from $B(HFFPOP\text{-}2)_2^-$ to $B(HFFPOP\text{-}3)_2^-$ to $B(HFFPOP\text{-}4)_2^-$, the C–F dipole rotates counterclockwise around the ring. For $B(HFFPOP\text{-}3)_2^-$ and $B(HFFPOP\text{-}4)_2^-$, the value of δ^- in the quadrupole should decrease relative to $B(HFPOP)_2^-$ as the C–F dipoles orient charge density away from the BO_4 region. Therefore, the ion-pairing strength of these two anions should be less than that of $B(HFPOP)_2^-$. This is evidenced by the higher conductivities for both $LiB(HFFPOP\text{-}3)_2$ (0.177 mS cm^{-1}) and $LiB(HFFPOP\text{-}4)_2$ (0.190 mS cm^{-1}) relative to $LiB(HFPOP)_2$ (0.137 mS cm^{-1}). Note also that the conductivity of $LiB(HFFPOP\text{-}4)_2$ is higher than $LiB(HFFPOP\text{-}3)_2$. The C–F dipole in the $B(HFFPOP\text{-}4)_2^-$ anion points directly to the end of the anion, which is more effective in reducing charge density in the BO_4 region than the C–F dipole in the $B(HFFPOP\text{-}3)_2^-$ anion. The surprisingly low conductivity of $LiB(HFFPOP\text{-}2)_2$ also supports this idea. The C–F dipole in this case is pointed *towards* the BO_4 core; this should increase the magnitude of the quadrupole δ^- component relative to $B(HFPOP)_2^-$, and therefore increase the ion-pairing strength of the anion. According to this model, the conductivity of $LiB(HFFPOP\text{-}2)_2$ should be lower than $LiB(HFPOP)_2$, and this is what was observed.

In the course of characterizing the $B(O_2L_f)_2^-$ anions, it was found that they possessed an overall dipole moment as well. Although it is weak, its relationship with conductivity was investigated. Dipole moments and magnitudes were obtained from the results of the quadrupole calculations described above (using the $C(O_2L_f)_2$ model). The dipole was oriented in the same direction for each anion analog, but the magnitudes differed. A plot of conductivity vs. dipole moment magnitude was made, as shown in Figure 9. Only a weak correlation is seen, in that a weaker dipole moment generally corresponds to a higher conductivity. Given this, and the fact that the dipole moment is weak, the anion dipole does not appear to be an important factor in determining conductivity.

The conductivity data for the new salts underscores an important issue in the design of weakly ion-pairing, or weakly coordinating anions. Namely, is perfluorination (a) necessary, and (b) desirable?[22] One needs to keep in mind the application in which the anion will be used to answer these questions, and consider the effect of fluorination on the properties of the salt (e.g. solubility, stability). However, in terms of creating an extremely weakly basic anion, the answer is often "yes" to both questions, due to the high degree of charge dispersal resulting from fluorination. The series of anions studied in this work represents a rare exception to this generally accepted rule. It was shown that the addition of a fluorine atom in the 2 position on the phenyl ring actually *increases* the ion-pairing strength. That is, a *lower* fluorine content is more desirable for decreasing anion ion-pairing strength, *if* placed in the correct positions.

Another strategy to decrease the ion-pairing strength of $B(HFPOP)_2^-$ was based physically blocking the BO_4 region. This should increase the distance between the charge density in this area and the $Li(DME)_2^+$ complex, and decrease the strength of the

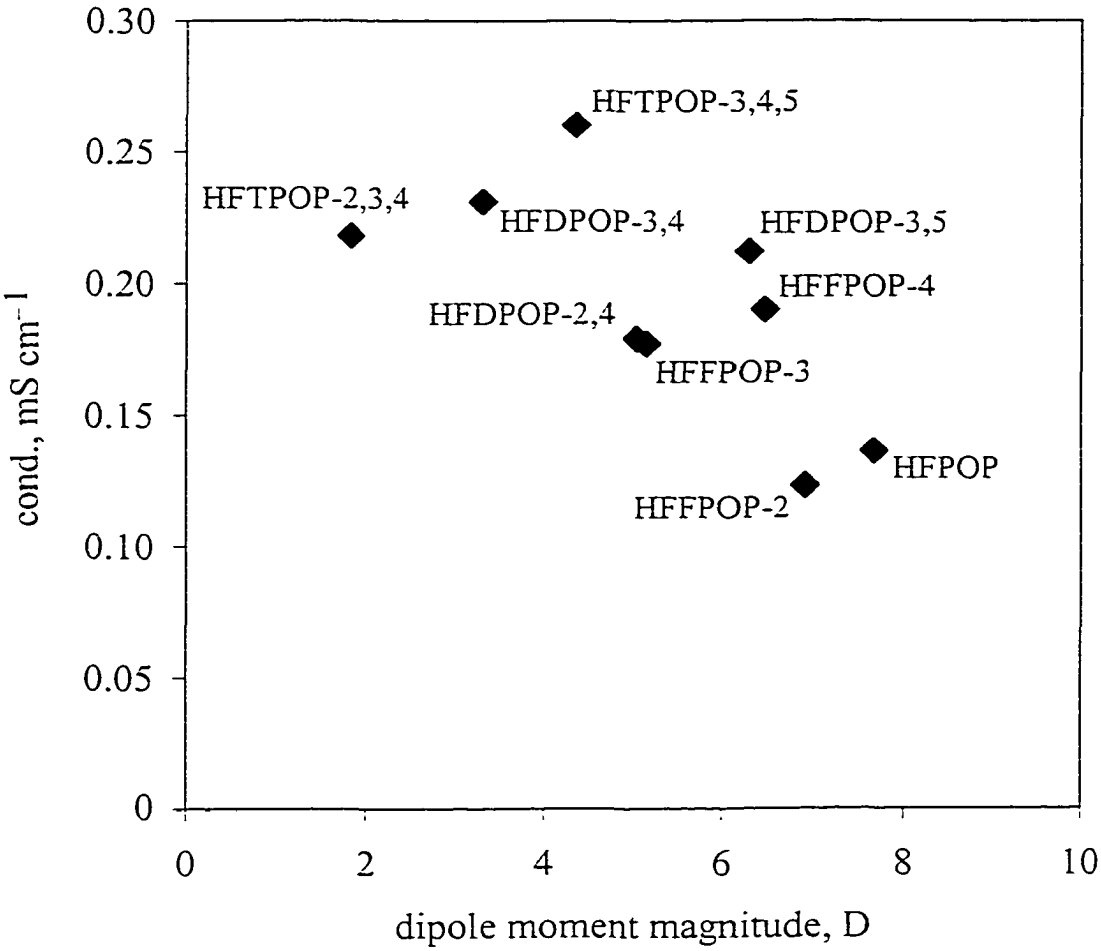

Figure 9. Plot of conductivity of $LiB(O_2L_f)_2$ salts (0.01 M, DME) vs. calculated dipole moment magnitude of $C(O_2L_f)_2$. See Table 2 for definitions of abbreviations.

monopole-monopole interaction. To accomplish this, the new anion $B(HFAPOP)_2^-$ was synthesized (see Table 2 for ligand structure). Each ligand contains a *t*-butyl group *ortho* to the phenoxy oxygen atom, and a methyl group in the *para* position. The methyl group was necessary for the successful synthesis of the ligand precursor (diol); without it, the hexafluoroacetone moiety preferentially substitutes in the *para* position. The 0.01 M conductivity of the lithium salt of this anion is 0.160 mS cm^{-1}, higher than that of $LiB(HFPOP)_2$ (0.137 mS cm^{-1}). Thus, the ion-pairing strength of the new anion is lower than that of $B(HFPOP)_2^-$, presumably due to the steric blocking effect of the *t*-butyl group.

$LiB(HFIPOP)_2$ is another salt to consider. Its conductivity is 0.157 mS cm^{-1}, higher than both $LiB(HFPOP)_2$ and the analogous $LiB(HFFPOP\text{-}2)_2$. Iodine is not as electronegative as fluorine, and does not exert as large an influence over the distribution of charge density in the ligand; if this were the case, a lower conductivity relative to $LiB(HFPOP)_2$ would have been the result. However, the steric effect of iodine on the ion-pairing strength of $B(HFIPOP)_2^-$ must be considered. This is not an issue in the case of $B(HFFPOP\text{-}2)_2^-$ due to the similar sizes of hydrogen and fluorine atoms. In contrast, iodine is large, and can physically block the phenoxy oxygen atom much like the *t*-butyl group of the HFAPOP ligand. This lowers the ion-pairing strength of $B(HFIPOP)_2^-$ relative $B(HFPOP)_2^-$, and a higher conductivity is observed.

In addition to $LiB(HFPOP)_2$, $LiB(HFTPOP\text{-}2,3,4)_2$ was also structurally characterized as an acetone adduct, as shown in Figure 10. Selected bond distances and angles are listed in Table 8. The structure consists of centrosymmetric dinuclear molecules composed of lithium(1+) and borate(1–) ions, as well as two acetone molecules. Each acetone bridges the two lithium cations, creating a planar Li_2O_2 core.

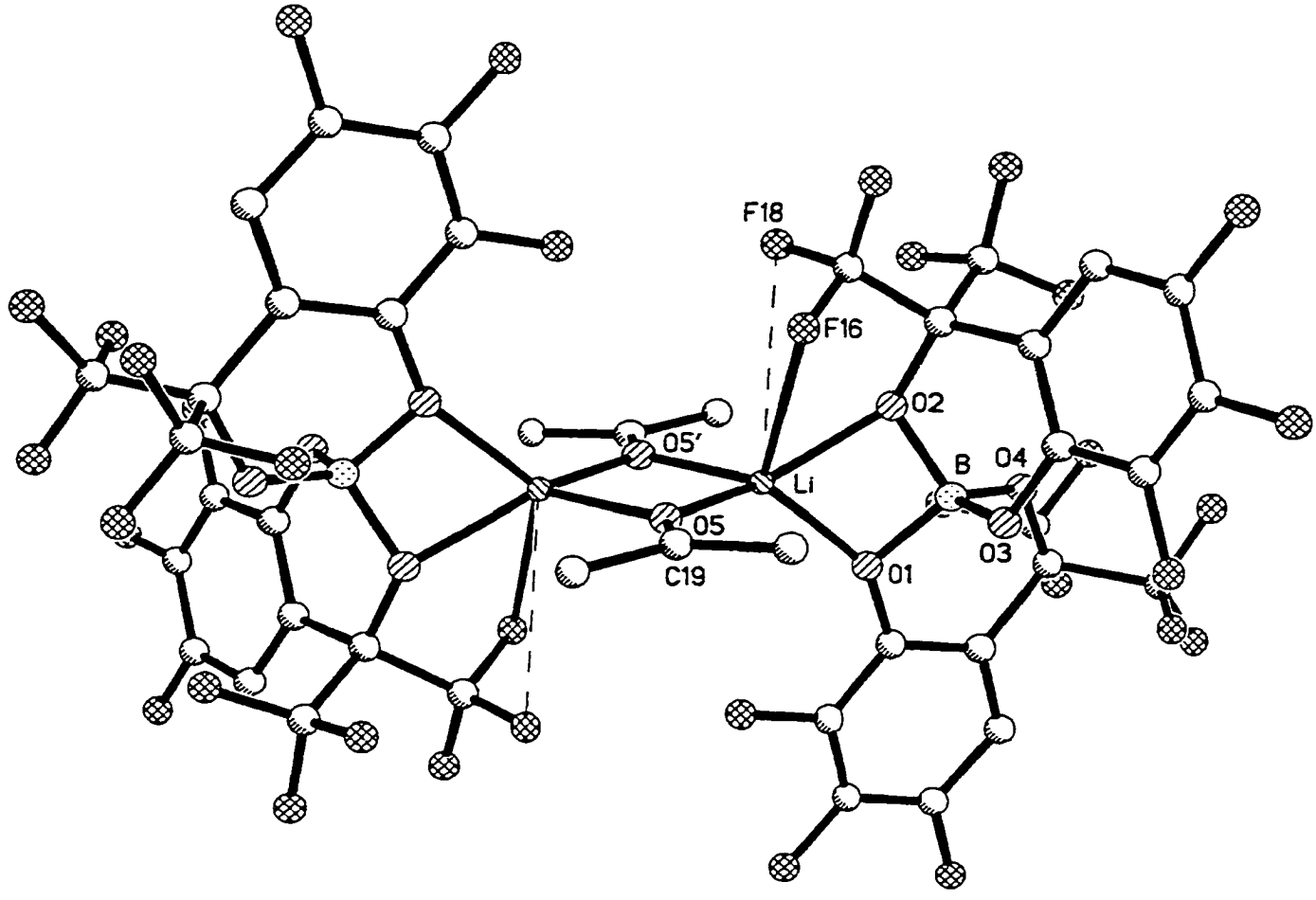

Figure 10. Drawing of the structure of $Li(OC(CH_3)_2)B(HFTPOP\text{-}2,3,4)_2$ (hydrogen atoms omitted for clarity). The unlabeled partially shaded circles are carbon atoms, and the unlabeled crosshatched circles are fluorine atoms. Selected interatomic distances (Å) and angles (deg): Li–O1, 1.964(7); Li–O2, 2.038(7); Li–O5, 1.950(7); Li–O5', 1.946(7); Li–F16, 2.780(7); Li–F18, 3.258(7); O1–Li–O2, 69.4(2). See Table 2 for definition of abbreviation.

Table 8. Selected interatomic distances (Å) and angles (deg) for $Li(OC(CH_3)_2)(HFTPOP\text{-}2,3,4)_2$.

Li–O1	1.964(7)	Li–O2	2.038(7)
Li–O5	1.950(7)	Li–O5'	1.946(7)
Li–F16	2.780(7)	Li–F18	3.258(7)
B–O1	1.468(5)	B–O2	1.480(5)
B–O3	1.445(6)	B–O4	1.431(5)
O4–B–O3	113.9(3)	O4–B–O1	112.6(4)
O3–B–O1	108.2(3)	O4–B–O2	109.9(3)
O3–B–O2	110.3(4)	O1–B–O2	101.3(3)
O5'–Li–O5	86.4(3)	O5'–Li–O1	122.5(4)
O5–Li–O1	124.0(4)	O5'–Li–O2	121.7(4)
O5–Li–O2	138.1(4)	O1–Li–O2	69.4(2)
F16–Li–F18	40.5(4)		

See Table 2 for definition of abbreviation.

Each B atom is tetrahedrally coordinated by two 2,3,4-trifluoro-6-(hexafluoropropoxy)phenoxide (HFTPOP-2,3,4) ligands. The two ligand chelate rings form O–B–O angles of 112.6(4)° (O1–B–O4) and 110.3(4)°, close to the ideal tetrahedral angle of 109.5°. The O3–B–O4 angle of 113.9(3)° is very similar to the other two, while the O1–B–O2 angle of 101.3(3)° is significantly smaller. The oxygen atoms from the anion that bridge the boron and lithium atoms form B–O bonds of 1.468(5) and 1.480(5) Å, which are considerably longer than the other two B–O bonds of 1.445(6) and 1.431(5) Å.

The Li^+ coordination sphere consists of one Li–F and four Li–O contacts. The O1–B–O2 unit forms a four-membered chelate ring with Li^+, with Li–O bond distances of 1.964(7) and 2.038(7) Å, and with an O1–Li–O2 bond angle of 69.4(2)°. Another four-membered ring with Li^+ is created by the O5–Li'–O5' unit, with Li–O bond distances of 1.946(7) and 1.950(7) Å, and with an O5–Li–O5' bond angle of 86.4(3)°. The single Li–F bond is at a distance of 2.785(7) Å, with the next closest Li···F contacts at 3.258(7) and 3.322(7) Å (Li–F18). While the first distance is longer than 3.165 Å, it is within the combined van der Waals radii for Li and F (3.29Å). The definition of $s = 0.03$ (Li–F distance of 3.165 Å) for effective bonding is admittedly arbitrary, and F18 may very well be bonding to Li. As such, the drawings of the overall structure of $LiB(OC(CH_3)_2)(B(HFTPOP\text{-}2,3,4)_2)$ and its coordination sphere (Figures 10, 11) include the Li–F18 contact by connecting these two atoms with a dotted line. For all other structures discussed in this work, Li–F contacts beyond 3.165 Å but within 3.29 Å will be denoted in this manner as well. Bond valence analysis was also performed, and values are listed in Table 9. There it can be seen that with or without the Li–F18 contact, the total valence is very close to one. The contribution made by Li–F bonding to the total

Table 9. Bond valence values for $Li(OC(CH_3)_2)B(HFTPOP\text{-}2,3,4)_2$.

bond	distance, Å	bond valence (s)
Li–O1	1.964(7)	0.237
Li–O2	2.038(7)	0.204
Li–O5	1.950(7)	0.244
Li–O5'	1.946(7)	0.246
Li–F16	2.780(7)	0.050
	total bond valence =	**0.981**
Li–F18	3.258(7)	0.027
	total bond valence =	**1.008**

The bond valence, s, is given by $s = (r/r_0)^{-N}$, where r_0(Li–O) = 1.378, N(Li–O) = 4.065, r_0(Li–F) = 1.288, and N(Li–F) = 3.9. See Table 2 for definition of abbreviation.

valence is low (<8%) in either case. Overall, the geometry of the LiO_4F (or LiO_4F_2) coordination sphere is irregular, and shown in Figure 11.

There are some interesting facets of this structure that deserve additional discussion. First, consider the Li–O1 and Li–O2 bond lengths. Li–O1 is significantly shorter than Li–O2 (>3σ), which provides an insight into the relative donor strengths of each oxygen atom. O1 is the phenoxy oxygen atom, and is assumed to be a stronger donor than O2, the alkoxide oxygen atom. This assumption is validated by the difference in bond lengths with Li: O1, being a stronger donor, makes a shorter bond with Li^+ than O2.

Another feature of this structure is the inclusion of acetone. The manner in which it bonds to Li^+ is consistent with the proposed model for Lewis acid catalysis. However, the O5–C19 bond length of 1.224(5) Å is not significantly longer (within 3σ) than the average $R_2C{=}O$ distance of 1.210 Å[23] (R = H or sp^3 C), indicating no significant distortion from uncomplexed acetone. A similar result was also observed by Barbarich *et al.* in the structure of Li(2-cyclohexen-1-one)(Al(OC(Ph)$(CF_3)_2)_4$).[24] These observations suggest that Li^+ acts as a Lewis-acid catalyst *not* by raising the ketone ground state energy, but by lowering the energy of the transition-state species. The inclusion of acetone also speaks to the weakly coordinating nature of B(HFTPOP-2,3,4)$_2^-$. The crystal was grown by sublimation at 180 °C under vacuum; the fact that acetone was not removed from the lithium salt under these conditions indicates an *extremely* Lewis acidic lithium cation.

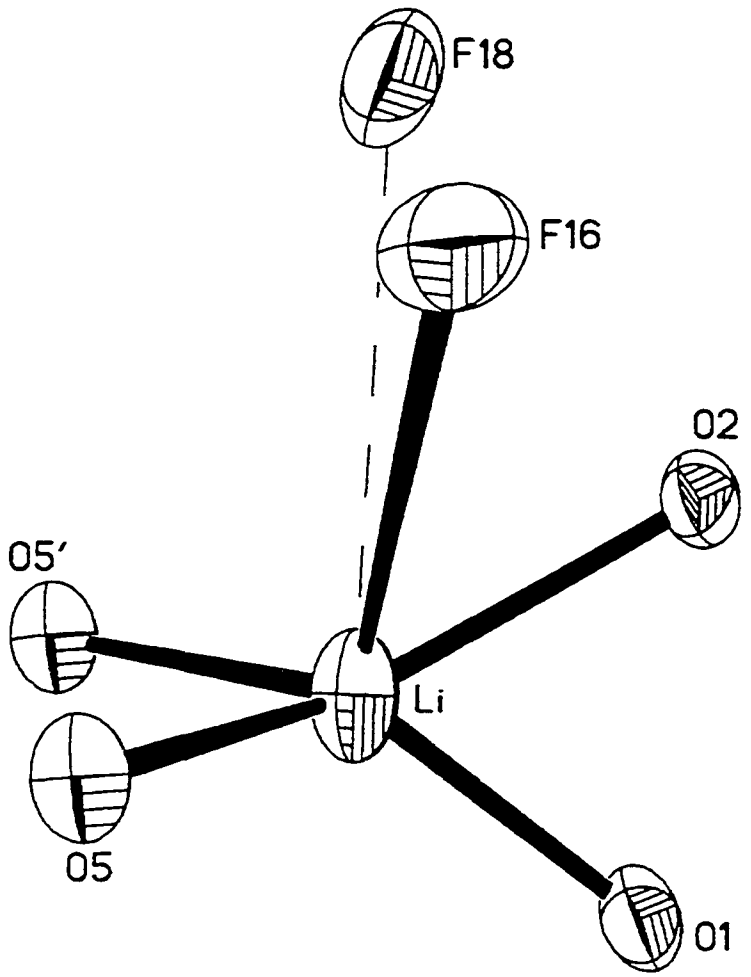

Figure 11. Drawing of the LiO_4F_2 coordination sphere of $Li(OC(CH_3)_2)B(HFTPOP\text{-}2,3,4)_2$ with 50% probability ellipsoids. See Table 2 for definition of abbreviation.

Electrochemical Stability of $LiB(O_2L_2)_2$

The electrochemical stability of the lithium borates was investigated using cyclic voltammetry. Oxidative and reductive stabilities were evaluated at a concentration of 0.1 M in EC/DMC (50:50 mol%) using a stainless steel working electrode, and lithium foil for the counter and reference electrodes. The oxidative stability was also measured at the same concentration in DME using a Pt disc working electrode, Pt mesh counter electrode, and lithium foil reference electrode.

Shown in Figure 12 is a voltammogram for $LiB(HFPOP)_2$ in EC/DMC illustrating the current response between 0 – 3 V (open-circuit potential E_R) vs. $Li^{0/+}$. There are two oxidation events at 1.2 and 2.1 V, and two reduction events at 0.5 and 1.9 V. All of these peaks are also observed in a $LiPF_6$ solution under the same conditions, and thus cannot be attributed to electrochemical reactions of the borate anion. They may be due to solvent impurities, or to the underpotential deposition and dissolution of lithium as proposed by Malik.[25] The residual current response over this potential range is essentially the same for all of the lithium borates studied; the only variation is in the current magnitude, which can be attributed to the different solution conductivities.

Figure 13 illustrates the reductive stability of $LiB(HFPOP)_2$ in EC/DMC in a voltammogram showing the current response between –0.5 – 3 V vs. $Li^{0/+}$. The reduction and oxidation events correspond to the plating and stripping of lithium. This occurs evenly, with a small loss in cycling efficiency as evidenced by a decreasing dissolution current. All other lithium borates exhibit similar behavior, and are stable with respect to reduction over this potential range.

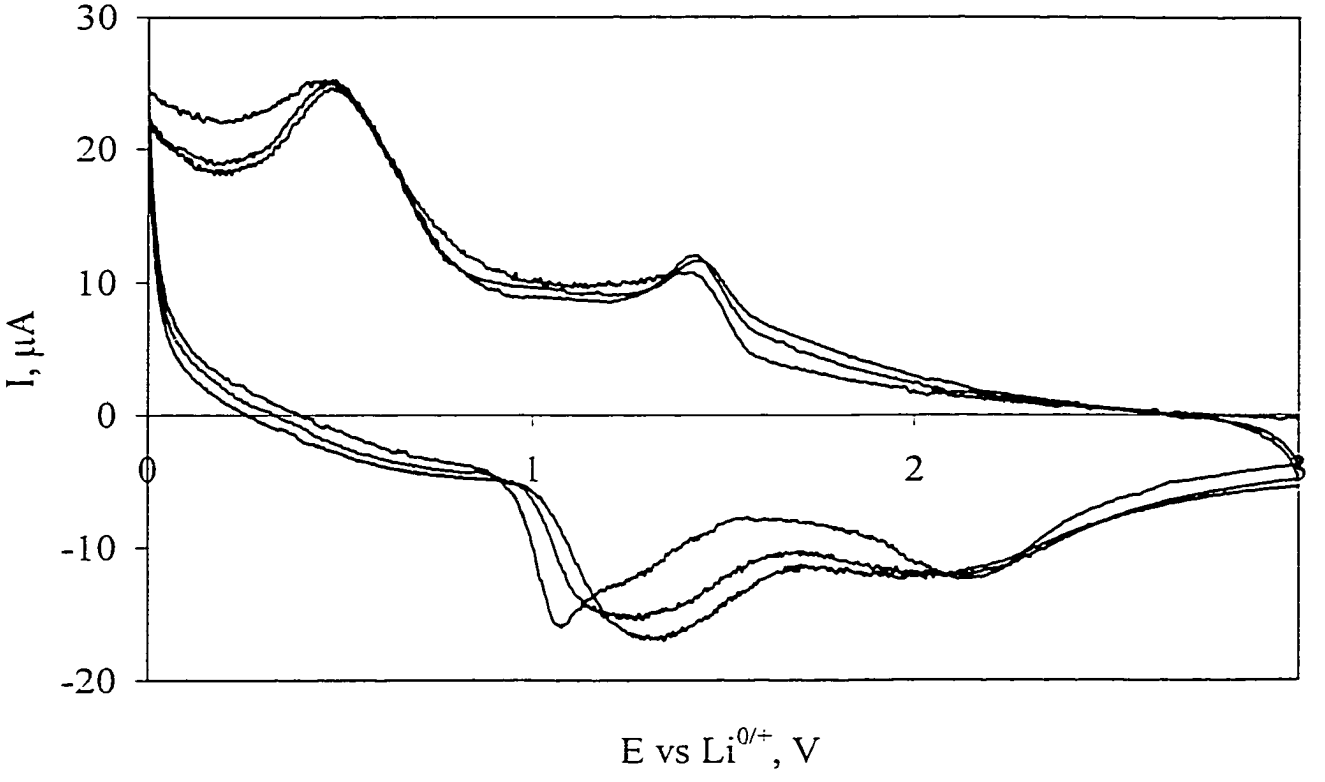

Figure 12. Voltammogram showing residual current over three scans (0 – 3 V vs. $Li^{0/+}$) for $LiB(HFPOP)_2$ in DME (0.1 M, stainless steel working electrode, Li metal counter and reference electrodes). See Table 2 for definitions of abbreviations.

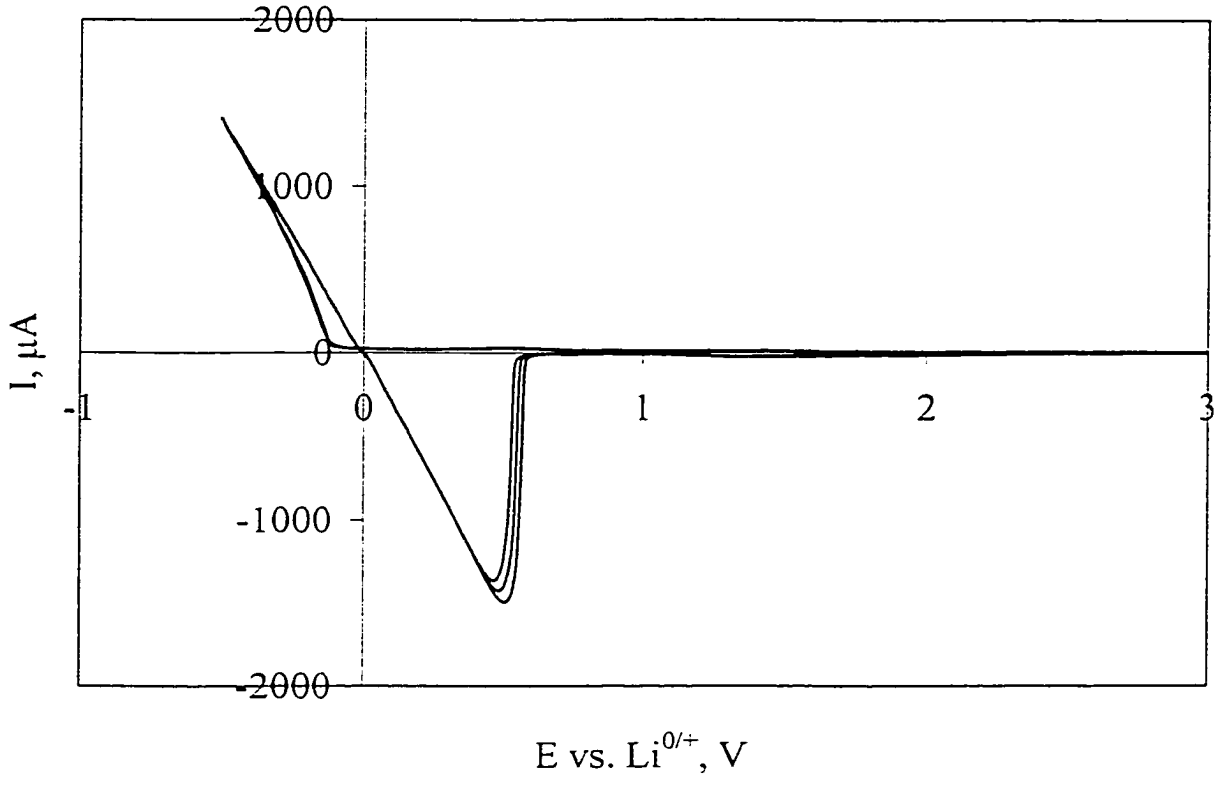

Figure 13. Voltammogram showing reductive stability for $LiB(HFPOP)_2$ and plating/stripping of lithium over three scans (–0.5 – 3 V vs $Li^{0/+}$) in DME (0.1 M, stainless steel working electrode, Li metal counter and reference electrode). See Table 2 for definitions of abbreviations.

The oxidative stability for each borate anion was also evaluated, and the potentials corresponding to anodic decomposition of each anion are listed in Table 10. E_{ox} was determined by linear extrapolation of the increasing oxidation current. Figure 14 shows the oxidative stability of four borate anions in EC/DMC: $B(HFPOP)_2^-$, $B(HFFPOP\text{-}4)_2^-$, $B(HFDPOP\text{-}3,4)_2^-$, and $B(HFTPOP\text{-}2,3,4)_2^-$. The sweep range is from E_R (3 V) to 6 V vs. $Li^{0/+}$, although only the first portion of the oxidation waves are shown. It can be seen that the addition of fluorine atoms to the ligand phenyl ring extends the oxidative limit of the borate anion to higher potentials, from 4.67 V ($B(HFPOP)_2^-$) to 5.16 V ($B(HFTPOP\text{-}2,3,4)_2^-$). This reflects a lowering of the anion HOMO energy resulting from fluorination; a similar effect was seen in the work of Barthel *et al.* with borates containing catecholate ligands with various degree of fluorine content.[1c] In contrast to conductivity, the potential at which the anion is oxidized does not appear to be significantly affected by the position of the fluorine atoms on the phenyl ring. Figure 15 illustrates the effect of increasing ligand fluorine content on the oxidative stability of the corresponding anion in a plot of E_{ox} vs. ring fluorine content. With the exception of the point for $B(HFPOP)_2^-$, each point on this plot corresponds to a mean value for the monofluoro, difluoro, and trifluoro derivatives. The relationship is linear, with an average increase of 0.15 V for each added fluorine atom.

The oxidative limits were also measured in DME using a Pt disk electrode. The same trend was observed as shown in Figure 16, but overall the potentials at which the anions are oxidized are lower (e.g. from 4.32 V for $B(HFPOP)_2^-$ to 4.84 V for $B(HFTPOP\text{-}2,3,4)_2^-$). These data are listed in Table 10. The potential shift could be due to the change in solvent or to the different working electrode. Figure 17 shows a plot similar to that in Figure 15, and again a linear relationship is seen between ring fluorine

Table 10. Potentials at which $B(O_2L_f)_2^-$ anions are oxidized in DME and EC/DMC vs. $Li^{0/+}$, as determined by linear extrapolation of the increasing oxidation current.

compound	E_{ox} in DME, V vs. $Li^{0/+}$	E_{ox} in EC/DMC,[a] V vs. $Li^{0/+}$)
$LiB(HFPOP)_2$	4.32	4.67
$LiB(HFFPOP\text{-}2)_2$	4.48	4.81
$LiB(HFFPOP\text{-}3)_2$	4.54	4.73
$LiB(HFFPOP\text{-}4)_2$	4.40	4.78
$LiB(HFDPOP\text{-}2,4)_2$	4.57	4.92
$LiB(HFDPOP\text{-}3,4)_2$	4.64	4.93
$LiB(HFDPOP\text{-}3,5)_2$	4.70	4.92
$LiB(HFTPOP\text{-}2,3,4)_2$	4.84	5.16
$LiB(HFTPOP\text{-}3,4,5)_2$	4.74	5.05
$LiB(HFAPOP)_2$	4.15	–

[a] 50:50 mol%. See Table 2 for definitions of abbreviations.

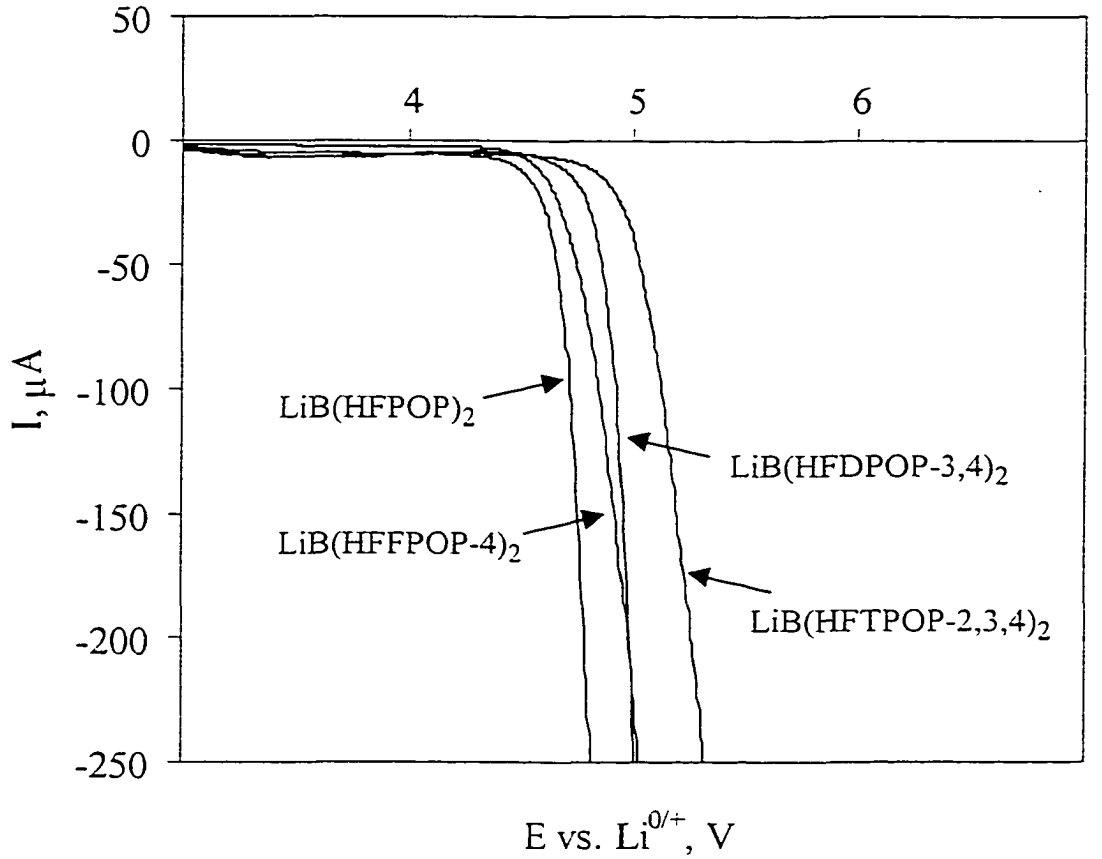

Figure 14. Oxidation of $B(O_2L_f)_2^-$ in EC/DMC (50:50 mol%) (0.1 M, stainless steel working electrode, Li metal counter and reference electrodes). See Table 2 for definitions of abbreviations.

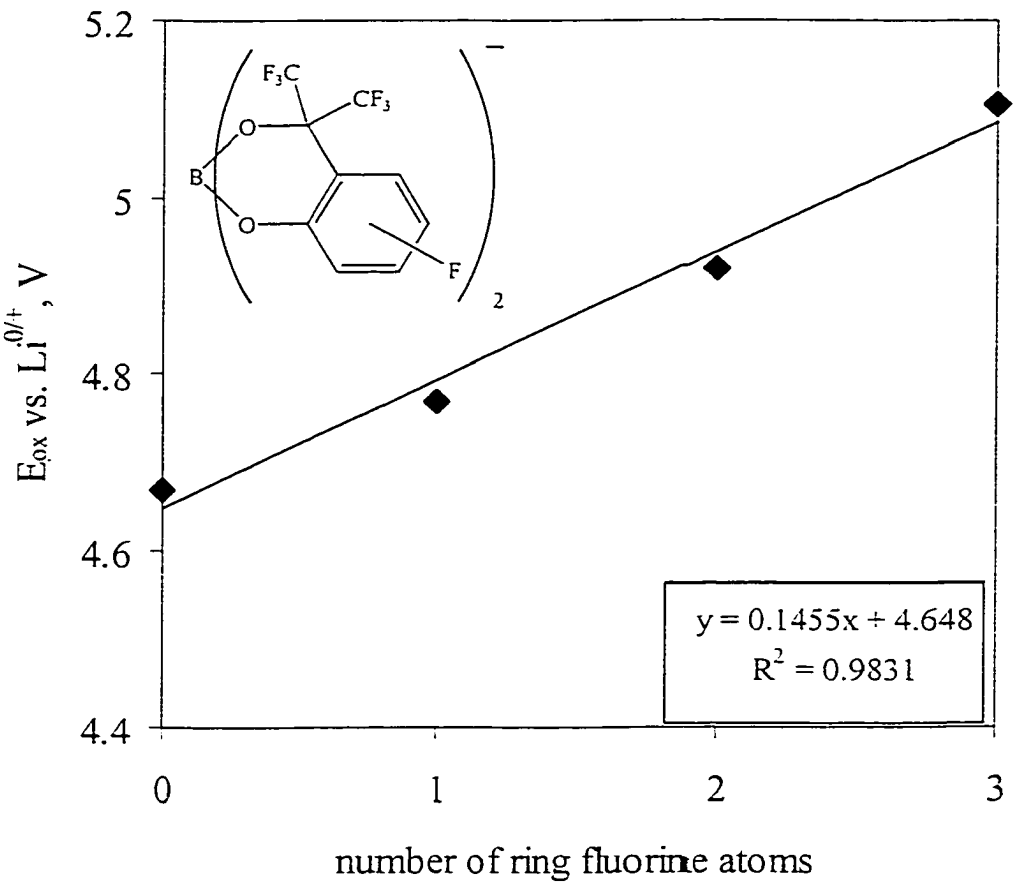

Figure 15. Plot showing the relationship between potential at which $B(O_2L_f)_2^-$ is oxidized and number of fluorine atoms on the ligand phenyl ring in EC/DMC (50:50 mol%). The points for F = 1, 2, 3 are mean values for the monofluoro, difluoro, and trifluoro isomers, respectively.

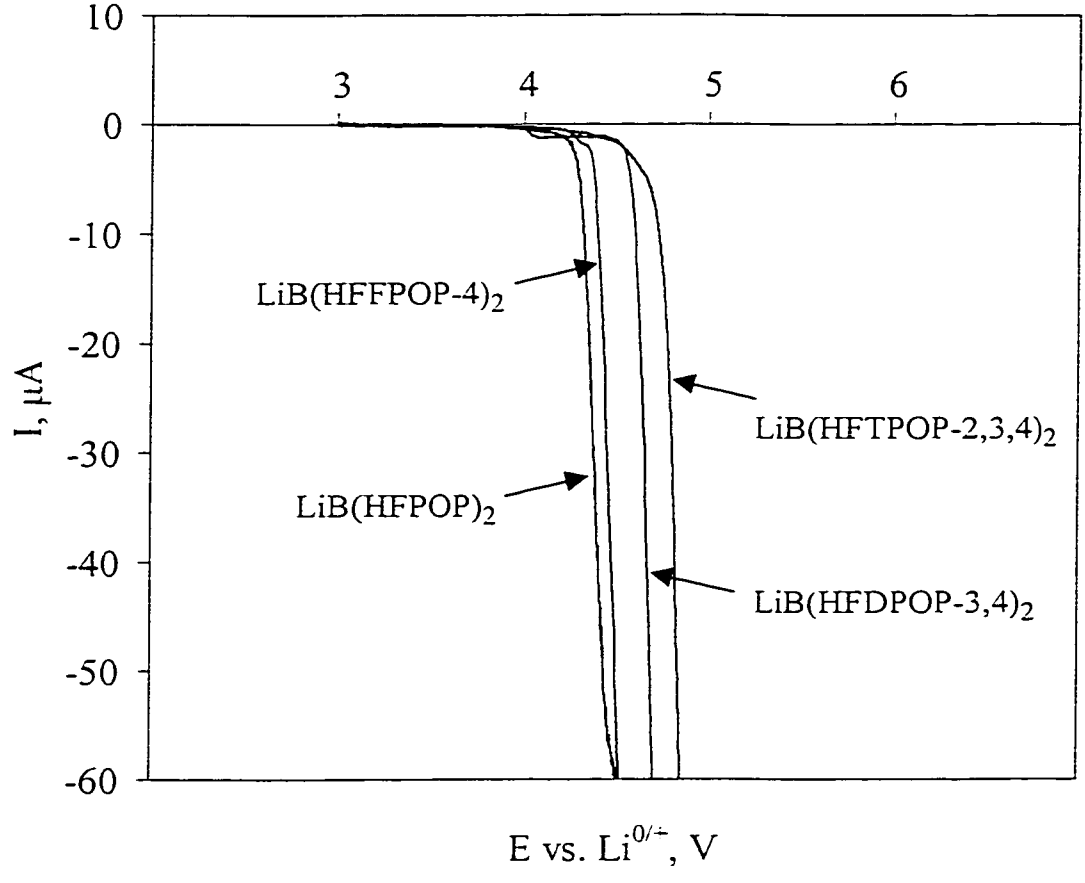

Figure 16. Oxidation of $B(O_2L_f)_2^-$ in DME (0.1 M, Pt disc working electrode, Pt mesh counter electrode, Li metal reference electrode). See Table 2 for definitions of abbreviations.

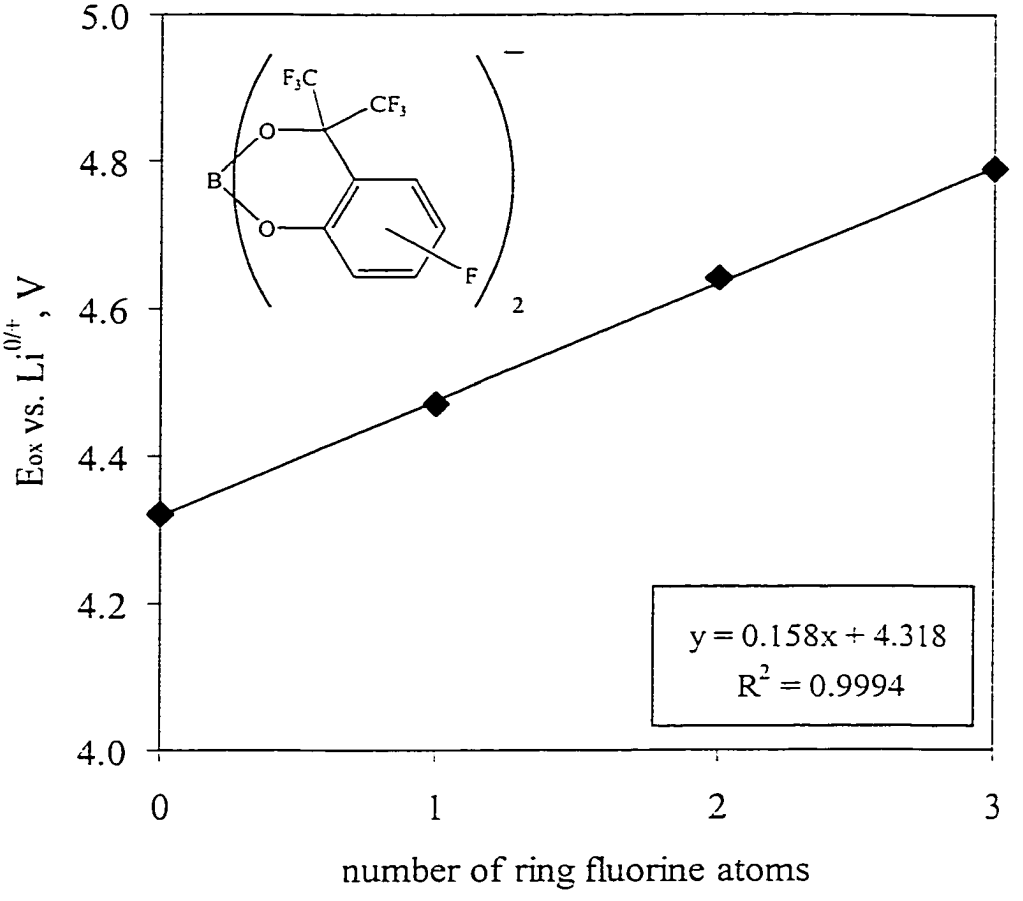

Figure 17. Plot showing the relationship between potential at which $B(O_2L_f)_2^-$ is oxidized and number of fluorine atoms on the ligand phenyl ring in DME. The points for F = 1, 2, 3 are mean values for the monofluoro, difluoro, and trifluoro isomers, respectively.

content and E_{ox}. The average increase of 0.16 V per added fluorine atom is virtually identical to that observed in EC/DMC. Overall, the data indicate that the new anions exceed the oxidative stability requirement of 4.2 V vs. $Li^{0/+}$, and do so in two solvents commonly used in lithium batteries.

As discussed earlier, two strategies, electronic and steric, were adopted to reduce the ion-pairing strength of the borate anions. The electronic approach of fluorination had the benefit of not only decreasing the ion-pairing strength, but also of increasing the oxidative stability as shown above. While the steric approach of incorporating a *t*-butyl group *ortho* to the phenoxy functionality was successful in decreasing the anion ion-pairing strength, the electronic effect was detrimental to oxidative stability. The electron-donating character of this group acts to increase the anion HOMO energy, thereby decreasing E_{ox}. This is illustrated in the voltammograms in Figure 18. The $B(HFAPOP)_2^-$ anion is oxidized at 4.15 V, lower than $B(HFPOP)_2^-$ and below the practical minimum. As such, this salt would not be a useful electrolyte for lithium batteries.

An interesting difference among the fluorinated borates is the presence or absence of electrode passivation as a result of anion oxidation. Its occurrence can be beneficial, in that electrolyte degradation due to oxidation is reduced after the initial passivation layer is formed. Of all the borates under study, only $B(HFPOP)_2^-$, $B(HFFPOP\text{-}3)_2^-$, and $B(HFDPOP\text{-}3,5)_2^-$ exhibit passivation, as shown in Figure 19. Each experiment was performed in DME with a Pt disc working electrode. The forward scan from 3–6 V vs. $Li^{0/+}$ is shown for each of three consecutive cycles; anion oxidation occurs in this range, and passivation is evidenced by a progressively decreasing current magnitude. The differences in current magnitudes among the three borates reflect different solution

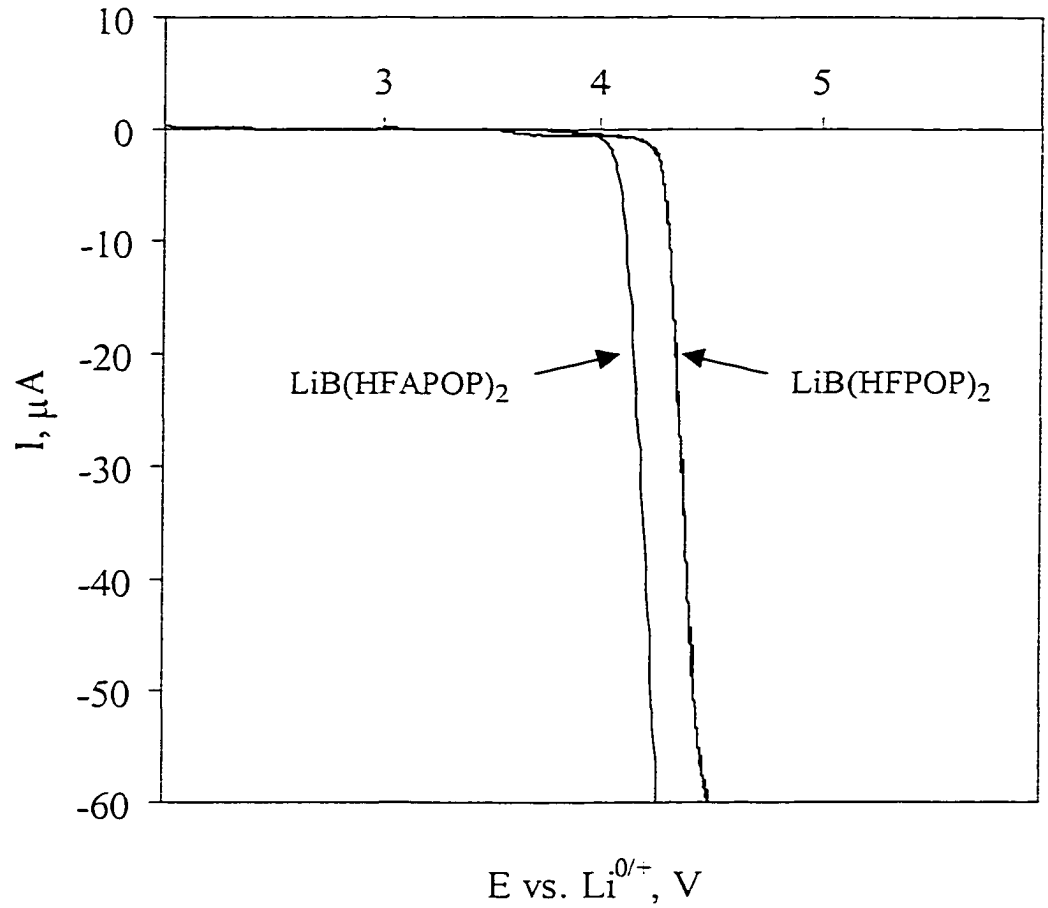

Figure 18. Oxidation of $B(O_2L_f)_2^-$ in DME (0.1 M, Pt disc working electrode, Pt mesh counter electrode, Li metal reference electrode). See Table 2 for definitions of abbreviations.

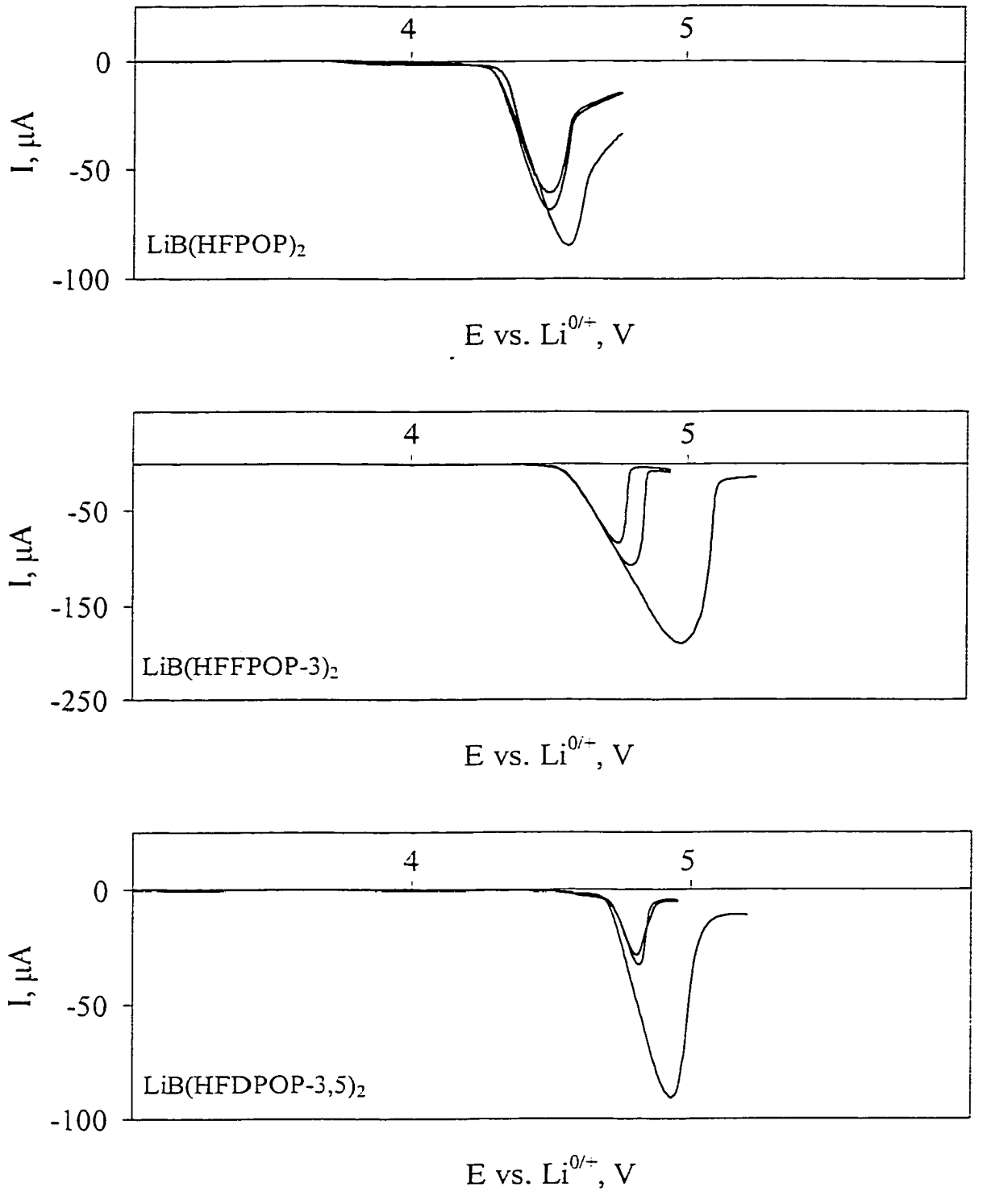

Figure 19. Oxidation of $B(O_2L_f)_2^-$ and electrode passivation in DME (0.1 M, Pt disc working electrode, Pt mesh counter electrode, Li metal reference electrode). Each set of voltammograms shows the forward scans for each of three consecutive cycles. See Table 2 for definitions of abbreviations.

conductivities, different rates of passivation, or a combination of both effects. All of the other borates under study did not exhibit this behavior; as an example, the cyclic voltammogram containing all three forward scans for the oxidation of $B(HFFPOP\text{-}4)_2^-$ is shown in Figure 20. The obvious difference between the two groups of anions is the incorporation of fluorine atoms in the *ortho* and *para* positions relative to the phenoxy functionality. Apparently, the oxidation products from anions of this type do not passivate the platinum surface. This could be due to their higher solubility in DME relative to the oxidation products from anions in the passivating group. It is especially interesting that anions with fluorine atoms in the *meta* position(s) on the phenyl ring *do* result in passivation. As was the case for determining conductivity, the pattern of fluorine substitution on the phenyl ring is also important in determining this behavior as well. The presence or absence of passivation was also investigated in EC/DMC using a stainless steel electrode, as shown in Figure 21. Similar results were observed, except that a higher degree of passivation (compared to experiments in DME) resulted from the oxidation of $B(HFPOP)_2^-$, $B(HFFPOP\text{-}3)_2^-$, and $B(HFDPOP\text{-}3,5)_2^-$. Also, only one scan was necessary to achieve a high degree of passivation.

The tendency of $LiB(O_2L_f)_2$ electrolytes to promote the corrosion of aluminum was investigated by chronoamperometric and cyclic voltammetric methods. Chronoamperometry was done at 4.2 V vs. $Li^{0/+}$, the required voltage minimum for practical use, for one hour. An acceptable current density is 1 $\mu A\ cm^{-2}$,[26] but for all salts the final current density was at least one order of magnitude less than this value, indicating no significant amount of Al corrosion under these conditions. A typical voltammogram is shown in Figure 22, for $LiB(HFFPOP\text{-}4)_2$. This figure also shows the response of $LiCF_3SO_3$ under the same conditions, which has been shown to promote the

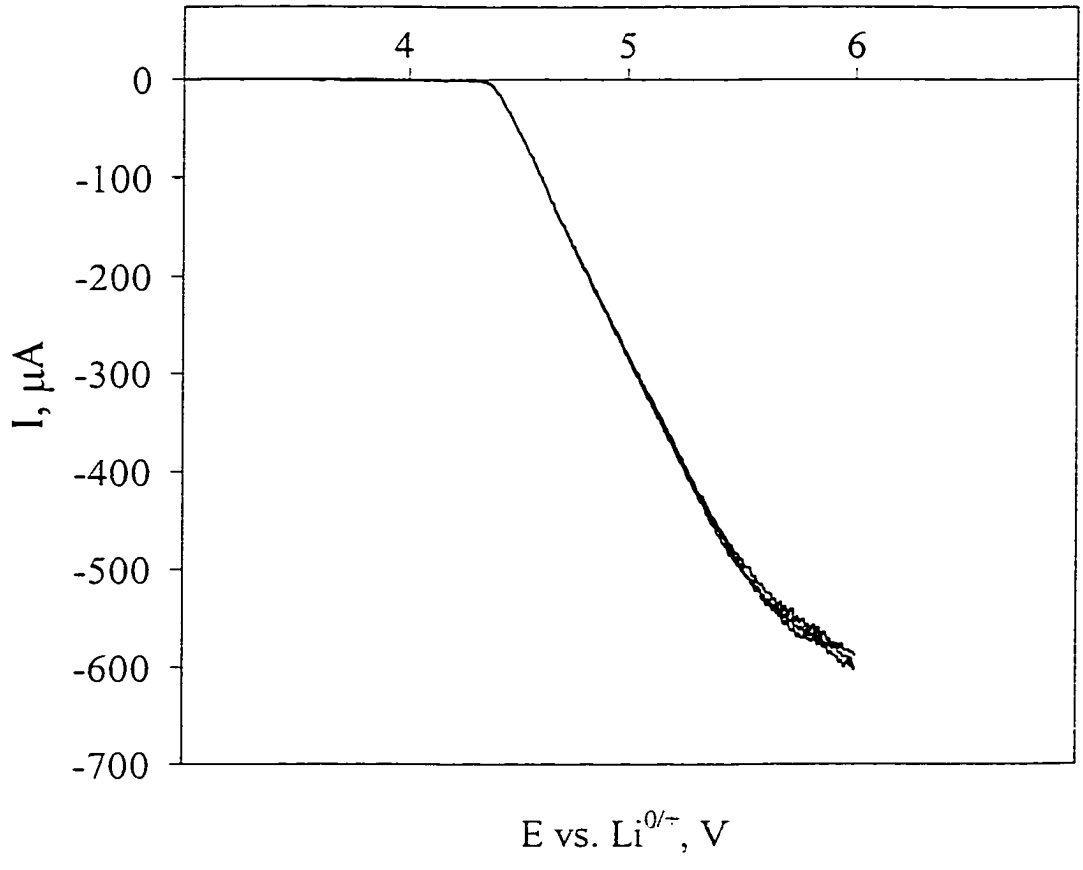

Figure 20. Oxidation of $B(HFFPOP\text{-}4)_2^-$ in DME (0.1 M, Pt disc working electrode, Pt mesh counter electrode, Li metal reference electrode). Forward scans of three consecutive cycles are shown. See Table 2 for definitions of abbreviations.

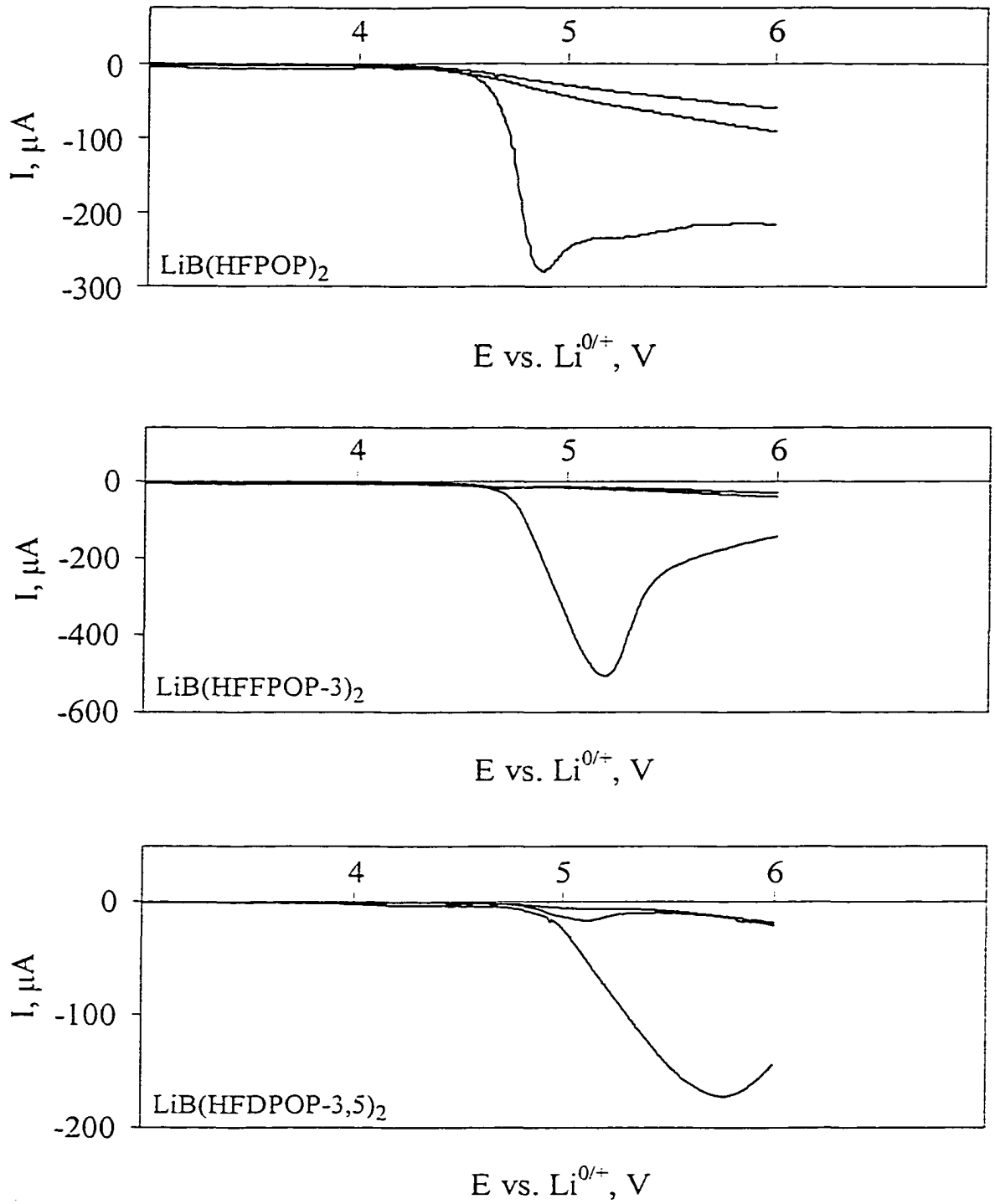

Figure 21. Oxidation of $B(O_2L_f)_2^-$ and electrode passivation in EC/DMC (50:50 mol%, 0.1 M, stainless steel working electrode, Li metal counter and reference electrodes). Each set of voltammograms shows the forward scans for each of three consecutive cycles. See Table 2 for definitions of abbreviations.

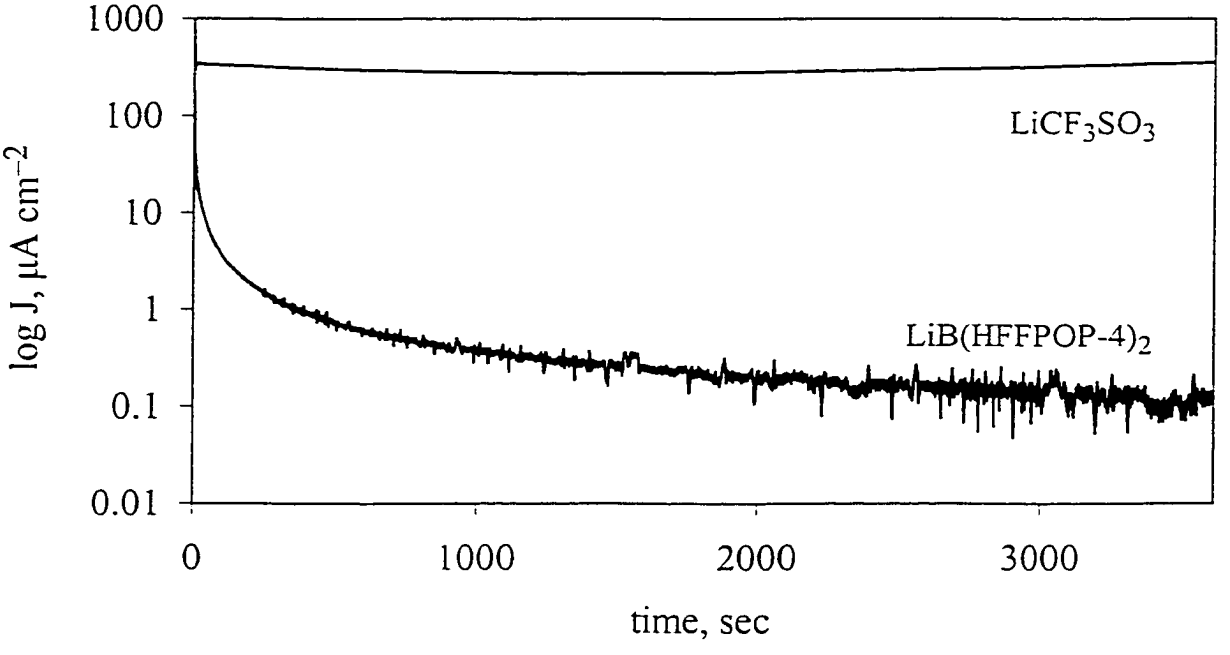

Figure 22. Plot showing the logarithm of current density at 4.2 V vs. $Li^{0/+}$ over one hour for 0.1 M LiB(HFFPOP-4)$_2$ and $LiCF_3SO_3$ in DME. Al foil working electrode, Li foil counter and reference electrodes. See Table 2 for definitions of abbreviations.

corrosion of aluminum even at 3.0 V.[27] Cyclic voltammetry was done to determine the potential at which significant Al corrosion occurs, if at all. Figure 23 illustrates a typical set of voltammograms for $LiB(HFFPOP\text{-}4)_2$, showing the current response over three scans. There is one oxidation event at ~4.8 V, and this is observed at approximately the same potential for every salt. If this were Al corrosion, the current should increase with each cycle, but this does not occur; instead, passivation is evidenced by a reduction in current magnitude. The two remaining possibilities are anion oxidation and solvent oxidation. It seems unlikely that all of the anions are being oxidized at the same potential, given the results from the oxidative stability tests. In terms of solvent oxidation, 4.8 V is below the potential at which DME is normally oxidized (5.1 V). However, it is possible that on an aluminum electrode, E_{ox} for DME is different, and could be lower. Given this possibility and the fact that the two potentials are similar, DME oxidation is a likely cause of the observed oxidation.

From a practical standpoint, it is desirable to know the maximum conductivity (κ_{max}) that can be achieved with a given electrolyte. Although minimum useful values vary depending on the application, a commonly cited figure of merit is 5 mS cm^{-1}.[28] The κ_{max} values for the $LiB(O_2L_f)_2$ salts were determined in DME and are listed in Table 11. Except for $LiB(HFAPOP)_2$, all of these exceed the 5 mS cm^{-1} minimum, and range from 5.39 to 8.39 mS cm^{-1} at a concentration of 0.5 M. In general, the trend in κ_{max} values agrees with the trend observed at 0.01 M, indicating that the conductivity at low concentration is a reliable predictor of the maximum conductivity that can be attained. The one exception to this is the relation between $LiB(HFFPOP\text{-}3)_2$ and $LiB(HFFPOP\text{-}4)_4$. At 0.01 M, the conductivity of the 4 isomer is greater than that of the 3 isomer. The same is true at 0.1 M, but at higher concentrations the conductivity of the

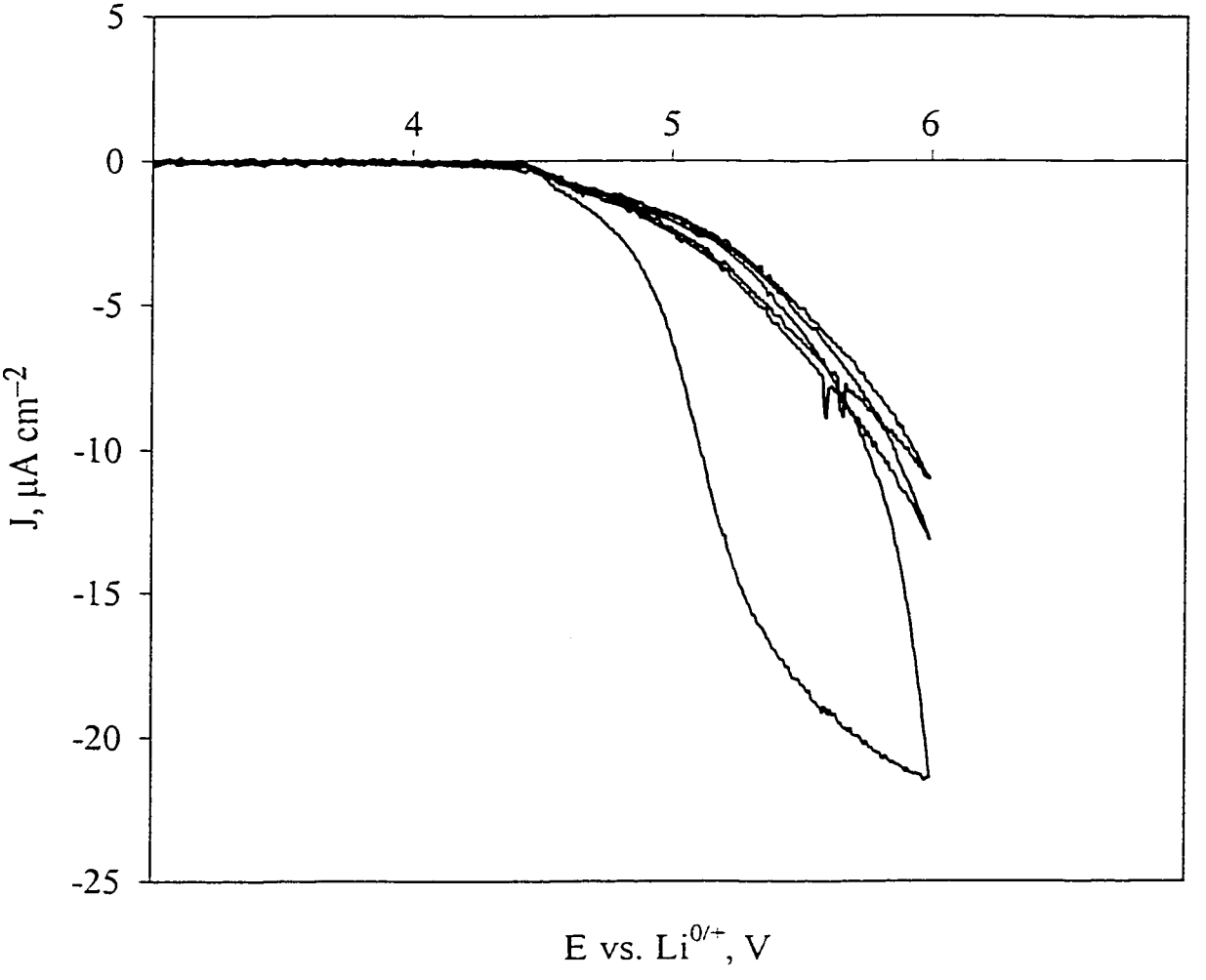

Figure 23. Voltammograms showing anodic current density for a cyclic voltammetry experiment with 0.1 M LiB(HFFPOP-4)$_2$ in DME. Al foil working electrode, Li foil counter and reference electrodes. See Table 2 for definitions of abbreviations.

Table 11. Maximum conductivities (κ_{max}) for $LiB(O_2L_f)_2$ salts in DME.

compound	κ_{max}, mS cm^{-1} [a]
$LiB(HFPOP)_2$	5.88
$LiB(HFFPOP\text{-}2)_2$	5.39
$LiB(HFFPOP\text{-}4)_2$	6.57
$LiB(HFFPOP\text{-}3)_2$	6.89
$LiB(HFDPOP\text{-}2,4)_2$	6.39
$LiB(HFDPOP\text{-}3,5)_2$	7.55
$LiB(HFDPOP\text{-}3,4)_2$	7.87
$LiB(HFTPOP\text{-}2,3,4)_2$	7.79
$LiB(HFTPOP\text{-}3,4,5)_2$	8.39
$LiB(HFAPOP)_2$	4.31

[a] Except for $LiB(HFAPOP)_2$ (0.4 M), all concentrations are 0.5 M. See Table 2 for definitions of abbreviations.

3 isomer is consistently higher. This is the only pair of salts that behaves in this manner, and the reason is unknown. The relatively low κ_{max} for $LiB(HFAPOP)_2$ reflects its large size. As mentioned earlier, both ion-pairing strength and ion mobility contribute to determining the overall conductivity. Even though the $B(HFAPOP)_2^-$ anion is more weakly ion-pairing that $B(HFPOP)_2^-$ as evidenced by 0.01 M conductivities, its large size does not allow a high κ_{max} to be achieved. The mobility of $B(HFAPOP)_2^-$ is low, and at high concentrations solutions of this salt presumably have a high viscosity, resulting in a low conductivity.

The determination of κ_{max} values is illustrated graphically in Figures 24, 25, and 26, for the monofluoro, difluoro, and trifluoro derivatives respectively. The same trend is seen in all of these: κ_{max} occurs at 0.5 M, followed by a decline in conductivity. The decline is most likely due to viscosity effects: as the concentration of electrolyte increases, the solution becomes more viscous, thereby reducing ion mobility. As the concentration increases a point is reached where the increase in charge carriers resulting from a concentration increase is overshadowed by a viscosity increase, and the conductivity begins to decrease. With the assumption that each borate anion is the same size, the observation that κ_{max} occurs at the same concentration in each case makes sense: each anion will have the same effect on limiting ion mobility in solution.

The maxima observed in DME for the $LiB(O_2L_f)_2$ salts are very encouraging, and the experimental conditions also represent a practical system, in that DME can be used as a solvent for primary lithium batteries. However, due to its reactivity with MCMB carbon (commonly used for the anode), it cannot be used in secondary (rechargeable) lithium-ion batteries. Instead, carbonate-based solvents are used, including ethylene carbonate (EC), dimethyl carbonate (DMC), diethyl carbonate (DEC), ethyl methyl

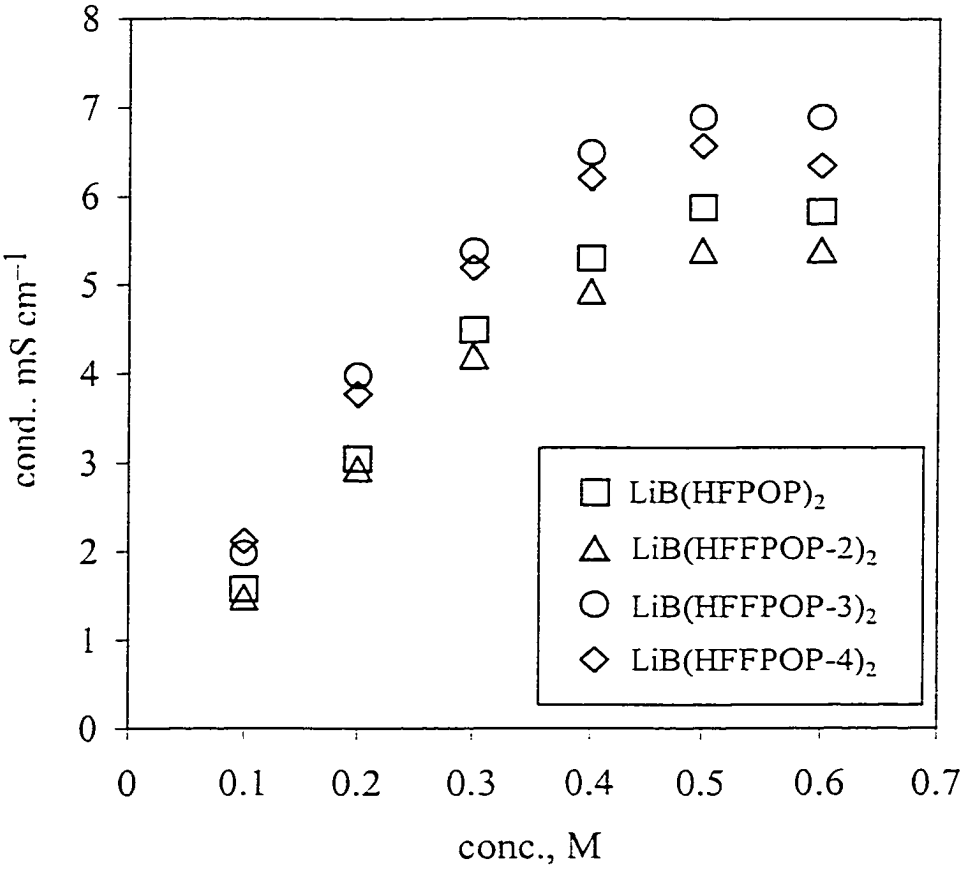

Figure 24. Plot of conductivity vs. concentration for monofluoro derivatives of $LiB(O_2L_f)_2$ salts in DME. See Table 2 for definitions of abbreviations.

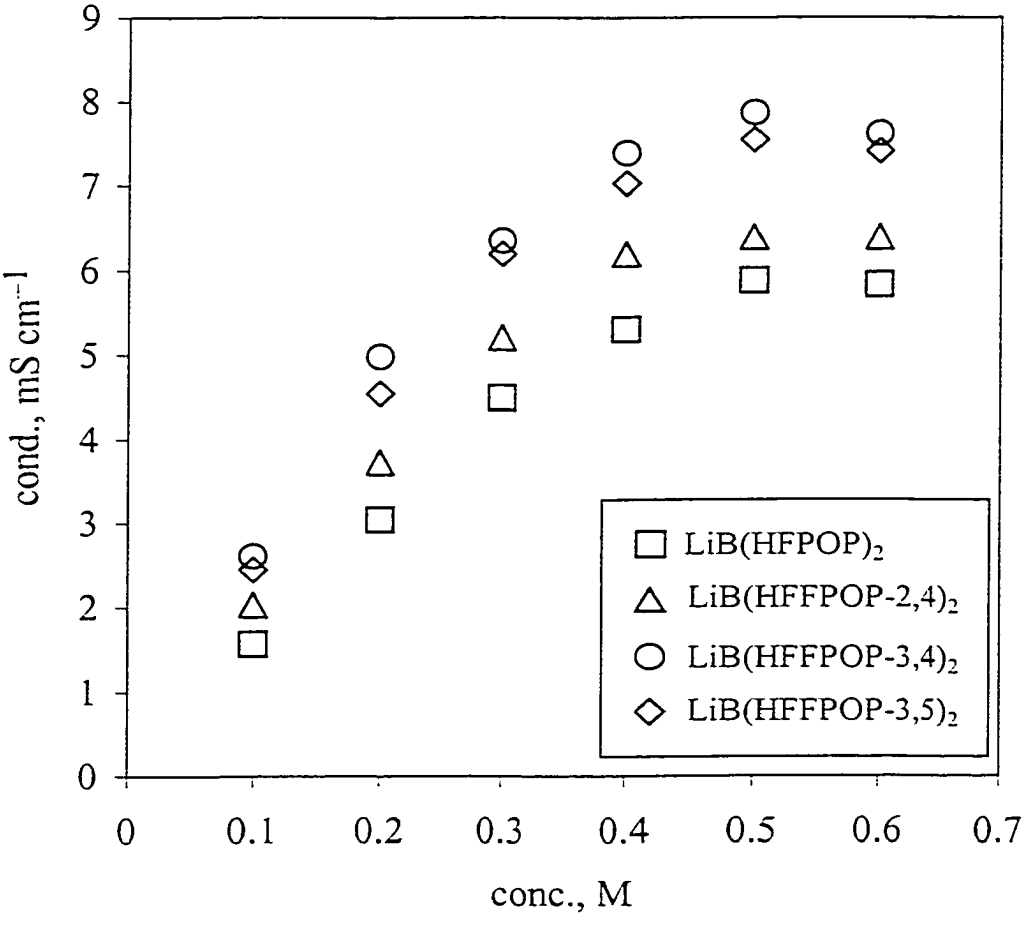

Figure 25. Plot of conductivity vs. concentration for difluoro derivatives of $LiB(O_2L_f)_2$ salts in DME. See Table 2 for definitions of abbreviations.

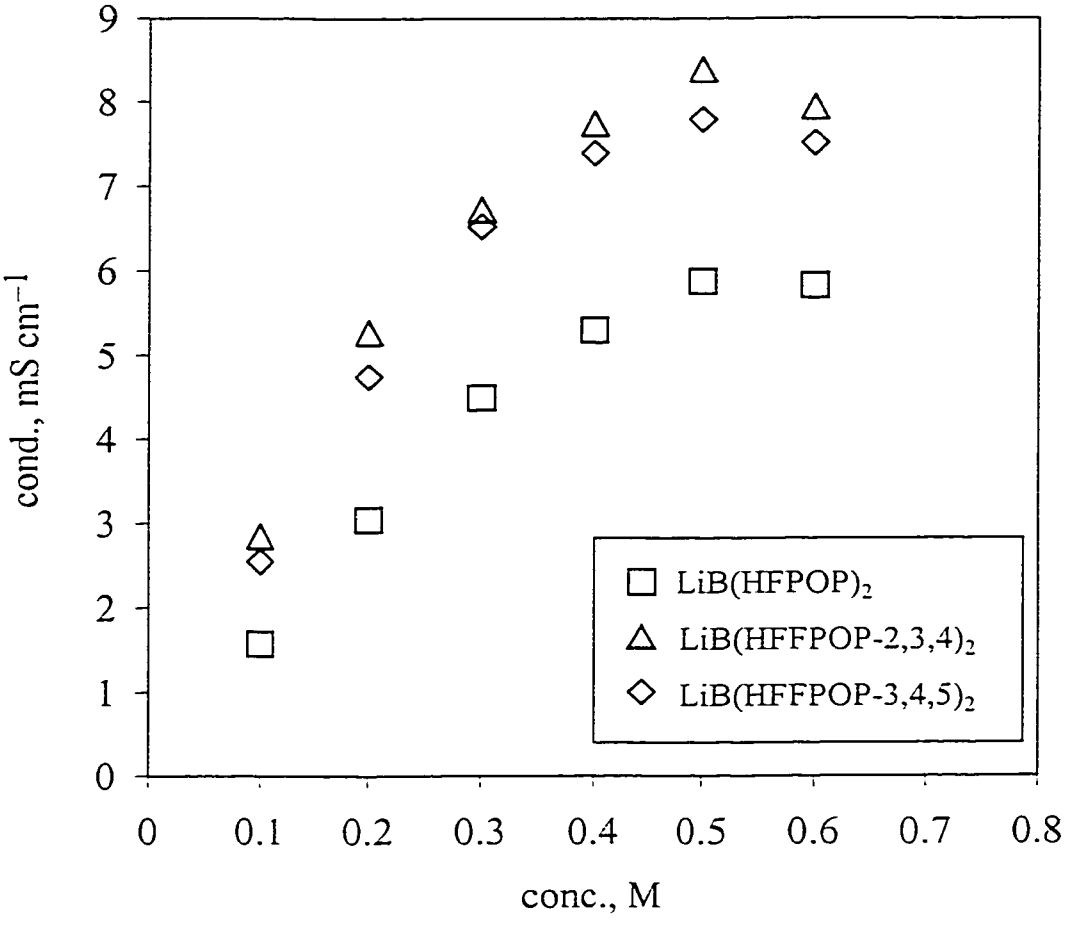

Figure 26. Plot of conductivity vs. concentration for trifluoro derivatives of $LiB(O_2L_f)_2$ salts in DME. See Table 2 for definitions of abbreviations.

carbonate (EMC), methyl propyl carbonate (MPC), and propylene carbonate (PC). One commonly used solvent is a 50:50 mol% mixture of EC and DMC, which combines the high permittivity of EC ($\varepsilon = 90.4$) with the low viscosity of DMC ($\eta = 0.59$ cP). The conductivity of $LiB(HFPOP)_2$ at 0.5 M was found to be 3.97 mS cm^{-1}, which is much lower than the maximum in DME, and below the practical minimum. The reduction in conductivity between solvents is most likely due to decreased ion mobilities. The EC/DMC mixture is more viscous that DME, and is thus more restrictive of ion movement.

Although the 50:50 mol% mixture of EC/DMC is a commonly used solvent for secondary batteries, this is only due to the nature of the lithium salts currently used. Specifically, $LiPF_6$ is the most commonly utilized lithium salt for these cells, and it has a maximum conductivity of 11.5 mS cm^{-1} in the EC/DMC mixture (25 °C, 1 M). The PF_6^- anion is much smaller than $B(HFPOP)_2^-$, and thus has a higher mobility. Its ion-pairing strength is greater than the borate anion, but the high solvent permittivity minimizes this problem. With this balance in mind, it was hoped that a similar optimal mixture could be found that would suit $LiB(HFPOP)_2$ and the other lithium borates. Less EC could be used, which would lower the viscosity, and the decrease in permittivity would not be a problem considering the weak ion-pairing strength of $B(HFPOP)_2^-$. Conductivities were measured at 0.5 M using various EC/DMC ratios, and the results are shown in Figure 27. Unfortunately, the desired effect was not observed: between 50% and 40% EC content, there is only an increase of 0.18 mS cm^{-1}, with a conductivity of 4.15 mS cm^{-1} in a 60/40 mol% EC/DMC mixture. Apparently, the viscosity is still too high to realize a high conductivity. The effect of permittivity can be seen upon further reducing the EC content; the conductivity steadily decreases to a value of 0.95 mS cm^{-1}

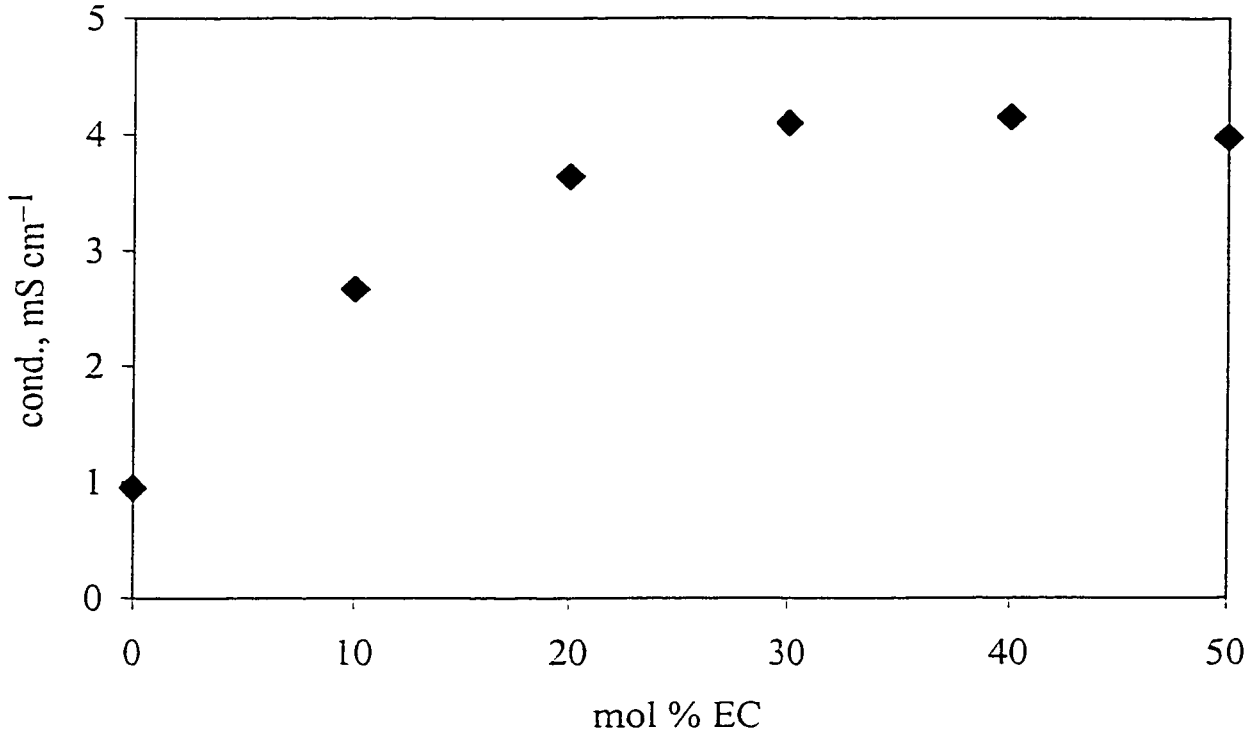

Figure 27. Plot of conductivity of 0.5 M LiB(HFPOP)$_2$ vs. mol% EC. The other solvent component is DMC. See Table 2 for definitions of abbreviations.

when the solvent is 100% DMC. It is also possible that the smaller donor numbers of both EC (16.4) and DMC (15.1) relative to DME (24) is having an effect. Although the fluorinated derivatives were not studied, it does not appear that EC and DMC in any ratio is a good solvent for $LiB(O_2L_f)_2$ electrolytes. A low-viscosity medium is necessary for these salts to yield a high conductivity.

A final detail to highlight is that not only do almost all of the new lithium salts exceed the practical minimum in DME, but also that they do so at a concentration of 0.5 M or lower. For many salts used commercially, a concentration of 1 M is required to achieve a useful conductivity. Consequently, even if the new salts are slightly more expensive than those used currently, the fact that less electrolyte would be required could result in a battery of similar or even lower cost.

Conclusions

A new class of weakly coordinating anions based on the general formula $B(O_2L_f)_2^-$ has been developed. Salts of these can be made readily and in high yield, and were found to be thermally and hydrolytically stable. Through conductivity studies, they were shown to be more weakly coordinating and more weakly ion-pairing than $CF_3SO_3^-$. The synthesis of a variety of anions that varied in terms of fluorine content and position on the ligand phenyl ring revealed the interesting effect that configuration can have on ion-pairing strength; in some comparisons it was found that the anion with *fewer* fluorine atoms had a weaker ion-pairing strength. Almost all of the lithium salts of the new anions were shown to satisfy the requirements for practical use in batteries, exhibiting high conductivities, oxidative and reductive stability, and stability in contact with

aluminum. Due to the combination of weak ion-pairing strength and stability under a variety of conditions, these anions should find use in many applications.

References

1. Farah, B.S.; Gilbert, E.E.; Litt, M.; Otto, J.A.; Sibilia, J.P. *J. Org. Chem.* **1965**, *30*, 1003.
2. Sheldrick, G.M., SMART/SAINT. Siemens Analyt. X-Ray Instr. Inc., Madison, WI, 1994.
3. Sheldrick, G.M., SHELXTL, vers. 5.03 (1994).
4. Flack, H.D. *Acta Crystallogr.* **1985**, *A39*, 876.
5. Bernardinelli, G.; Flack, H.D. *Acta Crystallogr.* **1985**, *A41*, 500.
6. Barbarich, T.J.; Handy, S.T.; Miller S.M.; Anderson, O.P.; Grieco, P.A.; Strauss, S.H. *Organometallics* **1996**, *15*, 3776.
7. (a) Barbarich, T.J.; Miller, S.M.; Anderson, O.P.; Strauss, S.H. *J. Mol. Catal.* **1998**, *128*, 289. (b) Ivanova, S.M; Nolan, B.G.; Kobayashi, Y.; Miller, S.M.; Anderson, O.P.; Strauss, S.H. *Chem. Eur. J.*, **2001**, *in press*.
8. (a) Barthel, J.; Wühr, Buestrich, R.; Gores, H.J. *J. Electrochem. Soc.* **1995**, *142*, 2527. (b) Barthel, J.; Buestrich, R.; Carl, E.; Gores, H.J. *J. Electrochem. Soc.* **1996**, *143*, 3565. (c) Barthel, J.; Buestrich, R.; Carl, E.; Gores, H.J. *J. Electrochem. Soc.* **1996**, *143*, 3572.
9. Tsujioka, S.T.; Strauss, S.H. *unpublished results*.
10. *Handbook of Chemistry and Physics*, 70th ed.; Weast, R.C., Lide, D.R., Astle, M.J., Beyer, W.H. Eds.; CRC Press: Boca Raton, 1989.
11. Dyachenko, V.I.; Galakhov, M.V.; Kolomiets, A.F.; Fokin, A.V. *Izv. Akad. Nauk SSSR, Ser. Khim.* **1989**, *4*, 923.

12. Dyachenko, V.I.; Kolomiets, A.F.; Fokin, A.V. *Izv. Akad. Nauk SSSR, Ser. Khim.* **1988**, *11*, 2557.

13. Farah, B.S.; Gilbert, E.E.; Sibilia, J.P. *J. Org. Chem.* **1965**, *30*, 998.

14. Barthel, J.; Gerber, R.; Gores, H.J. *Ber. Bunsenges. Phys. Chem.* **1984**, *88*, 616.

15. Fuoss, R.M.; Kraus, C.A. *J. Am. Chem. Soc.* **1933**, *55*, 2387.

16. Hojo, M.; Takiguchi, T.; Hagiwara, M.; Nagai, H.; Imai, Y. *J. Phys. Chem.* **1989**, *93*, 955.

17. (a) Hojo, M.; Tanio, A.; Miyauchi, Y.; Imai, Y. *Chem. Lett.* **1991**, 1827. (b) Hojo, M.; Imai, Y. *Bull. Chem. Soc. Jpn.* **1983**, *56*, 1963. (c) Bacelon, P.; Corset, J.; de Loze, C. *J. Solution. Chem.* **1980**, *9*, 129.

18. (a) Cavell, E.A.S.; Knight, P.C. *Z. Phys. Chem.* **1968**, *57*, 331. (b) Xu, M.; Obeid, N.; Eyring, E.M.; Petrucci, S. *J. Phys. Chem.* **1988**, *92*, 2789.

19. Gutmann, V. *Coordination Chemistry in Non-Aqueous Solvents*; Springer-Verlag: New York, 1968.

20. Nolan, B.G.; Barbarich, T.J.; Tsujioka, S.; Ivanova, S.M.; Fauber, B.P.; Brady, J.C.; Kriley, C.E.; Miller, S.M.; Anderson, O.P.; Bell, A.; Strauss, S.H. manuscript in preparation.

21. Urban, J.J.; von Tersch, R.L.; Famini, G.R. *J. Org. Chem.* **1994**, *59*, 5239.

22. Strauss, S.H. "New Weakly Coordinating Anions $CB_{11}H_{12-n}F_n^-$, $CB_9H_{10-n}F_n^-$, and $Al(OR_F)_4^-$: Is Perfluorination Achievable, and, If So, Is It Desirable," 215th ACS National Meeting, Dallas, TX (March/April 1998), abstract INOR 404.

23. Allen, F.H.; Kenard, O.; Watson, D.G.; Brammer, L.; Orpen, A.G.; Taylor, R. *J. Chem. Soc. Perkin Trans. II* **1987**, S1.

24. Barbarich, T.J., Ph.D. Dissertation, Colorado State University, 1999.

25. Malik, Y.; Aurbach, D.; Dan, P.; Meitav, A. *J. Electroanal. Chem.* **1990**, *282*, 73.

26. Tsujioka, S.T. *personal communication*.

27. Blomgren, G.E.; In *Lithium Batteries*; Gabano, J.P., Ed.; Academic Press, Inc.: New York, 1983; Ch. 2.

28. Barthel, J.; Wühr, Buestrich, R.; Gores, H.J. *J. Electrochem. Soc.* **1995**, *142*, 2527.

CHAPTER 3

New Weakly Coordinating Anions Based on Polyfluoroalkoxyaluminates

The class of weakly coordinating anions comprised of polyfluoroalkoxyaluminates possesses several beneficial properties, as described in Chapter 1 of this dissertation. This chapter describes the continued development of this class of anions, with the synthesis and characterization of new varieties with improved properties. The use of this class of compounds as a whole as potential battery electrolytes is also addressed. As in Chapter 2, many abbreviations are used for the fluoroalkoxide ligands; see Table 2 for definitions of these abbreviations and structures.

Experimental

Materials

Schlenk, glovebox, and high vacuum techniques were employed, with purified argon used when an inert atmosphere was required. All reagents and solvents were reagent grade or better. The compound $LiAlH_4$ was recrystallized from diethyl ether and stored in a glovebox. The compounds $HOC(CF_3)_3$ (H(PFTB); Fluorochem, 97%), $HOC(C_6H_5)(CF_3)_2$ (H(HFPP); Central Glass Co., Ltd.), $HOC(4\text{-}C_6H_4(CH_3))(CF_3)_2$ (H(HFTP); Fluorochem, 95%), and $HOCH(C_6H_5)(CF_3)$ (H(TFPE) (mixture of enantiomers); Fluorochem, 98%) were dried over activated 4Å molecular sieves and vacuum distilled. The compounds $LiAl(HFBuPP)_4$ and $LiAl(HFPP)_4$ were prepared according to the procedures developed by Mr. Shoichi Tsujioka.[1] The compound

$LiAl(HFTB)_4$ was prepared according to the procedure developed by Dr. Ingo Krossing.[2] The compounds $LiAl(PFTB)_4$ and $LiAl(HFTP)_4$ were prepared according to the procedures developed by Dr. Thomas Barbarich.[3] The compound $LiAl(TFPE)_4$ was prepared by Dr. Svetlana Ivanova and used as received. The following solvents were purified by distillation under nitrogen or under vacuum from the indicated drying agent: toluene (Fisher, Na); dichloromethane (Fisher, P_2O_5); 1,1,2-$C_3Cl_3F_3$ (Freon-113, Aldrich; P_2O_5); chlorotrifluoromethane (Aldrich, P_2O_5); acetonitrile (ACN, Fisher, P_2O_5); 1,2-dimethoxyethane (DME, Acros, Na); hexafluorobenzene (P_2O_5); 1,2-difluorobenzene (P_2O_5); acetonitrile-d_3 (Cambridge, CaH_2); benzene-d_6 (Cambridge, Na). Ethylene carbonate (EC, Mitsubishi Chem.) and dimethyl carbonate (DMC, Mitsubishi Chem.) were battery grade and were used as received. Hexane (Fisher) was stirred over concentrated sulfuric acid, passed through a column of alumina, and distilled under nitrogen from sodium.

HOC(*cyclo*-C_6H_{11})$(CF_3)_2$ (H(HFCP)). $HOC(C_6H_5)(CF_3)_2$ (19.1 g, 78.3 mmol) and rhodium on carbon (0.167 g 5% Rh/C, 0.081 mmol Rh) were combined to make a suspension. This mixture was stirred at room temperature under 80 psi H_2 for 4 d. After this time, the suspension was filtered through Celite to yield HOC(*cyclo*-C_6H_{11})$(CF_3)_2$ as a clear colorless liquid (18.2 g, 93%). ^1H NMR (C_6D_6) δ 2.12 (s, 1 H), 0.86 – 1.83 (11 H); ^{19}F NMR (C_6D_6/C_6F_6) δ –72.72 (s).

HOC(*cyclo*-C_6H_{11})$_2(CF_3)$ (H(DCTE)). $HOC(C_6H_5)_2(CF_3)$ (2.00 g, 7.93 mmol) was dissolved in 25 mL of ethanol, and Rh (0.2 g 5% Rh/C, 0.097 mmol Rh) was added to make a suspension. This mixture was stirred at room temperature under 80 psi H_2 for 4 d. After this time, the suspension was filtered through Celite and ethanol removed under vacuum to yield HOC(*cyclo*-$C_6H_{11})_2(CF_3)$ as a clear colorless liquid

(1.98 g, 95%). ^{1}H NMR (C_6D_6/C_6F_6) δ 1.55 (s, 1 H), 0.99 – 1.86 (22 H); ^{19}F NMR (C_6D_6/C_6F_6) δ –68.97 (s).

HOC(2-C_6H_4(HOC(CF_3)$_2$)(CF_3)$_2$ (H_2(1,2-HFAB)). $Li_2(OC(C_6H_4)(CF_3)_2)$ was generated following the procedure of Martin *et al.*[4] *n*-BuLi (86.9 mmol) and TMEDA (1.01 g, 8.69 mmol) were dissolved in 50 mL diethyl ether and stirred for 30 min. After degassing the solution and cooling to 0 °C, $HOC(C_6H_5)(CF_3)_2$ (9.634 g, 39.5 mmol) was added as a solution in ether (15 mL). This mixture was stirred at 0 °C for 30 min, then at room temperature for 20 h. After degassing this solution, hexafluoroacetone (6.56 g, 39.5 mmol), which had been measured out in a calibrated bulb using a high-vacuum line (10^{-5} torr), was added at 0 °C, and the mixture stirred for 2 d. After this time, an aqueous solution of H_2SO_4 was added. The organic layer was isolated, and the aqueous layer washed twice with 20-mL portions of ether. The organic fractions were combined, and washed twice with brine. Volatiles were then removed to leave a yellow oil. This was recrystallized from hexane/$CHCl_3$ (20:1 v:v) to yield HOC(2-C_6H_4(HOC(CF_3)$_2$)(CF_3)$_2$ as a slightly yellow solid (4.65 g, 29%). ^{1}H NMR (C_6D_6) δ 7.69 (m, 2 H), 6.72 (m, 2 H), 5.50 (s, 2 H); ^{19}F NMR (C_6D_6/C_6F_6) δ –72.81 (s).

LiAl(DPTE)$_4$. To a suspension of $LiAlH_4$ (0.226 g, 5.94 mmol) in hexane (200 mL) was added H(DPTE) (3.00 g, 11.9 mmol) as a solution in hexane (200 mL) at room temperature. This mixture was stirred at room temperature for 18 h, under reflux for 23 h, and then at room temperature again for an additional 50 h. After this time, there was much white solid suspended in a clear, colorless solution. This was filtered, and the filtered solid washed with 200 mL toluene. Volatiles were removed to yield $LiAl(DPTE)_4$ as a white solid (1.85 g, 60%). ^{1}H NMR (C_6D_6) δ 7.00 (m, 24 H), 7.27 (m,

16 H); ^{19}F NMR ($C_6D_6/CFCl_3$) δ –72.40 (s). Low-resolution mass spectrum ((–)ES-MS, CH_3CN solution) *m/z* 1031.0 [$(M - Li)^-$; calcd for $C_{56}H_{40}AlF_{12}O_4$ 1031.0].

LiAl(HFCP)$_4$. A suspension of $LiAlH_4$ (0.375 g, 9.86 mmol) was first prepared in hexane (40 mL). At 0 °C, H(HFCP) (4.93 g, 19.7 mmol) was added to this dropwise (over 10 min) as a solution in hexane (20 mL). This was stirred at 0 °C for 8.5 h, warmed to room temperature, and stirred for 12 h. The mixture was then stirred under reflux for 24 h. After this time, the cloudy gray mixture was filtered to leave a clear, colorless solution. Volatiles were removed from the filtrate to leave a clear colorless oil, which partially solidified after 18 h under vacuum. This was recrystallized from CH_2Cl_2, yielding LiAl(HFCP)$_4$ as clear colorless crystals (3.29 g, 65%). ^1H NMR (C_6D_6) δ 1.94 (m, 4 H), 1.89 (m, 2 H), 1.24 (m, 4 H), 1.02 (m, 1 H); ^{19}F NMR (C_6D_6/C_6F_6) δ –72.32 (s). Low-resolution mass spectrum ((–)ES-MS, CH_3CN solution) *m/z* 1023.2 [$(M - Li)^-$; calcd for $C_{36}H_{44}AlF_{24}O_4$ 1023.0].

Physical Measurements

Samples for NMR spectroscopy were solutions in 5 mm glass tubes. NMR spectra were recorded on a Varian 300 spectrometer operating at the indicated frequencies: ^1H, 300.1 MHz; ^{19}F, 282.4 MHz. Chemical shifts (δ scale) are relative to $SiMe_4$ (δ = 0 for ^1H NMR) and $CFCl_3$ (δ = 0 for ^{19}F NMR). Negative-ion electrospray ionization mass spectra (ES^-) were recorded on a Fisons VG Quattro-SQ mass spectrometer. Solution conductances were measured at 24±1 °C using a YSI Model 3403 conductivity cell calibrated for inverted use (k = 0.9988 cm^{-1}) and a YSI Model 32 conductivity bridge. The bridge was operated at 1 KHz (conductances > 100 μS) or at

line frequency (50–60 Hz, conductances <100 μS). Measurements made using both modes were the same, but a sharper null point is observed at 1 KHz for higher conductances, and at line frequency for lower conductances. All samples were anhydrous as determined by ^{1}H NMR spectroscopy, and solutions of these were prepared in volumetric flasks in the glovebox. The error in measurement was determined to be < 1% using the same batch of material. Variation from one batch to another was found to be 2% or less.

Crystals of $LiAl(HFCP)_4$ were grown from a hexane solution at 4 °C, and crystals of $LiAl(HFIP)_4$ were grown from a benzene/hexafluorobenzene (10:1 v:v) solution at room temperature. In both cases, suitable crystals were examined under an argon atmosphere and were placed in the cold nitrogen stream of the low-temperature LT-2 unit of a Siemens SMART CCD diffractometer system. The diffraction data collection and subsequent structural computations were performed using the crystallographic software supplied by Siemens[5] or by Professor G.M. Sheldrick.[6] Lorentz and polarization corrections were applied to the data. Details of the crystallographic experiment and subsequent computations are summarized in Tables A.3, A.4 (40%, 60% $LiAl(HFCP)_4$, respectively) and A.5 ($LiAl(HFIP)_4$), and can be found in the appendix.[7,8] The structures were solved by direct methods and were refined using full-matrix least-squares procedures on F^2 for all data. Non-hydrogen atoms were refined anisotropically. Hydrogen atoms were placed in calculated positions.

Results and Discussion

Synthesis of HOR_f

H(HFCP) and the new fluoroalcohol H(DCTE) were synthesized by catalytic hydrogenation of $HOC(C_6H_5)(CF_3)_2$ and $HOC(C_6H_5)_2(CF_3)$ over Rh/C. Alcohol/Rh ratios of 966:1 and 326:1 were used to make H(HFCP) and H(DCTE), respectively. Higher ratios were found to work as well, but the reaction times were longer. Overall, this method was very successful in synthesizing the two alcohols: the only purification necessary was filtration to remove Rh/C (and removal of ethanol in the case of H(DCTE)), and isolated yields were very high (95% for H(DCTE), 93% for H(HFCP)). The previously reported method for synthesizing H(HFCP) consisted of a free-radical-initiated reaction between cyclohexane and HFA,[9] resulting in a 69% isolated yield of the fluoroalcohol.

The synthesis of H_2(1,2-HFAB) completes the series of bis(2-hydroxyhexafluoro-2-propyl)benzene derivatives. The 1,3- and 1,4- varieties have been reported, and were made by $AlCl_3$-catalyzed electrophilic aromatic substitution of benzene with HFA.[10] The 1,2- isomer was not formed in this reaction, presumably due to steric hindrance. The first attempt to synthesize a 1,2-diol consisted of the reaction of H(HFBuPP) with HFA in the presence of $AlCl_3$. It was hoped that the *t*-butyl group would favor substitution of HFA in the *ortho* position by (a) blocking the *para* site, and (b) effectively blocking the *meta* site by steric hindrance. However, no reaction was observed. This could be due to excessive steric hindrance at both the *ortho* (from $-C(OH)(CF_3)_2$ group) and *meta* (from

t-butyl group) sites. The successful synthesis of H_2(1,2-HFAB) resulted from the reaction of *ortho*-lithiated $HOC(C_6H_5)(CF_3)_2$ (H(HFPP)) with HFA in diethyl ether. Adding two equivalents of *n*-BuLi to H(HFPP) in the presence of TMEDA leads to an *ortho*-lithiated dianion (after deprotonation of the alcohol).[4] This can then react with HFA, overcoming the steric hindrance barrier to form Li_2(1,2-HFAB). Protonation with H_2SO_4 followed by recrystallization yielded H_2(1,2-HFAB) in 29% yield. This diol may be useful as a bidentate ligand: both oxygen atoms are weak donors, but it could form stable complexes with a central atom by virtue of its chelating nature.

Synthesis of New $LiAl(OR_f)_4$ Salts

The first attempt to synthesize $LiAl(HFCP)_4$ utilized the same conditions for the successful synthesis of $LiAl(HFPP)_4$ (room temperature, hexane solvent, 2:1 alcohol:LAH ratio, 18 h reaction time, 95% isolated yield). However, unlike the crude product mixture for $LiAl(HFPP)_4$, numerous impurities were observed by NMR spectroscopy in the $LiAl(HFCP)_4$ mixture. Furthermore, the reaction did not go to completion as evidenced by some remaining H(HFCP). In another trial, the reaction mixture was heated at reflux after first stirring at room temperature for 18 hours. This resulted in a more complete reaction, but similar non-alcohol impurities were observed, and in similar relative amounts to the desired lithium aluminate. This indicated that the impurities were most likely formed in the initial stages of the reaction; based on this assumption, the next trial consisted of adding H(HFCP) dropwise to a suspension of LAH in hexane at 0 °C, followed by stirring at room temperature and then at reflux to drive the reaction to completion. Although the impurities were still observed in the crude mixture,

their amounts relative to $LiAl(HFCP)_4$ were much less. Recrystallization from dichloromethane yielded $LiAl(HFCP)_4$ in 65% yield with ~1% impurities as indicated by ^{19}F NMR spectroscopy. One of these was tentatively identified by negative-ion electrospray mass spectrometry as $LiAl(HFCP)_3(HFPP)$, indicating that the H(HFCP) reagent still contained some unhydrogenated H(HFPP).

The synthesis of $LiAl(HFIP)_4$ was also found to be the most successful (95% isolated yield) when the addition of H(HFIP) to LAH was done dropwise at 0 °C. In this case, Freon-113 was used as the solvent due to the extremely low solubility of H(HFIP) in hexane. A 5:1 H(HFIP):LAH ratio was found to be optimal. The mixture was stirred for 18 hours at 0 °C, and although no heat was required to drive the reaction to completion, the procedure includes an additional five days of stirring at room temperature following the initial 18 hours. After removing excess H(HFIP) and volatile materials, the crude reaction mixture consisted of only $LiAl(HFIP)_4$ as evidenced by ^1H and ^{19}F NMR spectroscopy.

The preparation of $LiAl(HFCP)_4$ was most efficient when only two equivalents of H(HFCP) were used (also for $LiAl(HFPP)_4$, $LiAl(HFTP)_4$, $LiAl(DPTE)_4$). One might expect that a mixed alkoxide/hydride species such as $LiAlH_2(OR_f)_2$ would be obtained from a reaction with this stoichiometry. This is even more expected considering that a Li–H bond in $LiAlH_4$ is probably more reactive than a Li–H bond in $LiAlH_3(OR_f)$. To explain this, the following reaction scheme is proposed.

$$LiAlH_{4(s)} + H(OR_f)_{(soln)} \xrightarrow[H_2]{\text{hexane, slow}} LiAlH_3(OR_f)_{(soln)} \qquad (1)$$

$$LiAlH_3(OR_f)_{(soln)} + 3\ H(OR_f)_{(soln)} \xrightarrow[3\ H_2]{\text{hexane, fast}} LiAl(OR_f)_4 \qquad (2)$$

The first protonolysis (1) is slow, as $LiAlH_4$ is completely insoluble in hexane and the reaction is heterogeneous. Once one OR_f group has bonded to Al, the salt probably achieves enough solubility in hexane to make the next protonolysis homogeneous. As more OR_f ligands are bonded to Al, the solubility should increase, leading to a faster rate of OR_f addition to Al despite the lower reactivity of the remaining hydrides relative to $LiAlH_4$. This allows the reaction to go to completion to form the tetrakis fluoroalkoxyaluminate anion, and precludes the formation of the "expected" $LiAlH_2(OR_f)_2$ species.

Structural Characterization of $LiAl(HFCP)_4$ and $LiAl(HFIP)_4$

The structure of $LiAl(HFCP)_4$, shown in Figure 28, consists of $LiAl(OC(cylco\text{-}C_6H_{11})(CF_3)_2)_4$ molecules composed of lithium(1+) and aluminate(1–) ions in a configuration best described as a penetrated ion pair. The thermal ellipsoid for Li^+ is large and elongated as shown in Figure 29, suggesting disorder; due to this condition, the structure was modeled using a two-site disorder for this atom. The electron density surrounding each site was determined using the EDEN function of the SHELXTL software, and is illustrated in an electron density contour map in Figure 30. Although it

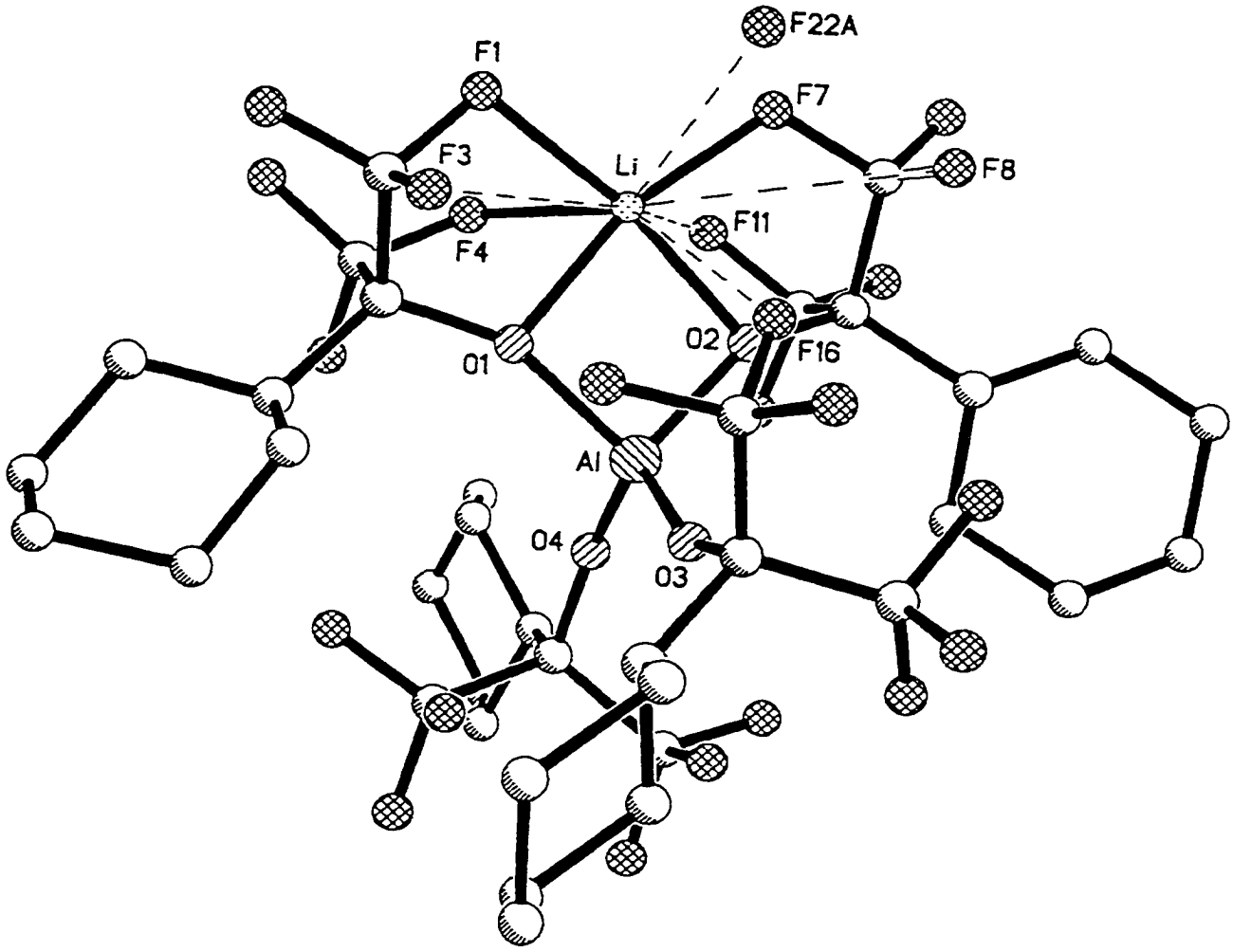

Figure 28. Drawing of the structure of $LiAl(HFCP)_4$ (hydrogen atoms omitted for clarity). The unlabeled partially shaded circles are carbon atoms, and the unlabeled crosshatched circles are fluorine atoms. See Table 2 for definition of abbreviation.

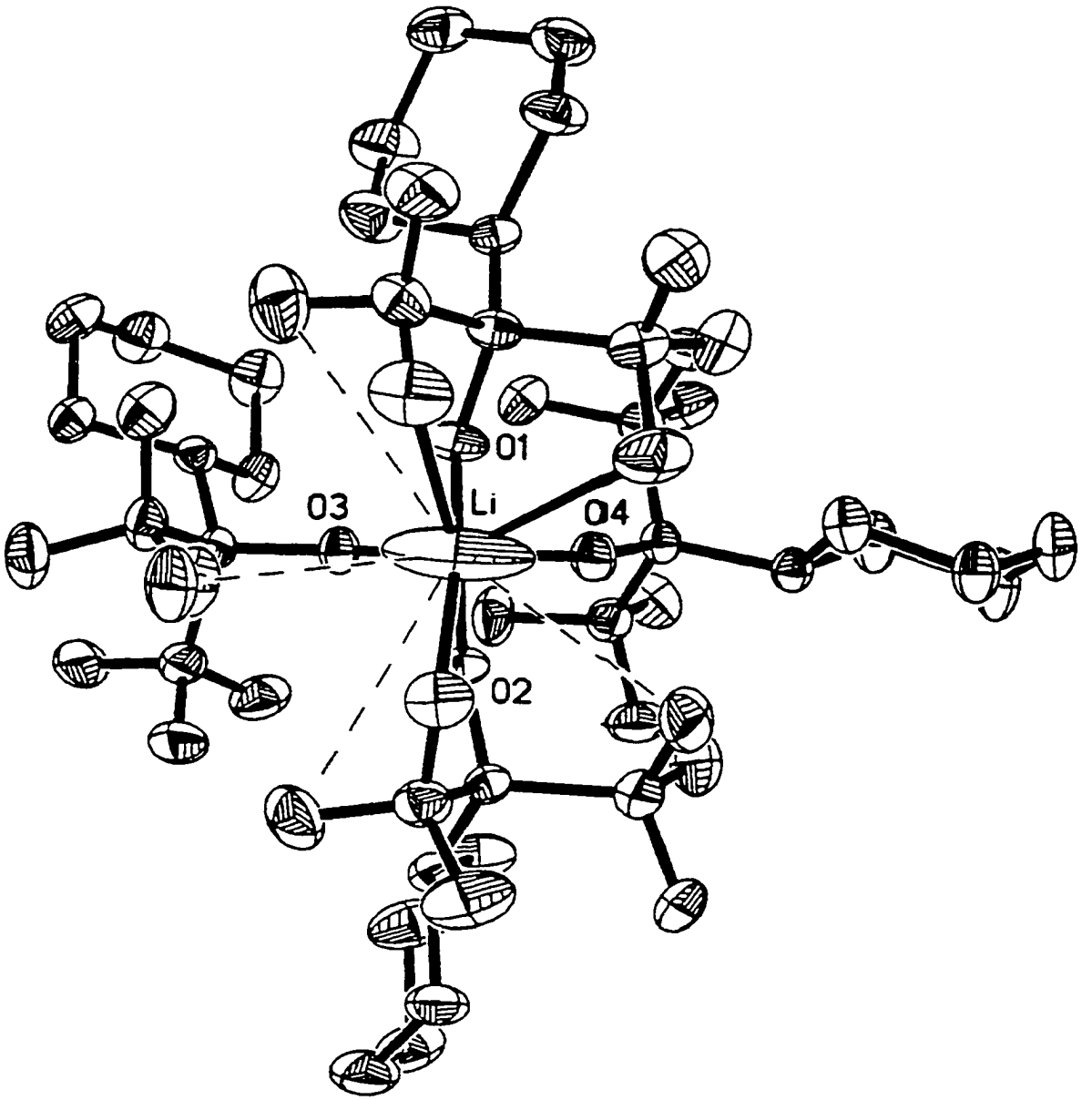

Figure 29. View of $LiAl(HFCP)_4$ with 50% probability ellipsoids showing elongated ellipsoid for Li^+. See Table 2 for definition of abbreviation.

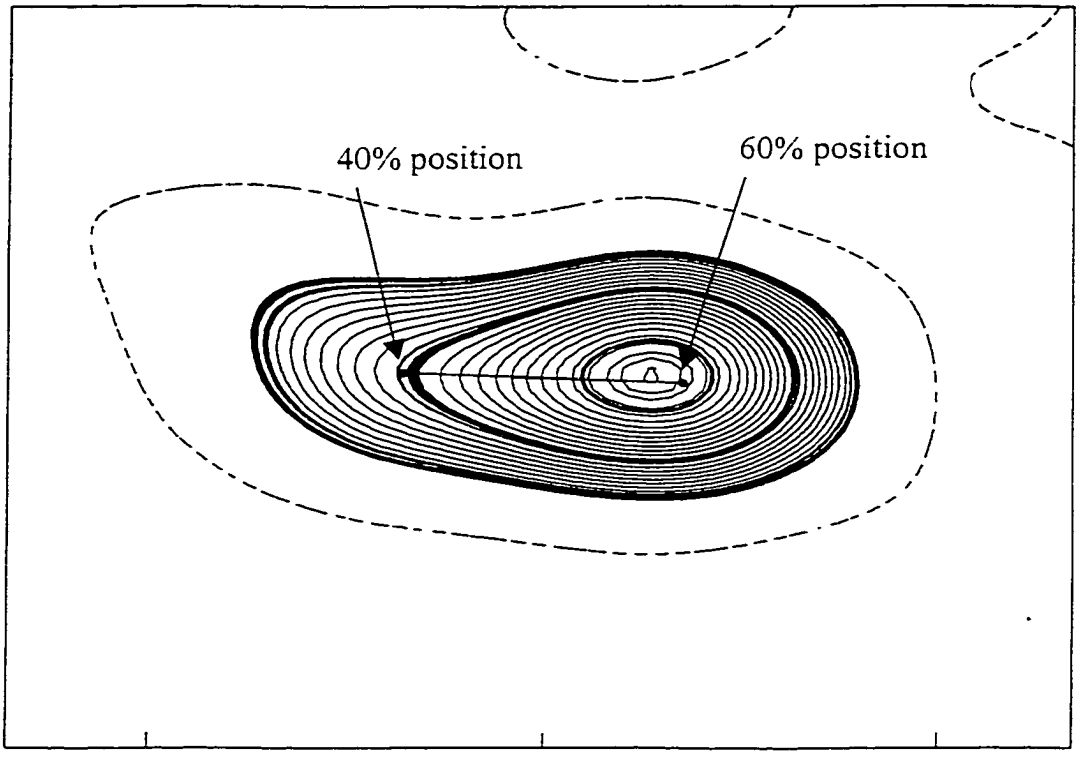

Figure 30. Electron density contour map of Li^{+} in $LiAl(HFCP)_4$. The structure was modeled with a two-site disorder, and both sites suggested by the SHELXTL software are shown. "40%" and "60%" correspond to the relative amounts of electron density at each site. See Table 2 for definition of abbreviation.

appears that the majority of the electron density is found near one site, the distribution was found to be approximately 60:40. For the purposes of evaluating the interactions of Li^+ with the anion, the structure was refined in two ways: with the lithium cation fixed in the 60% position, and with the lithium cation fixed in the 40% position. Selected bond distances and angles are listed in Tables 12 (40%) and 13 (60%).

In both models, the Al atom is tetrahedrally coordinated by four 1,1,1,3,3,3-hexafluoro-2-cyclohexyl-2-propoxide ($HFCP^-$) ligands. Although the true bond distances vary slightly between the two forms, the Al–O1 and Al–O2 bond lengths are longer than Al–O3 and Al–O4 in both cases. Also, the O1–Al–O2 bond angle is smaller than the other five O–Al–O angles, which are close to the ideal tetrahedral angle 109.5°.

The nature of the Li^+ coordination sphere differs between the two forms. In the 60% model, the $Al(HFCP)_4^-$ anion acts as a hexadentate chelating ligand for Li^+. The O1–Al–O2 unit forms a four-membered chelate ring with Li^+, with bond distances of 2.022(2) and 2.189(2) Å, and an O1–Li–O2 bond angle of 91.47(7)°. Four C–F bonds from four different CF_3 groups form four five-membered O–Li–F–C–C chelate rings, with Li–F bond distances of 1.711(2), 2.108(2), 2.141(2), and 2.716(2) Å. The next shortest Li···F contact is 3.292 Å. Overall, the LiO_2F_4 coordination sphere is best described as trigonal prismatic, and is shown in Figure 31. The two planes formed by O2–F7–F11 and O1–F1–F4 are twisted away from the ideal, eclipsed conformation by 3.1°.

In the 40% model, the $Al(HFCP)_4^-$ anion acts as an octadentate chelating ligand, and one additional Li–F intermolecular contact completes the coordination sphere of Li^+. The O1–Al–O2 unit forms a four-membered chelate ring with Li^+, with bond distances of 1.964(2) and 2.009(2) Å, and an O1–Li–O2 bond angle of 91.50(7)°. Five C–F bonds

Table 12. Selected interatomic distances (Å) and angles (deg) for 40% $LiAl(HFCP)_4$.

Li–O1	1.964(2)	Li–O2	2.009(2)
Li–F1	2.034(2)	Li–F3	3.016(2)
Li–F4	2.666(2)	Li–F7	1.960(2)
Li–F8	3.110(2)	Li–F16	2.765(2)
Li–F22'	2.753(2)	Al–O1	1.769(2)
Al–O2	1.776(2)	Al–O3	1.699(2)
Al–O4	1.703(2)	C–F(Li)[a]	1.313(3) – 1.375(3)
C–F[b]	1.322(2) – 1.348(3)		
O3–Al–O4	112.57(7)	O3–Al–O1	110.23(8)
O4–Al–O1	115.01(7)	O3–Al–O2	115.27(7)
O4–Al–O2	110.71(7)	O1–Al–O2	91.50(7)
O1–Li–O2	79.45(5)	F1–Li–F7	109.5(1)
F1–Li–F22'	79.4(1)	F1–Li–F8	135.9(1)
F1–Li–F16	115.3(1)	F1–Li–F3	45.1(1)
F1–Li–F4	67.6(1)	F7–Li–F22'	75.5(1)
F7–Li–F8	42.7(1)	F7–Li–F16	110.5(1)
F7–Li–F3	145.0(1)	F7–Li–F4	96.0(1)
F22'–Li–F8	62.3(1)	F22'–Li–F16	64.4(1)
F22'–Li–F3	75.8(1)	F22'–Li–F4	141.0(1)

Table 12. (continued)

F8–Li–F16	68.4(1)	F8–Li–F3	132.4(1)
F8–Li–F4	133.1(1)	F16–Li–F3	74.0(1)
F16–Li–F4	149.0(1)	F3–Li–F4	93.7(1)

[a] Range of C–F distances for those fluorine atoms that are within van der Waals contact of Li. [b] Range of C–F distances for those fluorine atoms that are not within van der Waals contact of Li. See Table 2 for definition of abbreviation.

Table 13. Selected interatomic distances (Å) and angles (deg) for 60% $LiAl(HFCP)_4$.

Li–O1	2.189(2)	Li–O2	2.022(2)
Li–F1	2.141(2)	Li–F4	2.108(2)
Li–F7	1.711(2)	Li–F11	2.716(2)
Al–O1	1.773(2)	Al–O2	1.776(2)
Al–O3	1.700(2)	Al–O4	1.702(2)
C–F(Li)[a]	1.343(3) – 1.373(3)	C–F[b]	1.316(3) – 1.348(3)
O3–Al–O4	112.62(7)	O3–Al–O1	110.27(8)
O4–Al–O1	114.95(8)	O3–Al–O2	115.26(7)
O4–Al–O2	110.71(7)	O1–Al–O2	91.47(7)
O2–Li–O1	74.13(5)	F1–Li–F4	77.67(6)
F1–Li–F7	115.30(6)	F1–Li–F11	142.4(6)
F4–Li–F7	130.28(6)	F4–Li–F11	72.6(6)
F7–Li–F11	70.6(6)		

[a] Range of C–F distances for those fluorine atoms that are within van der Waals contact of Li. [b] Range of C–F distances for those fluorine atoms that are not within van der Waals contact of Li. See Table 2 for definition of abbreviation.

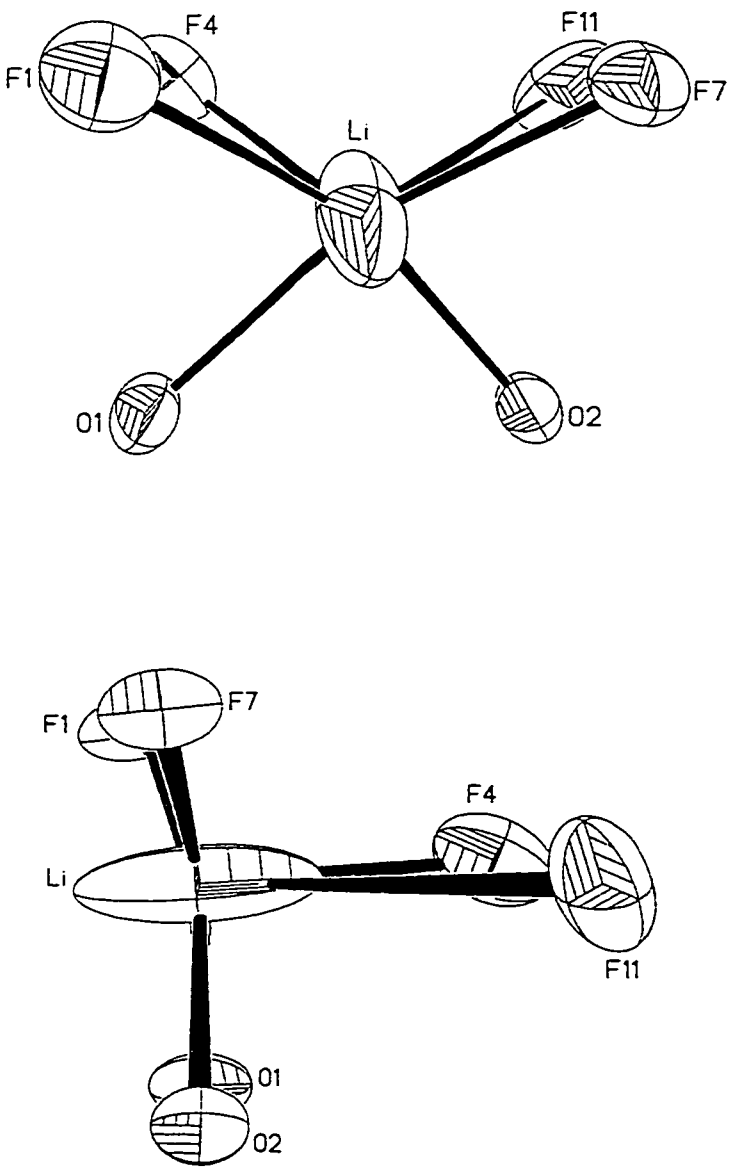

Figure 31. LiO_2F_4 coordination sphere of $LiAl(HFCP)_4$ with 50% probability ellipsoids (Li in 60% position). The two planes formed by O2–F7–F11 and O1–F1–F4 are twisted away from the ideal, eclipsed conformation by 3.1°. See Table 2 for definition of abbreviation.

from three different CF_3 groups form five five-membered O–Li–F–C–C chelate rings, with Li–F bond distances of 1.960(2), 2.009(2), 2.034(2), 2.666(2), 3.016(2), and 3.110(2) Å. The intermolecular Li–F contact has a distance of 2.753(2) Å. The next shortest Li···F contact is 3.371 Å. Overall, the LiO_2F_7 coordination sphere is irregular, and is shown in Figure 32.

Although the true solid-state Li–F and Li–O distances for $LiAl(HFCP)_4$ cannot be known from this structure, a semi-quantitative treatment of the bonding can still be done using the 60% and 40% structures. The lithium cation most likely resides in one of these positions, and an analysis of each case will give a good approximation of the nature of the cation-anion interactions. Bond valence methods were used to examine the bonding between Li^+ and the anion, as shown in Table 14. In both forms, the total bond valence for Li^+ is very close to one, and large contributions are made by Li–F bonds (57% of total valence for 40% structure, 65% for 60% structure). The geometry of the Li^+ coordination sphere is very different between the two, being trigonal prismatic for the 60% case, and irregular with one intermolecular Li···F contact for the 40% case. Similar lithium aluminates ($LiAl(HFPP)_4$, $LiAl(HFTP)_4$, $LiAl(HFBuPP)_4$) exhibit the same trigonal prismatic coordination geometry as the 60% structure, suggesting that this is the more likely form. If this turns out to be true, the Li–F7 bond distance of 1.711(2) Å is remarkable. Currently, the shortest known Li–F(C) contact is 1.956(3) Å,[11] which is significantly longer ($> 3\sigma$) than the Li–F7 distance. To confirm this, a structure of $LiAl(HFCP)_4$ is needed in which the lithium cation is not disordered.

Another interesting feature of this structure is a correlation between C–F(Li) and C–F bond distances. It has been previously observed that coordination of an organofluorine atom to a metal cation results in a lengthening of the participating C–F

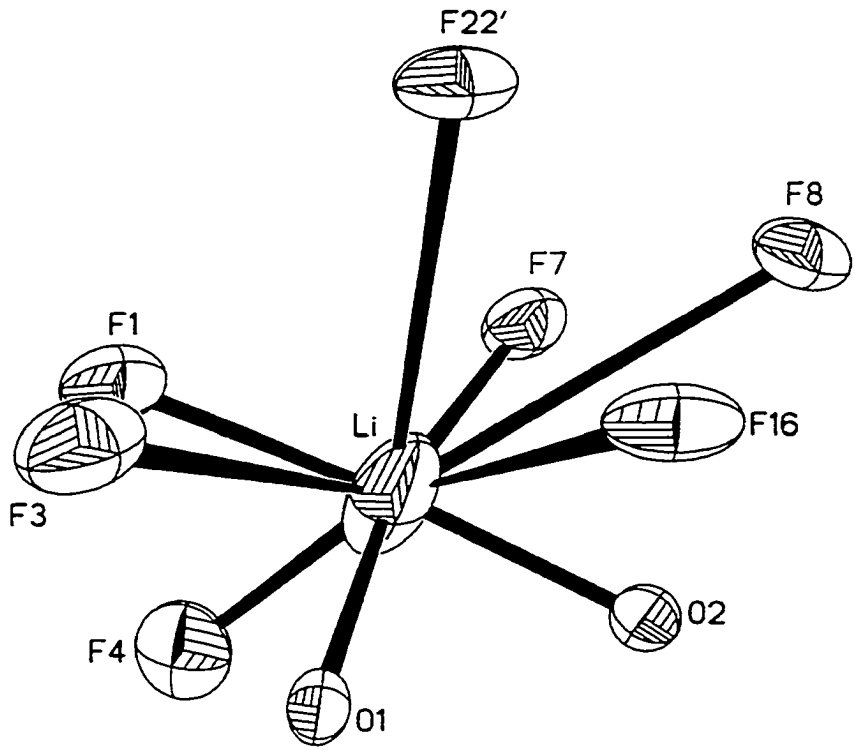

Figure 32. LiO_2F_7 coordination sphere of $LiAl(HFCP)_4$ with 50% probability ellipsoids (Li in 40% position). See Table 2 for definition of abbreviation.

Table 14. Bond valence values for 40% and 60% structures of $LiAl(HFCP)_4$.

40% structure			60% structure		
bond	distance, Å	bond valence (*s*)	bond	distance, Å	bond valence (*s*)
Li–O1	1.964(2)	0.237	Li–O1	2.189(2)	0.152
Li–O2	2.009(2)	0.216	Li–O2	2.009(2)	0.216
Li–F1	2.034(2)	0.168	Li–F1	2.141(2)	0.138
Li–F3	3.016(2)	0.036	Li–F4	2.108(2)	0.146
Li–F4	2.666(2)	0.059	Li–F7	1.711(2)	0.330
Li–F7	1.960(2)	0.194	Li–F11	2.716(2)	0.054
Li–F8	3.110(2)	0.032			
Li–F16	2.765(2)	0.051			
Li–F22'	2.753(2)	0.052			
total bond valence =		**1.045**	total bond valence =		**1.030**

The bond valence, *s*, is given by $s = (r/r_0)^{-N}$, where r_0(Li–O) = 1.378, N(Li–O) = 4.065, r_0(Li–F) = 1.288, and N(Li–F) = 3.9. See Table 2 for definition of abbreviation.

bond, accompanied by a shortening of the two remaining C–F bonds in the CF_3 group.[3] Figure 33 shows plots of the carbon-fluorine bond distances for each C–F bond in $LiAl(HFCP)_4$ for both the 60% and 40% $LiAl(HFCP)_4$ structures. The dotted line represents the average distance of all C–F bonds from unaffected CF_3 groups, and has a value of 1.336 Å. Although the correlation is better for the 60% case, in both it can be seen that the C–F bonds coordinated to Li^+ are generally longer than 1.336 Å, while the remaining two C–F bonds in the affected trifluoromethyl groups are shorter. The obvious outliers in the 40% case are C3–F3, C11–F8, and C21–F18. The first two are within the bonding distance boundaries established above, but are at the extreme and contribute only 3.6% and 3.2%, respectively, to the total valence of Li^+. As such, the lengthening of the C3–F3 and C11–F8 bonds resulting from coordination to Li^+ would not be expected to be dramatic. Furthermore, each of these fluorine atoms is part of a CF_3 group that also contains a strongly bonded fluorine atom (F1, F7 respectively). The effect of these bonds is to shorten the remaining two, and this should be significant considering the length of Li–F1 (2.034(2) Å) and Li–F7 (1.960(2) Å). This shortening of the C3–F3 and C11–F8 bonds apparently outweighs the lengthening as a result of coordination to Li^+, resulting in an overall bond distance that is shorter than 1.336 Å. The unexpected length of C21–F18 is more difficult to explain; this fluorine atom is not coordinated to Li^+. At this time, the origin of its anomalous length is not known.

The structure of $LiAl(HFIP)_4$ is shown in Figure 34. Selected bond distances and angles are listed in Table 15. The structure of this compound consists of centrosymmetric dinuclear molecules composed of two Li^+ and two tetrahedral $Al(HFIP)_4^-$ ions. Each $Al(HFIP)_4^-$ anion donates three of its four oxygen atoms to the Li^+ cations: one each to the two Li^+ cations and a third that bridges the two Li^+ cations

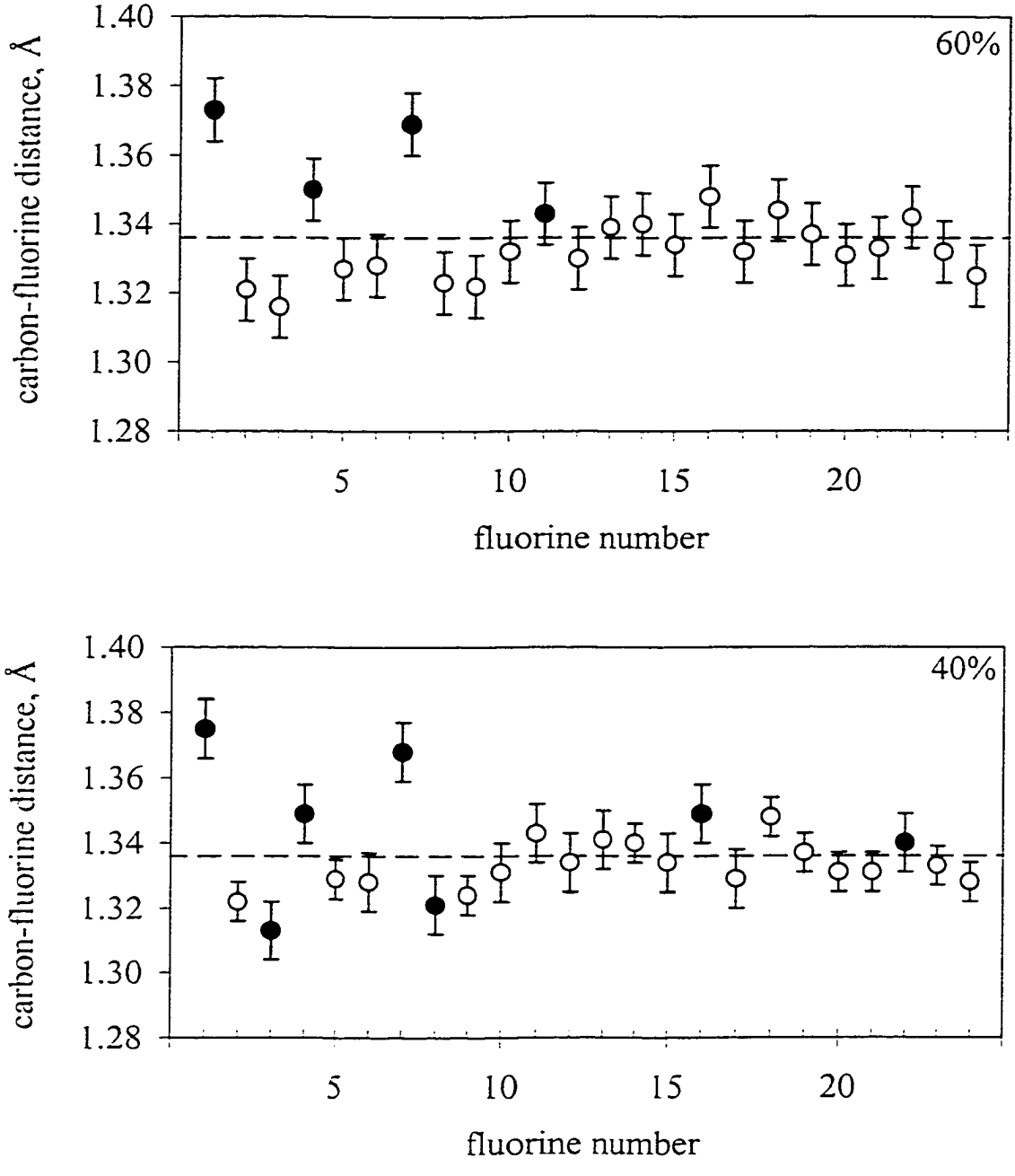

Figure 33. Plots of C–F distance vs. fluorine atom number for the 60% and 40% structures of $LiAl(HFCP)_4$. The error bars are $\pm 3\sigma$ for each individual distance. The filled circles represent the C–F(Li) bonds and the open circles represent all other C–F bonds. The dotted line in each plot corresponds to an average distance of all C–F bonds from CF_3 groups with no C–F(Li) bonds (1.336 Å). See Table 2 for definition of abbreviation.

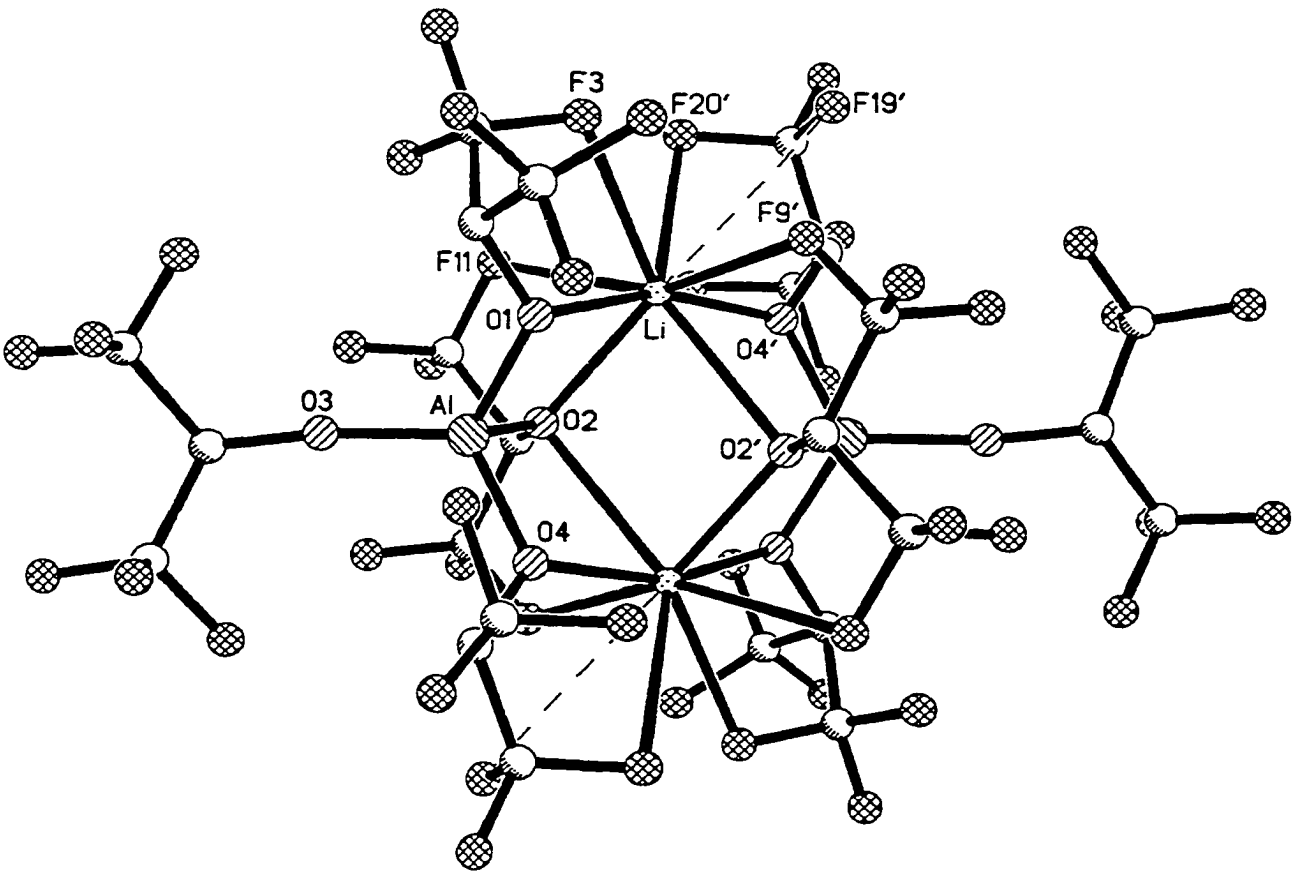

Figure 34. Drawing of the structure of $LiAl(HFIP)_4$ (hydrogen atoms omitted for clarity). The unlabeled partially shaded circles are carbon atoms, and the unlabeled crosshatched circles are fluorine atoms. Selected interatomic distances (Å) and angles (deg): Li–O1, 2.089(5); Li–O2, 2.166(6); Li–O2', 2.533(6); Li–O4', 2.016(5); Li–F1, 3.327(6); Li–F3, 2.366(6); Li–F11, 3.055(6); Li–F9', 2.414(6); Li–F19', 3.181(6); Li–F20', 2.798(6); O1–Li–O2, 75.0(2); O2'–Li–O4', 70.9(2). See Table 2 for definition of abbreviation.

Table 15. Selected interatomic distances (Å) and angles (deg) for $LiAl(HFIP)_4$.

Li–O1	2.089(5)	Li–O2	2.166(6)
Li–O2'	2.533(6)	Li–O4'	2.016(5)
Li–F1	3.327(6)	Li–F3	2.366(6)
Li–F11	3.055(6)	Li–F9'	2.414(6)
Li–F19'	3.181(6)	Li–F20'	2.798(6)
Al–O1	1.758(2)	Al–O2	1.771(2)
Al–O3	1.690(2)	Al–O4	1.766(2)
C–F(Li)[a]	1.320(4) – 1.354(4)	C–F[b]	1.310(4) – 1.337(4)
O3–Al–O1	111.1(1)	O3–Al–O4	112.1(1)
O1–Al–O4	112.41(9)	O3–Al–O2	127.1(1)
O1–Al–O2	94.49(9)	O4–Al–O2	98.17(9)
O1–Li–O2	75.0(2)	O1–Li–O2'	89.9(3)
O1–Li–O4'	160.4(3)	O2–Li–O2'	82.0(3)
O2–Li–O4'	97.5(2)	O2'–Li–O4'	146.8(3)
F1–Li–F3	39.9(3)	F1–Li–F11	56.5(3)
F1–Li–F9'	113.4(3)	F1–Li–F19'	102.5(3)
F1–Li–F20'	77.5(3)	F3–Li–F11	82.5(3)
F3–Li–F9'	79.2(3)	F3–Li–F19'	68.8(3)
F3–Li–F20'	64.7(3)	F11–Li–F9'	157.2(3)

Table 14. (continued)

F11–Li–F19'	97.2(3)	F11–Li–F20'	56.4(3)
F9'–Li–F19'	63.4(3)	F9'–Li–F20'	103.0(3)
F19'–Li–F20'	40.9(3)		

[a] Range of C–F distances for those fluorine atoms that are within van der Waals contact of Li. [b] Range of C–F distances for those fluorine atoms that are not within van der Waals contact of Li. See Table 2 for definition of abbreviation.

forming a planar Li_2O_2 core. Each Li^+ cation is also bonded to four fluorine atoms from four different CF_3 groups. As expected, the AlO_4 core is distorted from a tetrahedral geometry. Since O3 does not bond to the Li^+ ions, the Al–O3 bond distance, 1.690(2) Å, is considerably shorter than the other three Al–O distances, which range from 1.758(2) to 1.771(2) Å. The O1–Al–O2 and O2–Al–O4 bond angles are 94.49(9) and 98.17(9).° The other four O–Al–O angles range from 111.1(1) to 127.0(1)°. The LiO_4F_4 coordination sphere is shown in Figure 35. The top drawing shows all Li–O and Li–F contacts, including Li–F19' (3.181(6) Å), which has a distance greater than 3.165 Å but less than 3.29 Å. Disregarding this contact, the overall coordination geometry can be described as a distorted square antiprism (see bottom drawing in Figure 35). The Li–O1, Li–O2, Li–O2', and Li–O4' bond distances are 2.089(5), 2.166(6), 2.533(6), and 2.016(5) Å, respectively. The Li–F bond distances are 2.366(6), 2.414(6), 2.798(6), and 3.055(6) Å. The next shortest Li–F distance (after F19') is 3.327 Å. The four-atom planes indicated by the dashed lines make a dihedral angle of 15°.

Bond valence analysis was also performed for $LiAl(HFIP)_4$, and values are listed in Table 16. Without Li–F19', the total valence is 0.902, well below one, and bonding between Li and F accounts for 29% of the total valence in this case. Adding Li–F19', the total rises to 0.931, which is still low. However, if the next closest contact (Li–F1, 3.327 Å) is added, the total is 0.956, within 0.05 units of one. With this in mind, can F1 be considered to be bonded to Li? According to both the $s = 0.03$ definition stated above and the van der Waals radii, the answer would be no. However, if the total bond valence is taken into consideration, the answer may be yes. There is uncertainty in this case, which speaks to the fact that the perfect definition of when Li–F(C) bonding occurs does not exist. Each is based on assumptions, and situations will arise where one definition

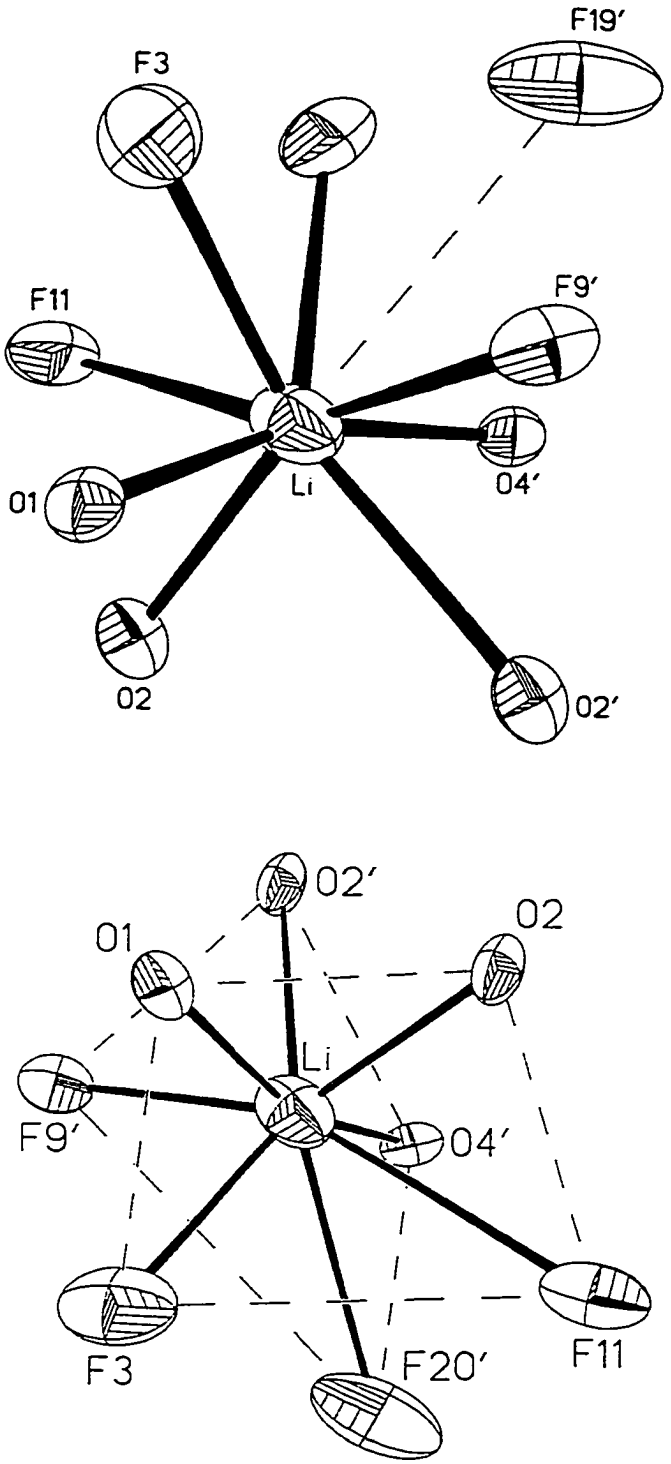

Figure 35. Drawings of the LiO_4F_6 (top) and LiO_4F_4 (bottom) coordination sphere of $LiAl(HFIP)_4$ with 50% probability ellipsoids. See Table 2 for definition of abbreviation.

Table 16. Bond valence values for $LiAl(HFIP)_4$.

bond	distance, Å	bond valence (s)
Li–O1	2.089(5)	0.184
Li–O2	2.166(6)	0.159
Li–O2'	2.533(6)	0.084
Li–O4'	2.016(5)	0.213
Li–F3	2.366(6)	0.093
Li–F11	3.055(6)	0.034
Li–F9'	2.414(6)	0.086
Li–F20'	2.798(6)	0.049
	total bond valence =	**0.902**
Li–F1	3.327(6)	0.025
Li–F19'	3.181(6)	0.029
	total bond valence =	**0.956**

The bond valence, s, is given by $s = (r/r_0)^{-N}$, where r_0(Li–O) = 1.378, N(Li–O) = 4.065, r_0(Li–F) = 1.288, and N(Li–F) = 3.9. See Table 2 for definition of abbreviation.

will contradict another. They are useful for describing coordination spheres, but none are the ultimate authority on the nature of Li–F bonding. The relationship between C–F(Li) and other C–F bonds in each CF_3 group was also investigated, as shown in the plot in Figure 36. There is fairly good agreement with the prediction discussed above for $LiAl(HFCP)_4$, especially in the cases of the CF_3 groups containing F4 and F9.

Hydrocarbon Solubility

In the course of characterizing new salts based on the $LiAl(OR_f)_4$ formula, it was found that many of them exhibit a high degree of hydrocarbon solubility. For example, $LiAl(HFPP)_4$ is soluble in hexane to a concentration of 37 mM. This, combined with the strong Lewis acidity of the Li^+ cation, results in species that have the potential to be used as catalysts in hydrocarbon solvents. In fact, $LiAl(HFPP)_4$ has been shown to be an active Lewis acid catalyst in *toluene solution* for the 1,4-conjugate addition of silyl ketene acetals to α,β-unsaturated carbonyl compounds and for the direct substitution of allylic acetates by silyl ketene acetals.[12] This behavior is unique among lithium salts of *WCA*s: while some exist that are hydrocarbon-soluble, before this work there were none known that also exhibited catalytic activity.

The origin of hydrocarbon solubility for certain varieties of $LiAl(OR_f)_4$ can be understood by examining the solid-state structure of $LiAl(HFPP)_4$, which is shown in Figure 37.[3] Two Li–O and four Li–F bonds create a coordination sphere whereby the $Al(HFPP)_4^-$ anion completely encapsulates the Li^+ cation. This "penetrated ion pair"[13] structure results in a lithium salt with no intermolecular bridging and a high degree of molecular character, affording it solubility in both aromatic and aliphatic hydrocarbons.

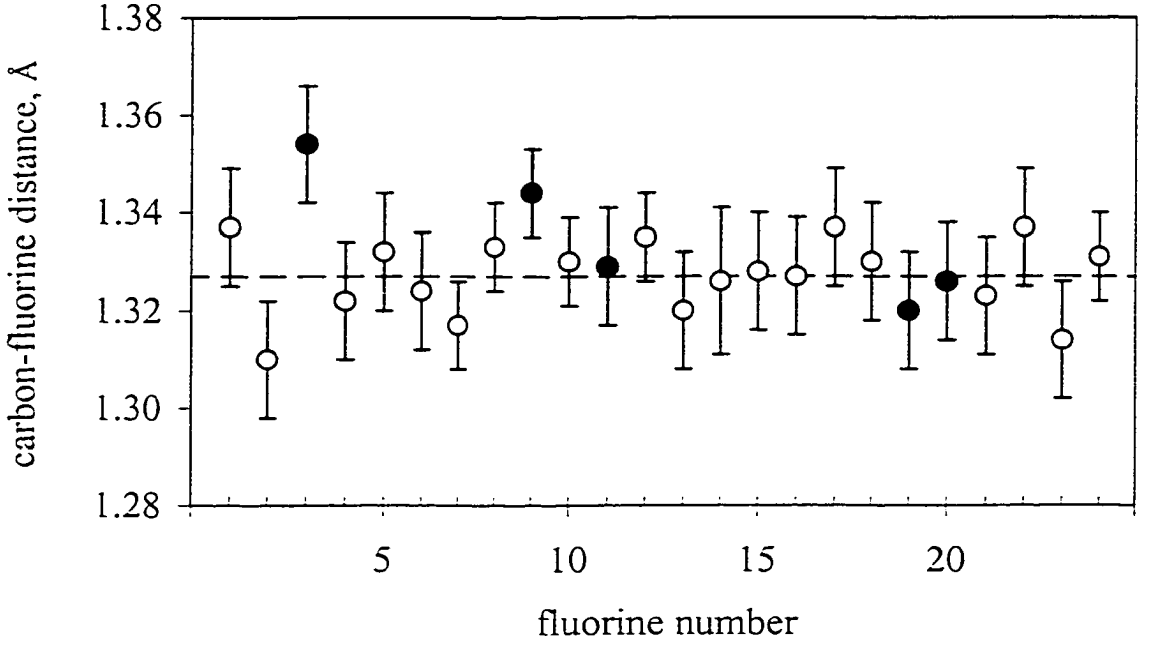

Figure 36. Plot of C–F distance vs. fluorine atom number for $LiAl(HFIP)_4$. The error bars are $\pm 3\sigma$ for each individual distance. The filled circles represent the C–F(Li) bonds and the open circles represent all other C–F bonds. The dotted line corresponds to an average distance of all C–F bonds from CF_3 groups with no C–F(Li) bonds (1.327 Å). See Table 2 for definition of abbreviation.

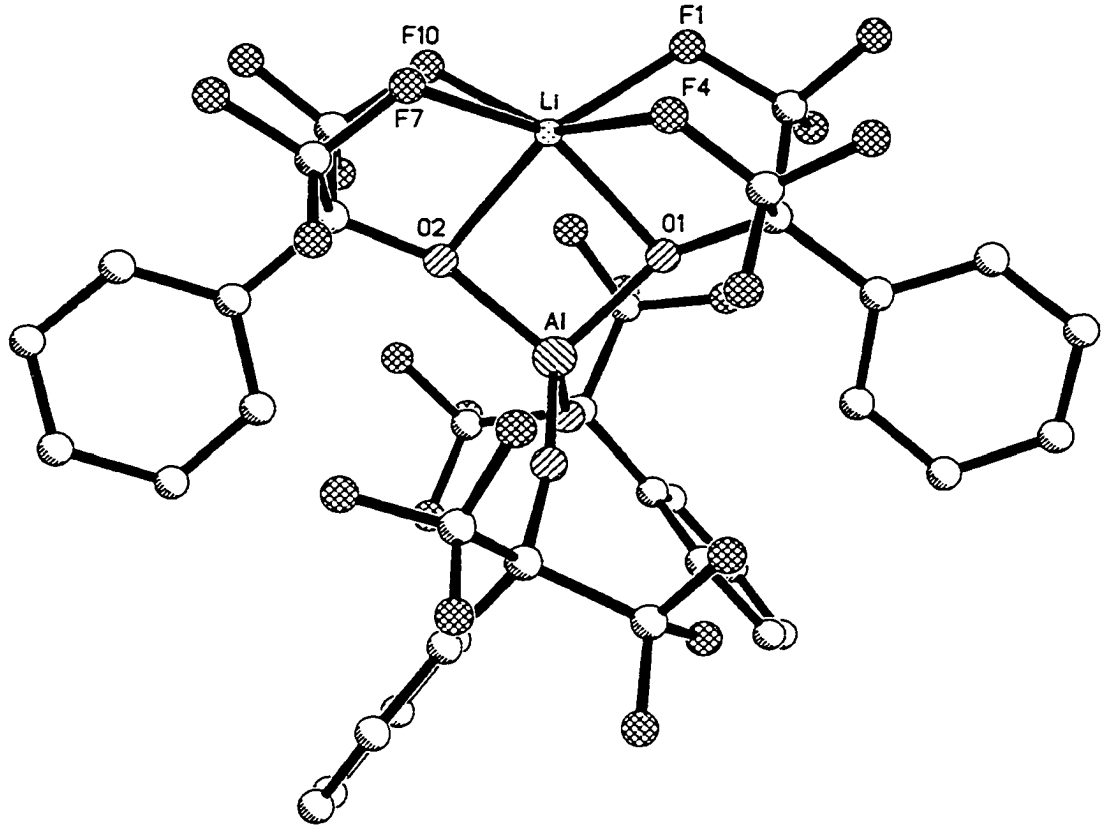

Figure 37. Drawing of the structure of $LiAl(HFPP)_4$ (hydrogen atoms omitted for clarity). The unlabeled partially shaded circles are carbon atoms, and the unlabeled crosshatched circles are fluorine atoms. See Table 2 for definition of abbreviation.

This observation illustrates an important principle in the design of hydrocarbon-soluble salts of *WCAs*: an effective weakly coordinating anion should coordinate strongly enough to the cation, and provide enough donor atoms for the cation, to prevent extensive bridging with neighboring molecular ion pairs, because this invariably leads to poor solubility in low-dielectric, low-donor-number solvents.[14,15] With this in mind, it can be proposed that multiple contacts of carbon–fluorine bonds to a cation may be more desirable in terms of solubility than multiple contacts of even more weakly coordinating carbon–hydrogen bonds. As a slightly stronger donor, C–F bonds will better stabilize a cation than C–H bonds, thereby eliminating the need for intermolecular contacts. For example, the Li^+ cation in the unfluorinated salt $LiNb(OEt)_6$ is bonded to only four ethoxide oxygen atoms from two adjacent $Nb(OEt)_6^-$ anions, forming a tetrahedral LiO_4 core.[16] Not surprisingly, $LiNb(OEt)_6$ is not soluble in aromatic hydrocarbon solvents, whereas the polyfluorinated compound $LiNb(HFIP)_6$ dissolves to an appreciable extent in benzene and toluene.[17]

After $LiAl(HFPP)_4$ was characterized and found to possess the unique combination of high solubility *and* catalytic activity in hydrocarbon solvents, new $LiAl(OR_f)_4$ salts were synthesized with the goal of enhancing either or both of these properties. In this section, the issue of hydrocarbon solubility is addressed. Several new salts were synthesized with modified fluoroalkoxide ligands (the compounds $LiAl(HFCP)_4$, $LiAl(HFIP)_4$, and $LiAl(DPTE)_4$ were prepared by the author), and their solubilities in hexane were quantified. The results are shown in Table 17.

Table 17. Hexane solubility of $LiAl(OR_f)_4$.

compound	solubility, mM
$LiAl(HFCP)_4$	385
$LiAl(HFTP)_4$	149
$LiAl(HFPP)_4$	37
$LiAl(HFTB)_4$	21
$LiAl(HFBuPP)_4$	9
$LiAl(DPTE)_4$	8
$LiAl(HFIP)_4$	~0

See Table 2 for definitions of abbreviations.

With the exception of $LiAl(DPTE)_4$, the only difference among these compounds is the identity of the R group in the fluoroalkoxide moiety $-OC\mathbf{R}(CF_3)_2$, which apparently has a profound impact on hexane solubility. However, solubility is a property governed by many factors, and it is extremely difficult to predict the solubility of a compound in a given solvent based solely on its molecular structure. Nevertheless, due to the similarity among the salts listed above, some interesting comparisons can be made in terms of the different R groups. For example, consider the results for $LiAl(HFPP)_4$ and $LiAl(HFCP)_4$, for which a difference in solubility of more than an order of magnitude was observed. Both of these salts are similar in terms of having penetrated ion pair structures, and also with respect to their shape and size (formula unit volume from solid state structures of 977 $Å^3$ for $LiAl(HFPP)_4$ vs. 1047 $Å^3$ for $LiAl(HFCP)_4$). Consequently, the observed difference can be attributed primarily to the nature of the R group. One possible explanation is that $LiAl(HFCP)_4$ has more aliphatic character (R = cyclohexyl) than $LiAl(HFPP)_4$ (R = phenyl), and is thus more soluble in the similarly

aliphatic solvent hexane. Another possibility is that intermolecular forces in the solid state are stronger for $LiAl(HFPP)_4$ than for $LiAl(HFCP)_4$. The phenyl rings on each HFPP ligand can interact *via* pi-stacking, while the cyclohexyl rings on each HFCP ligand cannot. Therefore, $LiAl(HFPP)_4$ should have a higher lattice energy than $LiAl(HFCP)_4$, and its solubility in hexane would be expected to be lower.

Also consider the solubilities of the three salts $LiAl(HFPP)_4$, $LiAl(HFTP)_4$, and $LiAl(HFBuPP)_4$, all of which have similar penetrated ion pair structures. It was hoped that adding alkyl groups to the phenyl ring of HFPP would increase the solubility of the corresponding lithium aluminate in hexane. This was based on both of the possible explanations for the differing solubilities of $LiAl(HFPP)_4$ and $LiAl(HFCP)_4$ discussed above: increasing the aliphatic character of the salt; or, by introducing bulky groups on the phenyl ring, the strength of pi-stacking interactions may be reduced due to steric considerations. It was found that the solubility of $LiAl(HFTP)_4$ increased relative to $LiAl(HFPP)_4$, but a *decrease* was observed for $LiAl(HFBuPP)_4$. Apparently, increasing the aliphatic character of the salt is not the determining factor for increasing solubility in hexane. The differences may be related to pi-stacking interactions, but overall the reason for these differences is not yet understood. It is also possible that anion size and/or shape may play a role.

Finally, consider the structures of $LiAl(HFPP)_4$ and $LiAl(HFIP)_4$, which illustrate the effect of bridging on hexane solubility. As mentioned above, intermolecular bridging results in poor solubility in low-dielectric, low-donor-number solvents; with this in mind, consider the structures of each lithium aluminate (Figures 37 and 34, respectively). $LiAl(HFPP)_4$ has no significant intermolecular contacts (other than potential pi-stacking interactions), and is highly soluble in hexane because it can dissolve as a molecular unit.

In contrast, $LiAl(HFIP)_4$ is completely insoluble in hexane, which can be attributed to the extensive bridging observed in its solid-state structure. This also reflects the extent to which the ionic portion (Al, Li, O atoms) of the molecule is exposed. In a nonpolar hydrocarbon solvent such as hexane, a highly exposed ionic portion invariably results in a low solubility. It can be seen from the two structures that an increase in bridging is accompanied by a greater degree of exposure, resulting in a lower solubility for $LiAl(HFIP)_4$.

Another way to consider the relationship between bridging and solubility is in the context of the penetrated ion pair structural theme. This was proposed earlier to be an important factor contributing to the hydrocarbon solubility of $LiAl(OR_f)_4$ salts, and it follows that the extent to which each salt can be described as having this structure may serve as an approximate indicator of its solubility. $LiAl(HFPP)_4$ is well-described as a penetrated ion pair, but this is not true for $LiAl(HFIP)_4$ due to the numerous intermolecular contacts. The relative solubilities of these two compounds agree with this interpretation as well.

Solution Conductivity

Lithium salts of the fluoroalkoxyaluminate anions were first characterized by measuring conductivities at various concentrations, c, in DME to gain insight into the nature of ion pairing in this solvent. Equivalent conductivities, Λ, were determined from these values, and plots of Λ vs. $c^{1/2}$ were made. Three salts were examined in this manner: $LiAl(HFIP)_4$, $LiAl(HFTB)_4$, and $LiAl(HFPP)_4$. The shape of the curves for $LiAl(HFIP)_4$ and $LiAl(HFTB)_4$, shown in Figure 38, are very similar to those for

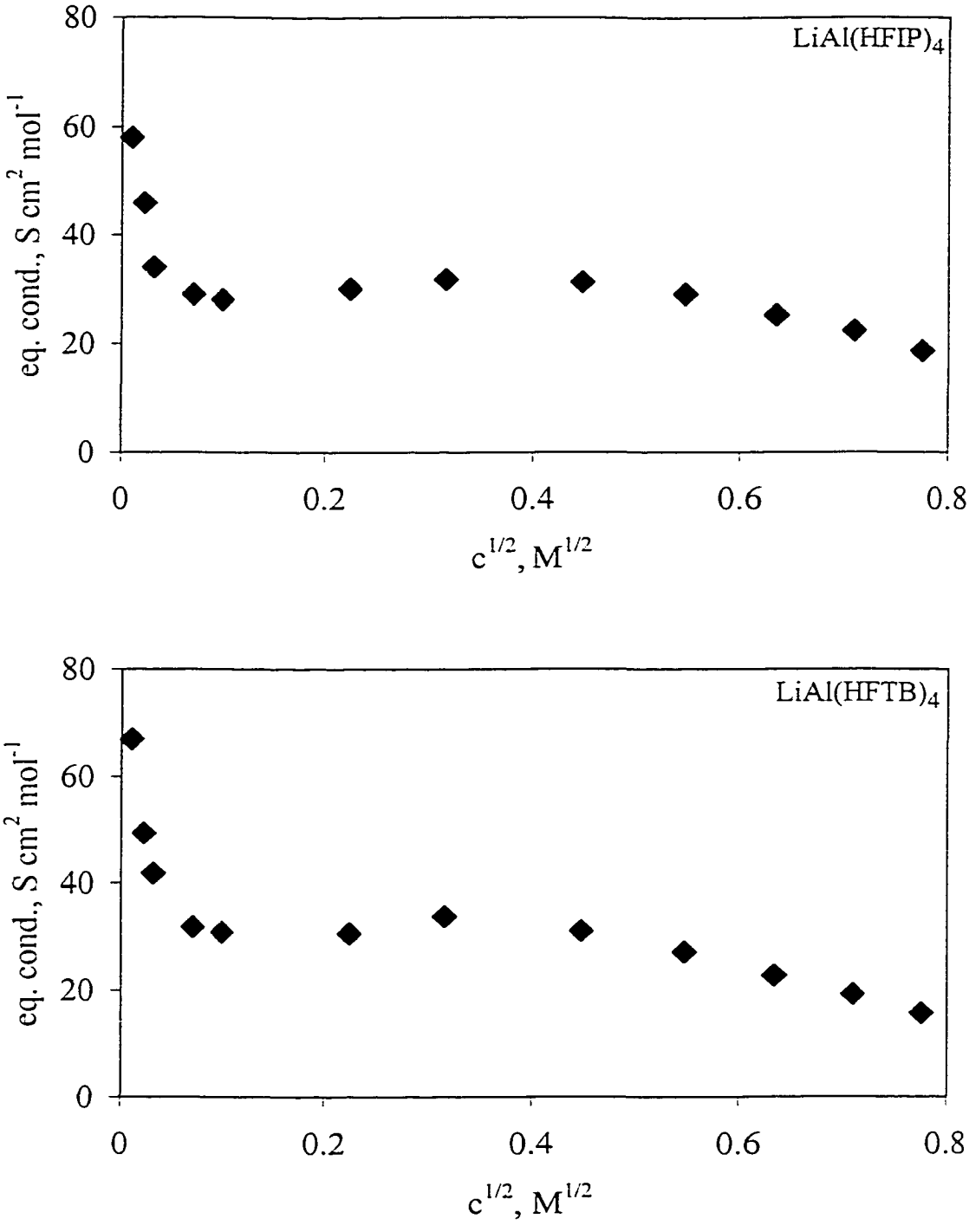

Figure 38. Plots of equivalent conductivity vs. square root of concentration for $LiAl(HFIP)_4$ and $LiAl(HFTB)_4$. See Table 1 for definitions of abbreviations.

$LiB(HFPOP)_2$ and $LiB(HFTPOP\text{-}2,3,4)_2$ displayed above in Figure 2. The local minima and maxima occur at the same concentrations, and the presence of a local minimum at approximately 0.1 $M^{1/2}$ (0.01 M) indicates the formation of triple ions.

The curve for $LiAl(HFPP)_4$, shown in Figure 39, differs from the others considered thus far. Unlike the other plots, a local minimum in equivalent conductivity is not observed at a concentration of approximately 0.01 M. Instead, the curve levels off, followed by a steady decrease at higher concentrations. This suggests that triple ions do not form to as significant an extent as for the other two salts in DME. The leveling region provides evidence for their existence, but the concentration is presumably low, as there is no increase in equivalent conductivity between 0.1 $M^{1/2}$ (0.01 M) and 0.32 $M^{1/2}$ (0.1 M) as was observed in the plots for $LiAl(HFIP)_4$ and $LiAl(HFTB)_4$. In this case, not enough triple ions are formed to increase Λ, and their concentration is not high enough to significantly increase the solution permittivity. The major difference among $LiAl(HFIP)_4$, $LiAl(HFTB)_4$, and $LiAl(HFPP)_4$ is the size of the R group on the $-OCR(CF_3)_2$ ligand. The R groups for HFIP and HFTB (H and CH_3, respectively) are small, allowing for the facile formation of triple ions. However, for HFPP the large and rigid phenyl group most likely results in a sterically strained $Li(Al(HFPP)_4)_2^-$ triple ion, resulting in a low concentration of this species. This explanation is in agreement with the solid-state structures for $LiAl(HFIP)_4$ and $LiAl(HFPP)_4$ (Figures 34 and 37, respectively). As discussed above, $LiAl(HFIP)_4$ has a dimeric structure, with many intermolecular contacts to Li^+, while the structure of $LiAl(HFPP)_4$ is monomeric, with no intermolecular contacts to Li^+. The explanation for this difference was based on steric considerations, and the same factors are most likely at play here as well. Furthermore,

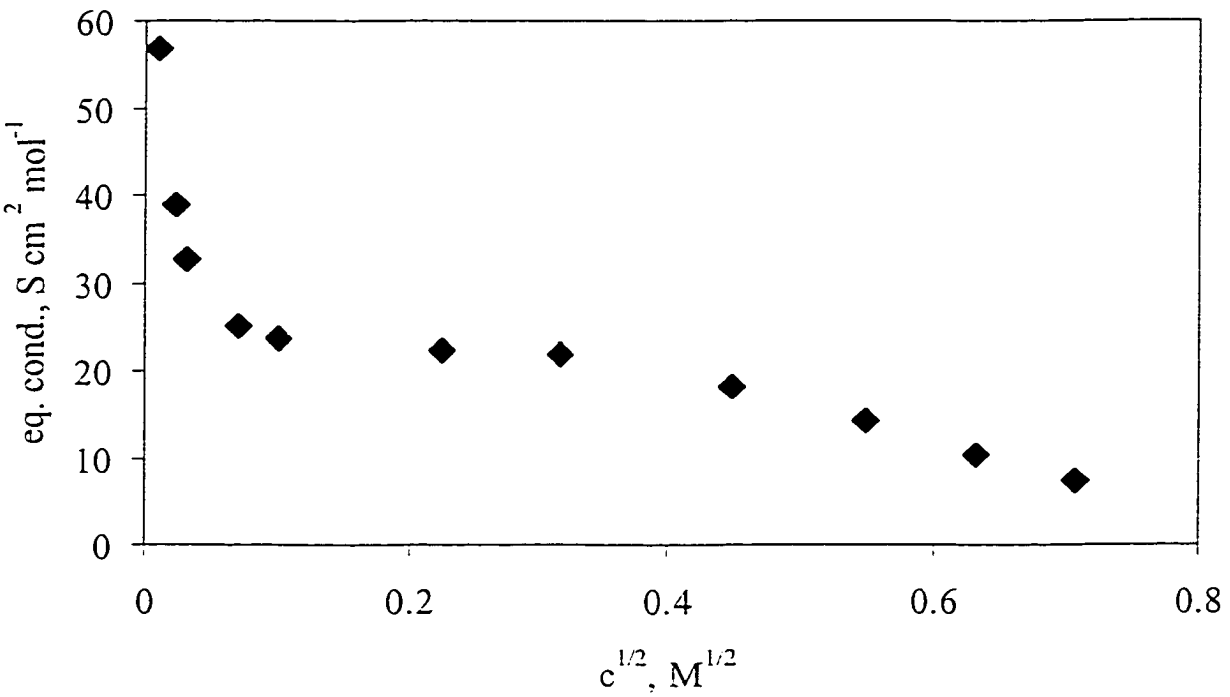

Figure 39. Plot of equivalent conductivity vs. square root of concentration for $LiAl(HFPP)_4$ in DME. See Table 2 for definitions of abbreviations.

solid-state structure of $[Li(Al(HFIP)_4)_2]^-$ has been determined by Dr. Svetlana Ivanova, providing evidence that this type of species does exist.

As for $LiB(HFPOP)_2$, $LiAl(OR_f)_4$ was compared to $LiCF_3SO_3$ by measuring conductivities at 0.01 M in the presence of two equivalents of 12-crown-4. Values are listed in Table 18. $LiAl(TFPE)_4$, the lithium aluminate with the lowest conductivity, was used for this study. As mentioned earlier, the conductivity of $LiCF_3SO_3$ increased by 150% when compared to a solution without added 12-crown-4. In contrast, the conductivity of $LiAl(TFPE)_4$ did not change, even when an excess of the cyclic ether was added. According to the discussion above for $LiB(HFPOP)_2$, this indicates that the $Al(TFPE)_4^-$ anion is more weakly coordinating than $CF_3SO_3^-$, and that the lithium cation exists primarily in the fully solvated $Li(DME)_2^+$ form in a DME solution of $LiAl(TFPE)_4$. Also, the higher conductivity of $LiAl(TFPE)_4$ under these conditions shows that $Al(TFPE)_4^-$ is more weakly ion-pairing than the triflate anion. Since $LiAl(TFPE)_4$ has the lowest conductivity of all $LiAl(OR_f)_4$ salts, it is likely that the same conclusions can be made regarding the other lithium aluminates.

Conductivities of a variety of $LiAl(OR_f)_4$ salts were measured in DME, and are listed in Table 18. The key component of the new *WCA*s is the OR_f ligand, and its properties determine the character of the anion. One objective in designing the ligands was to maximize the degree of charge dispersal. This was accomplished primarily with the incorporation of trifluoromethyl groups (e.g. $-OCR(CF_3)_2$, $-OCR_2(CF_3)$, $-OCRR'(CF_3)$ ligands), although it was expected that the nature of the R and R' groups would also have an effect. First consider the series of ligands based on the general formula $-OCR(CF_3)_2$. Increasing the electron-withdrawing power of R should enhance the degree of charge dispersal in the anion, thereby decreasing the ion-pairing strength

Table 18. Conductivities of $LiCF_3SO_3$, $LiAlF(HFPP)_3$, and $LiAl(OR_f)_4$.

compound	solvent	conc., M	conductivity, mS cm^{-1}
$LiAl(TFPE)_4$	DME	0.01	0.125
$LiAl(TFPE)_4$ + 2 eq. 12-c-4	DME	0.01	0.122
$LiAl(DPTE)_4$	DME	0.01	0.205
$LiAl(HFBuPP)_4$	DME	0.01	0.218
$LiAl(HFTP)_4$	DME	0.01	0.236
$LiAl(HFPP)_4$	DME	0.01	0.236
$LiAl(HFPP)_4$	1,2-$C_6H_4F_2$	0.01	0.003
$LiAl(HFPP)_4$	toluene	0.01	–[a]
$LiAl(HFCP)_4$	DME	0.1	0.283
$LiAl(HFIP)_4$	DME	0.01	0.300
$LiAl(HFTB)_4$	DME	0.01	0.308
$LiAl(PFTB)_4$	DME	0.01	0.342
$LiAl(HFPP)_4$	DME	0.1	2.05
$LiAlF(HFPP)_3$	DME	0.1	0.500
$LiCF_3SO_3$	DME	0.01	0.004
$LiCF_3SO_3$ + 2 eq. 12-c-4	DME	0.01	0.010
$LiAl(HFBuPP)_4$	ACN	0.01	0.786
$LiAl(HFTP)_4$	ACN	0.01	0.847
$LiAl(HFPP)_4$	ACN	0.01	0.883

Table 18 (continued).

$LiAl(HFCP)_4$	ACN	0.01	0.883
$LiAl(PFTB)_4$	ACN	0.01	0.927
$LiAl(HFIP)_4$	ACN	0.01	1.020
$LiAl(HFTB)_4$	ACN	0.01	1.020

[a] Too low to measure. 12-c-4 = 12-crown-4. See Table 2 for definitions of abbreviations.

of the anion and increasing the conductivity of its lithium salt. This prediction turned out to be true only in the case of $LiAl(PFTB)_4$, in which the trifluoromethyl group is much more electron-withdrawing than the other R moieties. For all other salts, the predicted ion-pairing strength does not correlate with conductivity. For example, the conductivity of $LiAl(HFTB)_4$ is higher than $LiAl(HFPP)_4$, even though a phenyl group is more electron-withdrawing than a methyl group (which is even slightly *electron-donating*). This idea is shown graphically in Figure 40, in a plot of conductivity vs. pK_a of the protonated fluoroalkoxide ligand. The fluoroalcohol pK_a values, listed in Table 19, provide a relative measure of the ability of each fluoroalkoxide ligand to disperse the negative charge of the corresponding anion; the lower the pK_a, the higher the degree of charge dispersal, and the weaker the ion-pairing strength. No obvious correlation was observed, and it does not appear that ion-pairing strength is primarily responsible for the observed differences in conductivity.

Ion pairing is not the only factor to consider when evaluating conductivity values. Ion mobility is also important, which is dependent on ion size. Both the cation and anion determine the conductivity, so it is necessary to consider the contribution of each. While the size of the $Li(DME)_2^+$ complex does not vary, the size of the anion is different for each salt, and this affects the conductivity. Figure 41 illustrates this relationship in a plot of conductivity vs. $LiAl(OR_f)_4$ formula unit volume. Formula unit volume was used to approximate anion size and was obtained from the appropriate solid-state structure, or estimated ($LiAl(HFTB)_4$ and $LiAl(PFTB)_4$) from very similar structures (values are listed in Table 19). In contrast to Figure 40, a strong ($R^2 = 0.68$) correlation is seen: as anion size increases, conductivity decreases.

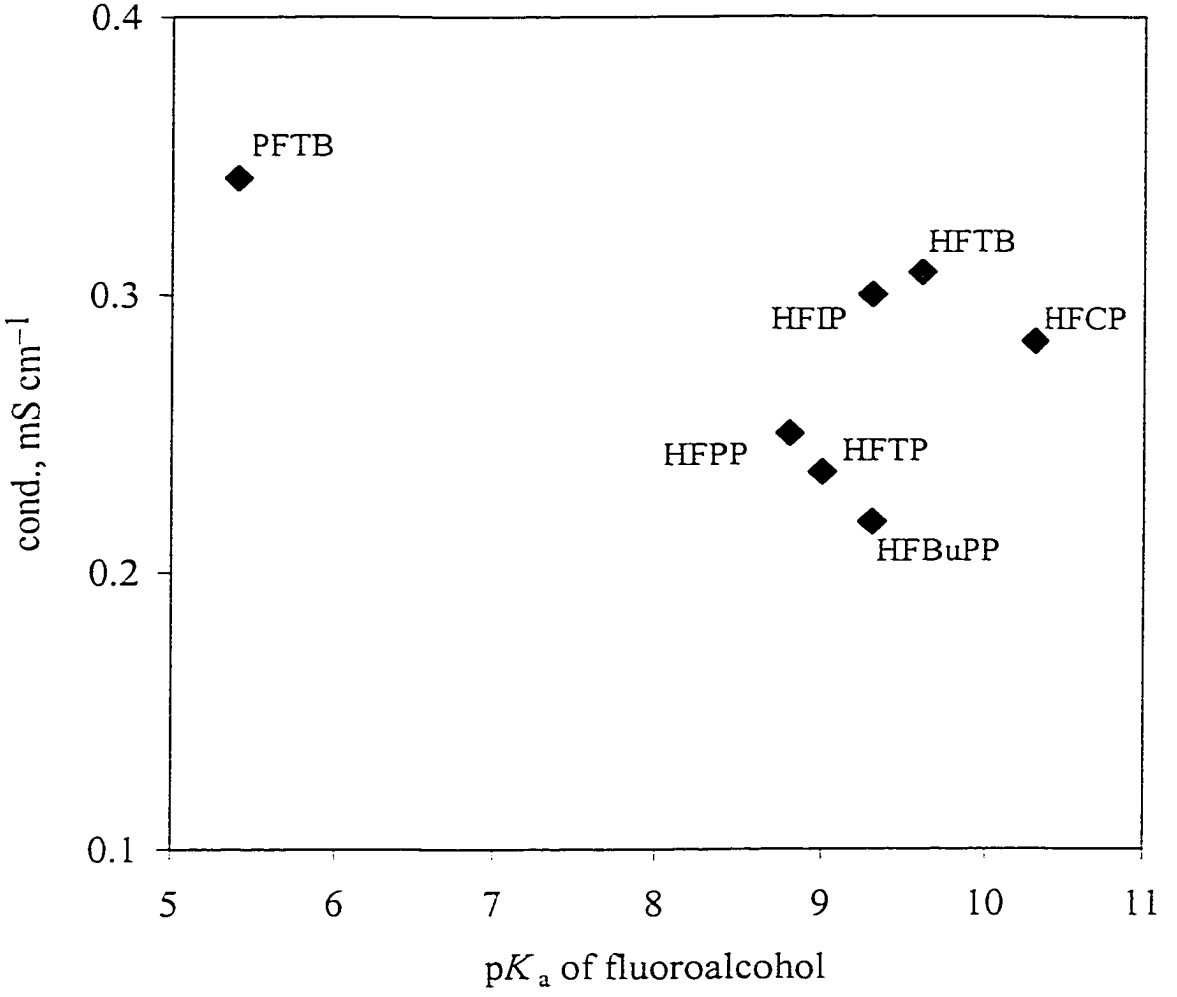

Figure 40. Plot of conductivity of $LiAl(OCR(CF_3)_2)_4$ salts in DME vs. pK_a of $HOCR(CF_3)_2$. See Table 2 for definitions of abbreviations.

Table 19. pK_a Values and formula unit volumes for $LiAl(OR_f)_4$ salts.

compound	pK_a of HOR_f [a]	formula unit volume of $LiAl(OR_f)_4$, Å^3
$LiAl(HFBuPP)_4$	9.3[18]	1507[b]
$LiAl(HFTP)_4$	9.0[18]	1124[b]
$LiAl(HFPP)_4$	8.8[18]	977.0[b]
$LiAl(HFCP)_4$	10.3[18]	1047[b]
$LiAl(PFTB)_4$	5.4[19]	750[c]
$LiAl(HFIP)_4$	9.3[19]	545[b]
$LiAl(HFTB)_4$	9.6[19]	700[c]

[a] Aqueous pK_a value. [b] from X-Ray structure determinations. [c] Estimated from structure of Li·(2-cyclohexenone)Al(HFTB)$_4$. See Table 2 for definitions of abbreviations.

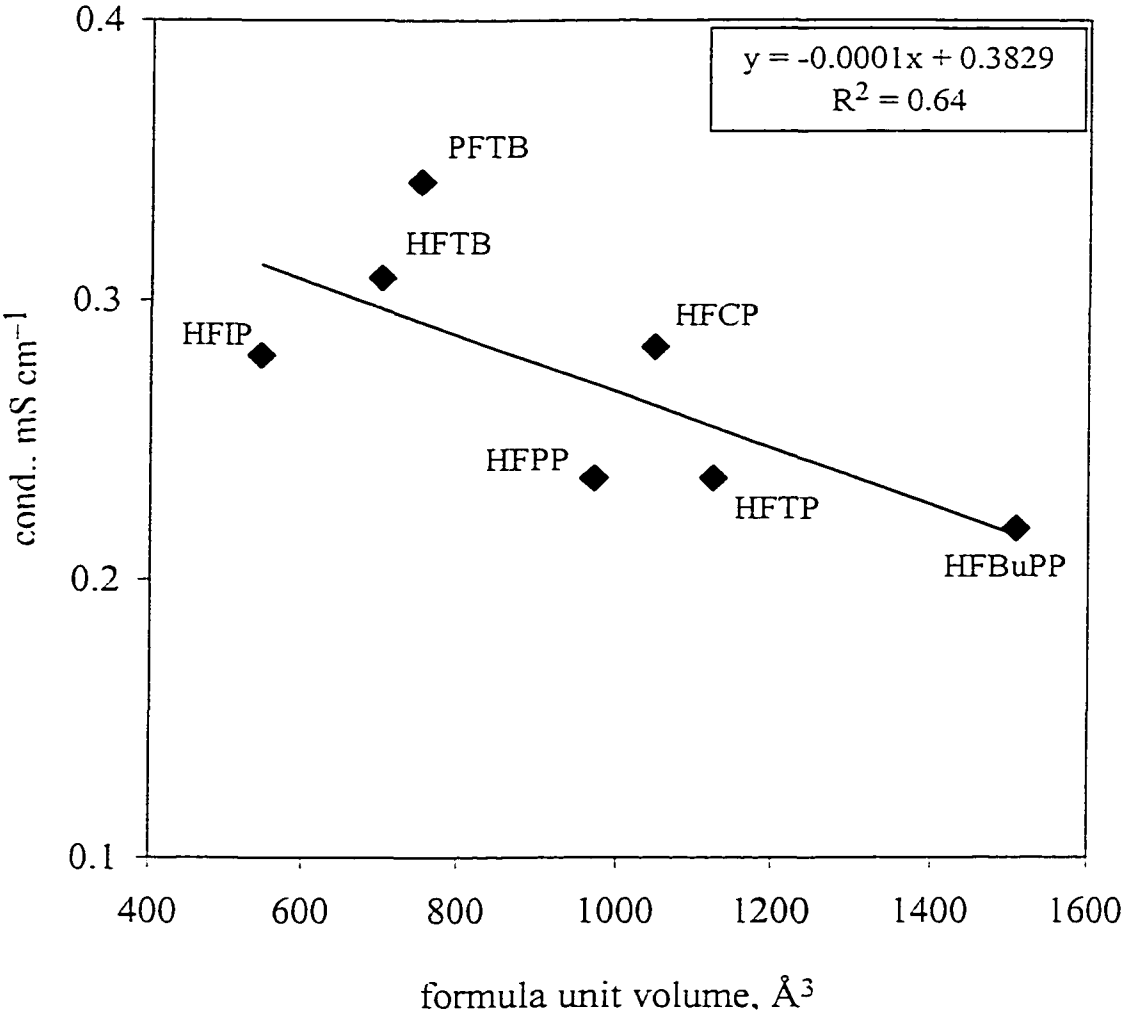

Figure 41. Plot of conductivity vs. formula unit volume for $LiAl(OCR(CF_3)_2)_4$ salts in DME. See Table 2 for definitions of abbreviations.

Another possible explanation for the observed trend in conductivities lies in the relative tendencies to form triple ions. As discussed above, triple ion formation acts to increase conductivity by producing more charge carriers. As the stability of these species increases, their concentration will also increase, leading to a higher conductivity. It was demonstrated that the formation of triple ions is favorable for $LiAl(HFIP)_4$ and $LiAl(HFTB)_4$, but is not as favorable for $LiAl(HFPP)_4$. Assuming that steric bulk is the determining factor, it is predicted that triple ion formation would be increasingly less favorable as the size of the R group increases. Based on this assumption, the conductivities of $LiAl(HFPP)_4$ (0.236 mS cm^{-1}), $LiAl(HFTP)_4$ (0.236 mS cm^{-1}), and $LiAl(HFBuPP)_4$ (0.218 mS cm^{-1}) can be explained according to their relative tendencies to form triple ions. The HFPP (R = phenyl) and HFTP (R = *p*-tolyl) ligands have similar sizes, but the HFBuPP (R = 4-*t*-butyl-phenyl) ligand is much larger. Thus, the anions composed of HFPP and HFTP ligands presumably have similar tendencies to form triple ions, and the anion composed of HFBuPP ligands a much lower tendency. As such, $LiAl(HFPP)_4$ and $LiAl(HFTP)_4$ have the same conductivity, while that of $LiAl(HFBuPP)_4$ is lower. The higher conductivity of $LiAl(HFCP)_4$ may be due to the more flexible R group (cyclohexyl) on each ligand, which would lead to more stable triple ions. The data fit this hypothesis based on triple ion stability, as well as the size hypothesis proposed above. In reality, the results most likely reflect a combination of both these effects.

Conductivities of $LiAl(OCR(CF_3)_2)_4$ were also measured at 0.01 M in acetonitrile (Table 18). The high dielectric constant (ε = 36) of this solvent disfavors triple ion formation, thereby simplifying the solution dynamics. The high permittivity also minimizes the effect of ion-pairing strength; while this was shown to have only a minor

influence on the conductivity of $LiAl(OCR(CF_3)_2)_4$ in DME, it was still a factor when $LiAl(PFTB)_4$ was considered. A plot of conductivity in ACN vs. pK_a shown in Figure 42 demonstrates this, in which no obvious correlation is observed between the two variables. In contrast, in a plot of conductivity in ACN vs. formula unit volume shown in Figure 43, a strong correlation ($R^2 = 0.90$) is observed. Assuming that the concentration of triple ions is negligible in all cases, anion size is left as the only significant variable, and is the determining factor for conductivity of $LiAl(OCR(CF_3)_2)_4$ salts in this solvent. Although Li^+ solvation is probably significantly different in ACN and DME, these data lend support to the hypothesis that anion size is the determining factor for the conductivity of $LiAl(OR_f)_4$ salts in DME as well.

All of the ligands discussed to this point are derived from the general formula – $OCR(CF_3)_2$. Another class under study is based on OR_f ligands with only one trifluoromethyl group, to investigate the effect of decreased fluorine content. Two new lithium salts have been synthesized: $LiAl(DPTE)_4$ and $LiAl(TFPE)_4$ (the former compound by the author, the latter by Dr. Svetlana Ivanova in the Strauss group). The conductivity of $LiAl(DPTE)_4$ is quite high, and is comparable to the bis(trifluoromethyl) derivatives, while the value for $LiAl(TFPE)_4$ is much lower. The only difference between the two anions is the substitution of a phenyl group for a hydrogen atom on each ligand, which has a large impact on anion size. This illustrates an important consideration in the design of *WCA*s: as the size of an anion increases, it generally becomes more weakly ion-pairing, due to the higher degree of charge dispersal and weakened electrostatic interaction. The $Al(DPTE)_4^-$ anion is larger than $Al(TFPE)_4^-$, and is thus presumably more weakly ion-pairing, resulting in a higher conductivity for its lithium salt. This argument may appear to contradict what was discussed above, but it is

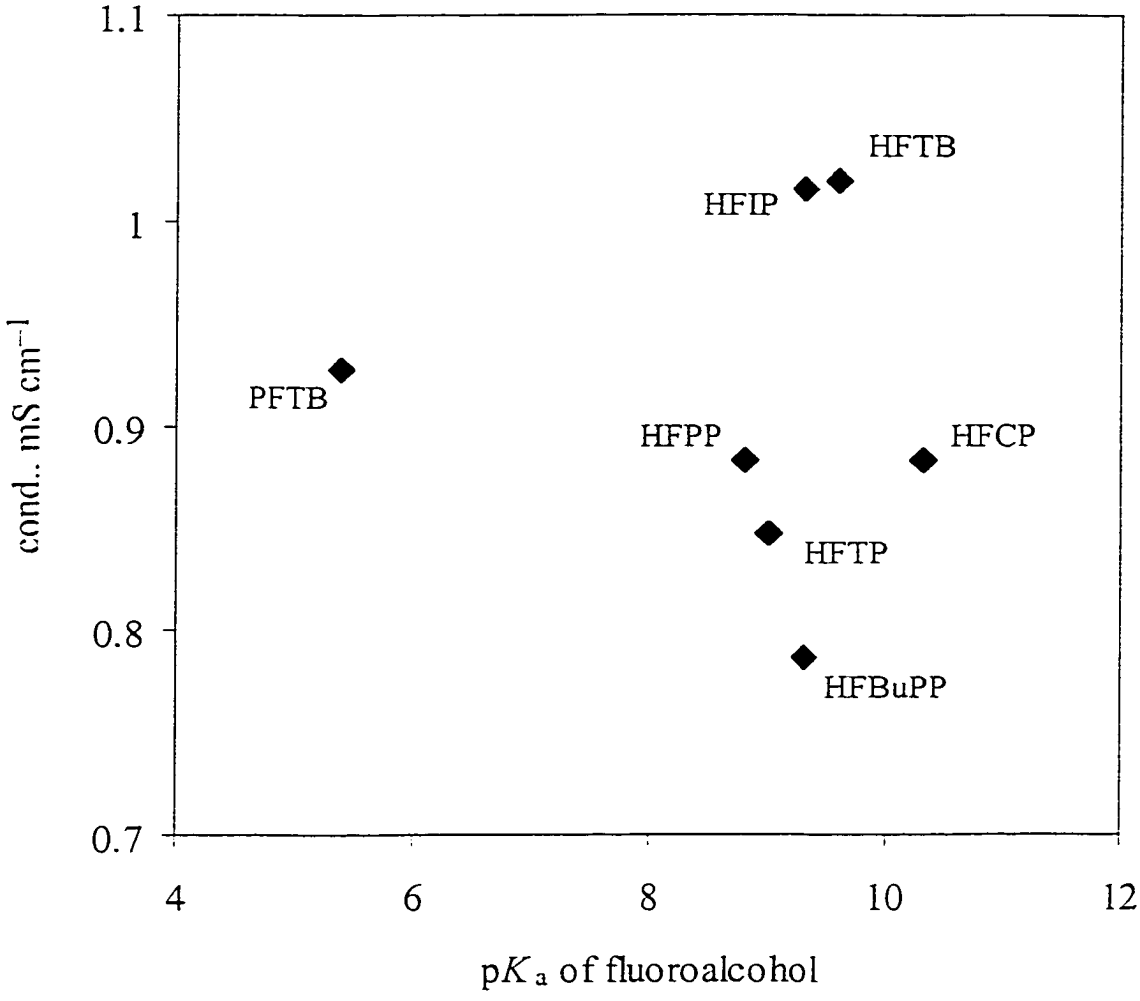

Figure 42. Plot of conductivity of $LiAl(OCR(CF_3)_2)_4$ salts in ACN vs. pK_a of $HOCR(CF_3)_2$. See Table 2 for definitions of abbreviations.

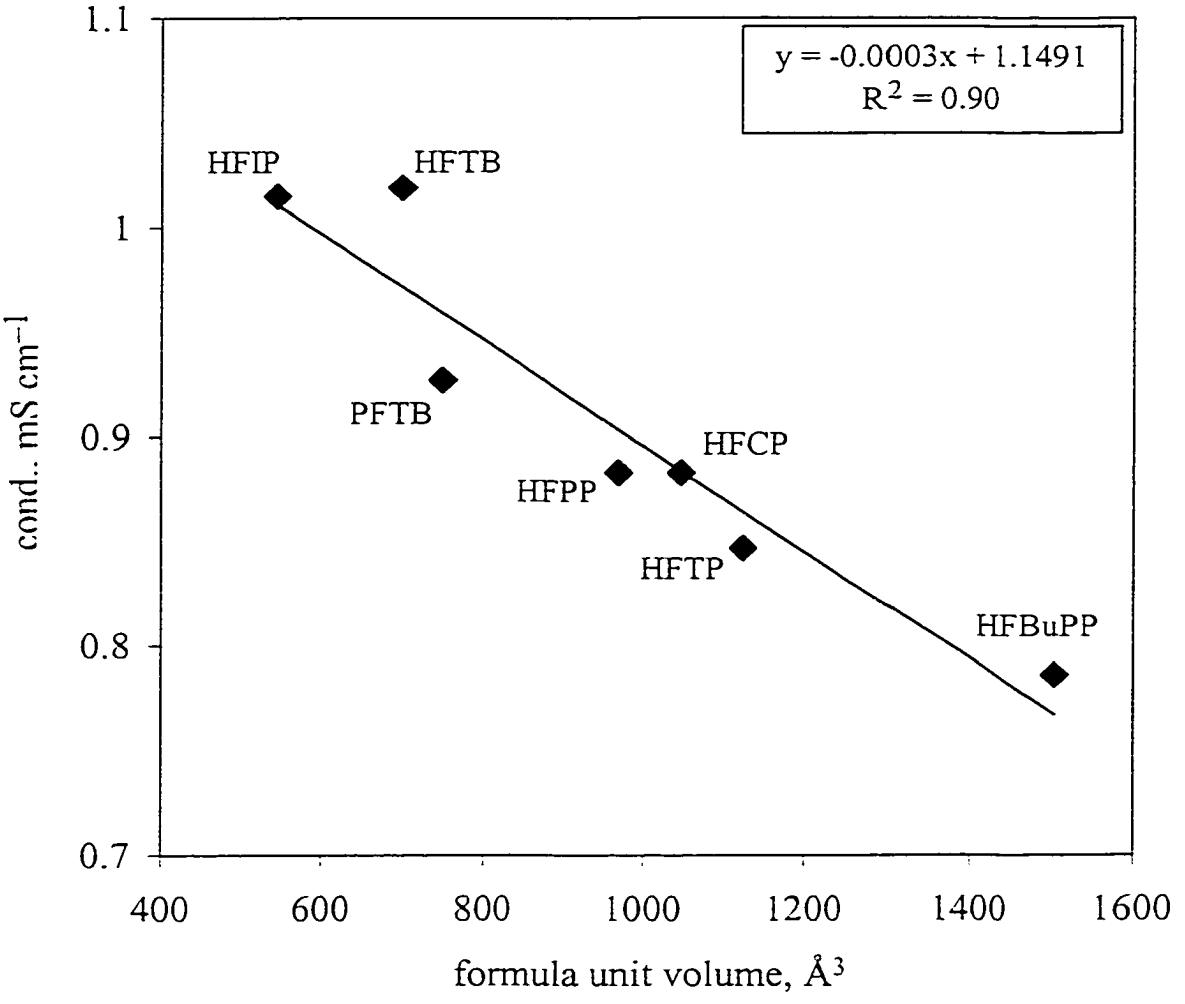

Figure 43. Plot of conductivity vs. formula unit volume for $LiAl(OCR(CF_3)_2)_4$ salts in ACN. See Table 2 for definitions of abbreviations.

important to keep in mind that conductivity is a convolution of ion mobility *and* ion-pairing. Although the $Al(TFPE)_4^-$ anion is weakly ion-pairing, its conductivity is low enough that both of these factors are most likely important, in contrast to the "extremely weak ion-pairing strength" regime of the other salts. Increasing anion size from $Al(TFPE)_4^-$ to $Al(DPTE)_4^-$ decreases conductivity in terms of ion mobility, but the increase due to weaker ion pairing outweighs this, leading to a higher conductivity overall.

The importance of effective fluoroalkoxyaluminate anions having four fluoroalkoxide substituents is illustrated by a comparison between the 0.1 M conductivities of $LiAl(HFPP)_4$ and $LiAlF(HFPP)_3$ (Table 18). The latter compound contains an anion with three HFPP ligands and one fluorine atom bonded to aluminum, and has a conductivity four times less than that of $LiAl(HFPP)_4$. The substitution of only one HFPP ligand for a fluorine atom has a dramatic effect on conductivity, and indicates a much higher ion-pairing strength for $AlF(HFPP)_3^-$.

Due to the extremely weak ion-pairing strength of $Al(OR_f)_4^-$ and the high solubility of certain $LiAl(OR_f)_4$ salts in low-polarity solvents, the use of alternative electrolyte solvents was investigated. The conductivity of $LiAl(HFPP)_4$ was measured at 0.01 M in toluene and 1,2-difluorobenzene (Table 18). The conductivity in toluene was too low to measure with the apparatus used, indicating a strongly bound ion pair. This suggests that the solution structure of this lithium aluminate in toluene is very similar to the solid-state structure (Figure 37). The conductivity in 1,2-difluorobenzene has a value of 0.003 mS cm^{-1}. Apparently, $LiAl(HFPP)_4$ is dissociated to a small extent in this solvent, indicating that 1,2-difluorobenzene is a strong enough donor to compete with $Al(HFPP)_4^-$ in coordinating to Li^+. Given the low donor strength of 1,2-difluorobenzene,

this provides additional evidence for the extremely weak ion-pairing strength of this aluminate anion. Furthermore, the fact that Li^+ is somewhat dissociated in this nonpolar solvent provides an insight into the origin of its catalytic activity as discussed earlier. Not only is $LiAl(HFPP)_4$ soluble in low-polarity solvents, but the anion is sufficiently weakly ion-pairing to yield a highly active Lewis acid.

Maximum Conductivity of $LiAl(OR_f)_4$

As for $LiB(O_2L_f)_2$ salts, the conductivity behavior of $LiAl(OR_f)_4$ was examined in DME at various concentrations to determine the κ_{max} values. Three salts were studied in this manner: $LiAl(HFIP)_4$, $LiAl(HFTB)_4$, and $LiAl(HFPP)_4$, and Figure 44 shows a plot of conductivity vs. concentration for each of these. $LiAl(HFIP)_4$ and $LiAl(HFTB)_4$ greatly exceed the practical minimum of 5 mS cm^{-1} (discussed in the Chapter 1 of this dissertation), and have κ_{max} values of 11.2 and 9.6 mS cm^{-1}, respectively. In contrast, $LiAl(HFPP)_4$ has a κ_{max} of only 4.2 mS cm^{-1}, below the practical minimum. One explanation for these differences stems from the different sizes of the fluoroalkoxide ligands that comprise each anion. As size increases, ion mobility as well as conductivity decreases. Another way to view this is in terms of viscosity. As ion size increases, solution viscosity also increases at a given concentration. This restricts the movement of both the cation and anion, resulting in a lower conductivity. In order of increasing size, the three anions are $Al(HFIP)_4^-$ > $Al(HFTB)_4^-$ > $Al(HFPP)_4^-$. The methyl group on HFTB does not result in a large increase in anion size from HFIP, but the phenyl group on HFPP does. Accordingly, the maximum conductivities follow the same order.

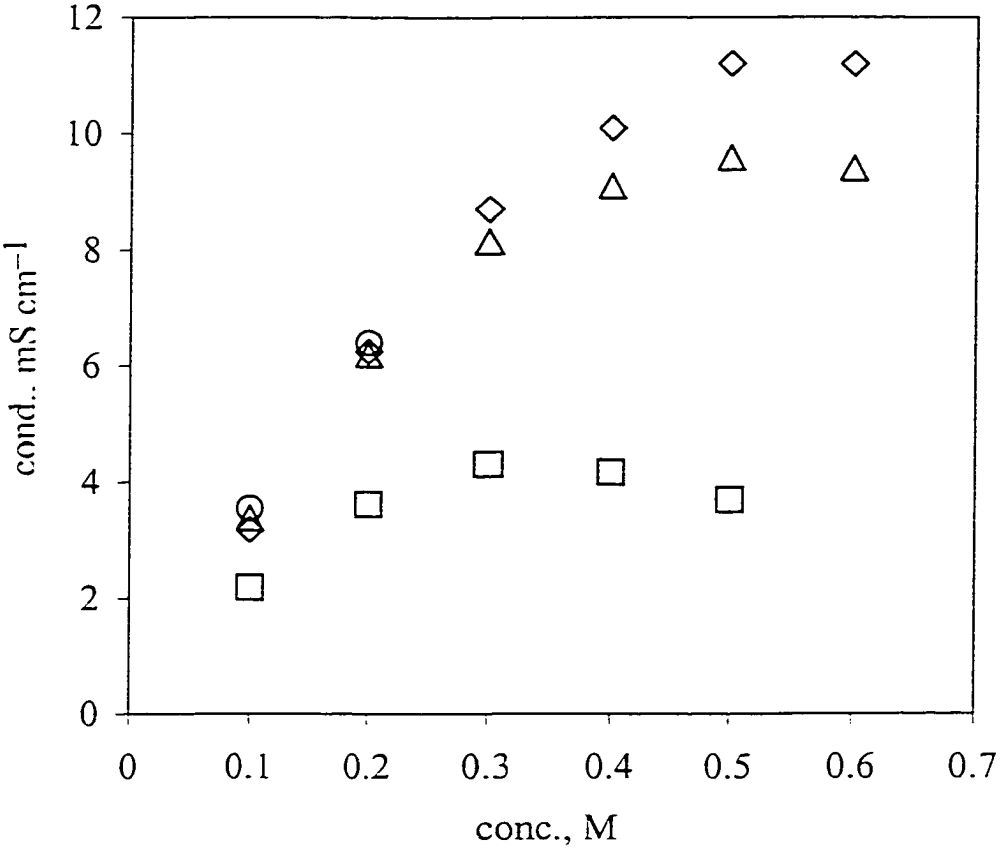

Figure 44. Plot of conductivity vs. concentration for $LiAl(OR_f)_4$ salts in DME. Squares – $LiAl(HFPP)_4$; circles – $LiAl(PFTB)_4$; triangles – $LiAl(HFTB)_4$; diamonds – $LiAl(HFIP)_4$. See Table 2 for definitions of abbreviations.

Another factor that may be contributing to the large difference in κ_{max} values between the $LiAl(HFIP)_4$ and $LiAl(HFTB)_4$ salts and $LiAl(HFPP)_4$ is the tendency to form triple ions. As discussed above, the formation of these affects the number of charge carriers in two ways: first, by physically creating more of these; second, by raising the solution permittivity, thereby shifting the dissociation equilibrium of $LiAl(OR_f)_4$ to form more ions. $LiAl(HFIP)_4$ and $LiAl(HFTB)_4$ were shown to behave in this manner, which may be partly responsible for their very high maxima relative to $LiAl(HFPP)_4$, which does not.

The maxima observed in DME for $LiAl(HFIP)_4$ and $LiAl(HFTB)_4$ are very encouraging, as they greatly exceed the practical minimum of 5 mS cm^{-1}. To determine its efficacy as *secondary* lithium battery electrolytes, the conductivity of $LiAl(HFIP)_4$ was also evaluated in EC/DMC. The conductivity maximum for this salt was found to be 6.1 mS cm^{-1} (also at 0.5 M) in this solvent by Mr. Shoichi Tsujioka (a former research associate in the Strauss group), which is much lower than the maximum in DME, but still above the practical minimum. The reduction in κ_{max} between solvents is most likely due to decreased ion mobilities. The EC/DMC mixture is more viscous that DME, and is thus more restrictive of ion movement. While $Al(HFIP)_4^-$ is the smallest aluminate anion, it is still relatively large, and its mobility will be noticeably affected by a change in solvent viscosity. As was done for $LiB(HFPOP)_2$, the conductivity of $LiAl(HFIP)_4$ was also measured in various mixtures of EC/DMC in an attempt to find an optimal solvent. Conductivities were measured at 0.5 M, and the results are shown graphically in Figure 45. Again, the desired effect was not observed: between 50% and 30% EC content, there is only an increase of 0.8 mS cm^{-1}. One possible explanation for this is that the viscosity is still too high to yield a high conductivity, even when the solvent is 100% DMC (η =

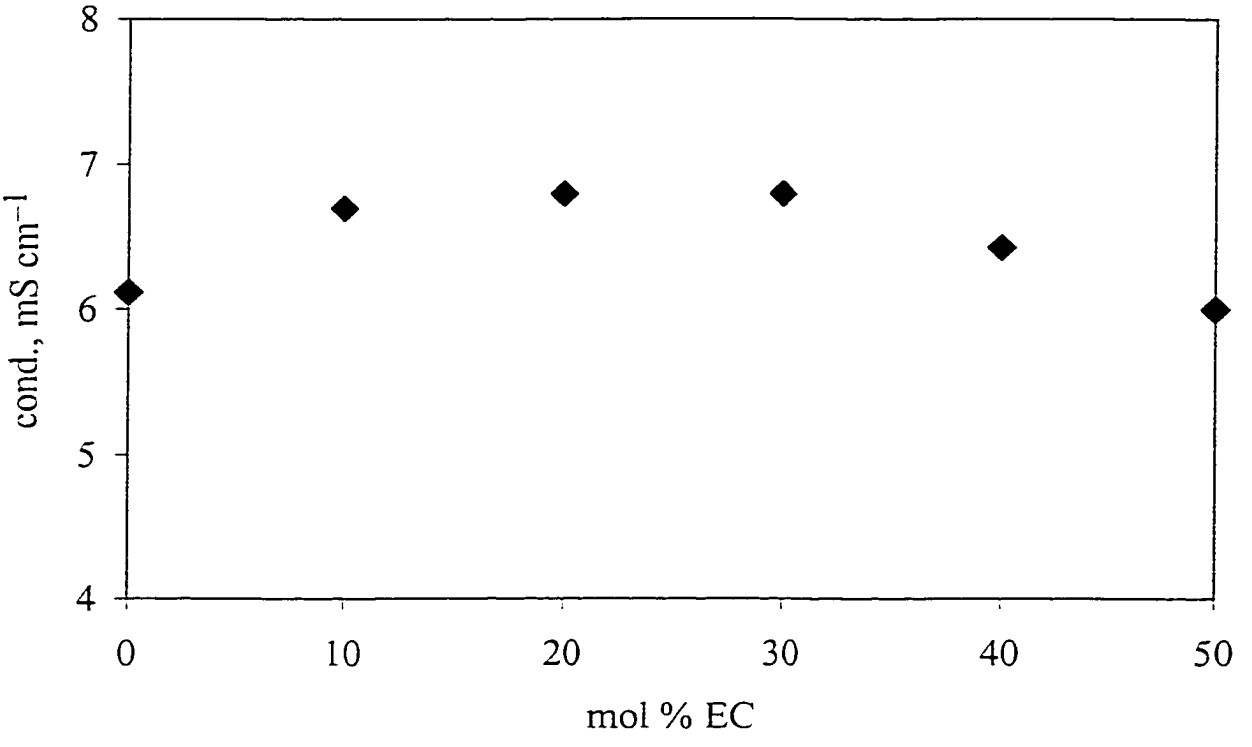

Figure 45. Plot of conductivity of 0.5 M $LiAl(HFIP)_4$ vs. mol% EC. The other component of the solvent is DMC. See Table 2 for definitions of abbreviations.

0.59 cP) . It was not expected that this rather small increase in viscosity (vs. 0.407 cP for DME) would have such a deleterious effect. Another possibility is the smaller donor number of both EC (16.4) and DMC (15.1) vs. DME (24).

A final point to consider is that as was the case with $LiB(O_2L_f)_2$, the concentrations of $LiAl(OR_f)_4$ involved the conductivity analyses do not exceed 0.6 M, and very high values are observed at 0.5 M. As was mentioned earlier, a concentration of 1 M is necessary to achieve a useful conductivity for a given lithium salt. However, for $LiAl(HFIP)_4$, a value of 11.2 mS cm^{-1} is observed at 0.5 M, *half* of the usual concentration. For this compound and $LiAl(HFTB)_4$, conductivities of 6.2 mS cm^{-1} are seen at 0.2 M, indicating that even less compound could be used in to reach the 5 mS cm^{-1} minimum. This could be very important if any of these salts are developed commercially. Even if the new lithium aluminates are more expensive than $LiPF_6$ (as an example), the fact that the amount required is much less could match, or be lower than, the production cost of a battery using the latter salt.

Electrochemical Stability of $LiAl(OR_f)_4$

The lithium fluoroalkoxyaluminates were characterized for their electrochemical stability in the same manner as for the lithium borates. This work was performed by Mr. Shoichi Tsujioka. Two salts were studied in detail: $LiAl(HFIP)_4$ and $LiAl(HFPP)_4$. Both were found to be oxidatively (>5.0 V vs. $Li^{0/+}$) and reductively stable in several solutions, and neither were found to promote the corrosion of aluminum. Additional tests were done to determine the stability of the electrolyte in contact with commonly used cathode ($LiCoO_2$) and anode (MCMB carbon) materials. It was found that both salts are

stable under these conditions as well. Due to its combination of favorable properties, $LiAl(HFIP)_4$ is currently being developed for commercialization.

Conclusions

New varieties of $Al(OR_f)_4^-$ based on the $Al(HFPP)_4^-$ prototype have been developed. Those that were structurally characterized showed that C–F bonds coordinated to Li are longer than those that are not, in agreement with previous results. The new salt $LiAl(HFCP)_4$ was found to have the highest hexane solubility of all known $LiAl(OR_f)_4$, and is an order of magnitude greater than that of $LiAl(HFPP)_4$. Conductivity studies showed that all $LiAl(OR_f)_4$ salts are very weakly ion-pairing when compared to PF_6^- and $CF_3SO_3^-$. In fact, the ion-pairing strengths of the new anions are so weak that ion mobility, and not ion-pairing, is the primary factor determining conductivity in DME and ACN. The maximum conductivity for $LiAl(HFIP)_4$ is very high in DME, and it was also found that this salt satisfies other requirements for practical use in battery systems.

References

1. Tsujioka, S.; Strauss, S.H. *unpublished results*.
2. Krossing, I. *Chem. Eur. J.* **2000**, *6*, 0000.
3. Barbarich, T.J., Ph.D. Dissertation, Colorado State University, 1999.
4. Perozzi, E.F.; Michalak, R.S.; Figuly, G.P.; Stevenson, W.H.; Ross, M.R.; Martin, J.C. *J. Org. Chem.* **1981**, *46*, 1049.
5. Sheldrick, G.M., SMART/SAINT. Siemens Analyt. X-Ray Instr. Inc., Madison, WI, 1994.
6. Sheldrick, G.M., SHELXTL, vers. 5.03 (1994).
7. Flack, H.D. *Acta Crystallogr.* **1985**, *A39*, 876.
8. Bernardinelli, G.; Flack, H.D. *Acta Crystallogr.* **1985**, *A41*, 500.
9. Howard, E.G.; Sargeant, P.B.; Krespan, C.G. *J. Am. Chem. Soc.* **1967**, *89*, 1422.
10. Maruta, T.; Nishinomiya, T. (Central Glass Co., Ltd., Japan) Jpn. Kokai Tokkyo Koho 03027338, 1991.
11. Guzei, I.A.; Radzewich, C.E.; Jordan, R.F. *Acta Crystallogr. C* **2000**, *C56*, 279.
12. Barbarich, T.J.; Handy, S.T.; Miller, S.M.; Anderson, O.P.; Grieco, P.A.; Strauss, S.H. *Organometallics* **1996**, *15*, 3776.
13. Boche, G. *Angew Chem. Int. Ed. Engl.* **1992**, *31*, 731.
14. Gutmann, V. *Coordination Chemistry in Nonaqueous Solvents*; Springer-Verlag: Wien-New York, 1969.
15. Gutmann, V. *Coord. Chem. Rev.* **1967**, *2*, 239.
16. Eichorst, D.J.; Payne, D.A.; Wilson, S.R.; Howard, K.E. *Inorg. Chem.* **1990**, *29*, 1458.

17. Rockwell, J.J.; Kloster, G.M.; Dubay, W.J.; Grieco, P.A.; Shriver, D.F.; Strauss, S.H. *Inorg. Chim. Acta* **1997**, *263*, 195.

18. Ivanova, S.M.; Nolan, B.G.; Kobayashi, T.; Miller, S.M.; Anderson, O.P.; Strauss, S.H. *Chem. Eur. J.* **2001**, *in press*.

19. (a) Dyatkin, B.L.; Mochaline, E.P.; Knunyants, I.L. *Tetrahedron*, **1965**, *21*, 2991. (b) Willis, C.J. *Coord. Chem. Rev.* **1988**, 133.

CHAPTER 4

Additional New Classes of Weakly Coordinating Anions

Aside from the two major classes of new weakly coordinating anions discussed above, several others were explored as well: compounds based on the general formula $B(OR_f)(C_6F_5)_3^-$; carborane anions; and a weakly coordinating anion consisting of a hydrogen-bonded complexe. All of these were characterized in terms of their conductivities in various solvents, and are the subject of this chapter.

Experimental

Materials

Schlenk, glovebox, and high vacuum techniques were employed, with purified argon or nitrogen used when an inert atmosphere was required. All reagents and solvents were reagent grade or better. The compounds *n*-BuLi (2.5 M, Aldrich) and CF_3CO_2H (Aldrich, 99+%) were used as received. To prove that the CF_3CO_2H was sufficiently dry, ^1H NMR spectra of it dissolved in dry acetonitrile-d_3, with and without added $(CF_3CO)_2O$, were obtained. The δ value for the acidic H atom was the same in both cases; control experiments demonstrated that traces of water cause a shift in δ(H). The compounds $LiCF_3CO_2$ (Aldrich, 95%) and $NEt_4(CF_3CO_2)$ (Aldrich, 98%) were dried by heating under vacuum for 18 h at 110 °C or 35 °C, respectively. The compound $B(C_6F_5)_3$ (Boulder Scientific Co.) was dried by stirring with 1 M BCl_3 in 30 mL toluene for 18 h. Toluene and traces of HCl were removed under vacuum at room temperature,

and $B(C_6F_5)_3$ was sublimed from traces of $B(OH)_3$ under dynamic vacuum at 81 °C. ^1H NMR spectroscopy confirmed that the product was dry, and ^{19}F NMR spectroscopy confirmed that it was pure. The following solvents were obtained from the indicated commercial vendors, and were purified by distillation under nitrogen or under vacuum from the indicated drying agent: tetrahydrofuran (THF, Fisher, Na); 1,2-dimethoxyethane (DME, Acros, Na); propylene carbonate (PC, Aldrich, 4Å molecular sieves); acetonitrile-d_3 (Cambridge, CaH_2).

[Li][$CB_{11}H_{12}$]. The compound $[NHMe_3][CB_{11}H_{12}]$[1] (0.998 g, 4.92 mmol) was dissolved in dry THF (25 mL) and treated with *n*-BuLi (4.92 mmol) dropwise at room temperature. The cloudy mixture was stirred for 1 h. At this point, all volatiles (THF and NMe_3) were removed under vacuum to leave a white solid, which was dried under vacuum at 210 °C for 6 h to yield $LiCB_{11}H_{12}$ as a white powder (0.590 g, 80% yield). $^{11}B\{^1H\}$ NMR (CD_3CN): δ –5.84 (int. 1), –12.31 (int. 5), –15.38 (int. 5).

[Li][7,8,9,10,11,12-$CB_{11}H_6Br_6$]. The compound $[NHMe_3][CB_{11}H_6Br_6]$[2] (0.223 g, 0.329 mmol) was dissolved in dry THF (20 mL) and treated with *n*-BuLi (0.332 mmol) dropwise at 0 °C. After the addition was complete, the cloudy mixture was warmed to room temperature and stirred for 1 h. At this point, all volatiles (THF and NMe_3) were removed under vacuum to leave a white solid, which was dried under vacuum at 150 °C for three days to yield $LiCB_{11}H_6Br_6$ as a white solid (0.139 g, 68%). ^1H NMR (CD_3CN) δ 2.90 (s, 1 H), 2.30 (q, $J_{B\text{-}H}$ = 174 Hz, 6 H).

[Li][1-CH_3-$CB_{11}F_{11}$]. The compound $[NHMe_3][1\text{-}CH_3\text{-}CB_{11}F_{11}]$[3] (0.255 g, 0.614 mmol) was dissolved in dry THF (15 mL) and treated with *n*-BuLi (0.614 mmol) dropwise at 0 °C. After the addition was complete, the cloudy mixture was warmed to room temperature and stirred for 3 h. At this point, all volatiles (THF and NMe_3) were

removed under vacuum to leave an off-white solid, which was dried under vacuum at 145 °C for 18 h to yield [Li][1-CH_3-$CB_{11}F_{11}$] as an off-white solid (0.144 g, 65%). ^{1}H NMR (CD_3CN) δ 1.54 (s, 3 H).

Physical Measurements

Samples for NMR spectroscopy were solutions in 5 mm glass tubes. NMR spectra were recorded on a Varian 300 spectrometer operating at the indicated frequencies: ^{1}H, 300.1 MHz; ^{19}F, 282.4 MHz. Chemical shifts (δ scale) are relative to $SiMe_4$ ($\delta = 0$ for ^{1}H NMR) and $CFCl_3$ ($\delta = 0$ for ^{19}F NMR). Solution conductances were measured at 24±1 °C using a YSI Model 3403 conductivity cell calibrated for inverted use ($k = 0.9988\ cm^{-1}$) and a YSI Model 32 conductivity bridge. The bridge was operated at 1 KHz (conductances > 100 μS) or at line frequency (50–60 Hz, conductances <100 μS). Measurements made using both modes were the same, but a sharper null point was observed at 1 KHz for higher conductances, and at line frequency for lower conductances. All samples were anhydrous as determined by ^{1}H NMR spectroscopy, and solutions of these were prepared in volumetric flasks in the glovebox. The error in measurement was determined to be < 1% using the same batch of material. Variation from one batch to another was found to be 2% or less.

Results and Discussion

Carborane Anions

The conductivities of $[Li][CB_{11}H_{12}]$, $[Li][7,8,9,10,11,12\text{-}CB_{11}H_6Br_6]$, and $[Li][1\text{-}CH_3\text{-}CB_{11}F_{11}]$ were determined at a concentration of 0.01 M in various solvents. The results are listed in Table 20.

Table 20. 0.01 M Conductivities of lithium carborane anions in DME, THF, and PC.

compound	solvent	cond., mS cm^{-1}
$[Li][CB_{11}H_{12}]$	THF	0.059
$[Li][CB_{11}H_{12}]$	PC	0.152
$[Li][CB_{11}H_6Br_6]$	THF	0.149
$[Li][CB_{11}H_6Br_6]$	PC	0.134
$[Li][1\text{-}CH_3\text{-}CB_{11}F_{11}]$	DME	0.170
$[Li][1\text{-}CH_3\text{-}CB_{11}F_{11}]$	PC	0.155

Tetrahydrofuran was used as the solvent for $[Li][CB_{11}H_{12}]$ and $[Li][CB_{11}H_6Br_6]$, and DME was the solvent for $[Li][1\text{-}CH_3CB_{11}F_{11}]$. Although these are different solvents, they are very similar in terms of both permittivity (ε = 7.39, 7.20 for THF, DME respectively), viscosity (η = 0.455, 0.46 cP for THF, DME respectively) and donor number (DN = 20, 24 for THF, DME respectively).[4] Thus, the conductivities of salts should be similar in both solvents, and this has been observed in past experiments.[5] The effect of halogen content can be seen in comparing the three salts: as this increases,

conductivity also increases, reflecting a decrease in ion-pairing strength as a result of enhanced charge dispersal.

The conductivities of $[Li][CB_{11}H_{12}]$, $[Li][CB_{11}H_6Br_6]$, and $[Li][1\text{-Me-}CB_{11}F_{11}]$ were also measured in propylene carbonate (Table 20), a solvent commonly used in battery systems. It has the advantage of high permittivity ($\varepsilon = 64.4$), but suffers from a high viscosity ($\eta = 2.53$ cP).[4] As such, it is well-suited for use in conjunction with electrolytes containing small anions, where ion-pairing strength, and not ion mobility, is the determining factor for conductivity. $[Li][1\text{-Me-}CB_{11}F_{11}]$ and $[Li][CB_{11}H_{12}]$ have essentially the same conductivity, while the value for $[Li][CB_{11}H_6Br_6]$ is lower. These are different from the results in DME, and reflect the importance of ion mobility. In PC, all three carborane anions are presumably weakly-ion paired with Li^+, and the degree of association does not determine conductivity. The F_{11} and H_{12} anions are approximately the same size, and thus have very similar conductivities. However, the Br_6 anion is significantly larger, has a lower mobility, and thus a lower conductivity.

$B(OR_f)(C_6F_5)_3^-$ Anions

Another class of anions that was investigated were those based on combining $B(C_6F_5)_3$ (FAB) with a lithium fluoroalkoxide. Using FAB as an anion receptor to generate weakly ion-pairing anions has been studied in the past by Lee *et al.*[6] Also, the types of compounds to be discussed are claimed in a patent filed by 3M Co.,[7] but prior to the work reported in this dissertation no experimental evidence existed for these species. Three $LiOR_f$ salts were used (LiHFIP, LiDPTE, LiPFTB), and the conductivities for 0.01 M DME solutions are listed in Table 21, as well as the value for LiHFIP.

Table 21. 0.01 M Conductivities of $LiB(OR_f)(C_6F_5)_3$ in DME.

compound	cond., mS cm^{-1}
$LiB(HFIP)(C_6F_5)_3$	0.176
$LiB(DPTE)(C_6F_5)_3$	0.129
$LiB(PFTB)(C_6F_5)_3$	0.137

See Table 2 for definitions of abbreviations.

The $B(OR_f)(C_6F_5)_3^-$ anion was generated *in situ*, by mixing one equivalent of each component in DME. Comparing the values for LiHFIP (too low to measure) and $LiB(HFIP)(C_6F_5)_3$, it can be seen that the FAB additive dramatically increases the conductivity. The negative charge on HFIP is more effectively dispersed by coordination to the Lewis acid, creating a more weakly ion-pairing anion. Adding FAB to LiDPTE yields a complex with a lower conductivity, reflecting either a larger anion size or the weaker electron-withdrawing framework of the DPTE alkoxide. The conductivity of the PFTB complex was unexpectedly low. This alkoxide is the most electron-withdrawing of all three studied, and is not much larger than HFIP. Considering these factors, the complex of LiPFTB with FAB should have the highest conductivity. One possible explanation is that the PFTB complex with FAB is not stable, and the weakly ion-pairing $B(PFTB)(FAB)^-$ anion was not formed to an appreciable extent.

The $B(OR_f)(C_6F_5)_3^-$ anions are specific examples or a more general class of *WCAs*: those in which a negative fragment is coordinated to a Lewis acid such that the overall charge is negative one (1–). This description can be applied to the major anions discussed in this work ($Al(OR_f)_4^-$, $B(O_2L_f)_2^-$), but in this case the two components do not exist independently. In contrast, for $B(OR_f)(C_6F_5)_3^-$, both FAB and $LiOR_f$ exist and are stable.

WCAs Based on Hydrogen-Bonded Complexes

Another class of *WCAs* based on the Lewis acid/neutral base theme consists of oxoanions A^- hydrogen-bonded to their conjugate acids HA to form HA_2^- anions.[8] Although the simplest example, $H(OH)_2^-$, might be expected to be rather strongly coordinating, anions such as $H(RCO_2)_2^-$ should be weakly coordinating because of the decrease in negative charge density on the oxygen atoms relative to the parent RCO_2^- anion. Gas phase dissociation enthalpies for the strongest O–H···O hydrogen bonds are ca. 30 kcal mol^{-1} (e.g., $H(CH_3CO_2)_2^-$, 29.3 kcal mol^{-1}).[9] Although this is considerably lower than the gas-phase enthalpies of F^- dissociation from BF_4^- (92(6) kcal mol^{-1}),[10] PF_6^- (101(8) kcal mol^{-1}),[11] and even HF_2^- (39(1) kcal mol^{-1}),[12] the fragmentation of a particular HA_2^- anion into HA and A^- may be sufficiently endothermic to afford stable complexes in some cases.

To determine if complexes of the type described above are weakly ion-pairing, the conductivities of THF solutions of $LiCF_3CO_2$ were measured with various amounts of added CF_3COOH. The results are shown graphically in Figure 46. The equivalent conductivity for 0.01 M $LiCF_3CO_2$ is a linear function of the concentration of added CF_3COOH ($[[CF_3COOH]_{total}]$) between 0 and 1 M added acid. The Λ value at 1 M added acid, 1.05 S cm^2 mol^{-1}, is 70 times larger than the Λ value with no added acid. The Λ vs. $[CF_3COOH]_{total}$ relationship is nearly linear for 0.1 M $LiCF_3CO_2$. As expected, the Λ values are higher for the 0.01 M electrolyte solution than for the 0.1 M solution.

As discussed earlier, the conductivity of an electrolyte solution at a finite concentration is dependent on many factors, including the relative mobilities of the ions,

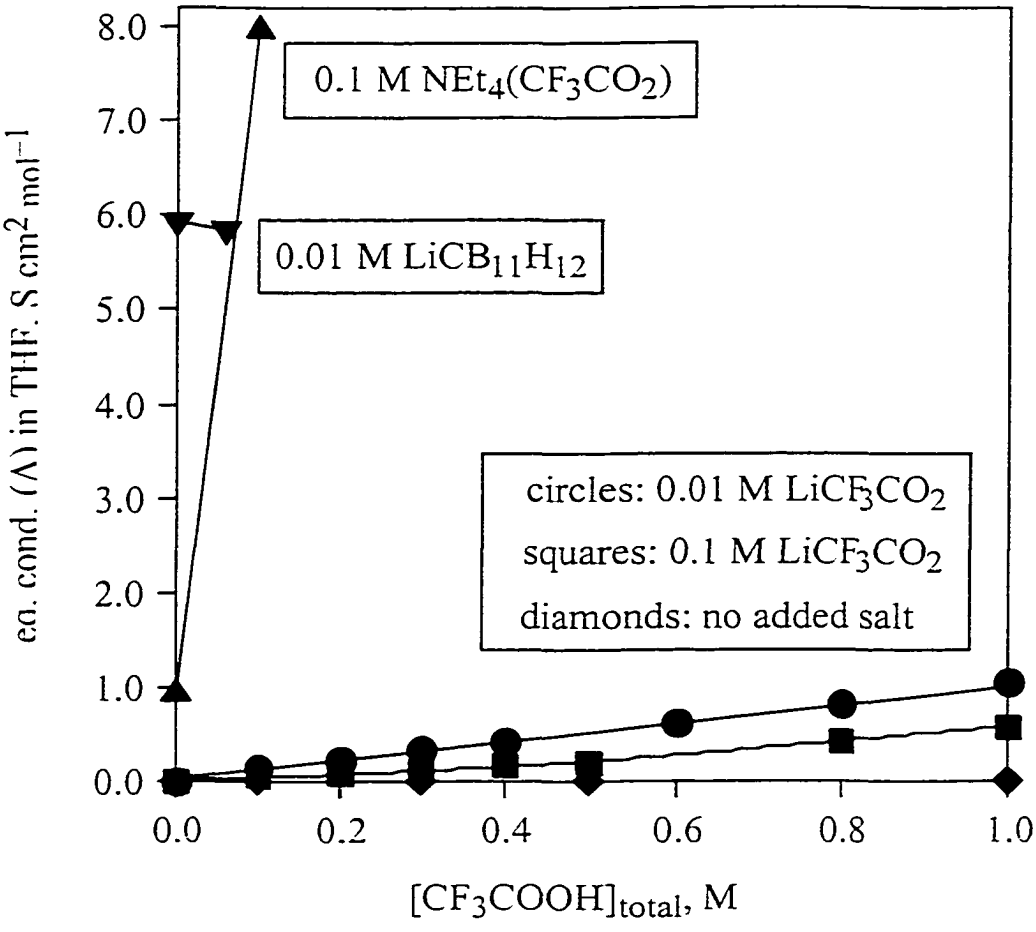

Figure 46. Plot of equivalent conductivity vs. concentration of CF_3COOH for THF solutions. The Λ value for 0.1 M $NEt_4(CF_3CO_2)$ with 1.0 M added CF_3COOH was 14.1(2) S cm^{-2} mol^{-1}.

specific ion–solvent interactions (i.e., Lewis acid–base interactions), and a variety of solvent properties such as permittivity, Lewis acidity and/or basicity, and viscosity.[13] These factors control the relative concentrations of free ions, solvent-separated ions, ion pairs, ion triplets, and higher aggregates, and these relative concentrations in turn alter the permittivity and viscosity of the solution from the permittivity and viscosity of the pure solvent. In view of these inherent complications, the goal of the present study was to demonstrate that $LiCF_3CO_2$ is more extensively ion paired in THF than $Li(H(CF_3CO_2)_2)$, and not to fully characterize and quantitate the wide variety of ionic species that are present in these solutions.

As a control experiment, we measured the conductivities of THF solutions of CF_3COOH, from 0 M added acid to 1 M added acid. For all concentrations of CF_3COOH, the observed Λ values were ~ 5.9×10^{-4} S cm^2 mol^{-1}, more than 10 times lower than even the lowest Λ value listed in Table 22. This demonstrates that there is no significant amount of ionization of CF_3COOH in THF at the concentrations used in this study. As another control experiment, we determined the equivalent conductivity of 0.01 M $LiCB_{11}H_{12}$ in THF and in THF containing 0.06 M CF_3COOH (the $CB_{11}H_{12}^-$ anion is an extremely weak base[14,15]). The Λ values, 5.90 and 5.82 S cm^2 mol^{-1}, respectively, are nearly the same. The small decrease may be due to the greater viscosity of CF_3COOH (η = 0.93 cP) relative to THF (η = 0.46 cP; note that the relative permittivities of THF and CF_3COOH, 7.4 and 8.6 at 20 °C, respectively, are similar). Therefore, the addition of CF_3COOH does not, *in general*, affect the conductivity of lithium salts in THF; there must be a specific effect operating when CF_3COOH is added to THF solutions of $LiCF_3CO_2$. This effect can be understood in terms of an admittedly simple model based on the following three equilibria (all species are solvated):

Table 22. Conductivities of $LiCF_3CO_2$ in THF with varying amounts of CF_3COOH.

conc. of added CF_3COOH, M	equivalent conductivity (Λ), S cm^2 mol^{-1} ($X^- = CF_3CO_2^-$)			
	0.01 M LiX	0.1 M LiX	0.1 M NEt_4X	0.01 M $LiCB_{11}H_{12}$
0.00	0.015(2)	0.008(2)	0.960(2)	5.90(2)
0.06				5.82(2)
0.10	0.139(2)	0.045(2)	8.00(2)	
0.20	0.232(2)	0.074(2)		
0.30	0.330(2)	0.114(2)		
0.40	0.430(2)	0.159(2)		
0.50		0.213(2)		
0.60	0.630(2)			
0.80	0.820(2)	0.431(2)		
1.00	1.14(2)	0.580(2)	14.1(2)	

$$Li^+CF_3CO_2^-(\text{ion pair}) \overset{K_1}{\rightleftharpoons} Li^+ + CF_3CO_2^-$$

$$CF_3CO_2^- + CF_3COOH \overset{K_2}{\rightleftharpoons} H(CF_3CO_2)_2^-$$

$$Li^+H(CF_3CO_2)_2^-(\text{ion pair}) \overset{K_3}{\rightleftharpoons} Li^+ + H(CF_3CO_2)_2^-$$

In a relatively low permittivity solvent, CF_3COOH forms a strong hydrogen bond with $CF_3CO_2^-$ (i.e., since $K_2 >> 1$) and K_1 is relatively small. Therefore, and if $H(CF_3CO_2)_2^-$ is more weakly ion pairing than $CF_3CO_2^-$ (i.e., $K_1 < K_3$), the conductivity of a solution of $LiCF_3CO_2$ in THF should increase as the concentration of CF_3COOH increases. This is what was observed. When CF_3COOH was added to a 0.1 M solution of $NEt_4(CF_3CO_2)$, the Λ value increased much more rapidly than in the 0.1 M $LiCF_3CO_2$ experiment. However, the Λ value did not increase linearly with concentration of acid; it seemed to approach a limiting value of 14.1 S cm^2 mol^{-1} at 1 M CF_3COOH. These two observations are consistent with a much larger K_1 value for $NEt_4(CF_3CO_2)$ than for $LiCF_3CO_2$, a sensible conclusion.

Others have studied the effect of added protic acids on the conductivities of solutions of electrolytes. In one study, de Almeida and Inocêncio investigated the effect of added formic acid on the conductivity of $LiClO_4$ in THF.[16] They noted a linear increase in Λ with increasing mass percent of HCOOH, but they attributed this increase to an increase in dielectric constant of the medium, not to hydrogen bond formation. In another study,[17] Kolthoff and Chantooni investigated the effect of added *p*-bromophenol

(HOAr) on the conductivity of 0.002 M NEt_4Cl in acetonitrile. Interestingly, addition of the phenol decreased Λ, an effect that can be rationalized if $K_1(NEt_4Cl)$ is very large when acetonitrile (ε = 37.5) is the solvent. In that case, addition of HOAr would not result in a larger concentration of ions but in the formation of a larger anion, $Cl\cdots HOAr^-$, with a smaller mobility. In a related study,[18] Pawlak investigated the effect of added proton donors on the conductivities of various lithium salts in sulfolane (ε = 34). The addition of $CHCl_2COOH$ to a sulfolane solution of $KCHCl_2CO_2$ also caused a modest decrease in Λ. Apparently, the effect of added HA on the conductivity of solutions of electrolytes such as LiA and KA depends on the permittivity of the solvent used. For high dielectric solvents such as acetonitrile and sulfolane, Λ decreases slightly because the mobility of the homoconjugated HA_2^- is less than the mobility of A^- and the electrolyte is already significantly ionized. For a low dielectric solvent such as THF, the decreased mobility of HA_2^- is of minor importance relative to the increased concentration of "free" ions, and Λ increases as more HA is added.

Conclusions

Preliminary studies were performed on three new classes of weakly coordinating anions. The carborane anions have the advantages of being very stable under a variety of conditions, and they may be good candidates for practical use upon further study. The new borate anions demonstrate that FAB is a highly effective additive for increasing the conductivity of solutions of weak electrolytes. The class based on hydrogen-bonded complexes is interesting, and presents another way in which to think about the

construction of *WCA*s. However, due to the presence of protons, their use in battery systems would be limited.

References

1. Plešek, J.; Jelínek, T.; Drdáková, E.; Hermánek, S.; Štíbr, B. *Coll. Czech. Chem. Commun.* **1984**, *49*, 1559
2. (a) Xie, Z.; Manning, J.; Reed, R.W.; Mathur, R.; Boyd, P.D.W.; Benesi, A.; Reed, C.A. *J. Am. Chem. Soc.* **1996**, *118*, 2922. (b) Xie, Z.; Bau, R.; Reed, C.A. *Inorg. Chem.* **1995**, *34*, 5403.
3. Ivanov, S.V.; Rockwell, J.R.; Polyakov, O.G.; Gaudinski, C.M.; Anderson, O.P.; Solntsev, K.A.; Strauss, S.H. *J. Am. Chem. Soc.* **1998**, *120*, 4224.
4. Morita, M.; Ishikawa, M.; Matsuda, Y. Organic Electrolytes for Rechargeable Lithium Ion Batteries. In *Lithium Ion Batteries Fundamentals and Performance*; Wakihara, M., Yamamoto, O., Eds.; Wiley-VCH: Weinheim, 1998; 156.
5. Nolan, B.G.; Strauss, S.H. *unpublished results*.
6. Lee, H.S.; Yang, X.Q.; Xiang, C.L.; McBreen, J.; Choi, L.S. *J. Electrochem. Soc.* **1998**, *145*, 2813.
7. Siedle, A.R.; Miller, J.A.; Lamanna, W.M. Tris(pentafluorophenyl)borate Complexes and Olefin Polymerization Catalysts Derived From Them. World Patent Appl. 96/26967 (Minnesota Mining and Mfg. Co.), 1996.
8. (a) Speakman, J. C. *Struct. Bonding* **1972**, *12*, 141. (b) Emsley, J. *Chem. Soc. Rev.* **1980**, *9*, 91.
9. (a) Yamdagni, R.; Kebarle, P. *J. Am. Chem. Soc.* **1971**, *93*, 7139. (b) Caldwell, G.; Rozeboom, M. D.; Kiplinger, J. P.; Bartmess, J. E. *J. Am. Chem. Soc.* **1984**, *106*, 4660. (c) Moet-Ner, M.; Sieck, L. W. *J. Am. Chem. Soc.* **1986**, *108*, 7525.

10. Mallouk, T. E.; Rosenthal, G. L.; Müller, G.; Brusasco, R.; Bartlett, N. *Inorg. Chem.* **1984**, *23*, 3167.

11. Bartlett, N. ; Okino, F.; Mallouk, T. E.; Hagiwara, R.; Lerner, M.; Rosenthal, G. L.; Kourtakis, K. *Adv. Chem. Ser.* **1990**, *226*, 391.

12. Larson, J. W.; McMahon, T. B. *J. Am. Chem. Soc.* **1982**, *104*, 5848.

13. (a) Barthel, J.; Gores, H. J.; Schmeer, G.; Wachter, R. *Top. Curr. Chem.* **1983**, *111*, 33. (b) Salomon, M. *J. Power Sources* **1989**, *26*, 9.

14. Lupinetti, A. J.; Strauss, S. H. *Chemtracts—Inorg. Chem.* **1998**, *11*, 565.

15. Reed, C. A. *Accounts Chem. Res.* **1998**, *31*, 133.

16. de Almeida, E. T.; Inocêncio, A. A. *J. Electrochem. Soc.* **1981**, *128*, 1177.

17. Kolthoff, I. M.; Chantooni, Jr., M. K. *J. Am. Chem. Soc.* **1969**, *91*, 4621.

18. Pawlak, Z. *Electrochim. Acta* **1983**, *28*, 1659.

Appendix

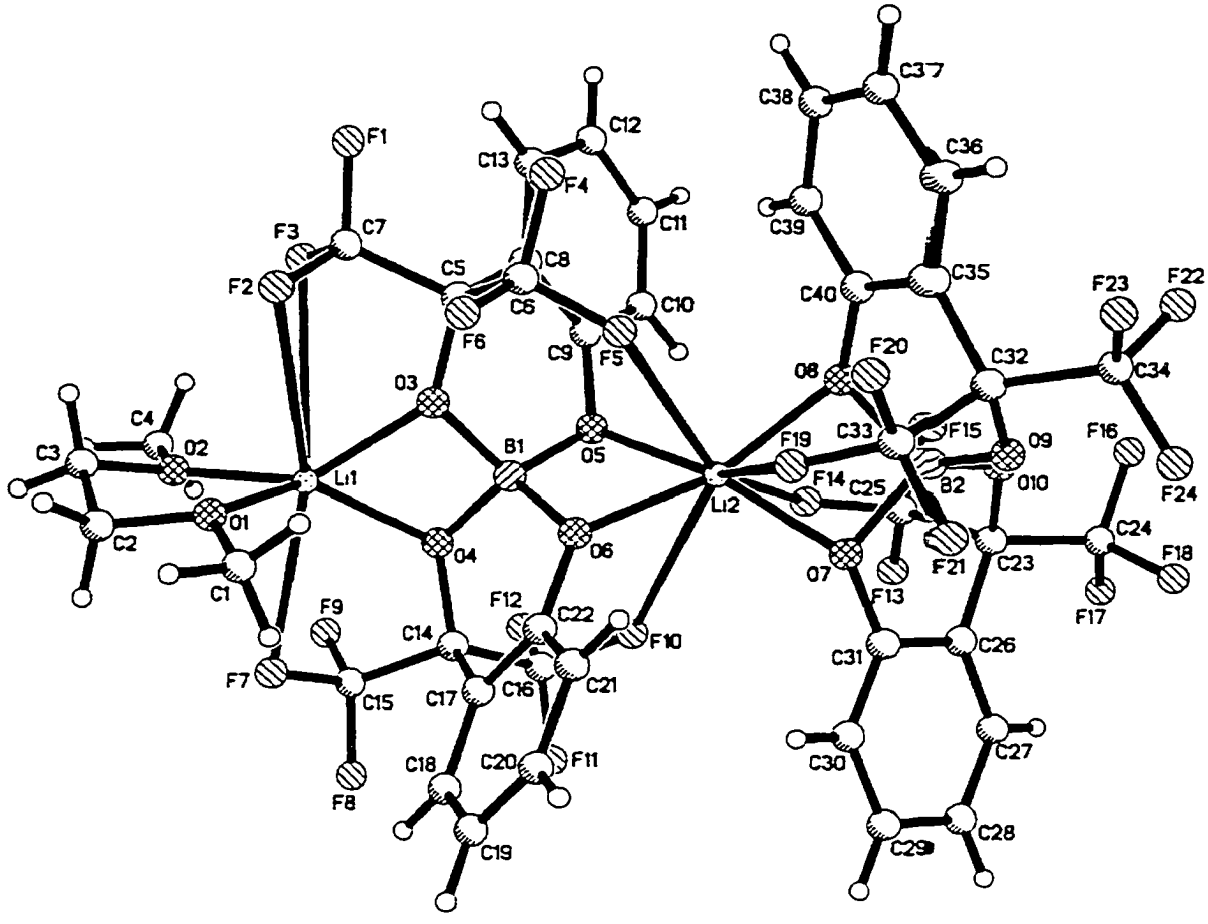

Figure A.1. Drawing of $Li_2(DME)(B(HFPOP)_2)_2$ with all but the hydrogen atoms labeled. See Table 2 for definitions of abbreviations.

Table A.1. Crystal data and structure refinement for $Li_2(DME)(B(HFPOP)_2)_2$.

Identification code	shsccd60 (Nolan/Strauss)
Empirical formula	$C_{40}H_{26}B_2F_{24}Li_2O_{10}$
Formula weight	1158.11
Temperature	166(2) K
Wavelength	0.71073 Å
Crystal system	Monoclinic
Space group	$P2_1/c$
Unit cell dimensions	a = 10.9434(3) Å alpha = 90° b = 23.6179(6) Å beta = 101.4090(10)° c = 18.0374(5) Å gamma = 90°
Volume, Z	4569.8(2) $Å^3$, 4
Density (calculated)	1.683 Mg/m^3
Absorption coefficient	0.180 mm^{-1}
F(000)	2312
Crystal size	0.30 x 0.30 x 0.40 mm, clear colorless cubes
θ range for data collection	1.44 to 28.44°
Limiting indices	$-14 \le h \le 10$, $-31 \le k \le 30$, $-24 \le l \le 23$
Reflections collected	29378
Independent reflections	10943 (R_{int} = 0.0440)
Absorption correction	SADABS
Refinement method	Full-matrix least-squares on F^2
Data / restraints / parameters	10942 / 0 / 704
Goodness-of-fit on F^2	1.005
Final R indices [$I>2\sigma(I)$]	R1 = 0.0475, wR2 = 0.1025
R indices (all data)	R1 = 0.0857, wR2 = 0.1194
Extinction coefficient	0.0002(2)
Largest diff. peak and hole	0.317 and -0.245 $eÅ^{-3}$

Table A.2. Atomic coordinates for $Li_2(DME)(B(HFPOP)_2)_2$.

	x	y	z	U(eq)
B(1)	4033(2)	4425(1)	2649(1)	25(1)
B(2)	1085(2)	6091(1)	2494(1)	26(1)
Li(1)	5219(4)	3510(2)	2404(2)	38(1)
Li(2)	2522(4)	5243(2)	2598(2)	41(1)
O(1)	4658(2)	2964(1)	1608(1)	46(1)
O(2)	6618(2)	3020(1)	2689(1)	48(1)
O(3)	4781(1)	4288(1)	2076(1)	26(1)
O(4)	4373(1)	3929(1)	3169(1)	27(1)
O(5)	4298(1)	4971(1)	2983(1)	28(1)
O(6)	2688(1)	4435(1)	2360(1)	27(1)
O(7)	908(1)	5503(1)	2731(1)	27(1)
O(8)	2317(1)	6050(1)	2275(1)	27(1)
O(9)	112(1)	6294(1)	1879(1)	29(1)
O(10)	1114(1)	6490(1)	3114(1)	30(1)
C(1)	3453(3)	2889(2)	1173(2)	90(1)
C(2)	5438(3)	2486(1)	1705(2)	61(1)
C(3)	6687(3)	2635(1)	2108(2)	57(1)
C(4)	7693(3)	3074(1)	3264(2)	60(1)
C(5)	5316(2)	4716(1)	1696(1)	27(1)
C(6)	4316(2)	4930(1)	1029(1)	33(1)
C(7)	6370(2)	4402(1)	1403(1)	36(1)
C(8)	5812(2)	5206(1)	2221(1)	27(1)
C(9)	5284(2)	5290(1)	2855(1)	26(1)
C(10)	5698(2)	5726(1)	3362(1)	31(1)
C(11)	6627(2)	6084(1)	3225(1)	37(1)
C(12)	7142(2)	6018(1)	2593(1)	38(1)
C(13)	6734(2)	5581(1)	2091(1)	32(1)
C(14)	3474(2)	3655(1)	3507(1)	28(1)
C(15)	4130(2)	3099(1)	3808(1)	37(1)
C(16)	3223(2)	4014(1)	4180(1)	39(1)
C(17)	2277(2)	3556(1)	2932(1)	29(1)
C(18)	1508(2)	3086(1)	2923(1)	40(1)
C(19)	444(2)	3029(1)	2370(1)	46(1)
C(20)	136(2)	3441(1)	1823(1)	42(1)
C(21)	884(2)	3911(1)	1818(1)	35(1)
C(22)	1958(2)	3965(1)	2370(1)	26(1)
C(23)	1007(2)	6320(1)	3840(1)	25(1)
C(24)	473(2)	6847(1)	4169(1)	35(1)
C(25)	2329(2)	6196(1)	4300(1)	32(1)
C(26)	187(2)	5798(1)	3840(1)	25(1)
C(27)	-539(2)	5682(1)	4377(1)	31(1)
C(28)	-1251(2)	5198(1)	4327(1)	36(1)
C(29)	-1240(2)	4817(1)	3748(1)	38(1)
C(30)	-521(2)	4920(1)	3215(1)	32(1)
C(31)	185(2)	5408(1)	3257(1)	26(1)
C(32)	251(2)	6296(1)	1127(1)	26(1)
C(33)	-73(2)	5707(1)	762(1)	33(1)

Table A.2 (continued).

C(34)	-730(2)	6735(1)	762(1)	37(1)
C(35)	1563(2)	6460(1)	1049(1)	26(1)
C(36)	1855(2)	6719(1)	408(1)	36(1)
C(37)	3074(2)	6838(1)	368(1)	44(1)
C(38)	4026(2)	6701(1)	965(1)	42(1)
C(39)	3763(2)	6449(1)	1606(1)	34(1)
C(40)	2535(2)	6326(1)	1644(1)	26(1)
F(1)	6911(1)	4709(1)	943(1)	49(1)
F(2)	5953(1)	3931(1)	1034(1)	52(1)
F(3)	7252(1)	4242(1)	1988(1)	51(1)
F(4)	4767(1)	5324(1)	628(1)	43(1)
F(5)	3374(1)	5167(1)	1294(1)	38(1)
F(6)	3832(1)	4516(1)	563(1)	48(1)
F(7)	4243(1)	2767(1)	3223(1)	46(1)
F(8)	3514(1)	2799(1)	4247(1)	52(1)
F(9)	5269(1)	3187(1)	4203(1)	52(1)
F(10)	2688(1)	4505(1)	3943(1)	48(1)
F(11)	2453(2)	3749(1)	4550(1)	64(1)
F(12)	4257(2)	4132(1)	4673(1)	70(1)
F(13)	2330(1)	6047(1)	5013(1)	46(1)
F(14)	2859(1)	5768(1)	3992(1)	45(1)
F(15)	3096(1)	6638(1)	4327(1)	50(1)
F(16)	1096(1)	7316(1)	4058(1)	44(1)
F(17)	511(2)	6811(1)	4916(1)	52(1)
F(18)	-716(1)	6927(1)	3836(1)	48(1)
F(19)	707(1)	5315(1)	1121(1)	41(1)
F(20)	43(1)	5695(1)	39(1)	50(1)
F(21)	-1222(1)	5543(1)	785(1)	60(1)
F(22)	-364(1)	7258(1)	980(1)	48(1)
F(23)	-933(1)	6730(1)	1(1)	53(1)
F(24)	-1831(1)	6651(1)	952(1)	53(1)

Table A.3. Bond lengths and angles for $Li_2(DME)(B(HFPOP)_2)_2$).

B(1)-O(5)	1.451(3)	B(1)-O(6)	1.462(3)
B(1)-O(3)	1.470(3)	B(1)-O(4)	1.481(3)
B(1)-Li(2)	2.552(4)	B(1)-Li(1)	2.583(4)
B(2)-O(9)	1.450(3)	B(2)-O(10)	1.459(2)
B(2)-O(7)	1.477(3)	B(2)-O(8)	1.482(3)
B(2)-Li(2)	2.531(4)	Li(1)-O(2)	1.907(4)
Li(1)-O(1)	1.937(4)	Li(1)-O(3)	1.962(4)
Li(1)-O(4)	2.060(4)	Li(1)-F(7)	2.650(4)
Li(1)-C(3)	2.734(4)	Li(1)-C(2)	2.759(4)
Li(2)-O(7)	1.929(4)	Li(2)-O(6)	1.972(4)
Li(2)-O(8)	1.993(4)	Li(2)-O(5)	2.034(4)
O(1)-C(2)	1.404(3)	O(1)-C(1)	1.407(3)
O(2)-C(3)	1.400(3)	O(2)-C(4)	1.412(3)
O(3)-C(5)	1.412(2)	O(4)-C(14)	1.413(2)
O(5)-C(9)	1.373(2)	O(6)-C(22)	1.370(2)
O(7)-C(31)	1.369(2)	O(8)-C(40)	1.371(2)
O(9)-C(32)	1.395(2)	O(10)-C(23)	1.396(2)
C(2)-C(3)	1.459(4)	C(5)-C(8)	1.526(3)
C(5)-C(6)	1.542(3)	C(5)-C(7)	1.549(3)
C(6)-F(6)	1.329(2)	C(6)-F(4)	1.333(2)
C(6)-F(5)	1.341(2)	C(7)-F(1)	1.326(2)
C(7)-F(2)	1.330(3)	C(7)-F(3)	1.337(3)
C(8)-C(9)	1.394(3)	C(8)-C(13)	1.397(3)
C(9)-C(10)	1.392(3)	C(10)-C(11)	1.381(3)
C(11)-C(12)	1.378(3)	C(12)-C(13)	1.387(3)
C(14)-C(17)	1.520(3)	C(14)-C(15)	1.544(3)
C(14)-C(16)	1.550(3)	C(15)-F(9)	1.324(3)
C(15)-F(7)	1.340(3)	C(15)-F(8)	1.338(2)
C(16)-F(12)	1.322(3)	C(16)-F(10)	1.331(3)
C(16)-F(11)	1.330(3)	C(17)-C(18)	1.391(3)
C(17)-C(22)	1.395(3)	C(18)-C(19)	1.381(3)
C(19)-C(20)	1.380(3)	C(20)-C(21)	1.379(3)
C(21)-C(22)	1.387(3)	C(23)-C(26)	1.524(3)
C(23)-C(24)	1.544(3)	C(23)-C(25)	1.546(3)
C(24)-F(16)	1.336(2)	C(24)-F(18)	1.334(3)
C(24)-F(17)	1.343(2)	C(25)-F(13)	1.334(2)
C(25)-F(15)	1.335(2)	C(25)-F(14)	1.339(2)
C(26)-C(31)	1.399(3)	C(26)-C(27)	1.396(3)
C(27)-C(28)	1.376(3)	C(28)-C(29)	1.381(3)
C(29)-C(30)	1.379(3)	C(30)-C(31)	1.382(3)
C(32)-C(35)	1.521(3)	C(32)-C(34)	1.543(3)
C(32)-C(33)	1.549(3)	C(33)-F(21)	1.324(2)
C(33)-F(20)	1.336(2)	C(33)-F(19)	1.336(2)
C(34)-F(22)	1.333(3)	C(34)-F(24)	1.331(3)
C(34)-F(23)	1.347(2)	C(35)-C(40)	1.391(3)
C(35)-C(36)	1.398(3)	C(36)-C(37)	1.380(3)
C(37)-C(38)	1.379(3)	C(38)-C(39)	1.380(3)
C(39)-C(40)	1.390(3)		

O(5)-B(1)-O(6)	102.8(2)	O(5)-B(1)-O(3)	112.5(2)
O(6)-B(1)-O(3)	114.7(2)	O(5)-B(1)-O(4)	115.7(2)
O(6)-B(1)-O(4)	111.2(2)	O(3)-B(1)-O(4)	100.6(2)
O(5)-B(1)-Li(2)	52.77(13)	O(6)-B(1)-Li(2)	50.37(12)
O(3)-B(1)-Li(2)	125.2(2)	O(4)-B(1)-Li(2)	134.1(2)

Table A.3 (continued).

O(5)-B(1)-Li(1)	139.0(2)	O(6)-B(1)-Li(1)	118.1(2)
O(3)-B(1)-Li(1)	49.00(12)	O(4)-B(1)-Li(1)	52.85(12)
Li(2)-B(1)-Li(1)	166.5(2)	O(9)-B(2)-O(10)	106.6(2)
O(9)-B(2)-O(7)	113.5(2)	O(10)-B(2)-O(7)	111.7(2)
O(9)-B(2)-O(8)	112.7(2)	O(10)-B(2)-O(8)	111.3(2)
O(7)-B(2)-O(8)	101.2(2)	O(9)-B(2)-Li(2)	131.1(2)
O(10)-B(2)-Li(2)	122.4(2)	O(7)-B(2)-Li(2)	49.40(12)
O(8)-B(2)-Li(2)	51.91(12)	O(2)-Li(1)-O(1)	85.1(2)
O(2)-Li(1)-O(3)	141.8(2)	O(1)-Li(1)-O(3)	112.2(2)
O(2)-Li(1)-O(4)	123.7(2)	O(1)-Li(1)-O(4)	134.3(2)
O(3)-Li(1)-O(4)	68.66(13)	O(2)-Li(1)-B(1)	149.3(2)
O(1)-Li(1)-B(1)	125.5(2)	O(3)-Li(1)-B(1)	34.42(8)
O(4)-Li(1)-B(1)	34.96(8)	O(2)-Li(1)-F(7)	80.72(14)
O(1)-Li(1)-F(7)	82.5(2)	O(3)-Li(1)-F(7)	133.4(2)
O(4)-Li(1)-F(7)	70.20(12)	B(1)-Li(1)-F(7)	100.42(14)
O(2)-Li(1)-C(3)	28.64(9)	O(1)-Li(1)-C(3)	57.61(12)
O(3)-Li(1)-C(3)	140.1(2)	O(4)-Li(1)-C(3)	148.6(2)
B(1)-Li(1)-C(3)	173.3(2)	F(7)-Li(1)-C(3)	85.76(13)
O(2)-Li(1)-C(2)	56.88(12)	O(1)-Li(1)-C(2)	28.49(9)
O(3)-Li(1)-C(2)	136.1(2)	O(4)-Li(1)-C(2)	144.9(2)
B(1)-Li(1)-C(2)	153.5(2)	F(7)-Li(1)-C(2)	75.89(12)
C(3)-Li(1)-C(2)	30.81(9)	O(7)-Li(2)-O(6)	117.4(2)
O(7)-Li(2)-O(8)	71.28(13)	O(6)-Li(2)-O(8)	150.6(2)
O(7)-Li(2)-O(5)	153.5(2)	O(6)-Li(2)-O(5)	69.28(13)
O(8)-Li(2)-O(5)	116.5(2)	O(7)-Li(2)-B(2)	35.55(9)
O(6)-Li(2)-B(2)	146.3(2)	O(8)-Li(2)-B(2)	35.80(9)
O(5)-Li(2)-B(2)	144.4(2)	O(7)-Li(2)-B(1)	147.4(2)
O(6)-Li(2)-B(1)	34.81(9)	O(8)-Li(2)-B(1)	141.1(2)
O(5)-Li(2)-B(1)	34.63(9)	B(2)-Li(2)-B(1)	176.8(2)
C(2)-O(1)-C(1)	116.6(2)	C(2)-O(1)-Li(1)	110.3(2)
C(1)-O(1)-Li(1)	128.5(2)	C(3)-O(2)-C(4)	116.6(2)
C(3)-O(2)-Li(1)	110.6(2)	C(4)-O(2)-Li(1)	130.6(2)
C(5)-O(3)-B(1)	122.6(2)	C(5)-O(3)-Li(1)	135.8(2)
B(1)-O(3)-Li(1)	96.6(2)	C(14)-O(4)-B(1)	121.2(2)
C(14)-O(4)-Li(1)	120.8(2)	B(1)-O(4)-Li(1)	92.19(14)
C(9)-O(5)-B(1)	121.8(2)	C(9)-O(5)-Li(2)	119.9(2)
B(1)-O(5)-Li(2)	92.6(2)	C(22)-O(6)-B(1)	121.1(2)
C(22)-O(6)-Li(2)	134.6(2)	B(1)-O(6)-Li(2)	94.8(2)
C(31)-O(7)-B(2)	118.8(2)	C(31)-O(7)-Li(2)	134.6(2)
B(2)-O(7)-Li(2)	95.0(2)	C(40)-O(8)-B(2)	120.5(2)
C(40)-O(8)-Li(2)	132.0(2)	B(2)-O(8)-Li(2)	92.3(2)
C(32)-O(9)-B(2)	123.1(2)	C(23)-O(10)-B(2)	122.6(2)
O(1)-C(2)-C(3)	110.8(2)	O(1)-C(2)-Li(1)	41.17(13)
C(3)-C(2)-Li(1)	73.7(2)	O(2)-C(3)-C(2)	110.2(2)
O(2)-C(3)-Li(1)	40.77(12)	C(2)-C(3)-Li(1)	75.5(2)
O(3)-C(5)-C(8)	111.8(2)	O(3)-C(5)-C(6)	108.3(2)
C(8)-C(5)-C(6)	110.3(2)	O(3)-C(5)-C(7)	103.4(2)
C(8)-C(5)-C(7)	112.2(2)	C(6)-C(5)-C(7)	110.7(2)
F(6)-C(6)-F(4)	108.3(2)	F(6)-C(6)-F(5)	107.1(2)
F(4)-C(6)-F(5)	107.1(2)	F(6)-C(6)-C(5)	112.5(2)
F(4)-C(6)-C(5)	111.7(2)	F(5)-C(6)-C(5)	109.7(2)
F(1)-C(7)-F(2)	107.2(2)	F(1)-C(7)-F(3)	107.9(2)
F(2)-C(7)-F(3)	106.3(2)	F(1)-C(7)-C(5)	113.3(2)
F(2)-C(7)-C(5)	111.5(2)	F(3)-C(7)-C(5)	109.7(2)
C(9)-C(8)-C(13)	118.5(2)	C(9)-C(8)-C(5)	117.7(2)
C(13)-C(8)-C(5)	123.8(2)	O(5)-C(9)-C(10)	117.5(2)
O(5)-C(9)-C(8)	121.7(2)	C(10)-C(9)-C(8)	120.7(2)
C(11)-C(10)-C(9)	119.4(2)	C(12)-C(11)-C(10)	120.9(2)

Table A.3 (continued).

C(11)-C(12)-C(13)	119.6(2)	C(12)-C(13)-C(8)	120.8(2)
O(4)-C(14)-C(17)	110.9(2)	O(4)-C(14)-C(15)	103.1(2)
C(17)-C(14)-C(15)	112.7(2)	O(4)-C(14)-C(16)	109.5(2)
C(17)-C(14)-C(16)	110.9(2)	C(15)-C(14)-C(16)	109.4(2)
F(9)-C(15)-F(7)	107.0(2)	F(9)-C(15)-F(8)	107.1(2)
F(7)-C(15)-F(8)	107.0(2)	F(9)-C(15)-C(14)	112.3(2)
F(7)-C(15)-C(14)	109.2(2)	F(8)-C(15)-C(14)	113.9(2)
F(12)-C(16)-F(10)	107.2(2)	F(12)-C(16)-F(11)	107.8(2)
F(10)-C(16)-F(11)	106.8(2)	F(12)-C(16)-C(14)	112.3(2)
F(10)-C(16)-C(14)	111.1(2)	F(11)-C(16)-C(14)	111.3(2)
C(18)-C(17)-C(22)	118.8(2)	C(18)-C(17)-C(14)	124.7(2)
C(22)-C(17)-C(14)	116.5(2)	C(19)-C(18)-C(17)	120.5(2)
C(20)-C(19)-C(18)	119.9(2)	C(19)-C(20)-C(21)	120.8(2)
C(20)-C(21)-C(22)	119.3(2)	O(6)-C(22)-C(21)	118.5(2)
O(6)-C(22)-C(17)	120.6(2)	C(21)-C(22)-C(17)	120.8(2)
O(10)-C(23)-C(26)	113.1(2)	O(10)-C(23)-C(24)	103.5(2)
C(26)-C(23)-C(24)	112.6(2)	O(10)-C(23)-C(25)	108.4(2)
C(26)-C(23)-C(25)	109.6(2)	C(24)-C(23)-C(25)	109.4(2)
F(16)-C(24)-F(18)	107.2(2)	F(16)-C(24)-F(17)	106.6(2)
F(18)-C(24)-F(17)	107.1(2)	F(16)-C(24)-C(23)	111.7(2)
F(18)-C(24)-C(23)	110.6(2)	F(17)-C(24)-C(23)	113.3(2)
F(13)-C(25)-F(15)	106.8(2)	F(13)-C(25)-F(14)	106.6(2)
F(15)-C(25)-F(14)	106.5(2)	F(13)-C(25)-C(23)	112.9(2)
F(15)-C(25)-C(23)	112.7(2)	F(14)-C(25)-C(23)	110.9(2)
C(31)-C(26)-C(27)	118.4(2)	C(31)-C(26)-C(23)	116.4(2)
C(27)-C(26)-C(23)	125.1(2)	C(28)-C(27)-C(26)	120.7(2)
C(27)-C(28)-C(29)	120.1(2)	C(30)-C(29)-C(28)	120.3(2)
C(29)-C(30)-C(31)	120.0(2)	O(7)-C(31)-C(30)	119.5(2)
O(7)-C(31)-C(26)	119.9(2)	C(30)-C(31)-C(26)	120.6(2)
O(9)-C(32)-C(35)	112.4(2)	O(9)-C(32)-C(34)	103.2(2)
C(35)-C(32)-C(34)	112.3(2)	O(9)-C(32)-C(33)	109.6(2)
C(35)-C(32)-C(33)	109.3(2)	C(34)-C(32)-C(33)	109.9(2)
F(21)-C(33)-F(20)	107.4(2)	F(21)-C(33)-F(19)	107.6(2)
F(20)-C(33)-F(19)	106.4(2)	F(21)-C(33)-C(32)	112.8(2)
F(20)-C(33)-C(32)	112.1(2)	F(19)-C(33)-C(32)	110.2(2)
F(22)-C(34)-F(24)	107.2(2)	F(22)-C(34)-F(23)	106.7(2)
F(24)-C(34)-F(23)	106.6(2)	F(22)-C(34)-C(32)	110.7(2)
F(24)-C(34)-C(32)	112.3(2)	F(23)-C(34)-C(32)	112.9(2)
C(40)-C(35)-C(36)	118.3(2)	C(40)-C(35)-C(32)	117.5(2)
C(36)-C(35)-C(32)	124.2(2)	C(37)-C(36)-C(35)	120.9(2)
C(38)-C(37)-C(36)	120.1(2)	C(37)-C(38)-C(39)	120.2(2)
C(38)-C(39)-C(40)	119.8(2)	O(8)-C(40)-C(35)	121.1(2)
O(8)-C(40)-C(39)	118.0(2)	C(35)-C(40)-C(39)	120.8(2)
C(15)-F(7)-Li(1)	99.35(14)		

Table A.4. Hydrogen atom coordinates for $Li_2(DME)(B(HFPOP)_2)_2$.

	x	y	z	U(eq)
H(1A)	2996(3)	3248(2)	1143(2)	135
H(1B)	3011(3)	2601(2)	1410(2)	135
H(1C)	3511(3)	2765(2)	663(2)	135
H(2A)	5486(3)	2327(1)	1204(2)	73
H(2B)	5082(3)	2194(1)	1993(2)	73
H(3A)	7131(3)	2289(1)	2324(2)	68
H(3B)	7164(3)	2806(1)	1752(2)	68
H(4A)	7537(3)	3352(1)	3638(2)	90
H(4B)	8394(3)	3200(1)	3042(2)	90
H(4C)	7893(3)	2707(1)	3512(2)	90
H(10A)	5346(2)	5777(1)	3798(1)	38
H(11A)	6915(2)	6381(1)	3572(1)	44
H(12A)	7773(2)	6270(1)	2501(1)	45
H(13A)	7086(2)	5536(1)	1653(1)	39
H(18A)	1716(2)	2802(1)	3300(1)	47
H(19A)	-75(2)	2706(1)	2367(1)	55
H(20A)	-599(2)	3401(1)	1446(1)	51
H(21A)	665(2)	4194(1)	1441(1)	42
H(27A)	-542(2)	5940(1)	4781(1)	37
H(28A)	-1750(2)	5126(1)	4632(1)	43
H(29A)	-1730(2)	4483(1)	3715(1)	46
H(30A)	-511(2)	4656(1)	2819(1)	38
H(36A)	1204(2)	6814(1)	-5(1)	43
H(37A)	3259(2)	7014(1)	-70(1)	53
H(38A)	4866(2)	6781(1)	934(1)	51
H(39A)	4419(2)	6360(1)	2019(1)	40

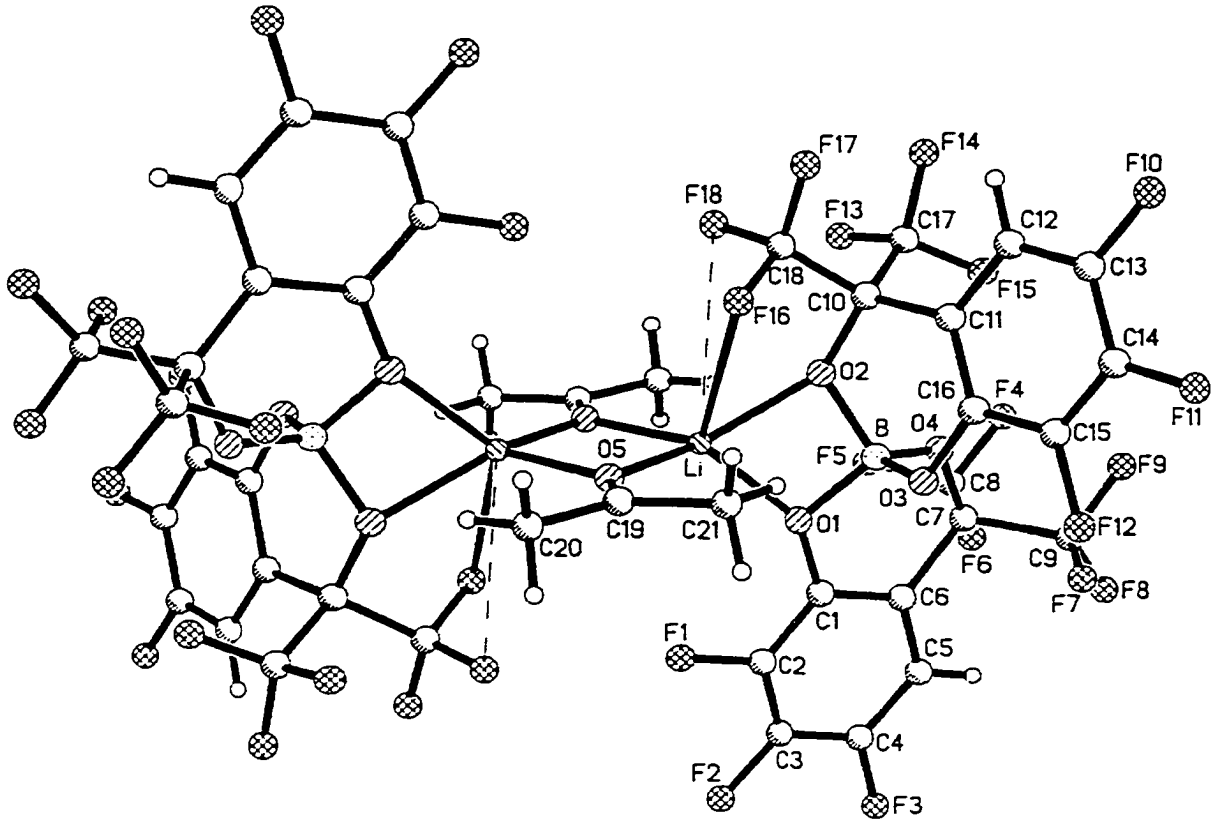

Figure A.2. Drawing of $Li(OC(CH_3)_2)B(HFTPOP\text{-}2,3,4)_2$ with all but the hydrogen atoms labeled. See Table 2 for definition of abbreviation.

Table A.5. Crystal data and structure refinement for $Li(OC(CH_3)_2)B(HFTPOP\text{-}2,3,4)_2$.

Identification code	sbscod41 (HFTPOP)
Empirical formula	$C_{21}H_8BF_{18}LiO_5$
Formula weight	700.02
Temperature	167(2) K
Wavelength	0.71073 Å
Crystal system	Triclinic
Space group	$P\bar{1}$
Unit cell dimensions	a = 8.4221(7) Å alpha = 104.202(2)° b = 11.5266(10) Å beta = 93.122(2)° c = 14.2693(12) Å gamma = 108.599(2)°
Volume, Z	1259.4(2) $Å^3$, 2
Density (calculated)	1.846 Mg/m^3
Absorption coefficient	0.214 mm^{-1}
F(000)	688
Crystal size	0.22 x 0.18 x 0.05 mm, clear colorless plates
θ range for data collection	1.49 to 28.37°
Limiting indices	$-11 \le h \le 10$, $-15 \le k \le 13$, $-16 \le l \le 19$
Reflections collected	8223
Independent reflections	5673 (R_{int} = 0.0553)
Absorption correction	SADABS
Refinement method	Full-matrix least-squares on F^2
Data / restraints / parameters	5672 / 0 / 416
Goodness-of-fit on F^2	0.887
Final R indices [$I>2\sigma(I)$]	R1 = 0.0766, wR2 = 0.1467
R indices (all data)	R1 = 0.1682, wR2 = 0.1872
Extinction coefficient	0.009(2)
Largest diff. peak and hole	0.374 and -0.375 $eÅ^{-3}$

Table A.6. Atomic coordinates for $Li(OC(CH_3)_2)B(HFTPOP\text{-}2,3,4)_2$.

	x	y	z	U(eq)
B	3075(6)	2247(5)	2558(3)	26(1)
Li	4205(9)	4039(7)	4116(5)	33(2)
O(1)	4164(4)	2328(3)	3428(2)	30(1)
O(2)	2310(3)	3220(3)	2959(2)	29(1)
O(3)	4146(4)	2629(3)	1852(2)	33(1)
O(4)	1779(4)	1025(3)	2186(2)	33(1)
O(5)	6262(4)	5532(3)	4547(2)	30(1)
C(1)	4549(5)	1274(4)	3455(3)	28(1)
C(2)	5910(5)	1422(4)	4101(3)	31(1)
C(3)	6386(6)	413(4)	4166(3)	41(1)
C(4)	5505(6)	-778(4)	3543(4)	48(1)
C(5)	4141(6)	-957(4)	2897(4)	41(1)
C(6)	3616(5)	60(4)	2845(3)	29(1)
C(7)	2019(6)	-113(4)	2191(3)	33(1)
C(8)	447(6)	-838(5)	2584(4)	44(1)
C(9)	2017(7)	-800(5)	1112(4)	47(1)
C(10)	1501(5)	3685(4)	2325(3)	30(1)
C(11)	2208(5)	3609(4)	1353(3)	27(1)
C(12)	1590(6)	4051(4)	628(3)	36(1)
C(13)	2301(6)	4001(4)	-220(3)	39(1)
C(14)	3575(6)	3503(5)	-380(3)	39(1)
C(15)	4162(6)	3066(4)	325(3)	37(1)
C(16)	3490(5)	3100(4)	1196(3)	30(1)
C(17)	-423(6)	2938(4)	2156(3)	36(1)
C(18)	1885(6)	5085(4)	2898(3)	36(1)
C(19)	7380(6)	6096(4)	4140(3)	28(1)
C(20)	8828(6)	7240(4)	4699(3)	41(1)
C(21)	7301(6)	5660(5)	3059(3)	38(1)
F(1)	6792(3)	2531(2)	4702(2)	45(1)
F(2)	7706(3)	568(3)	4820(2)	55(1)
F(3)	6006(4)	-1763(3)	3604(3)	71(1)
F(4)	-996(3)	-1028(3)	2050(2)	61(1)
F(5)	416(3)	-190(3)	3488(2)	52(1)
F(6)	445(4)	-1983(3)	2628(2)	58(1)
F(7)	3454(4)	-228(3)	811(2)	68(1)
F(8)	1903(4)	-2020(3)	986(2)	58(1)
F(9)	740(4)	-806(3)	527(2)	66(1)
F(10)	1728(4)	4433(3)	-924(2)	57(1)
F(11)	4253(4)	3458(3)	-1216(2)	54(1)
F(12)	5410(3)	2577(3)	162(2)	51(1)
F(13)	-992(3)	2806(3)	2997(2)	61(1)
F(14)	-1309(3)	3546(2)	1783(2)	47(1)
F(15)	-814(3)	1796(2)	1556(2)	46(1)
F(16)	3550(3)	5677(2)	3131(2)	54(1)
F(17)	1307(3)	5758(2)	2415(2)	43(1)
F(18)	1235(4)	5184(3)	3731(2)	53(1)

Table A.7. Bond lengths and angles for $Li(OC(CH_3)_2)B(HFTPOP\text{-}2,3,4)_2$.

B-O(4)	1.431(5)	B-O(3)	1.445(6)
B-O(1)	1.468(5)	B-O(2)	1.480(5)
B-Li	2.525(8)	Li-O(5)#1	1.946(7)
Li-O(5)	1.950(7)	Li-O(1)	1.964(7)
Li-O(2)	2.038(7)	Li-Li#1	2.840(13)
O(1)-C(1)	1.362(5)	O(2)-C(10)	1.403(5)
O(3)-C(16)	1.364(5)	O(4)-C(7)	1.390(5)
O(5)-C(19)	1.224(5)	O(5)-Li#1	1.946(7)
C(1)-C(2)	1.370(6)	C(1)-C(6)	1.400(5)
C(2)-F(1)	1.353(5)	C(2)-C(3)	1.367(6)
C(3)-F(2)	1.348(5)	C(3)-C(4)	1.380(6)
C(4)-F(3)	1.350(5)	C(4)-C(5)	1.361(7)
C(5)-C(6)	1.395(6)	C(6)-C(7)	1.524(6)
C(7)-C(8)	1.541(7)	C(7)-C(9)	1.548(6)
C(8)-F(5)	1.328(5)	C(8)-F(4)	1.324(5)
C(8)-F(6)	1.335(5)	C(9)-F(9)	1.322(5)
C(9)-F(7)	1.331(6)	C(9)-F(8)	1.344(6)
C(10)-C(11)	1.535(6)	C(10)-C(18)	1.539(6)
C(10)-C(17)	1.546(6)	C(11)-C(16)	1.387(6)
C(11)-C(12)	1.403(6)	C(12)-C(13)	1.377(6)
C(13)-F(10)	1.355(5)	C(13)-C(14)	1.375(7)
C(14)-F(11)	1.347(5)	C(14)-C(15)	1.366(7)
C(15)-F(12)	1.348(5)	C(15)-C(16)	1.389(6)
C(17)-F(15)	1.309(5)	C(17)-F(13)	1.340(5)
C(17)-F(14)	1.343(5)	C(18)-F(18)	1.329(5)
C(18)-F(16)	1.331(5)	C(18)-F(17)	1.334(5)
C(19)-C(20)	1.488(6)	C(19)-C(21)	1.492(6)

O(4)-B-O(3)	113.9(3)	O(4)-B-O(1)	112.6(4)
O(3)-B-O(1)	108.2(3)	O(4)-B-O(2)	109.9(3)
O(3)-B-O(2)	110.3(4)	O(1)-B-O(2)	101.3(3)
O(4)-B-Li	140.4(4)	O(3)-B-Li	105.7(3)
O(1)-B-Li	50.9(2)	O(2)-B-Li	53.8(2)
O(5)#1-Li-O(5)	86.4(3)	O(5)#1-Li-O(1)	122.5(4)
O(5)-Li-O(1)	124.0(4)	O(5)#1-Li-O(2)	121.7(4)
O(5)-Li-O(2)	138.1(4)	O(1)-Li-O(2)	69.4(2)
O(5)#1-Li-B	139.0(4)	O(5)-Li-B	133.9(4)
O(1)-Li-B	35.4(2)	O(2)-Li-B	35.9(2)
O(5)#1-Li-Li#1	43.3(2)	O(5)-Li-Li#1	43.1(2)
O(1)-Li-Li#1	138.8(5)	O(2)-Li-Li#1	150.6(5)
B-Li-Li#1	173.5(5)	C(1)-O(1)-B	117.5(3)
C(1)-O(1)-Li	148.5(3)	B-O(1)-Li	93.7(3)
C(10)-O(2)-B	120.1(3)	C(10)-O(2)-Li	134.6(3)
B-O(2)-Li	90.3(3)	C(16)-O(3)-B	115.8(3)
C(7)-O(4)-B	123.4(3)	C(19)-O(5)-Li#1	131.1(3)
C(19)-O(5)-Li	135.0(3)	Li#1-O(5)-Li	93.6(3)
O(1)-C(1)-C(2)	118.2(4)	O(1)-C(1)-C(6)	122.5(4)
C(2)-C(1)-C(6)	119.3(4)	F(1)-C(2)-C(3)	118.9(4)
F(1)-C(2)-C(1)	119.3(4)	C(3)-C(2)-C(1)	121.7(4)
F(2)-C(3)-C(2)	121.1(4)	F(2)-C(3)-C(4)	119.8(4)
C(2)-C(3)-C(4)	119.1(4)	F(3)-C(4)-C(5)	120.9(4)
F(3)-C(4)-C(3)	118.6(4)	C(5)-C(4)-C(3)	120.6(4)
C(4)-C(5)-C(6)	120.7(4)	C(5)-C(6)-C(1)	118.5(4)
C(5)-C(6)-C(7)	122.5(4)	C(1)-C(6)-C(7)	118.9(4)

Table A.7 (continued).

O(4)-C(7)-C(6)	113.8(3)	O(4)-C(7)-C(8)	103.7(3)
C(6)-C(7)-C(8)	109.7(4)	O(4)-C(7)-C(9)	106.3(4)
C(6)-C(7)-C(9)	112.1(4)	C(8)-C(7)-C(9)	110.9(4)
F(5)-C(8)-F(4)	107.7(4)	F(5)-C(8)-F(6)	106.7(4)
F(4)-C(8)-F(6)	106.7(4)	F(5)-C(8)-C(7)	109.9(4)
F(4)-C(8)-C(7)	113.2(4)	F(6)-C(8)-C(7)	112.3(4)
F(9)-C(9)-F(7)	108.3(5)	F(9)-C(9)-F(8)	107.1(4)
F(7)-C(9)-F(8)	106.7(4)	F(9)-C(9)-C(7)	112.0(4)
F(7)-C(9)-C(7)	110.2(4)	F(8)-C(9)-C(7)	112.4(5)
O(2)-C(10)-C(11)	112.4(3)	O(2)-C(10)-C(18)	103.4(3)
C(11)-C(10)-C(18)	110.1(4)	O(2)-C(10)-C(17)	109.0(4)
C(11)-C(10)-C(17)	110.9(3)	C(18)-C(10)-C(17)	110.8(3)
C(16)-C(11)-C(12)	119.8(4)	C(16)-C(11)-C(10)	119.0(4)
C(12)-C(11)-C(10)	121.2(4)	C(13)-C(12)-C(11)	119.1(4)
F(10)-C(13)-C(12)	119.9(4)	F(10)-C(13)-C(14)	118.7(4)
C(12)-C(13)-C(14)	121.4(4)	F(11)-C(14)-C(15)	120.3(4)
F(11)-C(14)-C(13)	120.6(5)	C(15)-C(14)-C(13)	119.1(4)
F(12)-C(15)-C(14)	118.8(4)	F(12)-C(15)-C(16)	119.6(4)
C(14)-C(15)-C(16)	121.6(4)	O(3)-C(16)-C(11)	123.8(4)
O(3)-C(16)-C(15)	117.3(4)	C(11)-C(16)-C(15)	118.9(4)
F(15)-C(17)-F(13)	107.6(4)	F(15)-C(17)-F(14)	107.5(3)
F(13)-C(17)-F(14)	106.4(4)	F(15)-C(17)-C(10)	112.2(4)
F(13)-C(17)-C(10)	111.2(4)	F(14)-C(17)-C(10)	111.6(4)
F(18)-C(18)-F(16)	106.9(4)	F(18)-C(18)-F(17)	106.7(3)
F(16)-C(18)-F(17)	106.7(4)	F(18)-C(18)-C(10)	111.7(4)
F(16)-C(18)-C(10)	109.9(3)	F(17)-C(18)-C(10)	114.6(4)
O(5)-C(19)-C(20)	121.5(4)	O(5)-C(19)-C(21)	120.3(4)
C(20)-C(19)-C(21)	118.2(4)		

Table A.8. Hydrogen atom coordinates for $Li(OC(CH_3)_2)B(HFTPOP\text{-}2,3,4)_2$.

	x	y	z	U(eq)
H(5A)	3542(6)	-1784(4)	2476(4)	49
H(12A)	693(6)	4380(4)	722(3)	43
H(20A)	8719(6)	7418(4)	5396(3)	61
H(20B)	8827(6)	7974(4)	4469(3)	61
H(20C)	9892(6)	7082(4)	4602(3)	61
H(21A)	6290(6)	4904(5)	2787(3)	57
H(21B)	8313(6)	5449(5)	2905(3)	57
H(21C)	7248(6)	6342(5)	2774(3)	57

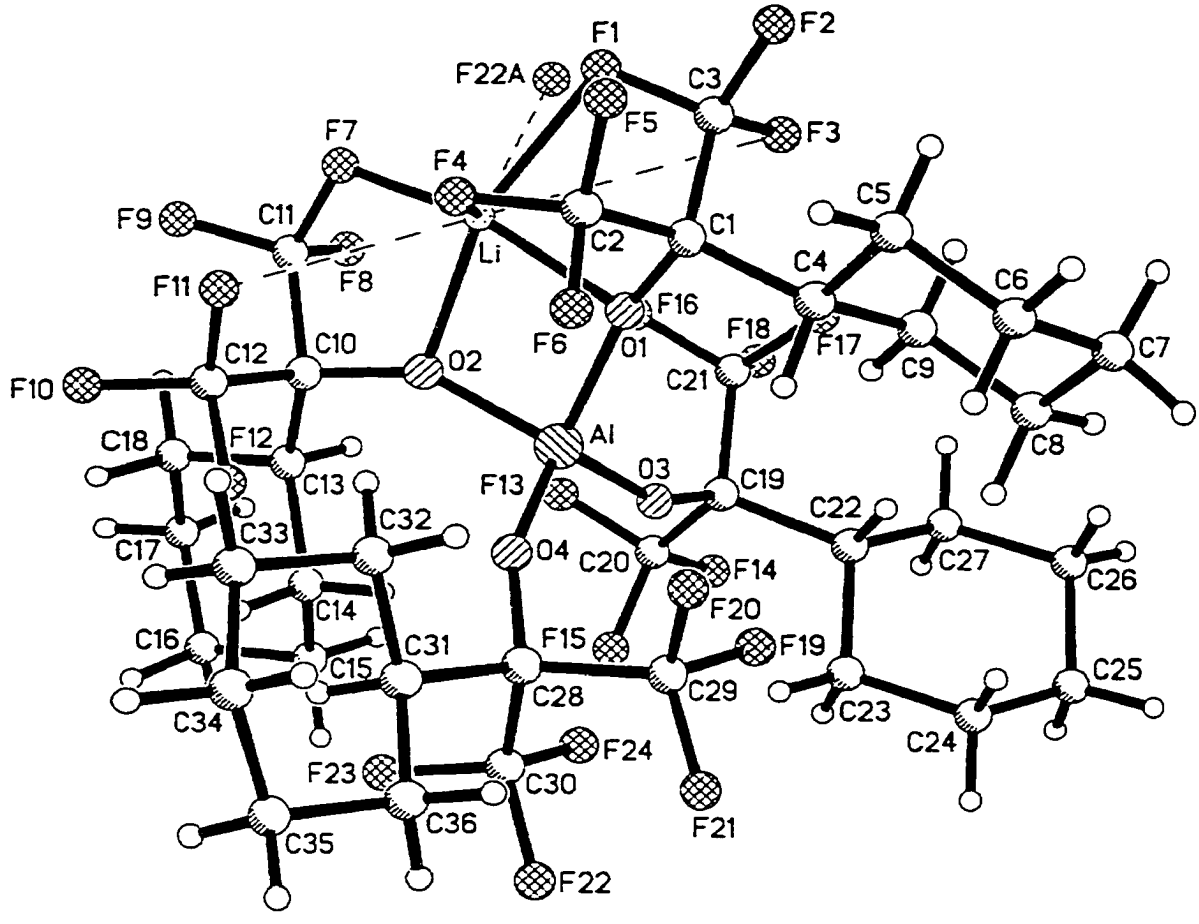

Figure A.3. Drawing of $LiAl(HFCP)_4$ with all but the hydrogen atoms labeled. See Table 2 for definition of abbreviation.

Table A.9. Crystal data and structure refinement for 40% $LiAl(HFCP)_4$.

Identification code	shs56m Li refined at 40% position
Empirical formula	$C_{36}H_{44}AlF_{24}LiO_4$
Formula weight	1030.63
Temperature	169(2) K
Wavelength	0.71073 Å
Crystal system	Monoclinic
Space group	$P2_1/n$
Unit cell dimensions	a = 11.4943(8) Å alpha = 90° b = 19.608(2) Å beta = 104.388(7)° c = 19.1934(14) Å gamma = 90°
Volume, Z	4190.2(6) $Å^3$, 4
Density (calculated)	1.634 Mg/m^3
Absorption coefficient	0.195 mm^{-1}
F(000)	2096
Crystal size	0.38 x 0.40 x 0.50 mm
θ range for data collection	1.51 to 28.39°
Limiting indices	$-15 \le h \le 15$, $-26 \le k \le 26$, $-25 \le l \le 19$
Reflections collected	27634
Independent reflections	10127 (R_{int} = 0.0515)
Absorption correction	SADABS
Refinement method	Full-matrix least-squares on F^2
Data / restraints / parameters	10126 / 0 / 593
Goodness-of-fit on F^2	1.101
Final R indices [I>2σ(I)]	R1 = 0.0490, wR2 = 0.1105
R indices (all data)	R1 = 0.0867, wR2 = 0.1238
Extinction coefficient	0.0016(2)
Largest diff. peak and hole	1.172 and -0.785 $eÅ^{-3}$

Table A.10. Atomic coordinates for 40% $LiAl(HFCP)_4$.

	x	y	z	U(eq)
Al	9159(1)	2253(1)	708(1)	19(1)
Li	8093	1878	-669	200(4)
O(1)	7848(1)	1787(1)	304(1)	32(1)
O(2)	9710(1)	2174(1)	-74(1)	25(1)
O(3)	8793(1)	3059(1)	902(1)	25(1)
O(4)	10100(1)	1863(1)	1423(1)	28(1)
C(1)	6982(2)	1286(1)	316(1)	26(1)
C(2)	7597(2)	587(1)	283(1)	32(1)
C(3)	6027(2)	1390(1)	-405(1)	35(1)
C(4)	6472(2)	1332(1)	985(1)	26(1)
C(5)	5656(2)	746(1)	1096(1)	40(1)
C(6)	5365(2)	808(1)	1825(2)	48(1)
C(7)	4790(2)	1487(1)	1914(1)	43(1)
C(8)	5581(3)	2069(1)	1785(2)	52(1)
C(9)	5865(2)	2011(1)	1058(1)	45(1)
C(10)	10654(2)	2191(1)	-411(1)	24(1)
C(11)	10028(2)	2176(1)	-1227(1)	33(1)
C(12)	11359(2)	1520(1)	-224(1)	34(1)
C(13)	11437(2)	2840(1)	-243(1)	28(1)
C(14)	12042(2)	2933(1)	553(1)	43(1)
C(15)	12618(2)	3638(2)	698(2)	59(1)
C(16)	13521(2)	3761(1)	261(2)	57(1)
C(17)	12949(3)	3653(1)	-531(2)	58(1)
C(18)	12381(2)	2950(1)	-680(1)	42(1)
C(19)	8215(2)	3678(1)	742(1)	24(1)
C(20)	9184(2)	4204(1)	681(1)	35(1)
C(21)	7308(2)	3624(1)	4(1)	32(1)
C(22)	7560(2)	3850(1)	1337(1)	24(1)
C(23)	8421(2)	3948(1)	2080(1)	32(1)
C(24)	7722(2)	3941(1)	2662(1)	43(1)
C(25)	6752(2)	4489(1)	2530(1)	44(1)
C(26)	5946(2)	4446(1)	1780(1)	42(1)
C(27)	6654(2)	4448(1)	1201(1)	32(1)
C(28)	10654(2)	1767(1)	2142(1)	23(1)
C(29)	9655(2)	1719(1)	2554(1)	29(1)
C(30)	11445(2)	2397(1)	2414(1)	29(1)
C(31)	11469(2)	1115(1)	2231(1)	25(1)
C(32)	10904(2)	518(1)	1767(1)	34(1)
C(33)	11822(2)	-46(1)	1788(1)	38(1)
C(34)	12377(3)	-285(1)	2542(1)	46(1)
C(35)	12900(2)	300(1)	3024(1)	49(1)
C(36)	12006(2)	878(1)	2998(1)	38(1)
F(1)	6566(1)	1313(1)	-965(1)	52(1)
F(2)	5124(1)	953(1)	-523(1)	48(1)
F(3)	5577(1)	2009(1)	-477(1)	53(1)
F(4)	8385(1)	618(1)	-133(1)	50(1)
F(5)	6848(1)	80(1)	22(1)	45(1)

Table A.10 (continued).

F(6)	8232(1)	395(1)	929(1)	44(1)
F(7)	9059(1)	1747(1)	-1368(1)	38(1)
F(8)	9588(1)	2781(1)	-1457(1)	49(1)
F(9)	10713(1)	1965(1)	-1646(1)	56(1)
F(10)	12300(1)	1458(1)	-506(1)	54(1)
F(11)	10655(1)	975(1)	-439(1)	51(1)
F(12)	11775(1)	1448(1)	486(1)	52(1)
F(13)	9555(1)	4123(1)	76(1)	49(1)
F(14)	8811(1)	4852(1)	684(1)	53(1)
F(15)	10158(1)	4142(1)	1225(1)	45(1)
F(16)	7747(1)	3252(1)	-464(1)	44(1)
F(17)	6294(1)	3320(1)	47(1)	41(1)
F(18)	7004(1)	4236(1)	-307(1)	45(1)
F(19)	8889(1)	2243(1)	2392(1)	49(1)
F(20)	8997(1)	1158(1)	2376(1)	41(1)
F(21)	10054(1)	1713(1)	3267(1)	47(1)
F(22)	11873(1)	2417(1)	3130(1)	44(1)
F(23)	12403(1)	2422(1)	2142(1)	45(1)
F(24)	10862(1)	2980(1)	2227(1)	46(1)

Table A.11. Bond lengths and angles for 40% $LiAl(HFCP)_4$.

Al-O(3)	1.6989(14)	Al-O(4)	1.7029(14)
Al-O(1)	1.769(2)	Al-O(2)	1.7762(14)
Al-Li	2.7246(6)	Li-F(7)	1.9597(13)
Li-O(1)	1.9636(14)	Li-O(2)	2.0093(13)
Li-F(1)	2.0337(14)	Li-C(3)	2.722(2)
Li-C(11)	2.761(2)	Li-C(1)	2.784(2)
O(1)-C(1)	1.403(2)	O(2)-C(10)	1.395(2)
O(3)-C(19)	1.382(2)	O(4)-C(28)	1.381(2)
C(1)-C(4)	1.541(3)	C(1)-C(3)	1.552(3)
C(1)-C(2)	1.551(3)	C(2)-F(5)	1.329(2)
C(2)-F(6)	1.328(3)	C(2)-F(4)	1.349(2)
C(3)-F(3)	1.313(3)	C(3)-F(2)	1.322(2)
C(3)-F(1)	1.375(3)	C(4)-C(9)	1.526(3)
C(4)-C(5)	1.532(3)	C(5)-C(6)	1.521(3)
C(6)-C(7)	1.516(3)	C(7)-C(8)	1.518(3)
C(8)-C(9)	1.514(3)	C(10)-C(12)	1.539(3)
C(10)-C(13)	1.546(3)	C(10)-C(11)	1.553(3)
C(11)-F(8)	1.321(3)	C(11)-F(9)	1.324(2)
C(11)-F(7)	1.368(3)	C(12)-F(12)	1.334(3)
C(12)-F(10)	1.331(3)	C(12)-F(11)	1.343(3)
C(13)-C(14)	1.524(3)	C(13)-C(18)	1.543(3)
C(14)-C(15)	1.527(3)	C(15)-C(16)	1.508(4)
C(16)-C(17)	1.513(4)	C(17)-C(18)	1.522(3)
C(19)-C(20)	1.543(3)	C(19)-C(21)	1.540(3)
C(19)-C(22)	1.559(3)	C(20)-F(15)	1.334(3)
C(20)-F(14)	1.340(2)	C(20)-F(13)	1.341(3)
C(21)-F(17)	1.329(3)	C(21)-F(18)	1.348(2)
C(21)-F(16)	1.349(2)	C(22)-C(23)	1.530(3)
C(22)-C(27)	1.532(3)	C(23)-C(24)	1.529(3)
C(24)-C(25)	1.524(3)	C(25)-C(26)	1.509(3)
C(26)-C(27)	1.530(3)	C(28)-C(29)	1.550(3)
C(28)-C(30)	1.546(3)	C(28)-C(31)	1.569(3)
C(29)-F(20)	1.331(2)	C(29)-F(21)	1.331(2)
C(29)-F(19)	1.337(2)	C(30)-F(24)	1.328(2)
C(30)-F(23)	1.333(2)	C(30)-F(22)	1.340(2)
C(31)-C(32)	1.516(3)	C(31)-C(36)	1.521(3)
C(32)-C(33)	1.522(3)	C(33)-C(34)	1.505(3)
C(34)-C(35)	1.502(3)	C(35)-C(36)	1.522(3)

O(3)-Al-O(4)	112.57(7)	O(3)-Al-O(1)	110.23(8)
O(4)-Al-O(1)	115.01(7)	O(3)-Al-O(2)	115.27(7)
O(4)-Al-O(2)	110.71(7)	O(1)-Al-O(2)	91.50(7)
O(3)-Al-Li	112.75(5)	O(4)-Al-Li	134.67(5)
O(1)-Al-Li	45.99(5)	O(2)-Al-Li	47.48(5)
F(7)-Li-O(1)	151.42(6)	F(7)-Li-O(2)	79.92(5)
O(1)-Li-O(2)	79.45(5)	F(7)-Li-F(1)	109.52(5)
O(1)-Li-F(1)	84.16(5)	O(2)-Li-F(1)	158.08(6)
F(7)-Li-C(3)	138.63(6)	O(1)-Li-C(3)	56.89(6)
O(2)-Li-C(3)	136.24(6)	F(1)-Li-C(3)	29.31(6)
F(7)-Li-Al	120.31(4)	O(1)-Li-Al	40.38(4)
O(2)-Li-Al	40.56(4)	F(1)-Li-Al	124.54(4)
C(3)-Li-Al	96.74(5)	F(7)-Li-C(11)	27.58(6)
O(1)-Li-C(11)	135.02(6)	O(2)-Li-C(11)	55.85(6)
F(1)-Li-C(11)	136.87(6)	C(3)-Li-C(11)	156.15(7)

Table A.11 (continued).

Al-Li-C(11)	96.18(5)	F(7)-Li-C(1)	147.56(6)
O(1)-Li-C(1)	28.17(6)	O(2)-Li-C(1)	104.47(5)
F(1)-Li-C(1)	56.82(5)	C(3)-Li-C(1)	32.72(6)
Al-Li-C(1)	67.99(4)	C(11)-Li-C(1)	154.33(6)
C(1)-C(1)-Al	152.26(13)	C(1)-C(1)-Li	110.47(11)
Al-O(1)-Li	93.63(6)	C(10)-O(2)-Al	150.61(13)
C(10)-O(2)-Li	117.43(11)	Al-C(2)-Li	91.86(6)
C(19)-O(3)-Al	154.16(13)	C(28)-O(4)-Al	155.35(13)
O(1)-C(1)-C(4)	113.1(2)	O(1)-C(1)-C(3)	104.0(2)
C(4)-C(1)-C(3)	113.8(2)	O(1)-C(1)-C(2)	106.6(2)
C(4)-C(1)-C(2)	110.9(2)	C(3)-C(1)-C(2)	107.9(2)
O(1)-C(1)-Li	41.36(8)	C(4)-C(1)-Li	151.11(13)
C(3)-C(1)-Li	71.46(11)	C(2)-C(1)-Li	92.85(12)
F(5)-C(2)-F(6)	107.0(2)	F(5)-C(2)-F(4)	106.1(2)
F(6)-C(2)-F(4)	105.8(2)	F(5)-C(2)-C(1)	114.7(2)
F(6)-C(2)-C(1)	111.3(2)	F(4)-C(2)-C(1)	111.4(2)
F(3)-C(3)-F(2)	108.0(2)	F(3)-C(3)-F(1)	105.2(2)
F(2)-C(3)-F(1)	106.4(2)	F(3)-C(3)-C(1)	112.8(2)
F(2)-C(3)-C(1)	114.8(2)	F(1)-C(3)-C(1)	109.0(2)
F(3)-C(3)-Li	89.59(13)	F(2)-C(3)-Li	151.7(2)
F(1)-C(3)-Li	46.38(9)	C(1)-C(3)-Li	75.82(11)
C(9)-C(4)-C(5)	109.4(2)	C(9)-C(4)-C(1)	113.8(2)
C(5)-C(4)-C(1)	116.5(2)	C(6)-C(5)-C(4)	110.5(2)
C(7)-C(6)-C(5)	112.0(2)	C(6)-C(7)-C(8)	110.3(2)
C(7)-C(8)-C(9)	111.6(2)	C(8)-C(9)-C(4)	111.0(2)
O(2)-C(10)-C(12)	107.2(2)	O(2)-C(10)-C(13)	113.8(2)
C(12)-C(10)-C(13)	114.2(2)	O(2)-C(10)-C(11)	104.3(2)
C(12)-C(10)-C(11)	107.8(2)	C(13)-C(10)-C(11)	109.0(2)
F(8)-C(11)-F(9)	108.2(2)	F(8)-C(11)-F(7)	105.1(2)
F(9)-C(11)-F(7)	105.4(2)	F(8)-C(11)-C(10)	111.3(2)
F(9)-C(11)-C(10)	115.0(2)	F(7)-C(11)-C(10)	111.2(2)
F(8)-C(11)-Li	92.38(12)	F(9)-C(11)-Li	145.9(2)
F(7)-C(11)-Li	41.55(8)	C(10)-C(11)-Li	80.14(11)
F(12)-C(12)-F(10)	106.5(2)	F(12)-C(12)-F(11)	105.4(2)
F(10)-C(12)-F(11)	106.9(2)	F(12)-C(12)-C(10)	111.3(2)
F(10)-C(12)-C(10)	114.6(2)	F(11)-C(12)-C(10)	111.5(2)
C(14)-C(13)-C(18)	108.8(2)	C(14)-C(13)-C(10)	113.9(2)
C(18)-C(13)-C(10)	116.9(2)	C(13)-C(14)-C(15)	111.1(2)
C(16)-C(15)-C(14)	111.8(2)	C(17)-C(16)-C(15)	110.4(2)
C(16)-C(17)-C(18)	112.0(2)	C(17)-C(18)-C(13)	110.6(2)
O(3)-C(19)-C(20)	106.8(2)	O(3)-C(19)-C(21)	108.8(2)
C(20)-C(19)-C(21)	108.3(2)	O(3)-C(19)-C(22)	109.3(2)
C(20)-C(19)-C(22)	113.1(2)	C(21)-C(19)-C(22)	110.4(2)
F(15)-C(20)-F(14)	106.9(2)	F(15)-C(20)-F(13)	106.4(2)
F(14)-C(20)-F(13)	106.7(2)	F(15)-C(20)-C(19)	111.1(2)
F(14)-C(20)-C(19)	113.3(2)	F(13)-C(20)-C(19)	112.1(2)
F(17)-C(21)-F(18)	106.9(2)	F(17)-C(21)-F(16)	106.1(2)
F(18)-C(21)-F(16)	106.5(2)	F(17)-C(21)-C(19)	112.3(2)
F(18)-C(21)-C(19)	112.8(2)	F(16)-C(21)-C(19)	111.7(2)
C(23)-C(22)-C(27)	109.2(2)	C(23)-C(22)-C(19)	113.0(2)
C(27)-C(22)-C(19)	118.5(2)	C(24)-C(23)-C(22)	110.1(2)
C(25)-C(24)-C(23)	111.6(2)	C(26)-C(25)-C(24)	111.5(2)
C(25)-C(26)-C(27)	112.5(2)	C(26)-C(27)-C(22)	109.6(2)
O(4)-C(28)-C(29)	107.5(2)	O(4)-C(28)-C(30)	108.4(2)
C(29)-C(28)-C(30)	108.3(2)	O(4)-C(28)-C(31)	109.5(2)
C(29)-C(28)-C(31)	113.1(2)	C(30)-C(28)-C(31)	109.2(2)
F(20)-C(29)-F(21)	106.5(2)	F(20)-C(29)-F(19)	106.0(2)
F(21)-C(29)-F(19)	106.6(2)	F(20)-C(29)-C(28)	111.4(2)

Table A.11 (continued).

F(21)-C(29)-C(28)	114.6(2)	F(19)-C(29)-C(28)	111.3(2)
F(24)-C(30)-F(23)	105.9(2)	F(24)-C(30)-F(22)	106.6(2)
F(23)-C(30)-F(22)	105.8(2)	F(24)-C(30)-C(28)	112.4(2)
F(23)-C(30)-C(28)	111.7(2)	F(22)-C(30)-C(28)	113.9(2)
C(32)-C(31)-C(36)	110.1(2)	C(32)-C(31)-C(28)	114.1(2)
C(36)-C(31)-C(28)	116.3(2)	C(31)-C(32)-C(33)	110.7(2)
C(34)-C(33)-C(32)	112.2(2)	C(35)-C(34)-C(33)	111.4(2)
C(34)-C(35)-C(36)	112.6(2)	C(35)-C(36)-C(31)	111.6(2)
C(3)-F(1)-Li	104.31(12)	C(11)-F(7)-Li	110.87(11)

Table A.12. Hydrogen atom coordinates for 40% $LiAl(HFCP)_4$.

	x	y	z	U(eq)
H(4A)	7187(2)	1310(1)	1406(1)	31
H(5A)	4902(2)	755(1)	711(1)	48
H(5B)	6060(2)	305(1)	1068(1)	48
H(6A)	4813(2)	435(1)	1879(2)	57
H(6B)	6114(2)	756(1)	2210(2)	57
H(7A)	4670(2)	1522(1)	2406(1)	52
H(7B)	3994(2)	1519(1)	1568(1)	52
H(8A)	6340(3)	2068(1)	2167(2)	62
H(8B)	5169(3)	2508(1)	1812(2)	62
H(9A)	6401(2)	2390(1)	998(1)	54
H(9B)	5113(2)	2049(1)	673(1)	54
H(13A)	10865(2)	3230(1)	-372(1)	34
H(14A)	12666(2)	2579(1)	708(1)	52
H(14B)	11439(2)	2877(1)	838(1)	52
H(15A)	11983(2)	3991(2)	579(2)	71
H(15B)	13021(2)	3679(2)	1215(2)	71
H(16A)	13831(2)	4233(1)	340(2)	68
H(16B)	14207(2)	3444(1)	419(2)	68
H(17A)	13567(3)	3708(1)	-806(2)	70
H(17B)	12326(3)	4006(1)	-699(2)	70
H(18A)	13012(2)	2596(1)	-550(1)	50
H(18B)	11993(2)	2906(1)	-1200(1)	50
H(22A)	7076(2)	3446(1)	1382(1)	29
H(23A)	9018(2)	3574(1)	2158(1)	38
H(23B)	8858(2)	4385(1)	2098(1)	38
H(24A)	7346(2)	3488(1)	2670(1)	52
H(24B)	8285(2)	4017(1)	3137(1)	52
H(25A)	6262(2)	4436(1)	2884(1)	53
H(25B)	7135(2)	4944(1)	2602(1)	53
H(26A)	5385(2)	4837(1)	1699(1)	51
H(26B)	5464(2)	4022(1)	1735(1)	51
H(27A)	7082(2)	4888(1)	1212(1)	39
H(27B)	6095(2)	4397(1)	720(1)	39
H(31A)	12173(2)	1250(1)	2043(1)	30
H(32A)	10588(2)	674(1)	1265(1)	41
H(32B)	10223(2)	339(1)	1942(1)	41
H(33A)	11425(2)	-436(1)	1496(1)	46
H(33B)	12462(2)	124(1)	1570(1)	46
H(34A)	11758(3)	-515(1)	2736(1)	55
H(34B)	13017(3)	-620(1)	2534(1)	55
H(35A)	13611(2)	477(1)	2879(1)	59
H(35B)	13172(2)	132(1)	3525(1)	59
H(36A)	12416(2)	1266(1)	3288(1)	45
H(36B)	11354(2)	721(1)	3213(1)	45

Table A.13. Crystal data and structure refinement for 60% $LiAl(HFCP)_4$.

Identification code	shscod56 li in 60% xyz
Empirical formula	$C_{36}H_{44}AlF_{24}LiO_4$
Formula weight	1030.63
Temperature	169(2) K
Wavelength	0.71073 Å
Crystal system	Monoclinic
Space group	$P2_1/n$
Unit cell dimensions	a = 11.4943(8) Å alpha = 90° b = 19.608(2) Å beta = 104.388(7)° c = 19.1934(14) Å gamma = 90°
Volume, Z	4190.2(6) $Å^3$, 4
Density (calculated)	1.634 Mg/m^3
Absorption coefficient	0.195 mm^{-1}
F(000)	2096
Crystal size	0.38 x 0.40 x 0.50 mm
θ range for data collection	1.51 to 28.39°
Limiting indices	$-15 \le h \le 15$, $-26 \le k \le 26$, $-25 \le l \le 19$
Reflections collected	27634
Independent reflections	10127 (R_{int} = 0.0515)
Absorption correction	SADABS
Refinement method	Full-matrix least-squares on F^2
Data / restraints / parameters	10126 / 0 / 593
Goodness-of-fit on F^2	0.923
Final R indices [$I>2\sigma(I)$]	R1 = 0.0490, wR2 = 0.1175
R indices (all data)	R1 = 0.0865, wR2 = 0.1371
Extinction coefficient	0.0016(3)
Largest diff. peak and hole	0.865 and -0.990 $eÅ^{-3}$

Table A.14. Atomic coordinates for 60% $LiAl(HFCP)_4$.

	x	y	z	U(eq)
Al	9160(1)	2254(1)	709(1)	19(1)
Li	8443	1551	-669	138(4)
O(1)	7846(1)	1786(1)	303(1)	32(1)
O(2)	9710(1)	2174(1)	-74(1)	25(1)
O(3)	8792(1)	3059(1)	902(1)	25(1)
O(4)	10099(1)	1863(1)	1423(1)	28(1)
C(1)	6984(2)	1287(1)	314(1)	26(1)
C(2)	7598(2)	586(1)	283(1)	32(1)
C(3)	6028(2)	1389(1)	-406(1)	35(1)
C(4)	6473(2)	1331(1)	986(1)	26(1)
C(5)	5657(2)	746(1)	1095(1)	41(1)
C(6)	5362(3)	808(1)	1823(2)	48(1)
C(7)	4788(2)	1487(1)	1914(2)	43(1)
C(8)	5579(3)	2069(1)	1787(2)	52(1)
C(9)	5859(3)	2012(1)	1052(2)	45(1)
C(10)	10655(2)	2191(1)	-409(1)	24(1)
C(11)	10028(2)	2176(1)	-1228(1)	33(1)
C(12)	11359(2)	1519(1)	-222(1)	33(1)
C(13)	11437(2)	2841(1)	-241(1)	28(1)
C(14)	12041(2)	2934(2)	552(1)	44(1)
C(15)	12612(3)	3638(2)	696(2)	59(1)
C(16)	13522(2)	3761(2)	259(2)	57(1)
C(17)	12949(3)	3652(1)	-531(2)	58(1)
C(18)	12380(2)	2948(1)	-681(2)	41(1)
C(19)	8218(2)	3678(1)	743(1)	24(1)
C(20)	9184(2)	4205(1)	680(1)	35(1)
C(21)	7308(2)	3625(1)	3(1)	32(1)
C(22)	7560(2)	3859(1)	1338(1)	24(1)
C(23)	8421(2)	3948(1)	2080(1)	32(1)
C(24)	7722(2)	3940(1)	2662(1)	43(1)
C(25)	6756(2)	4489(1)	2531(1)	45(1)
C(26)	5945(2)	4444(1)	1778(1)	42(1)
C(27)	6651(2)	4449(1)	1200(1)	32(1)
C(28)	10655(2)	1765(1)	2142(1)	24(1)
C(29)	9654(2)	1720(1)	2553(1)	29(1)
C(30)	11446(2)	2399(1)	2414(1)	29(1)
C(31)	11468(2)	1115(1)	2230(1)	25(1)
C(32)	10903(2)	517(1)	1767(1)	34(1)
C(33)	11821(2)	-46(1)	1788(1)	38(1)
C(34)	12379(3)	-286(1)	2544(1)	47(1)
C(35)	12902(3)	300(1)	3024(1)	49(1)
C(36)	12007(2)	877(1)	3001(1)	38(1)
F(1)	6567(1)	1311(1)	-964(1)	53(1)
F(2)	5125(1)	952(1)	-523(1)	48(1)
F(3)	5579(1)	2010(1)	-477(1)	53(1)
F(4)	8385(1)	618(1)	-134(1)	50(1)
F(5)	6848(1)	80(1)	23(1)	45(1)

Table A.14 (continued).

F(6)	8232(1)	395(1)	929(1)	44(1)
F(7)	9059(1)	1747(1)	-1369(1)	38(1)
F(8)	9588(1)	2782(1)	-1458(1)	49(1)
F(9)	10714(1)	1966(1)	-1646(1)	57(1)
F(10)	12300(1)	1458(1)	-507(1)	54(1)
F(11)	10654(1)	975(1)	-440(1)	51(1)
F(12)	11776(1)	1447(1)	485(1)	52(1)
F(13)	9555(1)	4123(1)	77(1)	49(1)
F(14)	8811(1)	4852(1)	686(1)	53(1)
F(15)	10158(1)	4141(1)	1225(1)	45(1)
F(16)	7746(1)	3252(1)	-465(1)	43(1)
F(17)	6292(1)	3320(1)	47(1)	41(1)
F(18)	7004(1)	4236(1)	-307(1)	45(1)
F(19)	8889(1)	2243(1)	2391(1)	49(1)
F(20)	8998(1)	1157(1)	2377(1)	41(1)
F(21)	10054(1)	1714(1)	3267(1)	47(1)
F(22)	11873(1)	2416(1)	3131(1)	45(1)
F(23)	12404(1)	2422(1)	2141(1)	45(1)
F(24)	10862(1)	2980(1)	2228(1)	46(1)

Table A.15. Bond lengths and angles for 60% $LiAl(HFCP)_4$.

Al-O(3)	1.700(2)	Al-O(4)	1.702(2)
Al-O(1)	1.773(2)	Al-C(2)	1.7764(14)
Al-Li	2.9128(6)	Li-F(7)	1.7106(13)
Li-O(2)	2.0216(14)	Li-F(4)	2.108(2)
Li-F(1)	2.141(2)	Li-O(1)	2.139(2)
Li-C(11)	2.635(2)	Li-C(10)	2.768(2)
O(1)-C(1)	1.396(2)	O(2)-C(10)	1.394(2)
O(3)-C(19)	1.378(2)	O(4)-C(28)	1.383(2)
C(1)-C(4)	1.546(3)	C(1)-C(3)	1.550(3)
C(1)-C(2)	1.553(3)	C(2)-F(5)	1.327(3)
C(2)-F(6)	1.328(3)	C(2)-F(4)	1.350(3)
C(3)-F(3)	1.316(3)	C(3)-F(2)	1.321(3)
C(3)-F(1)	1.373(3)	C(4)-C(5)	1.528(3)
C(4)-C(9)	1.530(3)	C(5)-C(6)	1.523(3)
C(6)-C(7)	1.516(4)	C(7)-C(8)	1.516(4)
C(8)-C(9)	1.526(4)	C(10)-C(12)	1.541(3)
C(10)-C(13)	1.546(3)	C(10)-C(11)	1.558(3)
C(11)-F(9)	1.322(3)	C(11)-F(8)	1.323(3)
C(11)-F(7)	1.369(3)	C(12)-F(12)	1.330(3)
C(12)-F(10)	1.332(3)	C(12)-F(11)	1.343(3)
C(13)-C(14)	1.520(3)	C(13)-C(18)	1.545(3)
C(14)-C(15)	1.524(4)	C(15)-C(16)	1.513(4)
C(16)-C(17)	1.512(4)	C(17)-C(18)	1.524(4)
C(19)-C(20)	1.543(3)	C(19)-C(21)	1.544(3)
C(19)-C(22)	1.560(3)	C(20)-F(15)	1.334(3)
C(20)-F(13)	1.339(3)	C(20)-F(14)	1.340(3)
C(21)-F(17)	1.332(3)	C(21)-F(18)	1.344(3)
C(21)-F(16)	1.348(2)	C(22)-C(23)	1.529(3)
C(22)-C(27)	1.537(3)	C(23)-C(24)	1.529(3)
C(24)-C(25)	1.522(4)	C(25)-C(26)	1.515(4)
C(26)-C(27)	1.529(3)	C(28)-C(29)	1.550(3)
C(28)-C(30)	1.553(3)	C(28)-C(31)	1.564(3)
C(29)-F(20)	1.331(2)	C(29)-F(21)	1.333(3)
C(29)-F(19)	1.337(2)	C(30)-F(24)	1.325(2)
C(30)-F(23)	1.332(2)	C(30)-F(22)	1.342(2)
C(31)-C(32)	1.517(3)	C(31)-C(36)	1.530(3)
C(32)-C(33)	1.520(3)	C(33)-C(34)	1.508(3)
C(34)-C(35)	1.501(4)	C(35)-C(36)	1.522(3)

O(3)-Al-O(4)	112.62(7)	O(3)-Al-O(1)	110.27(8)
O(4)-Al-O(1)	114.95(8)	O(3)-Al-O(2)	115.26(7)
O(4)-Al-O(2)	110.71(7)	O(1)-Al-O(2)	91.47(7)
O(3)-Al-Li	127.44(5)	O(4)-Al-Li	119.88(5)
O(1)-Al-Li	48.57(5)	O(2)-Al-Li	43.13(5)
F(7)-Li-O(2)	85.85(6)	F(7)-Li-F(4)	130.28(6)
O(2)-Li-F(4)	110.76(6)	F(7)-Li-F(1)	115.30(6)
O(2)-Li-F(1)	144.98(6)	F(4)-Li-F(1)	77.67(6)
F(7)-Li-O(1)	154.21(6)	O(2)-Li-O(1)	74.13(5)
F(4)-Li-O(1)	73.30(5)	F(1)-Li-O(1)	76.34(5)
F(7)-Li-C(11)	27.50(6)	O(2)-Li-C(11)	58.35(6)
F(4)-Li-C(11)	135.29(7)	F(1)-Li-C(11)	138.35(6)
O(1)-Li-C(11)	130.08(6)	F(7)-Li-C(10)	59.93(6)
O(2)-Li-C(10)	28.82(5)	F(4)-Li-C(10)	116.40(6)
F(1)-Li-C(10)	165.27(6)	O(1)-Li-C(10)	102.58(5)

Table A.15 (continued).

C(11)-Li-C(10)	33.41(6)	F(7)-Li-Al	121.89(4)
O(2)-Li-Al	36.92(4)	F(4)-Li-Al	90.23(4)
F(1)-Li-Al	112.54(4)	O(1)-Li-Al	37.38(4)
C(11)-Li-Al	94.69(5)	C(10)-Li-Al	65.30(4)
C(1)-O(1)-Al	152.32(14)	C(1)-O(1)-Li	103.93(12)
Al-O(1)-Li	94.04(6)	C(10)-O(2)-Al	150.49(13)
C(10)-O(2)-Li	106.82(11)	Al-O(2)-Li	99.96(6)
C(19)-O(3)-Al	154.19(13)	C(28)-O(4)-Al	155.47(14)
O(1)-C(1)-C(4)	113.2(2)	O(1)-C(1)-C(3)	104.2(2)
C(4)-C(1)-C(3)	113.8(2)	O(1)-C(1)-C(2)	106.7(2)
C(4)-C(1)-C(2)	110.6(2)	C(3)-C(1)-C(2)	107.9(2)
F(5)-C(2)-F(6)	107.2(2)	F(5)-C(2)-F(4)	106.3(2)
F(6)-C(2)-F(4)	105.9(2)	F(5)-C(2)-C(1)	114.7(2)
F(6)-C(2)-C(1)	111.3(2)	F(4)-C(2)-C(1)	111.1(2)
F(3)-C(3)-F(2)	108.1(2)	F(3)-C(3)-F(1)	105.2(2)
F(2)-C(3)-F(1)	106.5(2)	F(3)-C(3)-C(1)	112.6(2)
F(2)-C(3)-C(1)	114.9(2)	F(1)-C(3)-C(1)	108.9(2)
C(5)-C(4)-C(9)	109.4(2)	C(5)-C(4)-C(1)	116.5(2)
C(9)-C(4)-C(1)	113.4(2)	C(6)-C(5)-C(4)	110.5(2)
C(7)-C(6)-C(5)	112.2(2)	C(8)-C(7)-C(6)	110.3(2)
C(7)-C(8)-C(9)	111.5(2)	C(8)-C(9)-C(4)	110.4(2)
O(2)-C(10)-C(12)	107.2(2)	O(2)-C(10)-C(13)	113.8(2)
C(12)-C(10)-C(13)	114.3(2)	O(2)-C(10)-C(11)	104.3(2)
C(12)-C(10)-C(11)	107.6(2)	C(13)-C(10)-C(11)	109.0(2)
O(2)-C(10)-Li	44.36(8)	C(12)-C(10)-Li	93.46(13)
C(13)-C(10)-Li	150.63(13)	C(11)-C(10)-Li	68.62(11)
F(9)-C(11)-F(8)	108.3(2)	F(9)-C(11)-F(7)	105.5(2)
F(8)-C(11)-F(7)	105.1(2)	F(9)-C(11)-C(10)	115.0(2)
F(8)-C(11)-C(10)	111.2(2)	F(7)-C(11)-C(10)	111.2(2)
F(9)-C(11)-Li	132.7(2)	F(8)-C(11)-Li	107.89(14)
F(7)-C(11)-Li	35.25(8)	C(10)-C(11)-Li	77.97(11)
F(12)-C(12)-F(10)	106.5(2)	F(12)-C(12)-F(11)	105.6(2)
F(10)-C(12)-F(11)	106.8(2)	F(12)-C(12)-C(10)	111.3(2)
F(10)-C(12)-C(10)	114.5(2)	F(11)-C(12)-C(10)	111.5(2)
C(14)-C(13)-C(18)	108.9(2)	C(14)-C(13)-C(10)	113.9(2)
C(18)-C(13)-C(10)	116.6(2)	C(13)-C(14)-C(15)	111.0(2)
C(16)-C(15)-C(14)	111.7(2)	C(17)-C(16)-C(15)	110.2(2)
C(16)-C(17)-C(18)	112.1(2)	C(17)-C(18)-C(13)	110.3(2)
O(3)-C(19)-C(20)	107.0(2)	O(3)-C(19)-C(21)	108.9(2)
C(20)-C(19)-C(21)	108.0(2)	O(3)-C(19)-C(22)	109.3(2)
C(20)-C(19)-C(22)	113.1(2)	C(21)-C(19)-C(22)	110.4(2)
F(15)-C(20)-F(13)	106.3(2)	F(15)-C(20)-F(14)	106.9(2)
F(13)-C(20)-F(14)	106.9(2)	F(15)-C(20)-C(19)	110.9(2)
F(13)-C(20)-C(19)	112.1(2)	F(14)-C(20)-C(19)	113.3(2)
F(17)-C(21)-F(18)	107.0(2)	F(17)-C(21)-F(16)	106.1(2)
F(18)-C(21)-F(16)	106.7(2)	F(17)-C(21)-C(19)	112.0(2)
F(18)-C(21)-C(19)	112.9(2)	F(16)-C(21)-C(19)	111.7(2)
C(23)-C(22)-C(27)	109.2(2)	C(23)-C(22)-C(19)	112.9(2)
C(27)-C(22)-C(19)	118.6(2)	C(22)-C(23)-C(24)	110.1(2)
C(25)-C(24)-C(23)	111.5(2)	C(26)-C(25)-C(24)	111.5(2)
C(25)-C(26)-C(27)	112.3(2)	C(26)-C(27)-C(22)	109.3(2)
O(4)-C(28)-C(29)	107.4(2)	O(4)-C(28)-C(30)	108.0(2)
C(29)-C(28)-C(30)	108.8(2)	O(4)-C(28)-C(31)	109.6(2)
C(29)-C(28)-C(31)	113.5(2)	C(30)-C(28)-C(31)	109.3(2)
F(20)-C(29)-F(21)	106.5(2)	F(20)-C(29)-F(19)	106.2(2)
F(21)-C(29)-F(19)	106.6(2)	F(20)-C(29)-C(28)	111.3(2)
F(21)-C(29)-C(28)	114.4(2)	F(19)-C(29)-C(28)	111.4(2)
F(24)-C(30)-F(23)	106.2(2)	F(24)-C(30)-F(22)	106.6(2)

Table A.15 (continued).

F(23)-C(30)-F(22)	106.0(2)	F(24)-C(30)-C(28)	112.5(2)
F(23)-C(30)-C(28)	111.6(2)	F(22)-C(30)-C(28)	113.5(2)
C(32)-C(31)-C(36)	110.0(2)	C(32)-C(31)-C(28)	114.2(2)
C(36)-C(31)-C(28)	116.1(2)	C(31)-C(32)-C(33)	110.7(2)
C(34)-C(33)-C(32)	112.2(2)	C(35)-C(34)-C(33)	111.2(2)
C(34)-C(35)-C(36)	112.7(2)	C(35)-C(36)-C(31)	111.3(2)
C(3)-F(1)-Li	112.89(12)	C(2)-F(4)-Li	115.85(14)
C(11)-F(7)-Li	117.25(12)		

Table A.16. Hydrogen atom coordinates for 60% $LiAl(HFCP)_4$.

	x	y	z	U(eq)
H(4A)	7186(2)	1311(1)	1408(1)	31
H(5A)	4904(2)	756(1)	708(1)	49
H(5B)	6062(2)	305(1)	1067(1)	49
H(6A)	4808(3)	435(1)	1875(2)	57
H(6B)	6109(3)	754(1)	2209(2)	57
H(7A)	3992(2)	1520(1)	1568(2)	52
H(7B)	4668(2)	1521(1)	2406(2)	52
H(8A)	6339(3)	2066(1)	2167(2)	62
H(8B)	5168(3)	2508(1)	1817(2)	62
H(9A)	6391(3)	2392(1)	990(2)	54
H(9B)	5105(3)	2047(1)	669(2)	54
H(13A)	10865(2)	3231(1)	-371(1)	34
H(14A)	12666(2)	2580(2)	707(1)	52
H(14B)	11439(2)	2876(2)	838(1)	52
H(15A)	11976(3)	3990(2)	575(2)	71
H(15B)	13012(3)	3681(2)	1214(2)	71
H(16A)	13831(2)	4233(2)	338(2)	68
H(16B)	14207(2)	3444(2)	419(2)	68
H(17A)	13567(3)	3707(1)	-806(2)	69
H(17B)	12326(3)	4004(1)	-700(2)	69
H(18A)	13010(2)	2594(1)	-552(2)	50
H(18B)	11990(2)	2904(1)	-1201(2)	50
H(22A)	7076(2)	3445(1)	1382(1)	29
H(23A)	8857(2)	4386(1)	2098(1)	39
H(23B)	9019(2)	3574(1)	2168(1)	39
H(24A)	7344(2)	3488(1)	2669(1)	52
H(24B)	8285(2)	4015(1)	3138(1)	52
H(25A)	6267(2)	4438(1)	2886(1)	54
H(25B)	7141(2)	4944(1)	2601(1)	54
H(26A)	5379(2)	4833(1)	1698(1)	50
H(26B)	5467(2)	4019(1)	1734(1)	50
H(27A)	7079(2)	4889(1)	1213(1)	38
H(27B)	6094(2)	4398(1)	719(1)	38
H(31A)	12172(2)	1251(1)	2041(1)	30
H(32A)	10584(2)	671(1)	1265(1)	40
H(32B)	10224(2)	337(1)	1944(1)	40
H(33A)	11425(2)	-437(1)	1497(1)	46
H(33B)	12461(2)	124(1)	1570(1)	46
H(34A)	11761(3)	-515(1)	2739(1)	56
H(34B)	13019(3)	-621(1)	2536(1)	56
H(35A)	13609(3)	479(1)	2975(1)	59
H(35B)	13181(3)	134(1)	3524(1)	59
H(36A)	12417(2)	1265(1)	3291(1)	45
H(36B)	11355(2)	719(1)	3216(1)	45

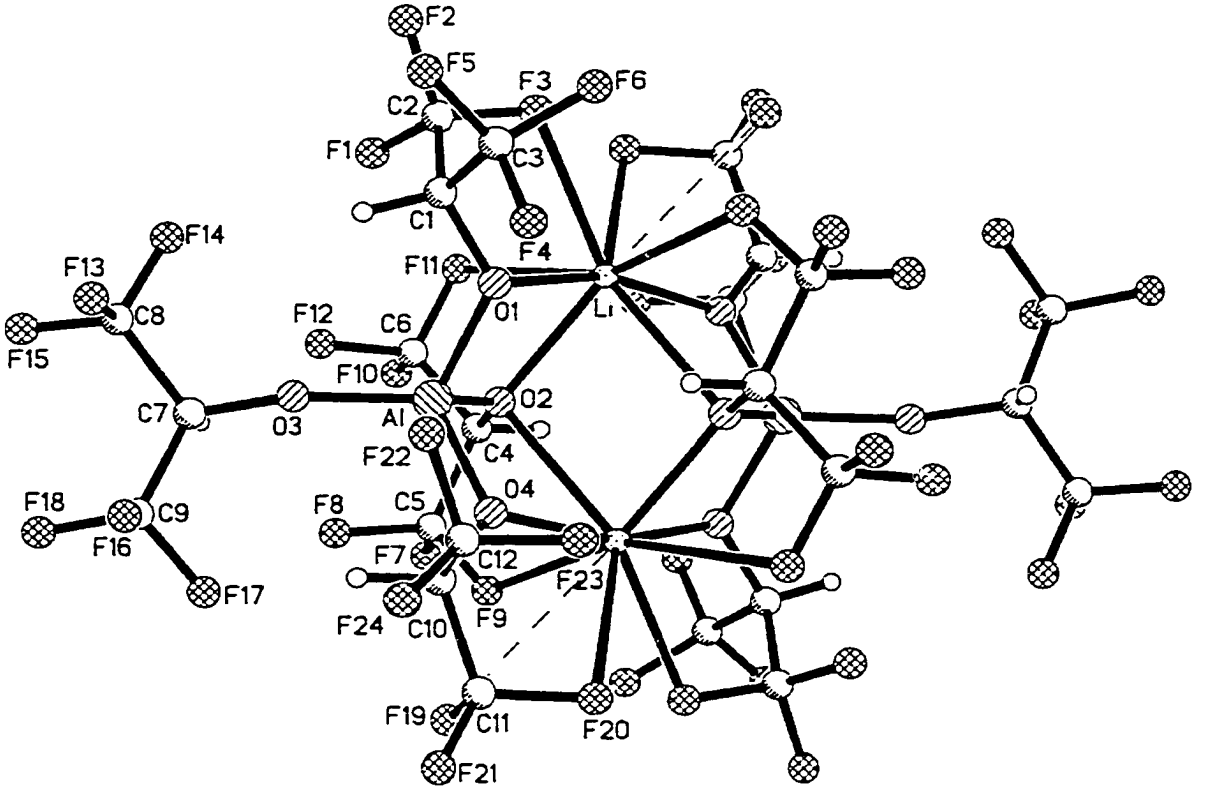

Figure A.4. Drawing of $LiAl(HFIP)_4$ with all but the hydrogen atoms labeled. See Table 2 for definition of abbreviation.

Table A.17. Crystal data and structure refinement for $LiAl(HFIP)_4$.

Identification code	shscod42 (Nolan/Strauss)
Empirical formula	$C_{12}H_4AlF_{24}LiO_4$
Formula weight	702.07
Temperature	173(2) K
Wavelength	0.71073 Å
Crystal system	Triclinic
Space group	$P\bar{1}$
Unit cell dimensions	a = 10.1184(7) Å alpha = 76.5870(10)°
	b = 10.5213(7) Å beta = 80.4790(10)°
	c = 11.6461(8) Å gamma = 65.0320(10)°
Volume, Z	1090.09(13) $Å^3$, 2
Density (calculated)	2.139 Mg/m^3
Absorption coefficient	0.319 mm^{-1}
F(000)	680
Crystal size	0.40 x 0.20 x 0.18 mm, clr. diamond shape
θ range for data collection	1.80 to 28.30°
Limiting indices	$-11 \le h \le 13$, $-14 \le k \le 13$, $-14 \le l \le 15$
Reflections collected	7230
Independent reflections	4997 (R_{int} = 0.0221)
Absorption correction	SADABS
Refinement method	Full-matrix least-squares on F^2
Data / restraints / parameters	4997 / 0 / 380
Goodness-of-fit on F^2	1.019
Final R indices [I>2σ(I)]	R1 = 0.0520, wR2 = 0.1213
R indices (all data)	R1 = 0.0822, wR2 = 0.1413
Extinction coefficient	0.0028(13)
Largest diff. peak and hole	0.408 and -0.427 $eÅ^{-3}$

Table A.18. Atomic coordinates for $LiAl(HFIP)_4$.

	x	y	z	U(eq)
Al	6340(1)	4131(1)	3318(1)	20(1)
Li	5897(7)	6184(6)	4755(4)	42(1)
O(1)	5958(2)	5964(2)	3007(2)	26(1)
O(2)	6597(2)	3918(2)	4829(2)	28(1)
O(3)	7568(2)	3284(2)	2284(2)	29(1)
O(4)	4741(2)	3795(2)	3513(2)	25(1)
C(1)	6616(3)	6646(3)	2063(2)	28(1)
C(2)	7739(4)	6937(4)	2548(3)	41(1)
C(3)	5491(4)	8000(4)	1417(3)	41(1)
C(4)	7506(3)	2882(3)	5673(2)	23(1)
C(5)	7501(3)	1433(3)	5696(2)	30(1)
C(6)	9038(3)	2867(3)	5433(3)	33(1)
C(7)	8817(3)	2145(3)	2000(2)	29(1)
C(8)	9803(4)	2587(4)	1087(3)	45(1)
C(9)	8398(4)	1106(4)	1577(3)	45(1)
C(10)	4329(3)	3258(3)	2694(2)	27(1)
C(11)	3494(4)	2376(4)	3382(3)	40(1)
C(12)	3460(3)	4468(3)	1766(3)	36(1)
F(1)	8867(2)	5719(3)	2894(2)	64(1)
F(2)	8257(3)	7790(3)	1805(2)	64(1)
F(3)	7156(3)	7517(3)	3533(2)	59(1)
F(4)	4326(3)	7802(3)	1276(2)	78(1)
F(5)	6050(3)	8407(2)	350(2)	67(1)
F(6)	5011(3)	9096(2)	1973(2)	61(1)
F(7)	8154(2)	472(2)	6598(2)	52(1)
F(8)	8121(2)	926(2)	4703(2)	52(1)
F(9)	6112(2)	1556(2)	5794(2)	41(1)
F(10)	9921(2)	1942(3)	6250(2)	60(1)
F(11)	8980(2)	4152(2)	5435(2)	51(1)
F(12)	9656(2)	2545(2)	4375(2)	49(1)
F(13)	9213(3)	3340(3)	70(2)	88(1)
F(14)	10095(3)	3612(3)	1491(3)	80(1)
F(15)	11078(2)	1641(3)	867(2)	67(1)
F(16)	7597(3)	1710(3)	651(2)	78(1)
F(17)	7586(2)	623(2)	2440(2)	61(1)
F(18)	9565(3)	-18(2)	1299(2)	65(1)
F(19)	4357(3)	1257(3)	4087(2)	80(1)
F(20)	2381(3)	3109(3)	4069(2)	76(1)
F(21)	2989(3)	1886(2)	2681(2)	61(1)
F(22)	4274(3)	5197(3)	1245(2)	67(1)
F(23)	2230(2)	5378(2)	2196(2)	64(1)
F(24)	3156(2)	4001(2)	915(2)	52(1)

Table A.18 (continued).

C(10)-O(4)-Li#1	130.0(2)	Al-O(4)-Li#1	103.8(2)
O(1)-C(1)-C(2)	108.0(2)	C(1)-C(1)-C(3)	111.6(2)
C(2)-C(1)-C(3)	112.0(3)	F(2)-C(2)-F(1)	107.9(3)
F(2)-C(2)-F(3)	107.8(3)	F(1)-C(2)-F(3)	105.7(3)
F(2)-C(2)-C(1)	114.5(3)	F(1)-C(2)-C(1)	110.5(3)
F(3)-C(2)-C(1)	110.1(3)	F(6)-C(3)-F(4)	106.4(3)
F(6)-C(3)-F(5)	106.7(3)	F(4)-C(3)-F(5)	108.0(3)
F(6)-C(3)-C(1)	113.9(3)	F(4)-C(3)-C(1)	111.0(3)
F(5)-C(3)-C(1)	110.6(3)	O(2)-C(4)-C(5)	110.4(2)
O(2)-C(4)-C(6)	109.9(2)	C(5)-C(4)-C(6)	112.4(2)
F(7)-C(5)-F(8)	108.4(2)	F(7)-C(5)-F(9)	107.8(2)
F(8)-C(5)-F(9)	105.8(2)	F(7)-C(5)-C(4)	112.5(2)
F(8)-C(5)-C(4)	112.8(2)	F(9)-C(5)-C(4)	109.3(2)
F(10)-C(6)-F(11)	107.9(2)	F(10)-C(6)-F(12)	108.0(3)
F(11)-C(6)-F(12)	106.6(2)	F(10)-C(6)-C(4)	111.8(2)
F(11)-C(6)-C(4)	109.9(2)	F(12)-C(6)-C(4)	112.4(2)
O(3)-C(7)-C(8)	109.6(2)	O(3)-C(7)-C(9)	109.7(2)
C(8)-C(7)-C(9)	112.5(3)	F(13)-C(8)-F(14)	107.3(3)
F(13)-C(8)-F(15)	107.8(3)	F(14)-C(8)-F(15)	106.8(3)
F(13)-C(8)-C(7)	113.1(3)	F(14)-C(8)-C(7)	109.7(3)
F(15)-C(8)-C(7)	111.8(3)	F(16)-C(9)-F(18)	108.4(3)
F(16)-C(9)-F(17)	106.4(3)	F(18)-C(9)-F(17)	107.5(3)
F(16)-C(9)-C(7)	112.7(3)	F(18)-C(9)-C(7)	112.0(3)
F(17)-C(9)-C(7)	109.4(3)	O(4)-C(10)-C(12)	110.2(2)
O(4)-C(10)-C(11)	107.8(2)	C(12)-C(10)-C(11)	113.3(2)
F(19)-C(11)-F(21)	106.9(3)	F(19)-C(11)-F(20)	106.6(3)
F(21)-C(11)-F(20)	108.4(3)	F(19)-C(11)-C(10)	110.3(3)
F(21)-C(11)-C(10)	112.4(3)	F(20)-C(11)-C(10)	112.0(3)
F(23)-C(12)-F(24)	108.3(3)	F(23)-C(12)-F(22)	107.1(3)
F(24)-C(12)-F(22)	106.7(2)	F(23)-C(12)-C(10)	113.9(2)
F(24)-C(12)-C(10)	112.2(3)	F(22)-C(12)-C(10)	108.3(3)
C(2)-F(3)-Li	108.1(2)	C(5)-F(9)-Li#1	122.2(2)

Symmetry transformations used to generate equivalent atoms:

#1 -x+1,-y+1,-z+1

Table A.19. Bond lengths and angles for $LiAl(HFIP)_4$.

Al-O(3)	1.690(2)	Al-O(1)	1.758(2)
Al-O(4)	1.766(2)	Al-O(2)	1.771(2)
Al-Li	2.877(5)	Al-Li#1	2.980(5)
Li-O(4)#1	2.016(5)	Li-O(1)	2.089(5)
Li-O(2)	2.166(6)	Li-F(3)	2.366(6)
Li-F(9)#1	2.414(6)	Li-O(2)#1	2.533(6)
Li-Al#1	2.980(5)	O(1)-C(1)	1.401(3)
O(2)-C(4)	1.398(3)	O(2)-Li#1	2.533(6)
O(3)-C(7)	1.382(3)	O(4)-C(10)	1.408(3)
O(4)-Li#1	2.016(5)	C(1)-C(2)	1.513(4)
C(1)-C(3)	1.519(4)	C(2)-F(2)	1.310(4)
C(2)-F(1)	1.337(4)	C(2)-F(3)	1.354(4)
C(3)-F(6)	1.324(4)	C(3)-F(4)	1.322(4)
C(3)-F(5)	1.332(4)	C(4)-C(5)	1.522(4)
C(4)-C(6)	1.523(4)	C(5)-F(7)	1.317(3)
C(5)-F(8)	1.333(3)	C(5)-F(9)	1.344(3)
C(6)-F(10)	1.330(3)	C(6)-F(11)	1.329(4)
C(6)-F(12)	1.335(3)	C(7)-C(8)	1.516(4)
C(7)-C(9)	1.526(4)	C(8)-F(13)	1.320(4)
C(8)-F(14)	1.326(5)	C(8)-F(15)	1.328(4)
C(9)-F(16)	1.327(4)	C(9)-F(18)	1.330(4)
C(9)-F(17)	1.337(4)	C(10)-C(12)	1.514(4)
C(10)-C(11)	1.520(4)	C(11)-F(19)	1.320(4)
C(11)-F(22)	1.323(4)	C(11)-F(20)	1.326(4)
C(12)-F(23)	1.314(4)	C(12)-F(24)	1.331(3)
C(12)-F(22)	1.337(4)	F(9)-Li#1	2.414(6)

O(3)-Al-O(1)	111.06(10)	O(3)-Al-O(4)	112.13(10)
O(1)-Al-O(4)	112.41(9)	O(3)-Al-O(2)	127.07(10)
O(1)-Al-O(2)	94.49(9)	O(4)-Al-O(2)	98.17(9)
O(3)-Al-Li	139.77(14)	O(1)-Al-Li	46.19(12)
O(4)-Al-Li	107.81(13)	O(2)-Al-Li	48.73(13)
O(3)-Al-Li#1	142.62(13)	O(1)-Al-Li#1	104.82(12)
O(4)-Al-Li#1	41.09(12)	O(2)-Al-Li#1	57.94(13)
Li-Al-Li#1	74.7(2)	O(4)#1-Li-O(1)	160.4(3)
O(4)#1-Li-O(2)	97.5(2)	O(1)-Li-O(2)	75.0(2)
O(4)#1-Li-F(3)	126.0(3)	O(1)-Li-F(3)	72.9(2)
O(2)-Li-F(3)	122.6(3)	O(4)#1-Li-F(9)#1	90.8(2)
O(1)-Li-F(9)#1	84.9(2)	O(2)-Li-F(9)#1	141.9(3)
F(3)-Li-F(9)#1	79.2(2)	O(4)#1-Li-O(2)#1	70.9(2)
O(1)-Li-O(2)#1	89.9(2)	O(2)-Li-O(2)#1	82.0(2)
F(3)-Li-O(2)#1	142.0(3)	F(9)#1-Li-O(2)#1	65.8(2)
O(4)#1-Li-Al	131.1(2)	O(1)-Li-Al	37.39(10)
O(2)-Li-Al	37.90(9)	F(3)-Li-Al	100.7(2)
F(9)#1-Li-Al	113.7(2)	O(2)#1-Li-Al	81.3(2)
O(4)#1-Li-Al#1	35.15(11)	O(1)-Li-Al#1	125.3(2)
O(2)-Li-Al#1	95.2(2)	F(3)-Li-Al#1	151.8(2)
F(9)#1-Li-Al#1	80.5(2)	O(2)#1-Li-Al#1	36.33(8)
Al-Li-Al#1	105.3(2)	C(1)-O(1)-Al	125.4(2)
C(1)-O(1)-Li	122.0(2)	Al-O(1)-Li	96.4(2)
C(4)-O(2)-Al	137.3(2)	C(4)-O(2)-Li	122.9(2)
Al-O(2)-Li	93.4(2)	C(4)-O(2)-Li#1	108.0(2)
Al-O(2)-Li#1	85.72(13)	Li-O(2)-Li#1	98.0(2)
C(7)-O(3)-Al	149.6(2)	C(10)-O(4)-Al	124.1(2)

Table A.19 (continued).

C(10)-O(4)-Li#1	130.0(2)	Al-O(4)-Li#1	103.8(2)
O(1)-C(1)-C(2)	108.0(2)	O(1)-C(1)-C(3)	111.6(2)
C(2)-C(1)-C(3)	112.0(3)	F(2)-C(2)-F(1)	107.9(3)
F(2)-C(2)-F(3)	107.8(3)	F(1)-C(2)-F(3)	105.7(3)
F(2)-C(2)-C(1)	114.5(3)	F(1)-C(2)-C(1)	110.5(3)
F(3)-C(2)-C(1)	110.1(3)	F(6)-C(3)-F(4)	106.4(3)
F(6)-C(3)-F(5)	106.7(3)	F(4)-C(3)-F(5)	108.0(3)
F(6)-C(3)-C(1)	113.9(3)	F(4)-C(3)-C(1)	111.0(3)
F(5)-C(3)-C(1)	110.6(3)	O(2)-C(4)-C(5)	110.4(2)
O(2)-C(4)-C(6)	109.9(2)	C(5)-C(4)-C(6)	112.4(2)
F(7)-C(5)-F(8)	108.4(2)	F(7)-C(5)-F(9)	107.8(2)
F(8)-C(5)-F(9)	105.8(2)	F(7)-C(5)-C(4)	112.5(2)
F(8)-C(5)-C(4)	112.8(2)	F(9)-C(5)-C(4)	109.3(2)
F(10)-C(6)-F(11)	107.9(2)	F(10)-C(6)-F(12)	108.0(3)
F(11)-C(6)-F(12)	106.6(2)	F(10)-C(6)-C(4)	111.8(2)
F(11)-C(6)-C(4)	109.9(2)	F(12)-C(6)-C(4)	112.4(2)
O(3)-C(7)-C(8)	109.6(2)	O(3)-C(7)-C(9)	109.7(2)
C(8)-C(7)-C(9)	112.5(3)	F(13)-C(8)-F(14)	107.3(3)
F(13)-C(8)-F(15)	107.8(3)	F(14)-C(8)-F(15)	106.8(3)
F(13)-C(8)-C(7)	113.1(3)	F(14)-C(8)-C(7)	109.7(3)
F(15)-C(8)-C(7)	111.8(3)	F(16)-C(9)-F(18)	108.4(3)
F(16)-C(9)-F(17)	106.4(3)	F(18)-C(9)-F(17)	107.5(3)
F(16)-C(9)-C(7)	112.7(3)	F(18)-C(9)-C(7)	112.0(3)
F(17)-C(9)-C(7)	109.4(3)	O(4)-C(10)-C(12)	110.2(2)
O(4)-C(10)-C(11)	107.8(2)	C(12)-C(10)-C(11)	113.3(2)
F(19)-C(11)-F(21)	106.9(3)	F(19)-C(11)-F(20)	106.6(3)
F(21)-C(11)-F(20)	108.4(3)	F(19)-C(11)-C(10)	110.3(3)
F(21)-C(11)-C(10)	112.4(3)	F(20)-C(11)-C(10)	112.0(3)
F(23)-C(12)-F(24)	108.3(3)	F(23)-C(12)-F(22)	107.1(3)
F(24)-C(12)-F(22)	106.7(2)	F(23)-C(12)-C(10)	113.9(2)
F(24)-C(12)-C(10)	112.2(3)	F(22)-C(12)-C(10)	108.3(3)
C(2)-F(3)-Li	108.1(2)	C(5)-F(9)-Li#1	122.2(2)

Symmetry transformations used to generate equivalent atoms:

#1 -x+1,-y+1,-z+1

Table A.20. Hydrogen atom coordinates for $LiAl(HFIP)_4$.

	x	y	z	U(eq)
H(1A)	7135(3)	5982(3)	1490(2)	34
H(4A)	7106(3)	3149(3)	6468(2)	28
H(7A)	9350(3)	1639(3)	2732(2)	34
H(10A)	5235(3)	2616(3)	2290(2)	32